Mathematical Modeling of Signal Transduction Pathways in Mammalian cells at the Example of the EGF induced MAP Kinase Cascade and TNF Receptor Crosstalk

Von der Fakultät für Maschinenbau der Universität Stuttgart zur Erlangung der Würde eines Doktor- Ingenieurs (Dr. -Ing.) genehmigte Abhandlung

Vorgelegt von

Dipl.-Ing. Birgit Schoeberl

aus Massenbachhausen

Hauptberichter:	Prof. Dr.-Ing. Dr. h.c. mult. E.D. Gilles
Mitberichter:	Prof. Dr. P. Scheurich
Tag der mündlichen Prüfung:	28.11.2003

Institut für Systemdynamik und Regelungstechnik der Universität Stuttgart

Max-Planck-Institut für Dynamik komplexer technischer Systeme

Sandtorstr. 1, 39106 Magdeburg

2003

Forschungsberichte aus dem Max-Planck-Institut
für Dynamik komplexer technischer Systeme

Band 7

Birgit Schoeberl

Mathematical Modeling of Signaltransduction Pathways in Mammalian Cells at the Example of the EGF induced MAP Kinase Cascade and TNF Receptor Crosstalk

D 93 (Diss. Universität Stuttgart)

Shaker Verlag
Aachen 2004

Bibliografische Information der Deutschen Bibliothek
Die Deutsche Bibliothek verzeichnet diese Publikation in der Deutschen Nationalbibliografie; detaillierte bibliografische Daten sind im Internet über http://dnb.ddb.de abrufbar.

Zugl.: Stuttgart, Univ., Diss., 2003

ISBN 3-8322-2985-X
ISSN 1439-4804

Shaker Verlag GmbH • Postfach 101818 • 52018 Aachen
Telefon: 02407 / 95 96 - 0 • Telefax: 02407 / 95 96 - 9
Internet: www.shaker.de • eMail: info@shaker.de

Vorwort

Die vorliegende Arbeit entstand während meiner Tätigkeit als wissenschaftliche Mitarbeiterin am Institut für Systemdynamik und Regelungstechnik an der Universität Stuttgart und dem Max-Planck-Institut für Dynamik komplexer technischer Systeme in Magdeburg. Die durchgeführten Forschungsarbeiten wurden im Rahmen des Sonderforschungsbereichs SFB 495 “Topologie und Dynamik von Signaltransduktionsprozessen” und dem Schwerpunkt Biosystemtechnik gefördert.

Mein Dank gilt Frau PD Dr. Gertraud Müller und Professor Dr. Peter Scheurich am Institut für Immunologie und Zellbiologie an der Universität Stuttgart für die vorzügliche Betreuung des zellbiologischen Teils meiner Arbeit. Ausserdem danke ich besonders Herrn Professor Dr.-Ing. h.c. mult. Ernst-Dieter Gilles für die Möglichkeit meine Dissertation in diesem sehr “neuen” Bereich der Systembiologie durchzuführen und in einer interdisziplinären sowie wissenschaftlich stimulierenden Umgebung zu arbeiten. Ausserdem möchte ich Herrn Professor Dr.-Ing. h.c. mult. Gilles für seine Anregungen und die interessanten Diskussionen danken.

Desweiteren möchte ich besonders Claudia Eichler-Jonsson am Institut für Immunologie und Zellbiologie an der Universität Stuttgart für die gelungene Zusammenarbeit danken. Wir haben gegenseitig viel voneinander, sowie interdisziplinär arbeiten gelernt. Wir haben während unserer Zusammenarbeit die jeweilige Sprache der Ingenieure und der Biologen verstehen und sprechen gelernt. Desweiteren möchte ich Mariola Fotin und Gudrun Zimmermann am Institut für Immunologie und Zellbiologie an der Universität Stuttgart für das zur Verfügungstellen ihrer experimentellen Daten und für die Erhebung neuer, Modell relevanter Daten danken. Auch möchte ich Thomas Eissing für die Diskussionen und seinen Beitrag zum TNF-Modell innerhalb seiner Diplomarbeit danken. Am Institut für Systemdynamik und Regelungstechnik in Stuttgart möchte ich Kerstin Falkner für die Einführung in die Mikroskopie und die “Starthilfe” danken. Am Institut für Systemtheorie technischer Prozesse an der Universität Stuttgart danke ich Dr.

Eric Bullinger für seine Hilfe und Diskussionen im Bereich der Modellanalyse. Am Max-Planck-Institut für Dynamik komplexer technischer System in Magdeburg möchte ich mich bei dem gesamten Institut bedanken, besonders jedoch bei der Gruppe Systembiologie für das gute Arbeitsklima. Mein besonderer Dank gilt hier Jörg Stelling für seine Hilfe im Bereich der Modellierung, Renate Müller für ihre Hilfe bei allen organisatorischen Dingen und dem Bibliotheksteam für das Beschaffen zahlreicher Literaturstellen.

Ausserdem möchte ich meiner Familie und meinen Freunden für Ihre Unterstützung während dieser Zeit danken.

Stuttgart, März 2003

Birgit Schoeberl

Für meine Eltern und Wolfgang

Contents

Constants

The following chapter contains all the symbols used in this thesis.

Φp	identification functional	
α	stoichiometric coefficient	[-]
β	stoichiometric coefficient	[-]
δ	stoichiometric coefficient	[-]
γ	dimensionless coefficient	[-]
ρ	dimensionless radius	[-]
τ	dimensionless time	[-]

Au	Autocrine Number	[-]
Da	Damköhler Number	[-]
C_i	molecular species	[-]
C	number of receptor complexes	
$\bar{C}$	dimensionless number of receptor complexes	[-]
D	diffusion coefficient	[$\mu^2 m$/s]
G	scaling Factor	[-]
I	identification functional with the standard defiation Q=1	
J_c	Jacobians for the states	
J_p	Jacobians for the parameters	
K_D	dissociation constant	[nM]
K_i	inhibitory constant	[nM]

L	ligand concentration	[nM]
$\bar{L}$	dimensionless ligand concentration	[-]
$\bar{L}$	dimensionless ligand concentration	[-]
$\bar{L}_S$	dimensionless ligand concentration at the cell surface	[-]
N_{AV}	Avogadro's Number	
Q	inverse of standard deviation	
R	receptor number	[receptors/cell]
$\bar{R}$	dimensionless receptor number	[-]
S_P	Protease synthesis rate	[Molecules/s]
S_j	set of species participating in reaction j	
U	sum of the squares of the deviation	
	of c values from their mean $\bar{c}$	
Vs	substrate volume	[l]
Vv	endosome volume	[l]
Vz	cell volume	[l]
W	dimensionless rate constant	[-]
Z	number of cells per well	[-]
c	compound concentration	[Molecules/Cell]
$\bar{c}$	mean concentration c	[Molecules/Cell]
e	error between model c(t_i,u,p)	
	and experiment c^M(t_i,u)	
k_{on}, $k_{1...n}$	overall forward constant	[1/(M · s)]
k_{off}, $k_{-1...n}$	overall backward constant	[1/s]
k_{df}	diffusion dependent movement	
	towards encounter complex	[1/(M · s)]
k_{db}	diffusion dependent movement	
	away from encounter complex	[1/s]
k_{rf}	reaction dependent association constant	[1/(M · s)]
k_{rb}	reaction dependent	
	dissociation constant	[1/s]

k_c	constitutive internalization rate	[1/s]
k_{cp}	constitutive protease internalization rate	[1/s]
k_{ap}	protease activation constant	[1/s]
k_e	receptor-ligand-complex internalization rate in autocrine model	[1/s]
k_{deg}	degradation rate	[1/s]
k_{ep}	protease internalization rate	[1/s]
p, p_i	model parameters	
r	cell radius	[μm]
r^2	r-squared value	
s	receptor synthesis rate	[molecules/s]
t	time	[min]
u	input function	
v	reaction rates	[Molecules/(M · s)]

x

Kurzfassung

Die mathematische Modellierung metaboler Netzwerke hat mittlerweile eine lange Tradition [65]. Im Bereich der Signaltransduktion ist die Modellierung jedoch immer noch ein sehr junges Forschungsgebiet. Dies liegt daran, dass die Strukturen der metabolen Netzwerke schon wesentlich früher aufgeklärt wurden, während sich die Signaltransduktionsnetzwerke immer noch in der Aufklärung befinden. Mathematische Modelle wurden bislang nur für Teilbereiche, wie die für MAP-Kinase-Kaskade [71] oder für Rezeptor-Ligand-Interaktionen [139] entwickelt. Aus diesem Grunde gibt es relativ viele quantitative Daten für metabole Netzwerke, jedoch kaum im Bereich der Signaltransduktion. Weiterhin wurden für die Analyse metaboler Netzwerke eine Reihe von Analysemethoden wie die Metabolic Control Analysis oder die Metabolic Flux Analysis entwickelt. Im Gegensatz zu metabolen Netzwerken, deren Verhalten im Gleichgewicht von Interesse ist, ist bei der Signalübertragung die Dynamik entscheidend. Zur Analyse von Signaltransduktionsnetzwerken können die existierenden Analysemethoden aufgrund des dynamischen Aspekts nur bedingt verwendet werden. Es mangelt ausserdem an mathematischen Modellen mit deren Hilfe neue Analysemethoden entwickelt und getestet werden können.

Erst kürzlich konnte am Beispiel der ERK Phosphorylierung gezeigt werden, dass die Dynamik eines Signals für die Zellantwort entscheidend ist. Der Vergleich von Zellen, die eine stark transiente ERK Phosphorlyierung aufweisen, mit Zellen, die durch eine langanhaltende bzw. sehr langsam abklingende ERK Phosphorylierung charakterisiert sind, zeigen unterschiedliche Auswirkungen auf die Aktivierung des Transkriptionsfaktors c-fos [105] und folglich Unterschiede in der physiologischen Zellantwort wie der Proliferation oder Differentiation.

Ziel der vorliegenden Arbeit besteht in der Entwicklung und Analyse mathematischer Modelle für die EGF induzierte MAP-Kinase-Kaskade und für die TNF induzierte Apoptose. Diese Modelle implizieren den derzeitigen Stand des Wissens über die jeweiligen Signaltransduktions-

netzwerke und bilden ein Forum für das publizierte Detailwissen.

Wachstumsfaktoren wie EGF spielen eine wesentliche Rolle bei der Regulation der Zellteilung. Störungen der durch Wachstumsfaktoren induzierten Signaltransduktion sind nachweislich an der Tumorentstehung und dem Tumorwachstum beteiligt. Tyrosin Kinase Rezeptoren, unter ihnen der EGF Rezeptor, aktivieren MAP (Mitogen Activated Protein) Kinasen, die Proliferations- bzw. Differentiationssignale in den Zellkern weiterleiten. Während die interagierenden Moleküle der MAP-Kinase-Kaskade strukturell und biochemisch gut charakterisiert sind, ist es nicht möglich, das Systemverhalten des Netzwerks aufgrund der positiven und negativen Feedback-Regulation rein intuitiv zu verstehen.

Zum besseren Verständnis der Dynamik der Signaltransduktion und um eventuell allgemeine Mechanismen der Signaltransduktion abzuleiten, haben wir ein mathematisches Modell der EGF induzierten MAP-Kinase-Kaskade entwickelt. Das Modell basiert auf gewöhnlichen Differentialgleichungen, deren kinetische Parameter grösstenteils der Literatur entnommen bzw. mit Hilfe eigener experimenteller Daten geschätzt wurden.

Nach einem einführenden Teil zeigen wir in Kapitel 3, dass das Modell in Hinblick auf Literaturdaten und eigene Experimente ein durchaus prädiktives Verhalten zeigt. Anhand von Simulationsdaten und experimentellen Ergebnissen diskutieren wir den Einfluss der EGF-Konzentration, der EGF-Rezeptorzahl und der Rolle der Rezeptorinternalisierung auf die ERK-Phosphorylierung sowie die physiologische Bedeutung der genannten Faktoren. Ausserdem erweitern wir das Modell der EGF induzierten MAP-Kinase-Kaskade, um einen weiteren positiven Feedback-Loop und implementieren den autokrinen Signaltransduktionsweg. Mit Hilfe dieses erweiterten Modells diskutieren wir die zu beobachtende Desensitisierung der EGF induzierten MAP-Kinase-Kaskade. Beispielsweise konnte experimentell beobachtet werden, dass nach einer impulsartigen Stimulation mit einer hohen EGF-Konzentration (1min, 50ng/ml EGF) keine zweite Stimulation mehr möglich ist, und die Zellen etwa 24-36 Stunden benötigen, um wieder ein maximales ERK-Signal nach Stimulation zu zeigen. Im Gegensatz dazu bleiben die Zellen stimulierbar, wenn es sich bei der ersten Stimulation um einen Impuls mit geringer EGF-Konzentration handelt (0.5ng/ml EGF). Mit Hilfe des Modells diskutieren wir verschiedene Möglichkeiten der Desensitisierung, Rezeptorinternalisierung und -degradation, Phosphorylierung und langsame Dephosphorylierung von Adaptermolekülen oder eine Limitierung bestimmter Adaptermoleküle. Weiterhin zeigen wir in Kapitel 3 eine praktische Anwen-

dung dieser mechanistischen biochemischen Modelle. Am Beispiel der EGF induzierten MAP-Kinase-Kaskade, zeigen wir, wie die Wirkung bestimmter Inhibitoren innerhalb der Kaskade vorausgesagt und die Kombination zweier Inhibitoren auf Synergieeffekte *in silico* untersucht werden kann.

In Kapitel 4 untersuchen wir das Systemverhalten des entwickelten Modells für die EGF induzierte MAP-Kinase-Kaskade genauer. Es wird die Robustheit des Systems gegenüber Variationen der Proteinkonzentrationen, aber auch gegenüber Variationen der kinetischen Parameter diskutiert. Ausserdem wird in diesem Kapitel gezeigt, dass die Stufen der MAP-Kinase-Kaskade unter Verwendung der kinetischen Parameter des hier vorgestellten Modells als unabhängige Module betrachtet und somit getrennt untersucht werden können. Wir diskutieren das Stabilitätsverhalten einer einzelnen Stufe der MAP-Kinase-Kaskade und zeigen deren Stabilität. Aufgrund des negativen Feedbacks von ERK-PP zu SOS, wobei SOS phosphorlyliert wird und zur Selbstabschaltung der MAP-Kinase-Kaskade führt, weist das gesamte Modul der MAP-Kinase-Kaskade in bestimmten Parameterbereichen jedoch ERK-PP-Oszillationen auf. Dabei wird angenommen, dass die Dephosphorylierung von SOS relativ schnell erfolgt und nicht zu einer Desensitisierung des Systems erfolgt. Diese Oszillationen hängen davon ab, ob das System mit einem Impuls oder einem konstanten Stimulus angeregt wird. Eine impulsartige Anregung zeigt gedämpfte Oszillationen bzw. nur eine Periode je nach Länge des Impulses. Der Einbau des oszillierenden Moduls in das gesamte Modell der EGF induzierten MAP-Kinase-Kaskade resultiert aufgrund des scharfen Ras-GTP Peaks und des Signalverhaltens der internalisierten Rezeptoren und der auf der Zellmembran verbleibenden Rezeptoren in einem stabilen Systemverhalen. Somit ist es fraglich, ob Oszillationen der MAP-Kinase-Kaskade experimentell zu beobachten sind. Eine zweite Anregung der ERK-Phosphorylierung wie z. B. im Falle radioaktiv bestrahlter Zellen zu beobachten ist, hat seine Ursache in der Anregung des autokrinen Signaltransduktionsweges und nicht in der Instabilität des Systems [26].

TNF ist ein pleiotropes Zytokin, das in einer Reihe von Krankheiten wie z.B. Rheumatismus eine wichtige Rolle spielt. Die zelluläre Wirkung des Zytokins Tumor-Nekrose-Faktor (TNF) wird über zwei spezifische Membranrezeptoren, TNF-R1 und TNF-R2, vermittelt. Die Kopplung an intrazelluläre Signalwege erfolgt über mehrere kürzlich beschriebene rezeptorassoziierte Proteine. So bindet der TNF-R1 z.B. TRADD (TNF-R1-associated death domain protein), das eine

sogenannte ”death domain” (DD) besitzt. Für TRADD konnte eine essentielle Bedeutung bei der TNF-induzierten Apoptose sowie bei der Aktivierung des Transkriptionsfaktors NF-κB und der c-Jun aminoterminalen Kinase (JNK) gezeigt werden. Im Gegensatz zur DD-vermittelten Induktion der Apoptose wird die Aktivierung von NF-κB und JNK durch den aminoterminalen Teil von TRADD durch Interaktion mit einem als TRAF2 (TNF-R2 assoziierten Faktor 2) bezeichneten Protein vermittelt. Bei der Betrachtung des antiapoptotischen Zweiges der TNF-R1 induzierten Signalwege spielen die durch NF-κB induzierten antiapoptotischen Proteine wie XIAP, c-IAP und c-FLIP eine wichtige Rolle.

Innerhalb dieser Arbeit wurde ein mathematisches Modell der TNF-Rezeptor-Interaktion erstellt, das die experimentellen Daten dreier Stimulationsprotokolle beschreibt. Um die TNF-Rezeptor-Interaktion zu analysieren, wurde die Caspase-8 und Caspase-3-Aktivierung bei TNF-R1 selektiver Stimulation, Costimulation von TNF-R1 / TNF-R2 und durch Prästimulation von TNF-R2 untersucht. Die einzelnen biochemischen Reaktionen, aus denen das Modell besteht, sind in Kapitel 5 detailiert aufgeführt.

Das Modell wurde mit in der Literatur veröffentlichten experimentellen Daten validiert und schliesslich zur Aufstellung neuer Hypothesen benutzt. Mit Hilfe dieses Modells konnte gezeigt werden, dass die TRAF2 Depletion durch das Binden von TRAF2 an TNF-R2 nicht ausreicht, um die experimentell beobachtete Depletion im Cytosol zu erklären. Während der Erstellung der Arbeit wurde experimentell gezeigt, dass c-IAP1 TRAF2 ubiquitiniert [94] und die aus dem Modell gewonnene Hypothese bestätigt. Weiterhin wurde die Rolle der antiapoptotischen Proteine XIAP, c-IAP und c-FLIP auf die Caspase-Aktvierung untersucht. Caspase-3 kann auf mehreren Wegen gespalten werden, entweder direkt durch Caspase-8 oder durch Caspase-9, die über den mitochondrialen Weg aktiviert wird. Innerhalb dieser Arbeit wird die Bedeutung des mitochondrialen Weges bei der Caspase-Aktivierung für die drei erwähnten Stimulationsprotokolle untersucht und die Rolle des positiven Feedbacks von Caspase-3 auf die Caspase-8-Aktivierung diskutiert.

In dieser Arbeit wird gezeigt, dass es möglich ist, mathematische Modelle für grosse Signalnetzwerke mit prädiktiven Charakter zu entwickeln. Wir konnten Hypothesen, die mit Hilfe des Modells gewonnen wurden, experimentell verifizieren und somit die Modelle innerhalb ihrer Grenzen validieren. Die in dieser Arbeit entwickelten Modelle ermöglichen somit ein ganzheitliches Verständnis dieser komplexen biologisch Signaltransduktionssysteme und die

Identifizierung regulatorischer Mechanismen innerhalb der Netzwerke. Dieses Wissen ist in Hinblick auf die Identifikation von neuen Drug-Targets äusserst wertvoll.

Während dieser Arbeit entstandene Publikationen:

- Schoeberl B., Fotin M., Mueller G., Wajant H., Gilles E.-D. and Scheurich P., A mathematical vision of TNF receptor interaction, Proceedings of the International Congress of Systems Biology 2001, Pasadena, CA, 158-167.
- Schoeberl B, Eichler-Jonsson C, Gilles ED, Muller G., Computational modeling of the dynamics of the MAP kinase cascade activated by surface and internalized EGF receptors. (2002), Nature Biotechnology, 20(4):370-5.
- Schoeberl B, Ginkel M., Gilles ED, Muller G., ”Mathematical Modeling of Signaling Cascades: Principles and Future Prospects” in Function and regulation of cellular systems: experiments and models, (Birkhäuser, Basel, 2003).

Während dieser Arbeit entstandene Konferenzbeiträge:

- B. Schoeberl and D. Lauffenburger, From Intracellular Signal Transduction to Cellular Oranization, Proceedings of In Silico Biology: Modeling Systems Biology for Research and Target Prioritzation, June 2-3 2002, San Diego, USA.
- B. Schoeberl, H. Wajant, G. Mueller, P. Scheurich and E. D. Gilles, A Mathematical Vision of TNF Receptor Interaction, Proceedings of the 2nd International Conference of Systems Biology, 4 - 7 November 2001, Pasadena, USA.
- B. Schoeberl, C. Eichler, K. Pfizenmaier, G. Mueller and E. D. Gilles, New Insights into Epidermal Growth Factor (EGF) Signal Transduction via Mathematical Modeling, Conference on Metabolic Engineering, October 2000, Colorado Springs, USA.
- B. Schoeberl, H. Wajant, P. Scheurich and E. D. Gilles, Quantification of Short Term Signaling by TNF-R1 and TNF-R2, Biotechnology 2000, 03-08 September, Berlin.
- B. Schoeberl, H. Wajant, P. Scheurich and E. D. Gilles, Mathematical Modeling of TNF Receptor Interaction, Proceeding of the 4th International Congress on Biochemical Engineering, 17 and 18 February 2000, Stuttgart, Germany. Stuttgart:Frauenhofer IRB Verlag.

Chapter 1

Introduction

As biology begins to move into the “postgenomic era” the question arises of how complex biomolecular networks of living cells or bacteria function as dynamic systems. In fact, the living cell functions as a complex chemical plant. Within the cytoplasm which is surrounded by a semipermeable membrane, the cell carries out thousands of chemical reactions and physical transformations which permit its own survival and reproduction. The cell must be able to respond to changes in the environment and to its own internal state, trapping raw materials and energy, avoiding toxins, repairing damaged parts and replicating. In order to meet all these demands of life the cell must be exquisitely regulated. All of these regulatory processes are carried out by the same molecular machinery that is itself being regulated: genes, proteins and metabolites [17], [152].

The proportion of identified components continues to increase and requires the development of mathematical and conceptual models, in order to understand these networks. Mathematical modeling has been a proven tool for a quantitative description of complicated systems and has been successfully applied in the field of Chemical Engineering. Mathematical modeling [136] can provide the necessary conceptual framework in order to:

1. integrate phenomena like crosstalk; positive or negative feedback within pathways or non-linear interactions into a coherent picture of the operation of metabolic or signal transduction networks;
2. identify design principles for the biochemical architecture of biological systems;
3. understand the responses of both wild-type and mutant organisms to stimuli;
4. verify the consistency and completeness of reaction sets hypothesized to describe specific

systems;

Comparing cells with chemical plants, an approach used according to the Modular Modeling Concept for biological systems proposed by Kremling [85] seems to be useful. In non-biological systems engineering is generally carried out in a hierarchical fashion. Thus a modular framework, that treats subsystems of complex molecular biological networks as functional units that perform identifiable tasks might be applied to biological systems. These functional units can then be represented by modeling objects [85], [140], which consist at the next lower level of elementary modeling objects. Likewise it is possible to model large systems in a transparent manner and to provide the complete information content of the system.

Prominent examples of these complicated biological networks are intracellular signaling cascades, metabolic pathways and cell-cell communication. Because signal flow is tightly regulated with positive and negative feedback control and is bidirectional with signals traveling from outside-in and inside-out, dynamic models that couple biophysical and biochemical elements are required to consider information processing both during transient and steady state conditions.

Metabolic engineering has now successfully applied mathematical modeling for more than 25 years [65]. Metabolic pathways in yeast or *E.coli* have already been well characterized and therefore, mechanistic modeling of the detailed metabolic reaction network has been possible. The increased knowledge gained during the last 20 years about signal transduction in mammalian cells has allowed similar modeling attempts to be undertaken.

In this work, we focus on intracellular signal transduction events triggered by cytokines. Cytokines are local messenger molecules, which transmit information between cells and have a major impact on growth regulation, cell division and apoptosis. Presently, more than 200 different cytokines have been identified such as interleukins, growth factors and chemokines. The key event in the initiation of intracellular signaling pathways, is the binding of the cytokine to the receptor and receptor oligomerization. The activated receptor triggers the binding of adapter molecules which then activate signaling cascades which lead to gene expression.

Each cytokine triggers multiple and diverse signaling pathways that stimulate diverse cellular responses, even though the signaling pathways often utilize the same molecular components. Analysis of the different pathways reveals the interaction of various signaling compounds at different levels within the signaling cascade. Thus, the response to a cytokine depends on

the degree of interaction with other signaling compounds. The primary function of the proteins that serve as signaling compounds is the transfer and processing of information rather than the chemical transformation of metabolic intermediates. These proteins allow information to be transferred from the cell membrane to the genome. In the signal transduction network they are linked into circuits that amplify and integrate information signals or serve as information storages [17]. In fact, signal transduction is analogous to chemical reactions of small molecules, allowing molecular interactions to be described using the languages of kinetics and thermodynamics.

Until now our understanding of these highly interconnected signal transduction systems as a whole has been very limited. As mentioned above, the attempt of mathematical modeling was considerably delayed because of the lack of biological knowledge about signal transduction networks. Due to the significant advances that have been made in the field of molecular cell biology in the past decade, it is now possible to quantify the concentration of signaling compounds, to isolate certain compounds, to create knock-outs or to study the translocation of signaling molecules with the help of fluorescence microscopy. The resultant pictures can be quantified with the help of digital image analysis and give an indication of the compartmentalization of certain compounds. Recently, the increasing availability of quantitative biological data enables the formulation of mathematical models of signal transduction networks similar to models of metabolic networks.

In the past, only parts of the signal transduction pathways have been modeled mathematically e.g. receptor-ligand interaction [91], [25], receptor internalization [139], the MAPK cascade [71], [36] or the caspase cascade [45]. From these models it is possible to derive a new functional understanding of certain mechanisms, like the ultrasensitivity of the MAP kinase cascade, which is known for its switch-like behavior. From the formulation and analysis of such mechanistic models of even larger systems, we hope to gain a better understanding of the system's behavior e.g. how the cell amplifies signals or how adaptation is regulated.

Amplification and adaptation are two of the most common responses of living cells towards external stimuli. Amplification enables a cell to transform the smallest changes in stimuli into substantial biochemical changes. Adaptation enables the cell to measure relative rather than absolute changes and to counterbalance the system. Examples of adaptation mechanisms are reduction of cell surface receptors due to internalization or negative feedback loops.

In fact, positive and negative feedback regulations are the most important features of signal transduction networks. Feedback means that the information on which the decision is based, is derived from the measurement of the output. Diverse types of feedback are possible including proportional (P), differential (D), and integral (I) as well as various combinations as PD, PID etc. As shown in Figure 1 in the total absence of adaptation, a new steady-state output is attained, partial adaptation reduces the “offset” of the new steady-state output value compared with the original prestimulus value, whereas perfect adaptation brings the system back to the original value. Besides adaptation, negative feedback might cause instability and bring about oscillations.

In this work, we focus on two pathways; a survival pathway, the EGF receptor induced MAP kinase cascade and an apoptotic pathway; the crosstalk between TNF-R1 and TNF-R2. For the mentioned pathways we have built mechanistic models which describe the detailed biochemical reaction network. Using these examples, we demonstrate how such models enable a model-driven biology and what can be learned from the models themselves.

EGF is an important mediator of cell survival and plays an important role during embryonal and postnatal development as well as in tumorgenesis. A substantial amount of quantitative data as well as kinetic rates have already been determined for the EGF receptor, making it a good model system to study. Simulating the dynamic behavior of the EGF induced MAP kinase cascade leads to an understanding of the signal transfer in a holistic manner. A possible application besides basic research is the incorporation of virtual inhibitors of the signaling cascade into the mathematical model. Likewise, the inhibitory effects on the cellular response can be simulated. In the future this may be a helpful tool in drug target development and drug design. Using the EGF induced signal transduction network we will show the predictive potential of these detailed biochemical reaction networks.

As it is becoming evident that autocrine loops play crucial roles in the regulation of EGF signaling and cell function, we include an autocrine loop into the EGF receptor model. Autocrine loops are established when soluble factors secreted by cells bind to and stimulate receptors on their own surfaces. They were first identified in tumor cells, where it was found that transformation of cells resulted in overexpression of certain ligands and unregulated proliferation of tumor cells [138]. In this context we examine the ability of cells to be stimulated for a second time after the ligand has been removed for a certain period of time and use the model to explain possible

mechanisms of desensitization.

Using the example of the EGF induced MAP kinase cascade we investigate the influence of different initial conditions on the system's behavior. This is important, as for most cell lines the protein concentrations are unknown. Of particular interest is whether the system retains its characteristic behavior though the set of initial conditions differs and consequently the set of kinetic parameters describing the system should differ as well. This would mean that the characteristic behavior is rather a structural property than a property related to the kinetic parameters and initial conditions. Furthermore the question of robustness vs. fragility of signal transduction networks will be discussed using the example of the parameter set used in the EGF model. The question of whether single parts of signal transduction networks can be treated as independent modules, will be addressed using the example of the MAP kinase cascade.

TNF induced apoptosis is the second biological system for which we have developed a mechanistic mathematical model. Defects in apoptotic cell death regulation contribute to many diseases, including disorders, where cell accumulation occurs (cancer, restenosis) or where cell loss ensues (stroke, AIDS, heart failure). In order to develop drugs it is very important to understand TNF induced cell signaling which is characterized by a very complex signal transduction network. The unique characteristics of the TNF-R1 signal transduction network is that it allows the possibility to trigger either gene induction or apoptosis (programmed cell death) to be stimulated.

From the modeling perspective, the TNF receptor interaction is a very interesting but also a very challenging question as it is a far less well characterized system than the EGF signaling network. We have developed a mathematical model for transfected HeLa cells in order to study TNF receptor crosstalk.

However, it could be shown that upon costimulation of TNF-R2 TNF-R1 induced cell death is drastically enhanced [166]. Utilizing the mathematical model we will discuss the competition of the two receptors for TRAF2 as a possible mechanism for the TNF-R2 mediated death enhancement. Furthermore we will analyze the influence of the distinct pathways of caspase activation.

The thesis is structured as follows: In Chapter 2, a general introduction to the model derivation is presented, in Chapter 3 we introduce the signal transduction networks triggered by EGF, describe the model derivation in detail and discuss the results obtained from the model. In

Chapter 4 we discuss issues like robustness and modularity using the example of the MAP kinase cascade. In Chapter 5 we present the mechanistic model of the TNF receptor interaction and discuss in particular pathways that induce cell death. The conclusions are presented in Chapter 6. The Appendix contains the detailed biochemical reaction networks, a short description of the experiments shown in the thesis as well as the original Western Blots. The Matlab files of the EGF and TNF models can be found under the following URLs:

http://www.mpi-magdeburg.mpg.de/model/EGF and

http://www.mpi-magdeburg.mpg.de/model/TNF.

This work was carried out in collaboration with the Institute of Cell Biology and Immunology at the University of Stuttgart. The experiments related to the EGF model were carried out by Claudia Eichler-Jonsson and can be found in more detail in [34] and the experiments related to the TNF model were carried out mostly by Gudrun Zimmermann and Mariola Fotin.

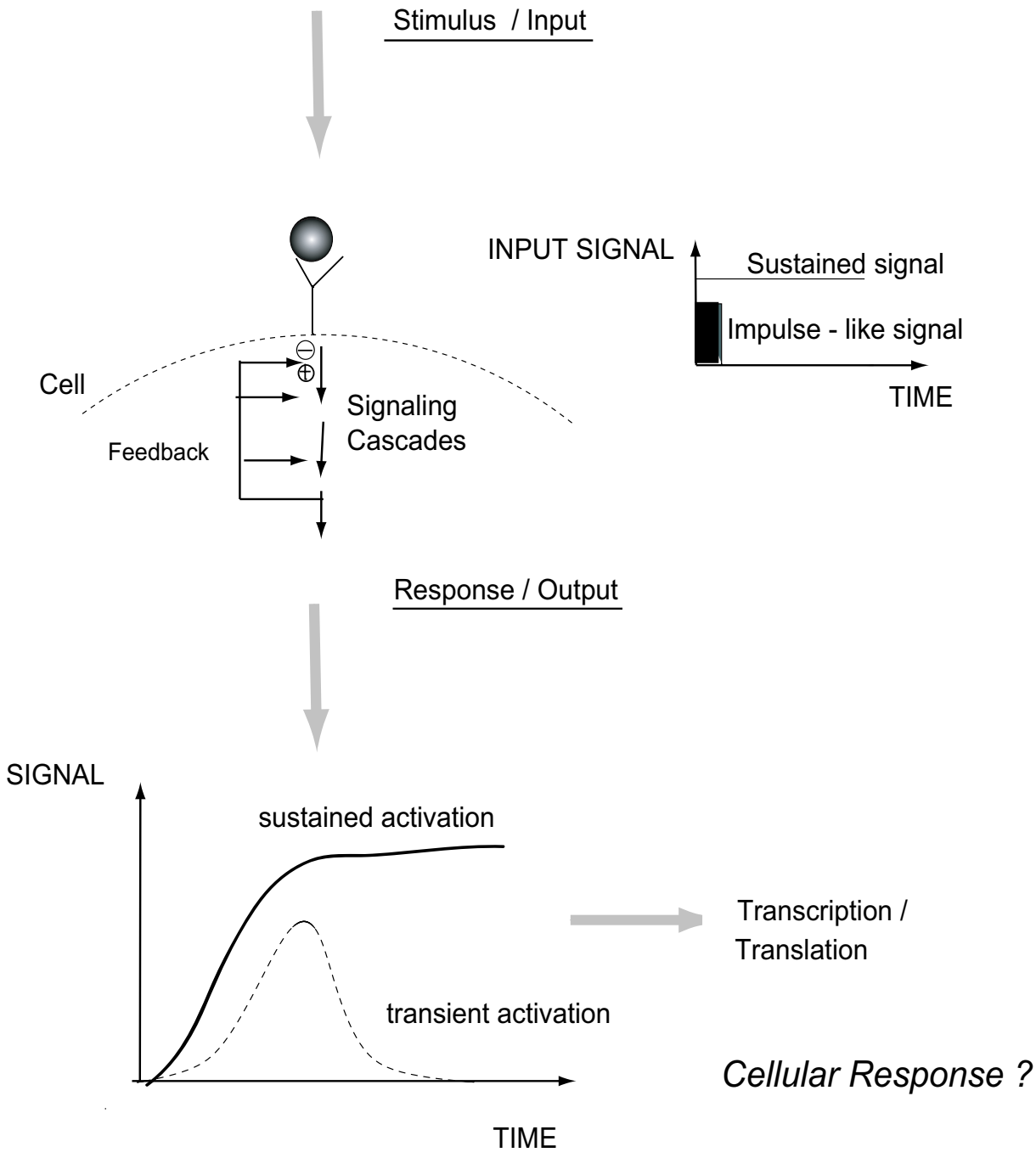

Fig. 1.1: Illustration of the dynamic responses of a system to a change in input.

8

Chapter 2

Mathematical Modeling and the Modular Modeling Concept

2.1 Model Derivation

The precision of mathematical language provides the opportunity for conceptualizing and understanding complex systems. Thus, mathematical models deliver a framework to integrate data and to gain insights into the static and dynamic behavior of complex biological systems such as networks of metabolic and signal transduction pathways or networks of interacting genes.

Figure 2.1 shows the general process that is undertaken in the model development of biological systems in order to study biological phenomena. First, biologists and modelers have to collaborate in order to determine which questions the model should help to answer. Based on this knowledge an appropriate analysis method must be selected. In the next step both groups should work on a model structure definition. In the case of mechanistic models, which are based on biochemical reactions, describing each step, this is the basis for the parameter determination. Once an operating model has been developed, it has to be made sure that the model passes several tests before it is applied to a real-world problem. One method is to challenge the model with “virtual” experiments, the results of which are described in the literature but have not been included during the model development process. Another method is a negative test, thus the model should not perform correctly with false input data. This methodology ascertains that the model performs well within its defined limits. Thus, it might take several iterative

rounds between model structure definition and model verification until an operational model is retrieved.

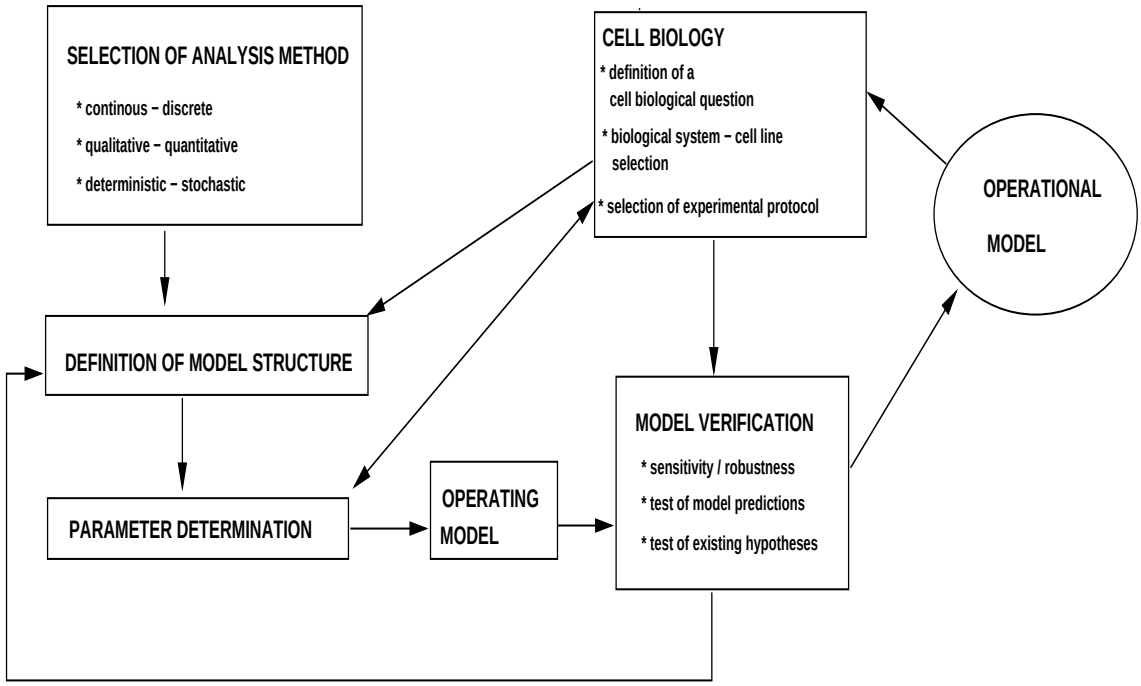

Fig. 2.1: Schematic representation of the major steps in the model development of biological systems.

In order to gain an understanding of the dynamics of EGF and TNF signaling pathways in their entity, we use mathematical modeling where all molecular interactions are described in terms of kinetic equations. The biochemical reaction network is represented with the help of a set of Ordinary Differential Equations (ODEs). The models presented in this work are compartment models which take the cell membrane, the endosomes and the cytoplasm into account. An idealized cell may be considered as a sphere with a diameter of 15 μm resulting in a cell volume of 1 x 10^{-12} l. The estimated radius of an average endosome is 100 nm, resulting in a volume of 4.2 x 10^{-18} l [62].

Usually, the kinetic equations of chemical reactions and the concentration are written in terms of molar concentrations. If the same compound participates in reactions taking place in different compartments with different volumes, the effective concentration of this compound is different in each compartment. As the number of receptor complexes formed at a certain concentration is usually calculated, the use of molecules per cell seemed more convenient for evaluating

the typical amplification steps in the cascade. Therefore, we converted the concentrations and the association rates occurring for the different compounds into molecules per cell using the proper volume for the particular compartment and Avogadro's Number. Due to the lack of further knowledge and the fact that proteins are present in considerable amounts (compare with the protein quantifications shown in Chapter 3 and Chapter 5) protein transport is not taken into consideration. Furthermore a deterministic approach based on ODEs has been chosen vs. a stochastic approach because of the high concentration of most signaling molecules.

2.2 Role of Protein Diffusion

The activation of signaling proteins by upstream activators or their activation of downstream effectors has been shown to involve binding interactions with adaptor complexes, cytoskeletal structures and subcellular membranes or with the targets and activators themselves. These localization processes can be highly regulated and rapidly reversible, leading to a dynamic view of signal transduction that diverges from the concept where receptor and signaling molecules stay largely in place and spatial signal transmission is made possible by the rapid diffusion of second messengers. Instead, signaling molecules translocate and undergo reversible reactions.

In order to build mathematical models of signal transduction pathways it is necessary to know the diffusion velocity of these molecules. If the diffusion process is rather slow, Partial Differential Equations (PDEs) need to be used. Alternatively, if the diffusion process is fast and if the signaling molecules are equally distributed, the signal transduction process can be described with Ordinary Differential Equations (ODEs) based on a formal kinetic approach.

The investigation of fluorescently conjugated proteins by different microscopy techniques has lead to new insights into the dynamic mechanisms of signaling processes. In nearly all cases studied a significant fraction of cytosolic, membrane bound or transmembrane proteins diffuse relatively freely within the cytosol and the membrane. Diffusion coefficients D of proteins are quite variable and differ from 0.05 μm^2/s for transmembrane receptors, up to 0.5 μm^2/s for membrane bound proteins and more than 10 μm^2/s for cytosolic proteins [107], [5].

The average distance that a protein diffuses from its origin along a given axis can be calculated as:

$$s = \sqrt{4 \cdot D \cdot t/\pi} \tag{2.1}$$

where D is the diffusion coefficient and t the time of diffusion. As an example, a cytosolic protein with a diffusion coefficient of D=10 μm^2/s diffuses on average 3.5 μm/s [147]. Figure 2.2 shows the differences between the average diffusion distance of receptors, membrane bound proteins and cyotosolic proteins. It can be seen that cytosolic proteins diffuse rapidly whereas membrane bound proteins can be regionally localized for longer time periods of seconds or even minutes. Therefore, initially, the usage of ODEs seems to be sufficient to describe the dynamics of intracellular reactions. This has the advantage that the systems can be analyzed more easily with the help of nonlinear systems theory.

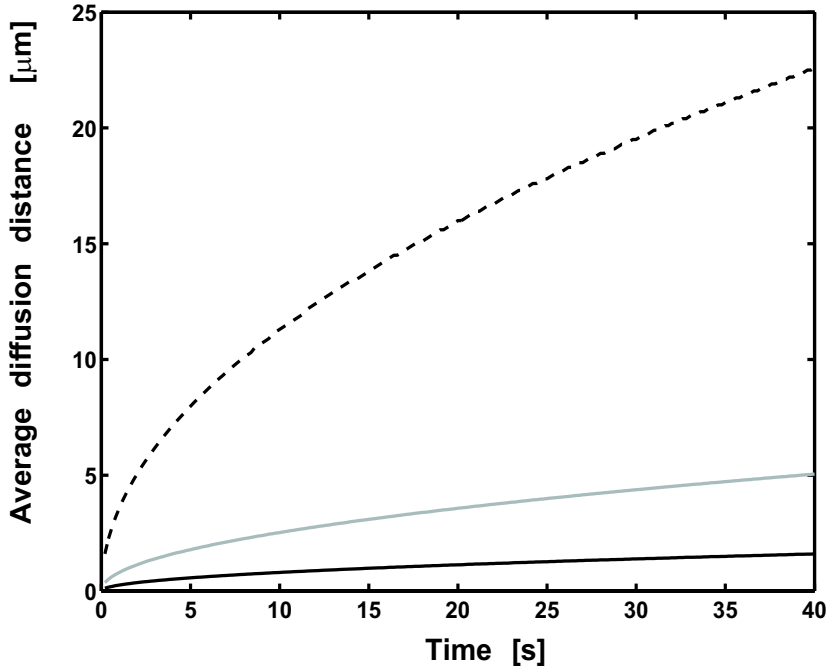

Fig. 2.2: Average diffusion distance of cytosolic - -, membrane bound proteins – or receptors –.

Chemical reactions of second order are usually treated as a one step process: However, chemical reactions are in reality two step processes, requiring first the molecular transport of the reaction partners A and B to interact and form an encounter complex before the reaction occurs and the complex AB is formed. The same approach is valid for the dissociation reaction. The diffusion dependent movement towards the encounter complex can be described by k_{df} and the following reaction step by k_{rf}. [35]. Thus the association rate constants measured in

kinetic experiments are theoretically a combination of the diffusion and the reaction step which represent an overall forward rate k_{on}. In the mathematical models presented in the following only the overall forward rate constant is used. Assuming the encounter complex to be in steady state, the overall forward rate constant k_{on} and in analogy the overall backward rate constant k_{off}, can be determined.

$$k_{on} = \frac{k_{rf} \cdot k_{df}}{k_{df} + k_{rf}}. \tag{2.2}$$

$$k_{off} = \frac{k_{rb} \cdot k_{db}}{k_{rb} + k_{db}}. \tag{2.3}$$

Hence, the kinetics measured in biochemical assays as well as the estimated parameters include intrinsically the diffusion steps in the rate constants, while the parameters obtained by estimation in our model include intrinsically the equations above. The components of the mathematical model are state variables, indicating the state of a system at a certain time (e.g. the number of molecules of a certain compound) and kinetic parameters. The kinetic parameters are the basis for the kinetic equations, which are retrieved from the literature and comprise Michaelis-Menten constants, turnover numbers and rate constants of association and dissociation.

The kinetic schemes of all the mathematical models described in this work are presented along with the mathematical models of the EGF induced MAP kinase cascade and the model of the TNF receptor interaction. The reactions are indicated with $v_{1..n}$ with n being the total number of reactions considered in the model. All the compounds are specified with numbers. All the mathematical models presented in the following chapters, consider receptor internalization and degradation. We assume that the receptors in the endosomes continue to signal. In comparison to the number of state variables the number of control variables is relatively small for the different models. The reason is the use of the same parameter set for the signal transduction triggered by internalized receptors and receptors retained at the cell surface. In addition, for identical reactions in different pathways also the same parameters are assumed. For example the association and dissociation rates are the same for protein A binding to B and forming an AB protein-complex or A binding to B which is part of the BC complex and forming an ABC complex.

To derive the mathematical equations, the entire biochemical reaction system with m molecular species C_i is decomposed into v elementary reactions j=1. . . n of the form

$$\alpha_{1,j} \cdot C_1 + \cdots + \alpha_{m,j} C_m \overset{k_j}{\rightarrow} \beta_{1,j} \cdot C_1 + \cdots + \beta_{m,j} \cdot C_m \tag{2.4}$$

Where k_j is the kinetic constant of the reaction, $\alpha_{i,j}$ and $\beta_{i,j}$ are the stoichiometric coefficients for substance C_i's involvement as educt or as product, respectively. Applying mass action kinetics, the mathematical equations (ODEs) are retrieved accordingly based on the biochemical reaction schemes. As proposed in [130], the differential equations of concentration c of the different compounds C_i (i = 1 . . . m) can be written as shown by the following equation:

$$\frac{dc_i}{dt} = \sum_{j=1}^{n} k_j \cdot (\beta_{i,j} - \alpha_{i,j}) \cdot \prod_{l \in S_j} c_l^{\alpha_{l,j}}. \tag{2.5}$$

Here, S_j represents the set of species actually participating in reaction j as educt, i.e. $\alpha_{l,j} \geq \forall$ $l \in S_j$.

Elementary chemical reactions instead of formal kinetics like Michaelis Menten rate laws are used for two major reasons: (i) Formal kinetics like Michaelis Menten rate laws imply assumptions on relative velocities for the elementary reactions, which beforehand, for a system with largely unknown parameter values, may not be applicable. (ii) Automatic model generation is relatively easy on the basis of elementary reactions as well as model analysis.

2.3 Parameter Estimation and Sensitivity Analysis

In order to estimate the kinetic parameters of the different reaction networks represented in the appendix, not yet accessible by published kinetic data, the model was fitted to time dependent quantitative observations described in the literature. In order to estimate the unknown parameters a sensitivity analysis was performed in DIVA. DIVA is a simulation tool which was developed at the Institute of System Dynamics and Control at the University of Stuttgart [57]. It has the advantage of powerful numerics and can solve an unlimited number of ODEs.

The mathematical model is a system S(c,u,p,t) of ODEs which depends on the state variables c (corresponding to the concentration vector c, which was introduced earlier), the input functions u (like number of receptors, ligand concentration etc.), the model parameters p and time t. Thus S can be written as:

$$\mathbf{S}(\mathrm{c}, \mathrm{u}, \mathrm{p}, \mathrm{t}) : \dot{\mathrm{c}} - \mathrm{f}(\mathrm{c}, \mathrm{u}, \mathrm{p}, \mathrm{t}) = 0. \tag{2.6}$$

and $t \geq t_o$, the functional f and the initial conditions $c(t_o)=c_o$.

Parameter estimation is based on the comparison of model behavior and the behavior of the real system. In order to estimate the parameters, an identification functional $\Phi(p)$ has to be minimized. In order to formulate the identification functional, the error e_i between model $c(t_i,u,p)$ and experiment $c^M(t_i, u)$ for each of the N measurements at a discrete time point is needed. The differences are furthermore weighted by the inverse of the standard deviation of the measurement Q_i. Therefore the identification functional can be written as

$$\Phi p = \sum_{i=1}^{N} [e_i^T \cdot Q_i \cdot e_i]. \rightarrow min. \tag{2.7}$$

with $e_i = e_i(t_i, u,p)=c(t_i, u, p) - c^M(t_i,u)$.

In order to minimize the identification functional to obtain an optimal set of parameters p*, an evolutional strategy, a genetic algorithm, based on the theory of Rechenberg [115] was applied. The evolutional strategy was implemented in Matlab at the Max-Planck-Institute for Dynamics of Complex Technical Systems. Genetic algorithms have been proven to be robust, flexible and efficient in complex spaces. Genetic algorithms use the idea of randomness when performing a search. However, genetic algorithms are not simply random search algorithms which can be inherently inefficient due to the directionless nature of their search. In contrast the evolutional strategy uses knowledge from previous generations of strings in order to construct a new generation that will approach a locally optimal solution.

The least squares criterion can be used to compare the quality of the curve fit for two or more parameter sets used to describe the same data. The function that gives the smallest identification functional $\Phi(p)$ gives the best fit. There is another measure of the quality of the curve fit, the coefficient of determination, also known as the r-squared value. It is defined as

$$r^2 = 1 - \frac{I}{U}. \tag{2.8}$$

I is the identification functional with the standard deviation of the measurement Q_i=1 and U is the sum of the squares of the deviation of the c_i values from their mean $\bar{c}$.

$$U = \sum_{i=1}^{N} [c_i - \bar{c}]^2. \tag{2.9}$$

For a perfect fit, I=0 and thus r^2=1. Thus the closer r^2 to 1 the better the fit. The value of U indicates of how much the data is spread around the mean, and the value of I indicates how much of the data spread is left unaccounted for by the model. A very good fit corresponds to values of $r^2 \geq 0.99$. In the following the r squared value is used as a measure of the quality of the curve fit.

Biochemical reactions networks show a certain robustness concerning parameter variations. Only a few parameters show a significant sensitivity towards parameter variations. With respect to the parameter estimation, only the estimation of those parameters sensitive to the measured time course of a certain compound is useful. Therefore, a parameter sensitivity analysis has to be carried out. The state sensitivities s_i, which are the partial derivatives of the concentration c with respect to the parameter p_i [159].

$$s_i = \frac{\partial c}{\partial p_i} \tag{2.10}$$

It has to be emphasized that the sensitivities are independent, so each can be computed in turn, once the state trajectory has been obtained. The sensitivities s_i are linear though they are time dependent as they depend on c and they are local with respect to parameter space.

In the recent years, the existence of robustness in biochemical reaction networks has been reported for a variety of biochemical networks [157, 2]. Of course nothing can be robust to absolutely all variations. However, some variations may not matter in terms of the functionality of the system in question. In this work, we are interested in the robustness to variations in kinetic parameters. Thus robustness, defined here, with respect to signal transduction networks, is a measure of the change in the dynamics of the output signal. The robustness characteristics were determined by analyzing in which range the kinetic parameters as well as the initial conditions can be varied without changing the output signal within certain limits (standard deviation $\leq$ 1 %). It was revealed that only certain parameters show a great sensitivity with respect to a certain output signal.

The robustness analysis presented here, is essentially a sensitivity analysis. In general, a sensitivity analysis is one measure of how much error is introduced by parametric errors.

2.4 Modularity - Modeling Entities - Modular Modeling Concept

The complexity of biological systems introduces several conceptual and practical difficulties. Among the most important is the difficulty of isolating smaller subsystems that could be analyzed separately. This has its origin in the engineering sciences, where this way of modular thinking has been successfully applied [90]. Therefore, a promising way to achieve a system level understanding of cells and organisms is to extend these theoretical concepts, which are already successfully applied for the analysis and synthesis of complex technical systems.

Focusing on the internal structure of cellular systems one central, increasingly accepted notion is that these systems are composed of 'functional units' or 'modules'. These functional units appear on each level of complexity and more complex units result from the aggregation of smaller less complex units. In contrast to 'man-made' systems, where the modules are defined by the designer of the system, biological systems evolved during evolution and are characterized by an enormous complexity. The challenge is now to decipher the modules that were created by nature and to find formal criteria that define modules or functional units.

Regarding the mathematical modeling of cellular systems, this modular structure raises the possibility of developing mathematical models for each of the functional units independently. These submodels, which correspond to functional units in the biological system, can then be connected to larger models, describing the particular biological system of interest. Possible criteria to structure complex biological systems are:(i) common physical goal, (ii) belong to a single genetic unit or (iii) a common signal transduction system [93].

On the top level, a cell can be divided into a regulatory and a metabolic network [85],[86]. These networks feature different characteristics. The metabolic network is mainly occupied with substance transformation, e.g. to provide cellular metabolites and cellular structures. The main function of the regulatory network is information processing, e.g. to adjust the expression level of receptors or proteins in order to provide an appropriate response of the biological system to internal or external changes. Mass flow plays only a minor role in the regulatory network. In this sense the regulatory network is superimposed to the metabolic network and fulfills the functions

of a controller in a technical process. The interaction between both networks is necessarily bound to substance exchange due to the requirements for precursors and proteins. However, the main interaction consists of directed signal flow like sensor signals and control action like protein expression.

With the help of elementary modeling objects it is possible to describe the particular biochemical reactions such as enzymatic processes or polymerization processes. In general, there are three classes of elementary modeling objects as depicted in Figure 2.3. In the class of substance storage, the distinction between storages with and without genetic information is made. The class of substance transformers consists of an elementary modeling object describing enzymatic processes, polymerization or degradation. Furthermore, there is the class of signal transformers, which is divided into a modeling object describing the control of polymerization processes and a modeling object describing Protein/DNA/RNA interactions. As this work models signal transduction processes, which consist for the main part of complex building or phosphorylation reactions, the substance storage module and the signal transformer are of great importance. The substance storage modules include all the states of the compounds as well as the initial conditions. The actual equations are placed in the signal transformer. This concept is realized in the graphical interface of the modeling tool PROMOT [49].

In order to gain a transparent model, which includes all the detailed information the elementary reactions can be grouped into so called functional units. These functional units can be analyzed separately with methods of dynamic system control theory. The following the Modular Modeling Concept is applied to the EGF and TNF signal transduction network.

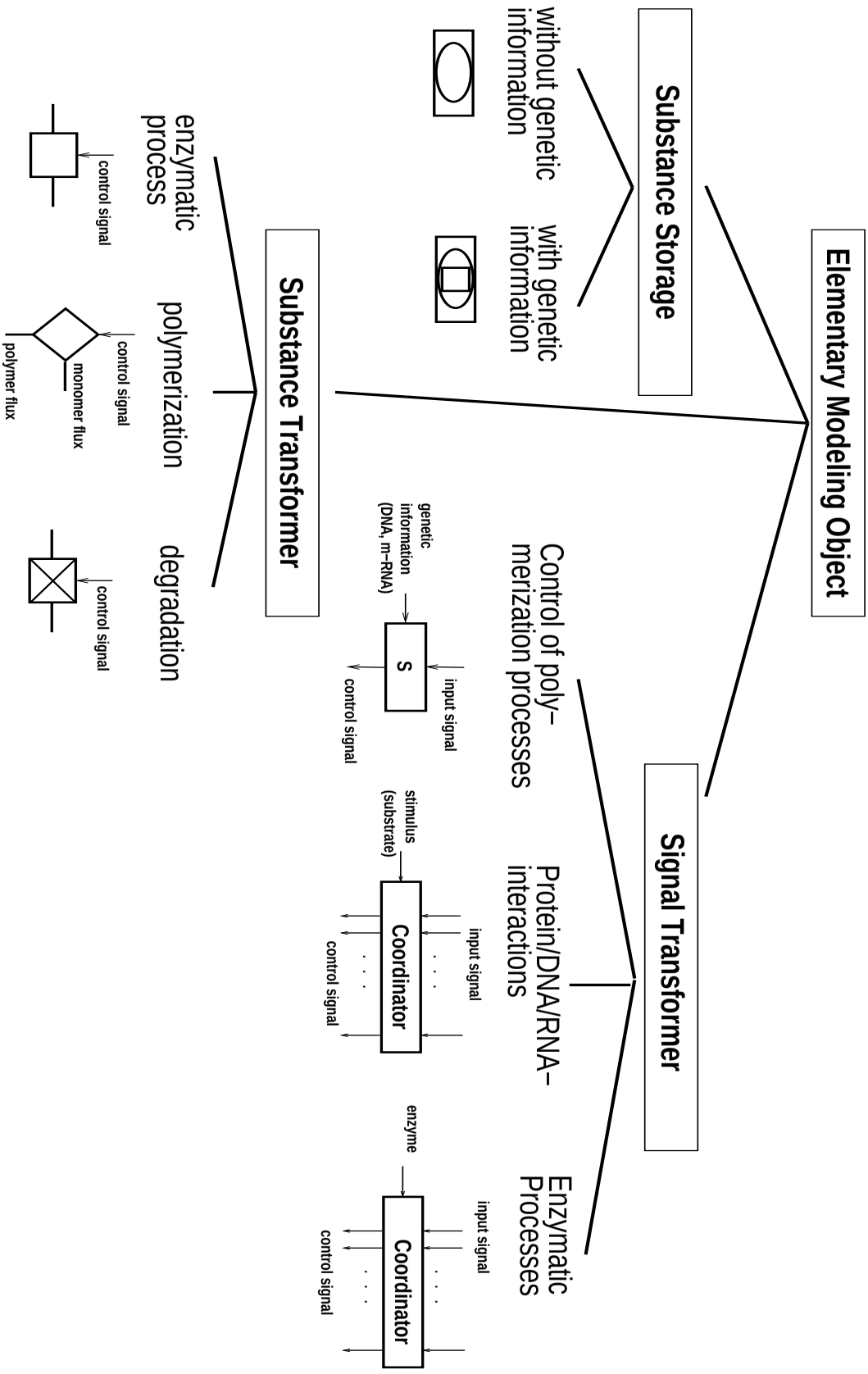

Fig. 2.3: Elementary modeling objects for cellular systems adapted from [140].

Chapter 3

A Mathematical Model of the EGF induced MAP Kinase Cascade

3.1 The EGF induced MAP Kinase Cascade

The EGF (epidermal growth factor) receptor belongs to the family of tyrosine kinase receptors and is expressed in virtually all organs of mammals. EGF receptors play a complex role during embryonic and postnatal development and the progression of tumors [133], [132]. For example, an increased expression of EGF receptor is found in human carcinomas [83] and glioblastomas [171]. The EGF receptor binds a number of related peptide growth factors, including epidermal growth factor (EGF), transforming growth factor (TGF-β) and heregulins [54], [56], [102]. Binding of ligand to the EGF receptor induces receptor dimerization (EGFR2) and cross-phosphorylation (EGFR2*) of specific carboxy terminal tyrosyl residues. As a consequence a multitude of signaling proteins are recruited to the activated receptors via phosphotyrosine specific recognition motifs, the SH2 domains, including Shc, Grb2, PI3-kinase, phospholipase$C\gamma$ (PLCγ), RasGTPase activating protein (GAP) and Shp-1 [127], [74], [11], [18], [80], [161]. This association of signaling molecules to the receptor results in either phosphorylation, transmission of conformational change or proximal translocation to membrane associated target molecules such as Ras/GDP. Each adaptor molecule funnels to different effector proteins inducing separate downstream signaling cascades with distinct physiological responses. Two principal pathways leading to the activation of Ras by the guanyl nucleotide exchange protein Sos (son of sevenless) are initiated. EGFR2* binds Grb2-Sos directly [18] as well as indirectly

through Shc [11] as shown in Figure 3.1 and in the biochemical reaction network in the Appendix Figure 3.2. Tyrosine phosphorylation of Shc leads to the assembly of a Shc-Grb2-SOS complex which is generally thought to be the major pathway for Ras activation. The GTP-bound form of Ras stimulates the activation of the MAP kinase cascade via the serine/threonine kinase Raf [103], and the dual-specificity tyrosine/threonine kinases MEK and ERK-1/2. Active ERKs phosphorylate and regulate several cellular proteins, comprising protein kinases, cytoskeletal components, phospholipase A2 and nuclear transcription factors such as Elk-1 which mediates transcriptional activation of many genes, including c-fos [98], [169].

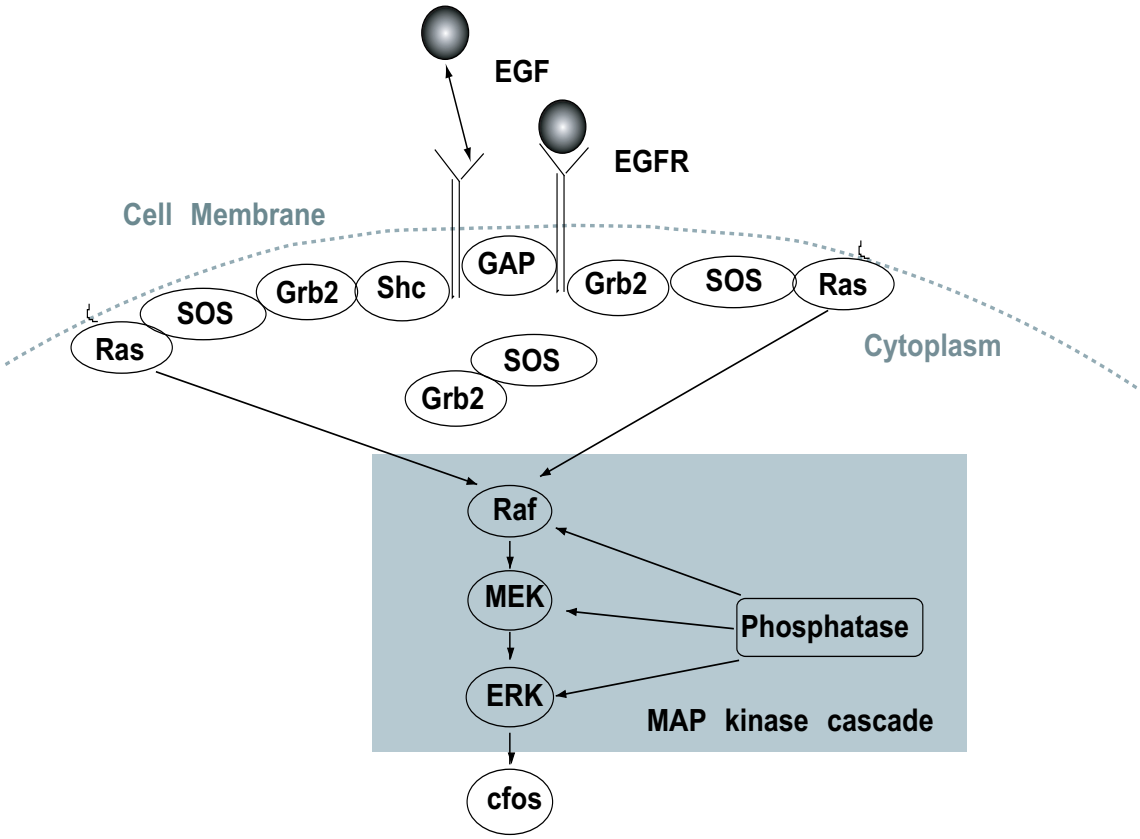

Fig. 3.1: Biological scheme of the EGF induced MAP Kinase cascade.

The inactivation of EGF receptor signaling is a complicated process and not fully understood. At least three different mechanisms seem to be involved in signal attenuation at the receptor level: Internalization, ubiquitination and interaction with caveolin. Ligand binding to the EGF receptor induces a structural change of the receptor that exposes coated pit targeting domains in the cytoplasmic domain that initiate internalization [19]. In addition this requires downstream receptor

signaling [89]. Following endocytosis, receptor-ligand complexes are delivered to early endosomes, where molecules are sorted for recycling back to the cell surface or degradation in lysosomes [20]. The net depletion of ligand and receptor from the cell surface has been recognized as an attenuation mechanism for EGF receptor long term signaling. Some evidence suggests that EGF receptor complexes continue to signal in the endosomal compartment, however, the relative signal contribution of external and internalized receptors is still unclear. The existence of functional EGFR2*-Shc-Grb2-Sos complexes in endosomes has been demonstrated [55], while the activity of PLCγ is downregulated in this compartment [63].

The EGF receptor is destined for lysosomal degradation through a mechanism that includes recruitment of c-Cbl and receptor poly-ubiquitination [163] and proteolytic cleavage by Cathepsin B [7]. Truncated EGF receptors that were internalization defective but retained their kinase activity, led to enhanced mitogenesis and cellular transformation, implying a relationship between internalization and signal attenuation [168]. Apart from its role in growth and differentiation, the EGF receptor participates in complex transactivation procedures of TGF - and of G-protein coupled receptors [56] and is involved in crosstalk mechanisms with receptors mediating opposite physiological effects, such as apoptosis signaling induced by TNF receptor or Fas receptor [104], [48].

The EGF receptor is one of the most extensively researched tyrosine kinase receptors and a lot of biochemical, structural and kinetic data of its intracellular signaling molecules has been published in the literature. While the principle hierarchy of downstream signaling components and its activation sequence is well known, the complicated kinetic network of these cascades is less well understood. Especially the critical signaling events which direct EGF receptor induced signals into such divergent patterns of cellular responses such as cell growth, survival and differentiation, are poorly understood. Recent data suggests that the physiological outcome of tyrosine kinase receptors signaling critically depends on the timing, duration, and amplitude of activation of the involved signaling components [98], [32], [121].

3.1.1 Derivation of a Mechanistic Model of the EGF Receptor Signal Cascade

The complete kinetic scheme of the biochemical network of the EGF receptor signaling cascade utilized for the computational simulation is shown in Figure 3.2. In principle, the model may be divided into several parts: 1. EGF binding, receptor dimerization and crossphosphory-

lation, 2. signaling complex formation at the cytoplasmic tail of the receptor (association of GAP, recruitment of Shc*-Grb2-Sos and Grb2-Sos), 3. and 4. Ras activation by two separate pathways leading each to the stimulation of the MAP kinase cascade. 5. receptor internalization, recycling, degradation and de novo synthesis. In Figure 3.1 the biological scheme of a signal transduction pathway of the EGF induced MAP kinase cascade is represented. Figure 3.3 shows how this pathway can be represented according to the Modular Modeling Concept. Due to the modularity implied in the pathway structure the main characteristics are receptor activation, the two independent pathways of receptor complex formation and the MAP kinase cascade and these can be represented in a very transparent fashion. The components (proteins and protein-complexes) are represented in storage modules, whereas the ODEs can be found in the coordinator modules. As can be observed in Figure 3.3 it is possible to zoom into the different coordinators down to the level of the elementary reactions. Thus, this concept provides transparency without the loss of detailed information about the elementary biochemical reaction steps which were taken into account in the model.

In step 1, EGF molecules bind to the receptor in a 2:2 ratio leading to receptor dimerization and immediate autophosphorylation of the receptors which is followed by the association of signaling molecules. GAP binds to the dimerized phosphorylated receptor EGFR2* [161]. Ras-GTP activation can be initiated by two pathways. Either Grb2 associates directly to the EGFR2*-GAP complex or Shc associates to EGFR2*-GAP to be phosphorylated by the receptor kinase and Grb2 binds to the EGFR2*-GAP-Shc* complex. Sos finally binds to these signaling complexes and allows the Ras-GDP, Ras-GTP exchange [23]. Ras-GTP forms a complex with Raf initiating activation to Raf*, which is a complicated multistep process [103], simplified to only one phosphorylation step in the model presented here. It is assumed that one Ras-GTP molecule activates only one Raf molecule which is then recycled to Ras-GDP by activated GAP after dissociation from Raf [129], [144]. The association of the different adaptor molecules is assumed to be competitive. A further assumption is that binding of signaling molecules protects the corresponding phosphotyrosine residues against phosphatases and the decay in EGFR phosphorylation is primarily due to proteolytic degradation after internalization. The activated Raf* (MAPKKK*) is the first step of the MAPK cascade. This part of the model is based on an already existing steady state MAPK cascade model [71]. The model by Huang and Ferrel predicts ultrasensitivity of the MAP kinase cascade, which implies a tendency of the cascade to

switch-like responses [71]. Increasing the number of steps as well as the number of phosphorylation sites leads to the switch-like behavior as shown in Chapter 4. Raf* phosphorylates MEK at the first or the second phosphorylation site of MEK. MEK-PP (MAPKK) catalyzes the dual phosphorylation of ERK. These phosphorylation reactions are implemented as dual collision mechanisms in the model and imply that the phosphorylating complexes of Raf* and MEK as well as of MEK-PP and ERK have first to dissociate before the second phosphorylation occurs, requiring a new phosphorylating complex formation. The same mechanism also applies for the dephosphorylation steps by phosphatases [71]. For the association of EGF and signaling proteins with the receptor as well as for enzyme substrate binding, we use second order kinetics. In addition, for enzyme activities such as EGF receptor autophosphorylation, formation of Ras-GTP, MEK-P, MEK-PP, ERK-P, ERK-PP and phosphatase reactions we apply first and second order kinetics, according to enzymatic reactions.

In the biochemical reaction scheme, shown in Figure 3.2, all the mechanistic steps described above can be found. Each reaction rate is indicated by v1...n, with n being the total number of reaction rates occuring in the network. The kinetic rate constants are indicated as follows: the overall association rate is indicated by $k_{+1...n}$ and the overall dissociation rate by $k_{-1...n}$. The numbers associated with k correspond to the number of the according biochemical reaction. The gray arrows indicate the biochemical reactions, which were introduced to simulate the system's behavior in response to an EGFR, a Grb2 and a MEK inhibitor respectively.

3.1.2 Modeling of EGF Receptor Internalization

Assuming that receptors at the cell surface and internalized receptors in endosomal compartments induce identical signaling cascades, the same kinetic constants are used for the reactions triggered by either an extracellular receptor or an internalized receptor. The topological separation of the two signaling pathways enables the investigation of the relative contribution by the internalized receptors and by the receptors remaining on the cell surface repectively, to the total signal which is triggered by all receptors. The first steps of the internalization of the EGF receptor in the model presented here, have been adapted from a model developed by C. Starbuck [139]. The dimerized receptors are supposed to be internalized by two pathways, a major coated pit path and a minor second path [96]. The coated pit path starts with the association of the coated pit proteins to the receptors (EGFR-Prot) and is considered a second order

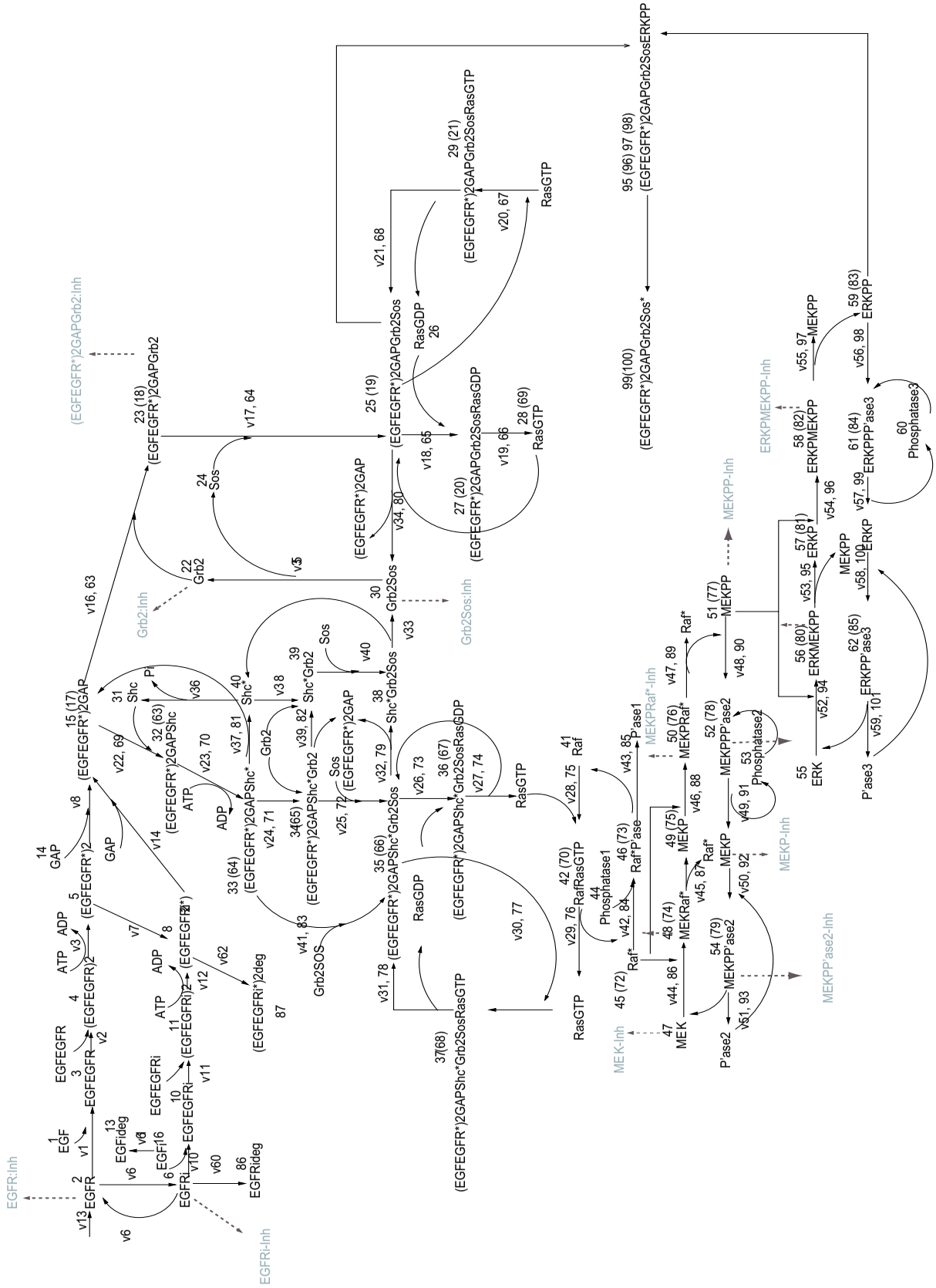

Fig. 3.2: Detailed biochemical reaction scheme of the EGF induced MAP Kinase cascade. The gray arrows indicate the inhibitor reactions.

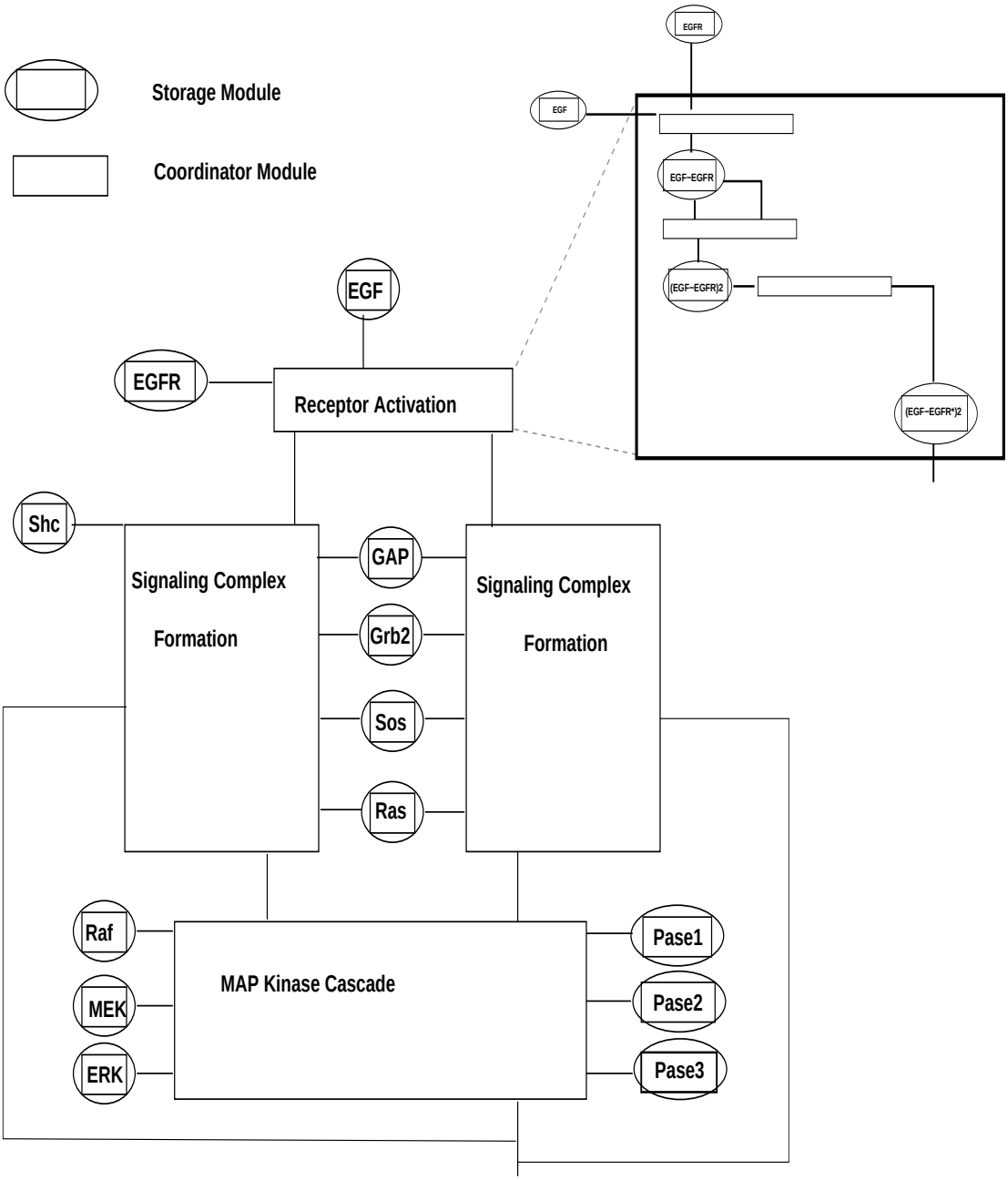

Fig. 3.3: Representation of the EGF induced MAP Kinase Cascade according to the Modular Modeling Concept.

process comprising the assembly of dimerized receptors into the coated pit k_{+4} and k_{-4} and the internalization rate k_5. The minor second internalization pathway is a first-order process with the internalization rates k_6 and k_7. The receptors internalized by the two pathways merge in the endosome [58]. The endosomal receptors are either recycled with the recycling rates k_{-6} and k_{-7} or degraded with degradation rates k_{60} and k_{62} for receptors and k_{61} for the ligand EGF [170], [139]. In order to represent the complete endocytic trafficking cycle in the mathematical model, the receptor synthesis has to be taken into account. The first order rate constant k_{13} describes the receptor synthesis in the model and acts like a source for new receptors.

3.1.3 Model Parameters

As different cell lines are characterized by a quite distinct behavior, we chose HeLa cells as a biological system to develop the mechanistic model. HeLa cells are well characterized and relatively easy to handle. The quantification of EGF receptors resulted in about 50 000 receptors being expressed on HeLa cells [13], [170]. EGF binding studies on HeLa cells reveals the presence of three receptor types [13], [122]. The K_D of the low affinity receptors was reported to range from 0.4 - 37nM, the K_D of the high affinity receptor ranges from 0.01nM to 0.6nM [22]. Therefore an average value for the K_D of 0.1nM is used in the model. The initial values for the concentrations of the different compounds are represented in Table 3.1.

3.1.4 Simulation of Signal Cascades as a function of EGF Concentration

We developed a mathematical model describing the dynamics of the EGF signal transduction pathway starting with the complex formation of EGF receptor and ending in ERK activation. The mathematical model calculates the change in concentration over time for the 85 compounds after EGF stimulation. The complete set of equations can be found in the code provided on the web site given in the introduction. In the figures presented here, only selected simulation results are shown that provide insights about the dynamic behavior of the most important contributors of the signal cascade. The modeling results have been obtained by using the initial conditions and the kinetic parameters shown in Table 3.1 and Table 3.4. In Table 3.2 and Table 3.4 reversible biochemical reactions are presented by leftright arrows and irreversible reactions by right arrows. The unknown kinetic parameters were fitted to a trainingset of experimental data

Internalization: A Coated pit path: Shc pathway

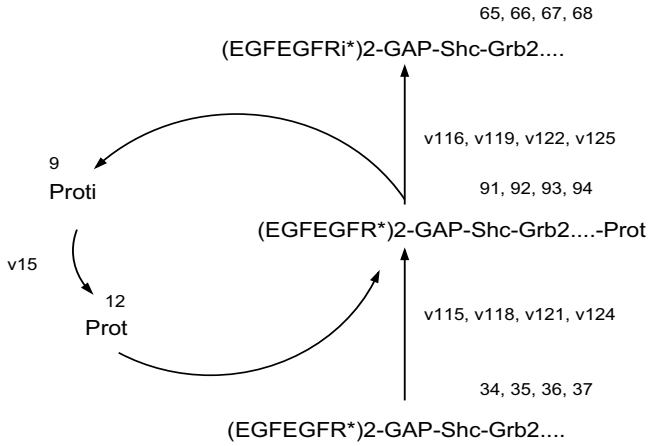

B Coated pit path: Shc deficient pathway

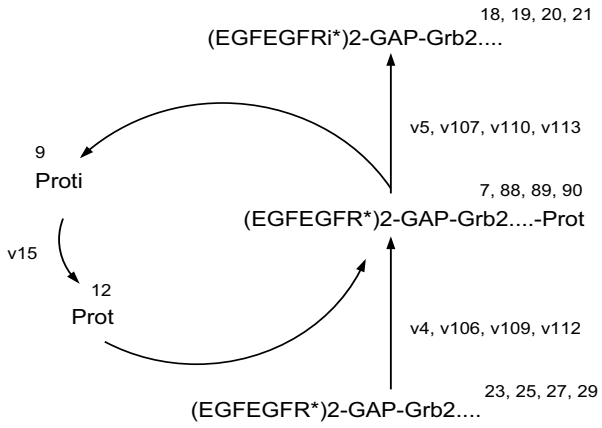

C Constitutive internalization

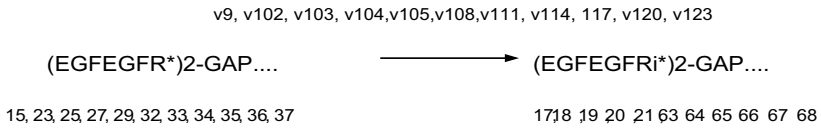

Fig. 3.4: Biochemical reaction schemes describing the receptor internalization of the EGF receptor as implemented in the mathematical model.

Tab. 3.1: Signaling protein levels.

Protein	Concentration [nM]	Number of Molecules/Cell	References
Receptors		50000	[13]
GAP	20	12000	Estimation
Shc	168	101000	experimental data
Grb2	85	51000	[81]
Sos	111	66300	experimental data
Ras-GDP	19000	11400000	experimental data
Raf Kinase	67	40000	Estimation
MEK	41667	25000000	experimental data
ERK	35000	21000000	experimental data
Phosphatase1	67	40000	Estimation
Phosphatase2	67	40000	Estimation
Phosphatase3	16667	10000000	Estimation
Coated Pit Protein	135	81000	[139]

retained from own experiments and literature data. The results are shown in Figure 3.5. The time course of EGF receptor autophosphorylation, of total phosphorylated Shc molecules, of Ras-GTP activation as well as of the phosphorylation of Raf, MEK and ERK is resolved as a function of different EGF concentrations. The solid lines represent the simulation results and the symbols the experimental data.

Autophosphorylation of the EGF receptor (EGFR*) is known to peak after 15s for concentrations between 10 and 120ng/ml EGF [124] which is in accordance with the simulation results shown. At 50ng/ml EGF, the model predicts complete phosphorylation of EGF receptors of the cell (50,000) within 15s. The decline in the total number of phosphorylated EGFR* calculated for each concentration shown in Figure 3.5A is in accordance with literature data as well [55], [164]. After reaching the maximum (in this model due to internalization) at 0.08nM (0.5ng/ml) EGF, only 50% receptors are phosphorylated, and even less at lower EGF concentrations. The initial velocities of EGF receptor autophosphorylation differ dramatically and show a concentration dependent pattern over the concentration ranges modeled, e.g. 45 000 or only 7000 receptor molecules/cell are phosphorylated per second and in the presence of 8nM (50ng/ml) or 0.08nM (0.5ng/ml) EGF, respectively. This array of initial velocities of EGF receptor autophosphorylation is very similar to the initial kinetics of EGF binding to the receptor with a parallel concentration dependent increase (data not shown).

The comparison of the kinetics of Shc phosphorylation triggered by the receptor kinase with the phosphorylation dynamics of the EGF receptor autophosphorylation reveals different phosphorylation patterns. The initial slope of Shc* phosphorylation decreases only slightly with descending EGF concentration, whereas the initial slope of EGF receptor autophosphorylation shows a strong EGF concentration dependence as depicted in Figure 3.5 B. Despite two orders of magnitude difference in stimulus (50ng/ml and 0.5ng/ml EGF) almost the same phosphorylation amplitude is reached. Due to the fast phosphorylation kinetics of Shc almost all cytoplasmic Shc molecules are phosphorylated within 2min [61] from 50ng/ml down to 0.08nM (0.5ng/ml) EGF) and persist over a long period, seen by the saturation curve. Receptor association of phosphorylated Shc, Grb2 and Sos occurs with similar kinetics, as can be seen in Table 3.1.

The activation of Ras-GTP shows a clear concentration dependent signal, with decreasing amplitudes and maxima that are shifted to later times for lower EGF concentrations (Figure 3.5C). The maximum number of Ras-GTP is predicted at about 1min after EGF stimulation, followed

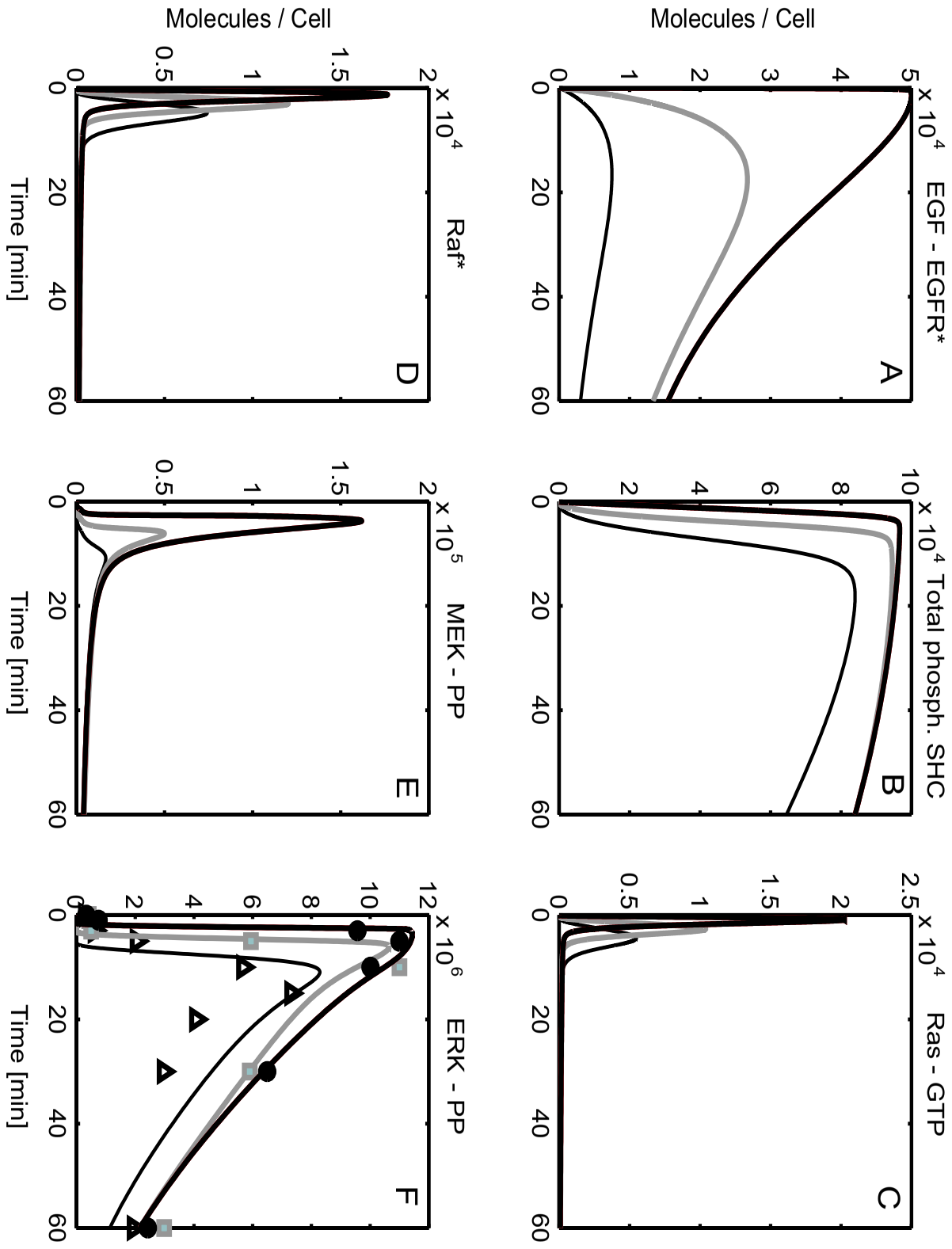

Fig. 3.5: Concentration dependence of the EGF induced MAP kinase cascade. Simulation and experimental results: –, ● 8 nM (50ng/ml), –, □, 0.08nM (0.5ng/ml,), -, △0.02 nM (0.125ng/ml) EGF.

by a rapid recovery to the inactive GDP bound state by 5min [164]. According to the model the ratio of the maximal number of Ras-GTP to the total number of Ras-GDP is about 0.25%, which is consistent with experimental findings [23]. Raf kinase shows a similar signaling pattern as Ras-GTP [154] as does MEK activation but not ERK phosphorylation. For Raf, MEK and ERK a time shift of the corresponding peak maxima towards later times along with increasing relative amplitudes can be noticed. Interestingly, the amplification steps from Raf to MEK (Figure 3.5D and E) are similar for all EGF concentrations (about 1:10). In the next step down the cascade, from MEK to ERK (Figure 3.5E and F) a significant amplification step of almost 1000 fold for all concentrations analyzed can be observed.

The ERK phosphorylation response signal is invariant over two orders of magnitude of ligand concentration resulting in the same amplitude and similar duration. Although the inititial signal of receptor autophosphorylation is below 10% of maximum at this low EGF concentration, shown in Figure 3.5 A, the model predicts that ERK activation still reaches about 70% of the maximum amplitude. Thus, in this last step of the MAP kinase cascade, a switch like activation of ERK should occur. This is in accordance with the steady state model by Huang and Ferrel [42]. Interestingly, the kinetics of the peak maximum correlates more with the temporal pattern of phosphorylated Shc bound to the receptors than with the initial kinetics of EGFR* phosphorylation. The simulated signal patterns for ERK activation could be experimentally well confirmed by the experimental analysis of time courses of ERK phosphorylation in HeLa cells for the indicated EGF concentrations [34]. The normalized data shown in Figure 3.5 F have been calculated from densitometric evaluation of westernblot bands and are represented by symbols. The actual westernblots are shown in Figure 6.1 in the Appendix. The Appendix contains a short description of the experimental methods. A more detailed description of the experimental methods can be found in [34]. In the concentration range of 8nM (50ng/ml) to 0.08nM (0.5ng/ml) EGF induced ERK-1/2 phosphorylation shows a maximum signal with delayed peak maxima between 1 and 10min, but identical signal duration (Figure 3.5 F). At saturating EGF concentrations, ERK-1/2 activation is known to peak after 1 to 5min, depending on the cell type at saturating conditions and declining thereafter [60]; [4]. Only at a concentration of 0.02nM (0.125ng/ml) EGF a significant reduction in peak height is noticeable, as well as a significant signal delay of 15min.

In the next two paragraphs we treat the system as a simple input output system. First, we com-

pare receptor activation patterns, which is the input of our system, with the ERK phosphorylation pattern as output signal. Second, we will look at ERK phosphorylation and its downstream signal, c-fos expression, which can also be considered as a simple input - output system.

Interestingly, the comparison between the time courses of the EGFR and ERK activation at 0.08nM (0.5ng/ml) shows that the maximum of ERK phosphorylation is reached before the maximal number of EGFR is phosphorylated. This is in contrast to the wide assumption that the maximum of EGFR receptor phosporylation determines the output signal. Therefore, the maximum of activated EGFR does not seem to be important for the ERK response as shown in Figure 3.6 rather the initial slope of EGF receptor phosporylation. Furthermore, simulation results also showed that an impulse-like stimulation with 0.08nM for 1min of the EGF receptor is sufficient to achieve the full ERK signal. This could be proven by first experiments (data not shown). From these findings, it seems that the initial velocity of receptor phosphorylation determines the signal output.

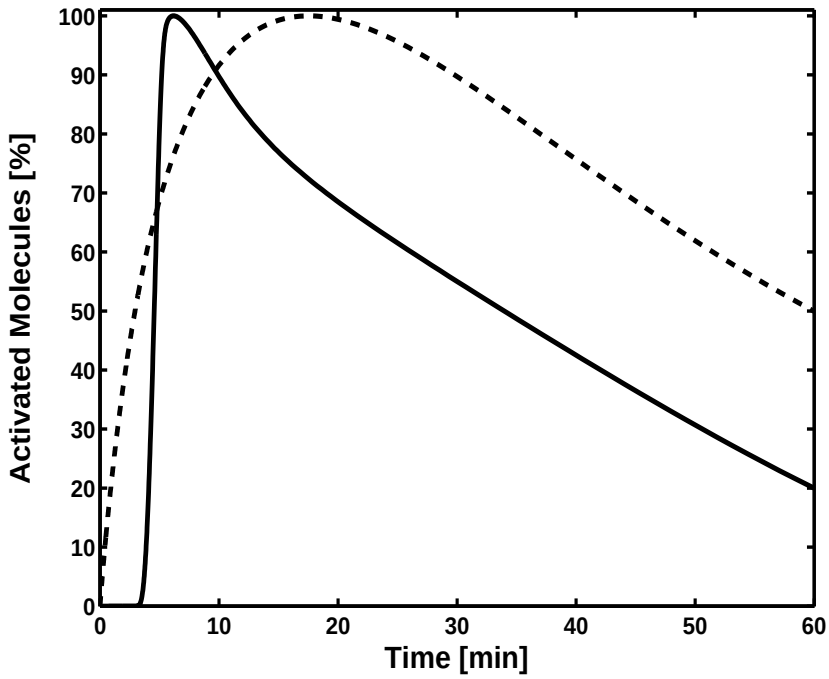

Fig. 3.6: Peak maximum of EGF-R phosphorylation does not determine ERK activation. **-** ERK-PP and **- -** (EGFR*)2.

Furthermore, the downstream effect of the ERK phosphorylation is of interest. Expression of the fos family of transcription factors is stimulated by growth factors. Within minutes of growth

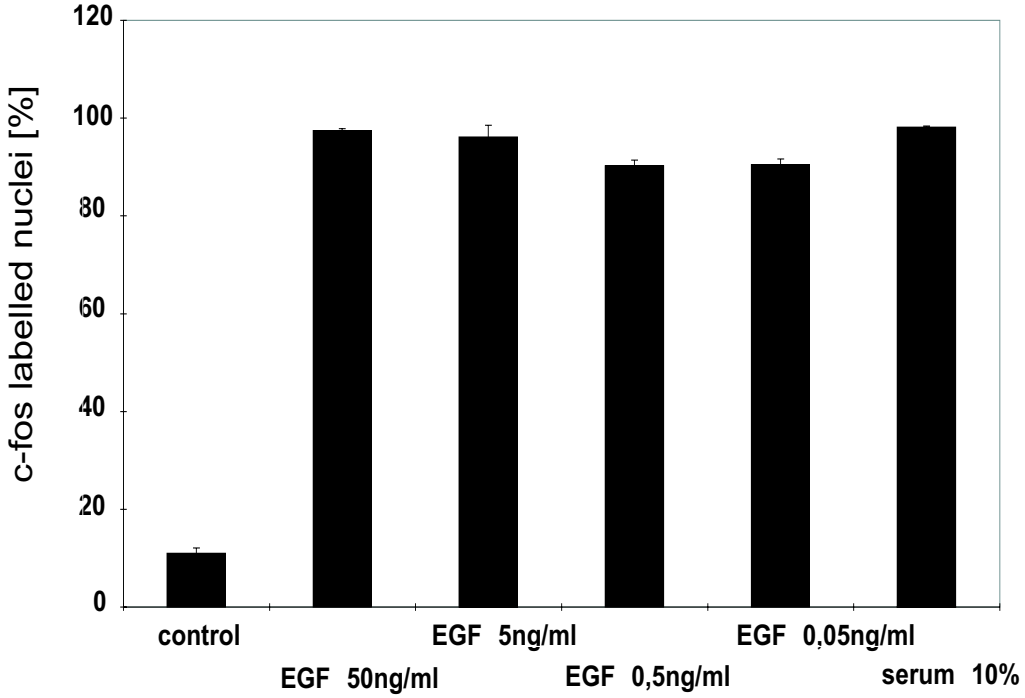

Fig. 3.7: c-fos expression in response to EGF stimulation.

factor stimulation the expression of fos family genes is induced, which include c-fos, fosB, fra-1, and fra-2 [66]. Fos family proteins form heterodimers with members of the Jun or ATF family. By binding to specific sites within the regulatory region of target genes, these Fos complexes may regulate the transcription of late-response genes the expression of which might be critical for cell cycle reentry. Comparing the maxima of the ERK phosphorylation time courses with c-fos expression triggered by a 60min EGF treatment, a similar dose response behavior can be observed experimentally for the c-fos expression. After overnight incubation the c-fos expression was determined microscopically at the single cell level. The experimental methods as well as the images taken can be found in Figure 6.7 in the Appendix. As shown in Figure 3.7 c-fos expression is maximal over two orders of magnitude from 8nM (50ng/ml) to 0.08nM (0.5ng/ml) EGF and declines for concentrations below the EGF receptor K_D in the same way as ERK-1/2 activation.

3.1.5 Relative Signal Contribution of External and Internalized Receptors

Another relevant question in EGF signaling, to date not resolved conclusively, is the contribution of activated internalized receptors to EGF signaling. After internalization, a considerable amount of phosphorylated receptor and phosphorylated Shc has been found associated with endosomes. However, it seemed difficult to prove its contribution in signaling experimentally. Therefore, we included receptor internalization into our model and investigated *insilico* the role of internalized receptors and the receptors remaining at the cell surface for the generation of a cellular responses, namely ERK phosphorylation in a quantitative manner.

In order to analyze theoretically the contribution of the internalized receptors versus the receptors remaining on the cell membrane we applied the model. Assuming that the internalized receptors signal through the same pathways as the external receptors and assuming the same kinetic rates as well as by keeping the signals of the internalized and external receptors separate, the contribution of internalized receptors versus the receptors remaining on the cell membrane can be analyzed.

In Figure 3.8 the signal cascade after EGF stimulation with 8nM (50ng/ml) is shown in a model derived from the same conditions as shown in Figure 3.5. The three curves in each graph follow the behavior of the total receptors (thick black line), of the extracellular receptors (gray line) and the internalized receptors (thin black line). In Figure 3.8A EGFR* is phosphorylated maximally after 15s at the plasma membrane, then is rapidly internalized and the maximum of the endosomal receptors was reached at about 15min. These findings correspond well with reported data from a preparative subcellular fractional approach, carried out to address receptor internalization in liver [55].

Comparing the kinetics of activation of the different signaling molecules, it can be seen that the majority of the signal results from the receptors at the plasma membrane for the concentration of 8nM (50ng/ml). The phosphorylation and association of phosphorylated Shc to receptors at the surface is so fast that e.g. Ras-GTP activation is maximal and already decayed to less than 50% before endocytosed receptors appear to a significant extent and can contribute to Ras activation of about 10% of the total signal. This implies that all the following steps of the MAP kinase cascade exhibit kinetics closely following activation of plasma membrane receptors. Thus, the high initial velocity of EGFR* phosphorylation seems to be sufficient to dominate ERK activation. However, at low (sub K_D) concentrations of EGF, the model predicts a distinct

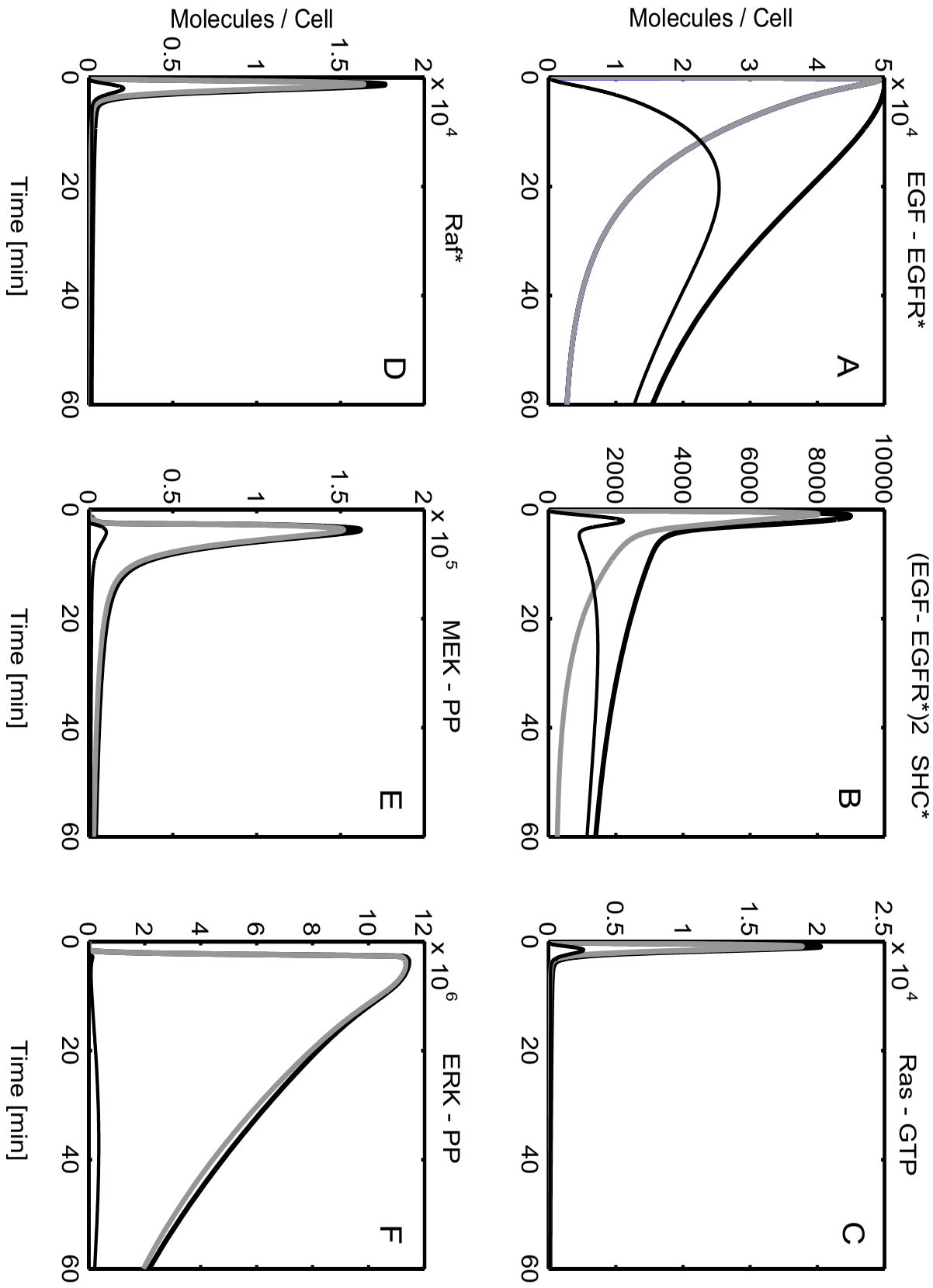

Fig. 3.8: Receptor internalization at 8nM of EGF (– signal triggered by total number of receptors, – Signal triggered by internalized receptors, – signal triggered by external receptors).

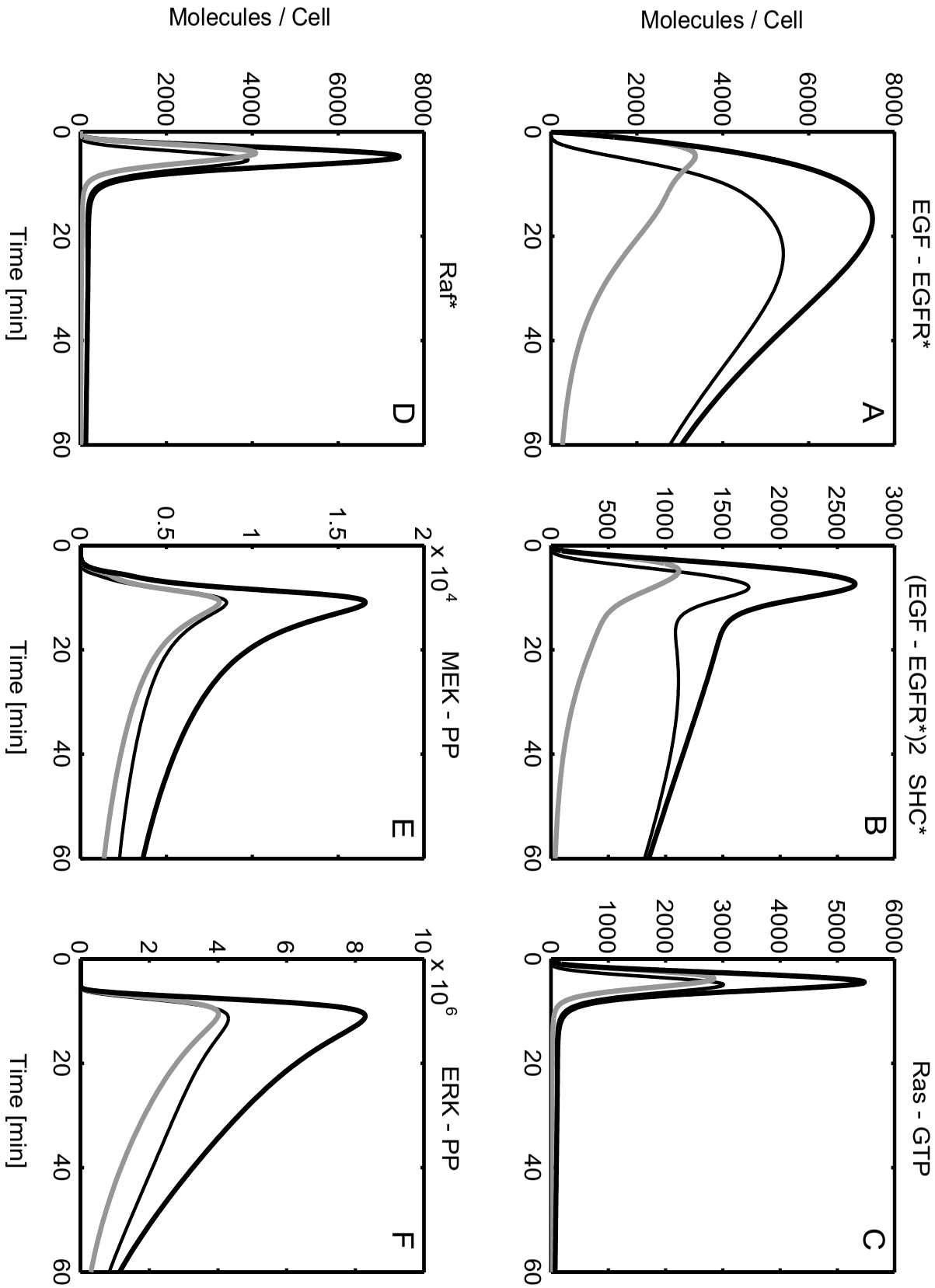

Fig. 3.9: Receptor internalization at 0.02nM EGF. (– signal triggered from total number of receptors, – signal triggered by internalized receptors, – signal triggered by external receptors).

contribution to ERK activation of plasma membrane and of internalized receptors. Similar calculations as in Figure 3.8 but at an EGF concentration of 0.02nM (0.125ng/ml) predict that at this low EGF concentration EGF receptor autophosphorylation becomes slow and only 10% of the total receptors are activated (Figure 3.9). This activation kinetics now is rather similar to the internalization rate of receptors and the ratio of internalized to externally exposed receptors after 5min is about 1:1. This implies that the relative signal contribution of internalized receptors throughout the cascade is considerably higher than at saturating EGF concentrations. Taken together, internalization appears to play a dual role in signal transduction: at high EGF concentrations internalization seems to attenuate the response whereas at low concentrations internalization amplifies the response.

3.1.6 Role of the Two Redundant Pathways of Ras Activation

To further investigate the validity of the mathematical model, an analysis to determine, which of the two pathways for Ras-GTP activation - the Shc dependent or independent pathway - would have priority in signaling, is carried out. The two pathways are depicted in Figure 3.3. Therefore, Shc wildtype and Shc mutant cells which show a Shc deficiency, are simulated. According to the experiments described in [88], two cases are studied: (i) ERK activation at a high EGF concentration e.g. 50ng/ml and (ii) a very low EGF concentration of 0.5ng/ml.

Simulating the mutant cells, the initial Shc concentration in the mathematical model is set to zero. In contrast to the data published by Pawson et al. [88], where only the amount of ERK activation after 5min is investigated, we simulated the entire time course of ERK activation. Comparing the simulation results for 50ng/ml EGF presented in Figure 3.10A the same ERK responses were obtained in the considered time frame of 10min, indicating, that the Shc deficient pathway does not contribute to the ERK-PP output signal at high EGF concentrations. Shc deficient cells show the same amount of activated ERK for high EGF concentrations and at the same time an increase of Ras-GTP activation. The increase of Ras-GTP in the mutant occurs in the simulation as well (data not shown), since more Ras is shuttled into the second pathway if the first pathway is inactivated.

However, ERK activation of the wild type and the mutant cells is different for the low EGF concentration of 0.5ng/ml. As shown in Figure 3.10B the simulation predicts a decrease of ERK activation of the mutant cells during the first 30min. This observation could also be found

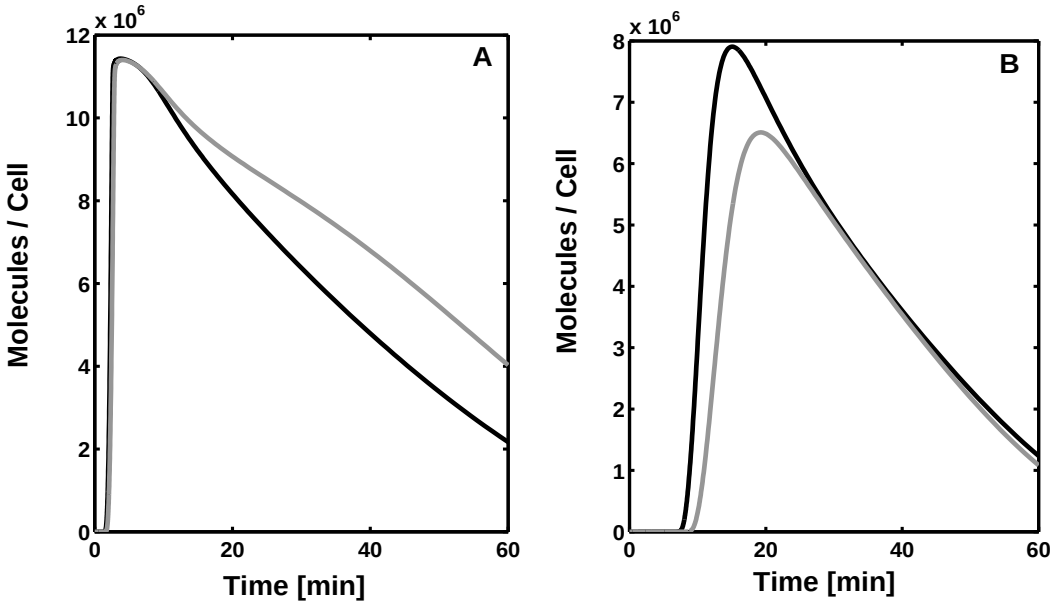

Fig. 3.10: ERK phosphorylation in the presence and absence of the adapter molecule Shc: – mutant, – wild type, **A** 8nM (50 ng/ml) EGF, **B** 0.02nM (0.125ng/ml) EGF.

experimentally [88]. Whether the simulation of ERK activation after 30min of EGF stimulation corresponds with actual experimental data remains to be elucidated.

Thus, Shc seems to be dispensable for MAPK activation in response to moderate concentrations of EGF but is necessary for efficient MAPK activation in cells exposed to low EGF concentrations of EGF and sensitizes the cellular machinery of MAPK activation.

3.1.7 Determination of ERK Signal Duration by EGF Receptor Number

As discussed in the example of Figure 3.8 and Figure 3.9 receptor internalization can have a signal amplifying or a signal attenuating effect. In the following the effect of receptor overexpression in combination with receptor internalization will be discussed.

Assuming a 10-fold increase in EGF receptors without changing parameters of internalization, our model predicts that the duration of the ERK signal is prolonged as shown in Figure 3.11. It has been shown that experimental overexpression of EGF receptors per se is sufficient for an increase in mitogenic or differentiation potency of EGF [150]. For example, the epidermal growth factor receptor and HER2/c-ErbB-2, both of which activate the Ras-MAPK pathway, are overexpressed in tumor cells up to 20% [32]. Since the high receptor number is subject to prolonged exposure to EGF at the surface and ERK is already maximally activated, the maximum

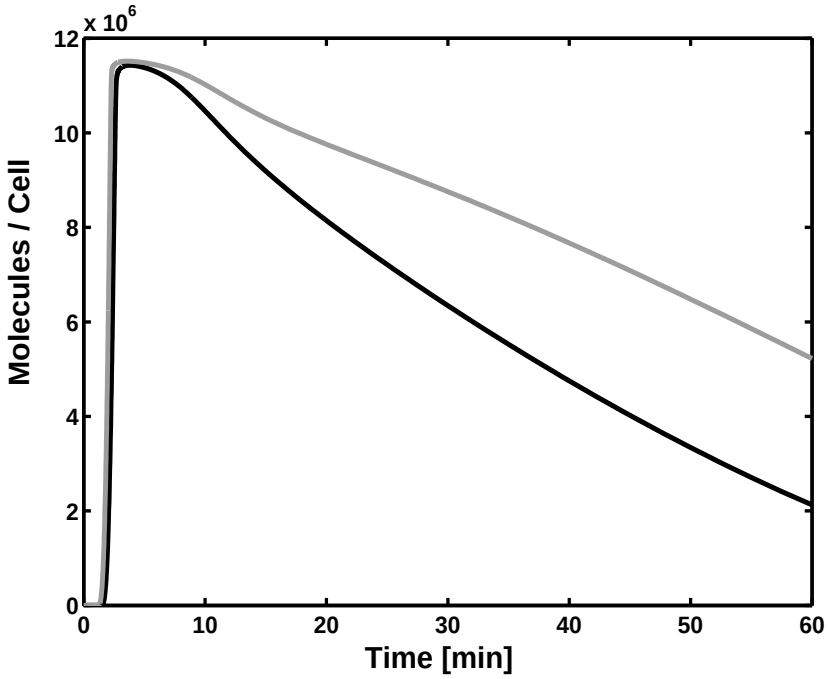

Fig. 3.11: ERK phosphorylation as a function of EGFR expression: – 500 000 EGFR, **–** 50000 EGFR.

amplitude is not changed. Due to saturation effects within the endosomes, receptor endocytosis is dramatically retarded under these hypothetical conditions. Likewise, when the internalization rate in the model is assumed to be zero, at low or normal receptor number, the attenuation in ERK signaling is reduced or abolished. Thus the internalization rate seems to be a major determinant in signal limitation. These findings are supported by the experimental data that show that the internalization rate decreases with an increasing receptor number [170]. Moreover, the model supports the mechanistic explanation, that due to a reduced internalization capacity the overexpression of EGF receptor appears sufficient for the continuous ERK activation, a key step in deregulated proliferative capacity of cells (see also Chapter 3.3).

3.1.8 Restimulation of the EGF induced MAP Kinase Cascade

In the experiments discussed so far, HeLa cells are stimulated permanently with EGF. As a consequence the question arises of how cells respond to an impulse-like stimulation and whether it is possible to restimulate cells.

As in the preceding graphs, all simulation results are indicated by solid lines and all experi-

mental data by dots in the figures presented in the following. The simulation results for cells that are exposed to a 1min-pulse of 50ng/ml EGF, which is above saturation, show that this pulse is sufficient to obtain a maximal ERK-PP response. This is shown in Figure 3.12, where the black solid lines represent the simulation result for an EGF impulse of 1min. The gray solid lines depict the simulation of phosphorylated EGFR* and of ERK phosphorylation for a continuous stimulation of the cells for 60min. An impulse-like stimulation of 1min leads to the same maximal EGFR* activation with the continuous presence of EGF but shows a small decrease of activated EGFR* towards later time points. With regard to the ERK phophorylation this results in an identical time course of activation. The experimental data; the black bullets for the impulse-like stimulation and the gray bullets for the permanent stimulation shown in Figure 3.12 are consistent with the simulation results.

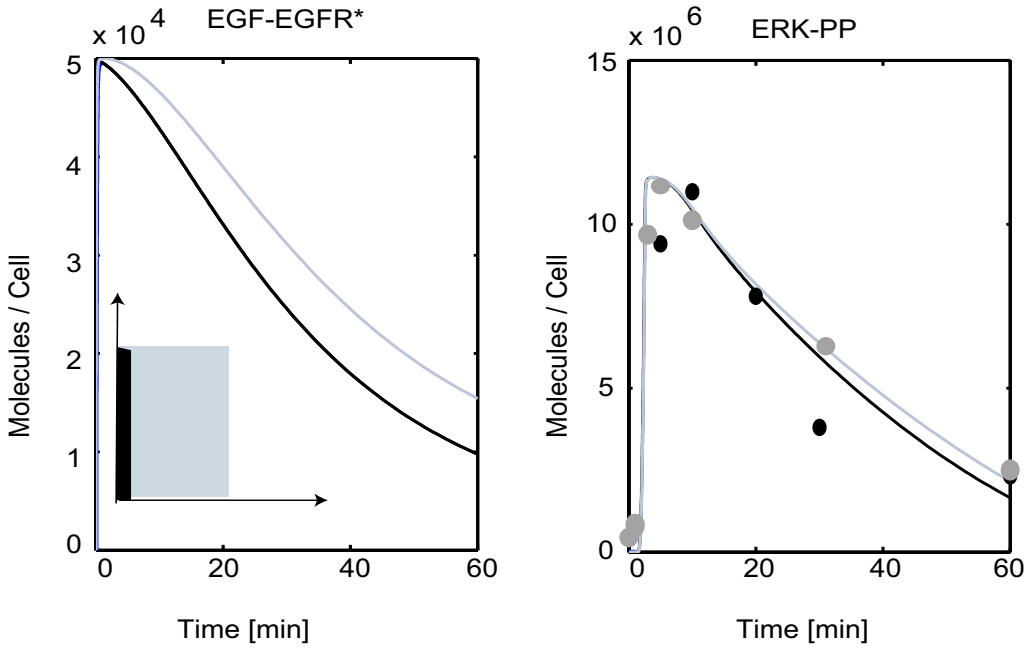

Fig. 3.12: Impulse-like stimulation of EGFR: – simulation of permanent EGF stimulation for 60min with 50ng/ml, – simulation for a 1min-EGF pulse(50ng/ml), • experimental data for permanent stimulation with 50ng/ml EGF, • experimental data for a 1min-EGF pulse (50ng/ml).

Autocrine signaling is an example where restimulation occurs in nature and where the phenomenon of desensitization is of major interest. In this section, the possibility to restimulate the

cells with EGF, while EGF has been removed, will be discussed. In the original model a second stimulation of the cells with EGF is not possible, because the system reaches a different steady state after the first stimulation. Thus, comparing the steady state levels of different components with the initial conditions used, the levels of Ras-GDP, Grb2, Sos and GAP concentration are diminished after the first stimulation and do not reach the initial value due to receptor internalization and degradation. In contrast, if we restimulate and increase the level of Ras-GDP, Grb2 and GAP back to the initial values, it is possible to stimulate the system a second time. In order to test these two possibilities, the HeLa cells where stimulated for 1min with EGF, washed and restimulated with EGF after 60min. In order to analyze the signaling effect, phosphorylated ERK1/2 was determined after 5, 10, 20, 30 and 60min after the second stimulation. Indeed, as depicted in Figure 3.13 and in the westernblots in Figure 6.8 in the Appendix only a small peak could be detected. Thus from this experiment, it seems that some kind of desensitization does take place.

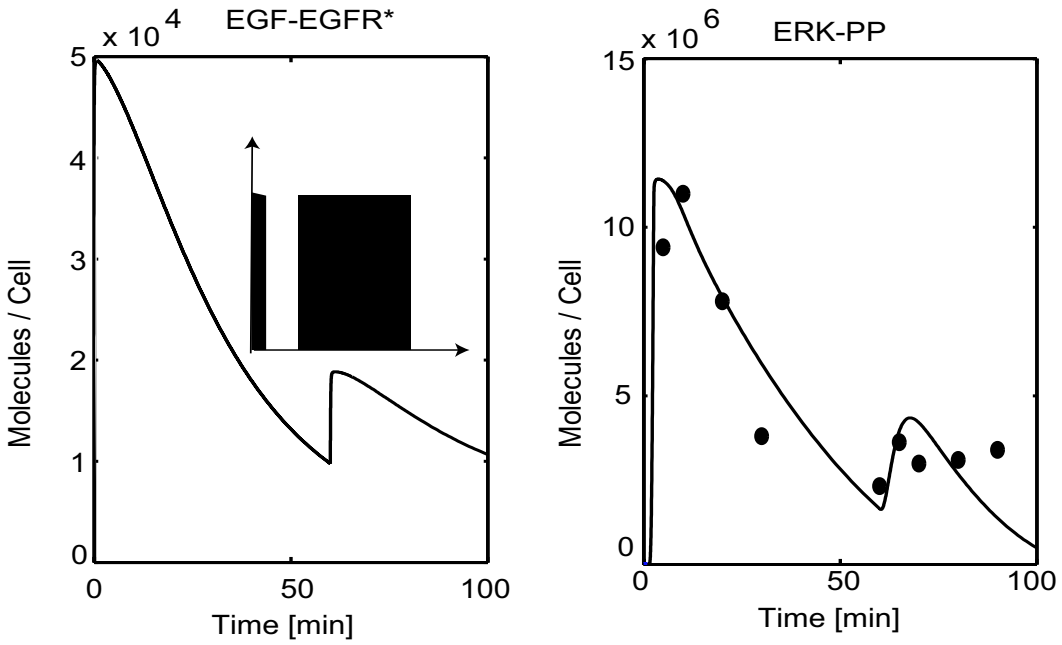

Fig. 3.13: Impulse-like stimulation and restimulation in HeLa cells:– simulation of 1min EGF impulse-like stimulation, removal of EGF and restimulation after 60min, • experimental data.

These findings show that a certain desensitization of ERK activation in HeLa cells occurs after a first stimulation. In order to study the effect of desensitization in an autocrine cell line we switch from HeLa to A431 cells. Figure 3.14 shows the increase in phosphorylated ERK with increase

in time between the first and the second stimulation. Each dot represents the measured maximal ERK activation after 5min of secondary stimulation of the washed and restimulated cells from 1hr to 36hrs. The washing process is necessary in order to hinder the EGF remaining on the cell surface to signal. After 24hrs the cells have almost recovered and the restimulation shows around 75% of the maximal ERK activation. After 36hrs the cells seem to have reached their initial physiological state again as shown in Figure 3.14. The same findings hold true for HeLa cells. However, when considering A431 cells, which are autocrine cells we show that the desensitization is a common regulatory mechanism, which is used by the cells in order to prevent perturbations in the desired signal response.

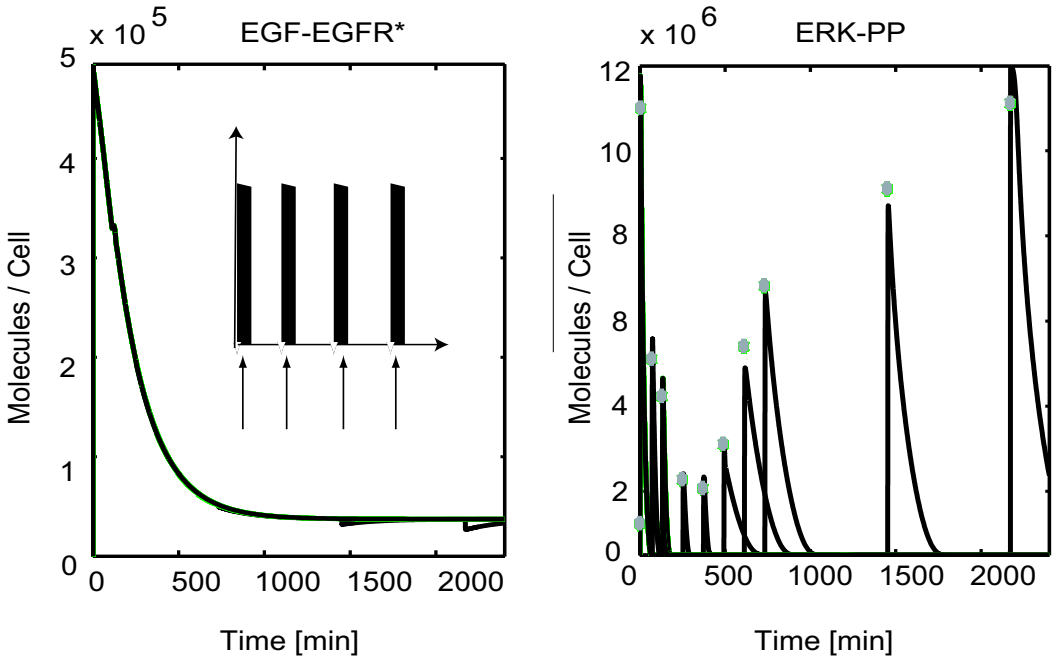

Fig. 3.14: Impulse-like restimulation of A431 cells; inital stimulation for 5min and restimulation at the indicated time points with – 50ng/ml EGF, • experimental data.

There are three possible mechanisms which could lead to desensitization: receptor downregulation and slow synthesis, the negative feedback loop from ERK-PP to SOS, which leads to the phosphorylation and thus inactivation of SOS or the downregulation of GAP, Shc or SOS. This downregulation of the mentioned adapter molecules might be due to phosphorylation effects or due to receptor internalization and degradation. In the following we want to elucidate the

proposed mechanisms.

3.2 Autocrine Epidermal Growth Factor Signaling

Autocrine receptor/ligand interactions were first identified in tumor cells, where it was found that transformation of cells resulted in overexpression of certain growth factors leading to unregulated proliferation of the tumor cells [138]. However, later on autocrine signaling has been found to operate in numerous physiological situations, including wound healing [148] and tissue organization during development [162] and reproductive cycles [172].

Autocrine loops are established, when soluble factors secreted by cells bind to and stimulate receptors on their own surfaces [137]. Commonly, secretion of autocrine ligands is tightly regulated. In the Epidermal Growth Factor Receptor (EGFR) system, ligands such as the Transforming Growth Factor alpha (TGFα) are synthesized in the form of membrane bound precursors [99]. Following synthesis, ligand-releasing proteases, so called “sheddases” process the membrane associated precursors into their active, soluble forms [99]. Autocrine cells generally express high levels of cognate receptors which makes them very effective in recapturing endogenous ligand [92], [108]. Besides the mechanisms for ligand release and capture, autocrine systems are equipped with numerous mechanisms for cross-activation. For example, different primary stimuli like exogenous growth factor or ionizing radiation can lead to ligand release and recapture, resulting then in the stimulation of the intracellular signaling. In non-autocrine cells, soluble growth factors were shown to activate sheddases through the Ras/MAPK pathway [39]. This discovery suggests that, in the autocrine EGFR system, a ligand, the receptor, the sheddases and the signaling network can form a positive feedback loop. This has been shown in a very elegant manner with the help of a mathematical model [131].

In this work we focus on radiation induced ERK activation followed by autocrine secretion of TGF-α. It could be shown that the exposure of A431 cells to ionizing radiation has been associated with short transient increases of epidermal growth factor receptor (EGFR) tyrosine phosphorylation and activation of the MAP kinase and c-Jun NH_2-terminal kinase (JNK) pathways. Irradiation of A431 cells with 2Gy causes immediate primary activation of the EGFR and the MAPK and JNK pathways which are followed by a second prolonged activation of the MAPK pathway. Both the primary as well as the secondary MAPK activation are abolished by

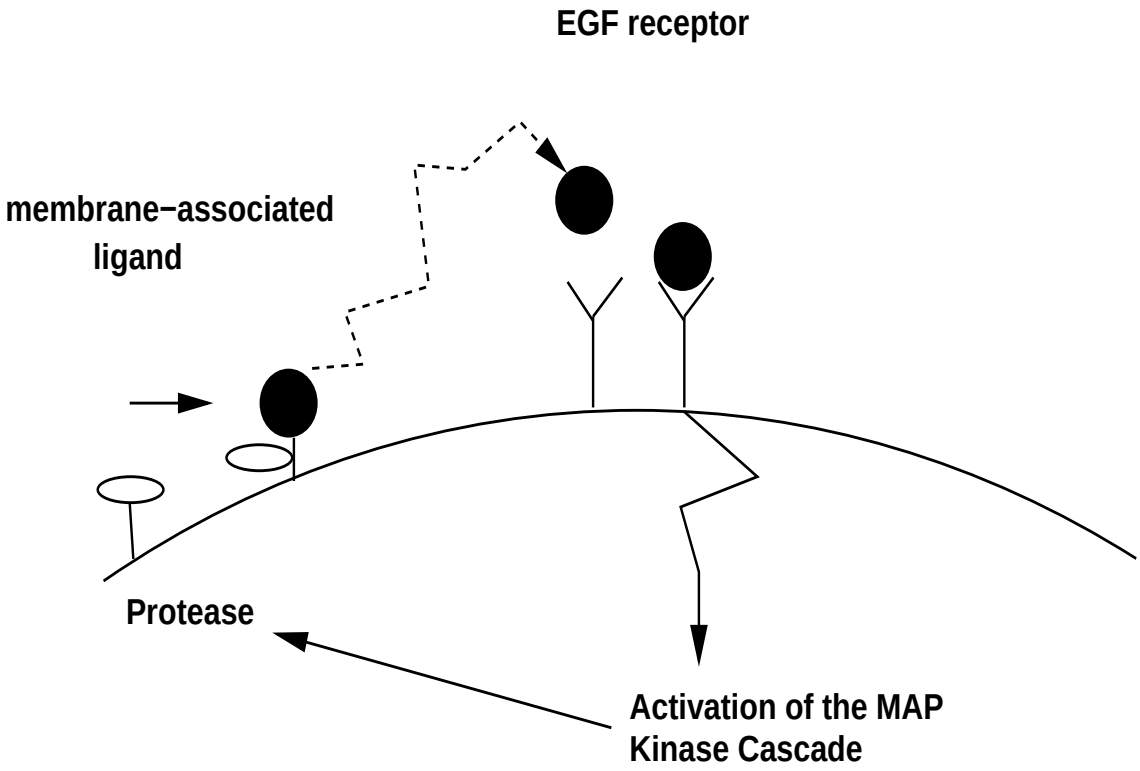

Fig. 3.15: Schematic representation of the autocrine loop.

the inhibition of EGFR phosphorylation as well as of Ras function [26]. It has been shown that irradiation can induce EGFR activation [78], which then in turn can activate the MAPK pathway. Experiments indicate that the addition of neutralizing monoclonal antibody versus TGF-α has no effect on the primary activation, neither on the primary activation of EGFR nor on the primary JNK or MAPK activation, and no secondary activation of MAPK and JNK could be detected [26]. Interestingly, media that was taken 60min after irradiation to stimulate new cells, induced no MAPK activation whereas due to increased pro-TGF-α cleavage 120-180min after exposure a secondary MAPK peak is observable. Thus, radiation causes primary and secondary activation of MAPK and JNK pathways. The secondary activation is dependent on radiation-induced cleavage and autocrine action of TGF-α.

3.2.1 Model Extension: Inclusion of Autocrine Signaling

As described earlier, autocrine loops are established when soluble factors secreted by cells bind to and stimulate receptors on their own surfaces. Generally, the secretion of autocrine

ligands is tightly regulated. In the EGFR system, ligands such as the Transforming Growth Factor alpha (TGFα) are synthesized in the form of membrane bound precursors [99]. As shown in Figure 3.15 ligand-releasing proteases process the membrane-associated precursors into their active soluble form, which can then be recaptured.

According to the mechanistic model of autocrine loops by Shvartsman et al. [131] the following Partial Differential Equation (PDE) and boundary condition for the ligand concentration L(r,t) in addition to the presented model can be derived:

$$\frac{\partial L}{\partial t}(r,t) = D[\frac{\partial^2 L}{\partial r^2} + \frac{2}{r}\frac{\partial L}{\partial r}], \tag{3.1}$$

$$r_{cell} \leq r \leq \infty, \qquad 0 \leq t \leq \infty,$$

$$\frac{dR(t)}{dt} = -k_{on}R(t)L(r_{cell}) + k_{off}C(t) + s - k_cR(t), \tag{3.2}$$

$$\frac{dC(t)}{dt} = k_{on}R(t)L(r_{cell}) - k_{off}C(t) - k_eC(t). \tag{3.3}$$

Where D represents the diffusion coefficient of the ligand diffusing into the extracellular medium and as we consider the cell as a sphere, r is the radius. R represents the number of unoccupied receptors, L the ligand concentration in the media, C the number of complexes formed, k_e the internalization rate of the receptor-ligand-complexes C, k_c the constitutive internalization rate, k_{on} and k_{off} the association and dissociation rates and s the receptor synthesis rate.

The boundary governing boundary condition is:

$$D\frac{\partial L}{\partial r}(r_{cell},t) = -Q + k_{on}R(t)L(r_{cell},t) - k_{off}C(t), \qquad L(\infty,t) = 0. \tag{3.4}$$

Q represents the ligand secretion rate in [# of molecules/(cell s)].

With the help of the following transformations the system can be rendered dimensionless:

$$\rho = \frac{r}{r_{cell}}, \qquad \tau = k_{off}t, \qquad \gamma = \frac{k_c}{k_{off}}, \qquad \delta = \frac{k_e}{k_e + k_{off}}, \tag{3.5}$$

$$\bar{L} = \frac{L}{K_D}, \qquad \bar{C} = \frac{C}{R_T}, \qquad \bar{R} = \frac{R}{R_T}, \tag{3.6}$$

$$Au = \frac{Qr_{cell}}{ADK_D}, \qquad Da = \frac{konr_{cell}s}{k_cDA}. \tag{3.7}$$

The cell radius scales the coordinate. The time t is scaled by the inverse dissociation rate k_{off}, the Ligand concentration L is scaled by the dissociation constant K_D=k_{off}/k_{on} and the

occupied and free receptors are scaled by the total number of receptors. The ligand secretion rate Q is assumed to be uniform over the cell surface area A. We consider the cells as spheres with a radius r of 5μm. Ligand released into the extracellular medium diffuses with a diffusion coefficient D, and binds reversibly to cell surface receptors with the dissociation constant K_D. The exact derivation of the dimensionless numbers can be found in [131]. The rescaled problem takes then the following form:

$$\epsilon \frac{\partial \bar{L}}{\partial \tau}(\rho, \tau) = \frac{\partial^2 \bar{L}}{\partial \rho^2} + \frac{2}{\rho}\frac{\partial \bar{L}}{\partial \rho}, \tag{3.8}$$

$$1 \leq \rho \leq \infty, \qquad 0 \leq \tau \leq \infty,$$

$$\frac{d\bar{R}(\tau)}{d\tau} = -\bar{R}(\tau)\bar{L}(1) + \gamma(1 - \bar{R}(\tau)) + \bar{C}(\tau), \tag{3.9}$$

$$\frac{d\bar{C}(\tau)}{d\tau} = \bar{R}(\tau)\bar{L}(1) - \frac{1}{1-\delta}\bar{C}(\tau). \tag{3.10}$$

The boundary conditions rescale to:

$$\frac{\partial \bar{L}}{\partial \rho}(1, \tau) = -Au + \delta Da \bar{R}(\tau)\bar{L}(1, \tau), \qquad \bar{L}(\infty, \tau) = 0. \tag{3.11}$$

The time scale of extracellular diffusion is defined by

$$\epsilon = r_{cell}^2 k_{off}/D. \tag{3.12}$$

For high values of secreted ligand diffusivity ($\epsilon \ll 1$), concentrations of soluble species evolve on a time scale that is much shorter than that of surface receptors and ligand/receptor complexes. In this regime, the binding/transport model can be simplified by using steady state approximation for the concentration of endogenous ligand. The concentration L at the surface of an autocrine cell is defined as:

$$\bar{L}_S(1) = \frac{Au + Da\bar{C}}{1 + Da\bar{R}}. \tag{3.13}$$

Au represents the *Autocrine Number* and Da the so called *Damköhler Number* both of which are dimensionless. The rates ke and s represent the receptor internalization rate and the receptor synthesis rate respectively.

In order to complete the model of autocrine signaling, the protease activation has to be included. The amount of the surface proteases P is determined by the balance between the processes for its synthesis, activation and degradation. Ligand releasing proteases are not specific and are capable of processing a wide range of surface molecules e. g. members of the EGF receptor ligand family. Sheddases are regulated by various intracellular processes. Secretion of the proteases is composed of a slow process mediating the constitutive release and a faster inducible process. The activation of the proteases is followed by its removal from the surface, most likely, via the endocytotic pathway [30].

The first kinetic analysis of the proteolytic release of the EGF-family ligands has been recently reported. It was shown that the rate of ligand release obeys the pseudo-first order kinetics with respect to the amount of surface protease [31]. In the absence of more detailed information, linear gains provide the simplest possible parameterization of the nonlinear interconnections between the modules comprising the ERK-PP induced protease activation. This is taken into account with the help of the scaling factor G. In the model the newly synthesized protease is inserted in the membrane with the rate S_P and constitutively internalized with the rate constant k_{cp}. The protease P gets activated with the rate constant k_{ap}, which is mediated by a MAPK dependent and independent process. The MAPK dependent process is simplified by a scaling factor G and the ratio of ERK-PP versus ERK_{tot}. Internalization of protease P(t) occurs with k_{ep}. Thus the differential equations for activated protease Pa(t) can be derived as follows:

$$\frac{dP(t)}{dt} = S_P - k_{cp}P(t) - (k_{ap} + Gk_{ep}\frac{[ERK-PP]}{[ERK_{tot]}})P(t), \tag{3.14}$$

$$\frac{dPa(t)}{dt} = (k_{ap} + Gk_{ep}\frac{[ERK-PP]}{[ERK_{tot}}])P(t) - k_{ep}P_a(t). \tag{3.15}$$

In the following the ordinary differential equations (ODEs) and the corresponding kinetic parameters are listed as they are used in the current mechanistic model of autocrine signaling which is basically an extension of the model of the EGF induced MAP kinase cascade described earlier, using the simplified model by [131]. The detailed biochemical reactions are depicted in Figure 3.16. Therefore we used the equations listed above in their unscaled form.

In order to describe the release of EGF by activated proteases mechanistically, the reactions v132 and v133 are included. The reversible reaction v132 describes the binding of activated protease to autocrine EGF (here refered to as [EGFauto]), which is still bound to the surface.

The irreversible reaction v133 describes the dissociation of the [EGFauto-Pa] complex, which results in the release of EGF and the still active protease from the cell surface. The reactions are summarized in Table 3.2. The parameter k_{13} stands for the EGF receptor synthesis rate and k_5 is the constitutive EGF receptor internalization rate. The exact values can be found in Table 3.3.

[Pi] comprises the concentration of the constitutively internalized protease [P] and the internalized activated protease [Pa] concentration, which then get degraded with k_{deg} to [Pideg].

EGF concentration in the media:

$$\frac{d[EGF]}{dt}(t) = v133 - v134 - v1. \tag{3.16}$$

Protease synthesis and activation:

$$\frac{d[P]}{dt}(t) = S_P - k_{cp}[P] - (k_{ap} + G\frac{[ERK-PP]}{[ERK_{tot}]}k_{ep})[P], \tag{3.17}$$

$$\begin{aligned}\frac{d[Pa]}{dt}(t) &= -v132 + v133 + k_{ap}[P] - k_{ep}[Pa] + \\ &\quad G\frac{[ERK-PP]}{[ERK_{tot}]}k_{ep}[P].\end{aligned} \tag{3.18}$$

Processing of EGF:

$$\begin{aligned}\frac{d[EGFauto]}{dt}(t) &= Au + Da\frac{[EGF-EGFR]kd1/k1}{(k13/k5)(1+Da[R]/(k13/k5))} \\ &\quad -v132,\end{aligned} \tag{3.19}$$

$$\frac{d[EGFauto-Pa]}{dt} = v132 - v133. \tag{3.20}$$

Total protease internalization and degradation:

$$\frac{d[Pi]}{dt}(t) = k_{cp}[P] + k_{ep}[Pa] - k_{deg}[Pi], \tag{3.21}$$

$$\frac{d[Pideg]}{dt}(t) = k_{deg}[Pi]. \tag{3.22}$$

Stimulated by a paper published by [26], we compared whether the effect of desensitization and the observation of two ERK-PP peaks after irradiation can be explained by mathematical modeling. [26] showed that irradiation (2Gy) of A431 cells caused immediate primary activations (0-10min) of the EGFR and the MAPK pathway, which was surprisingly followed by later

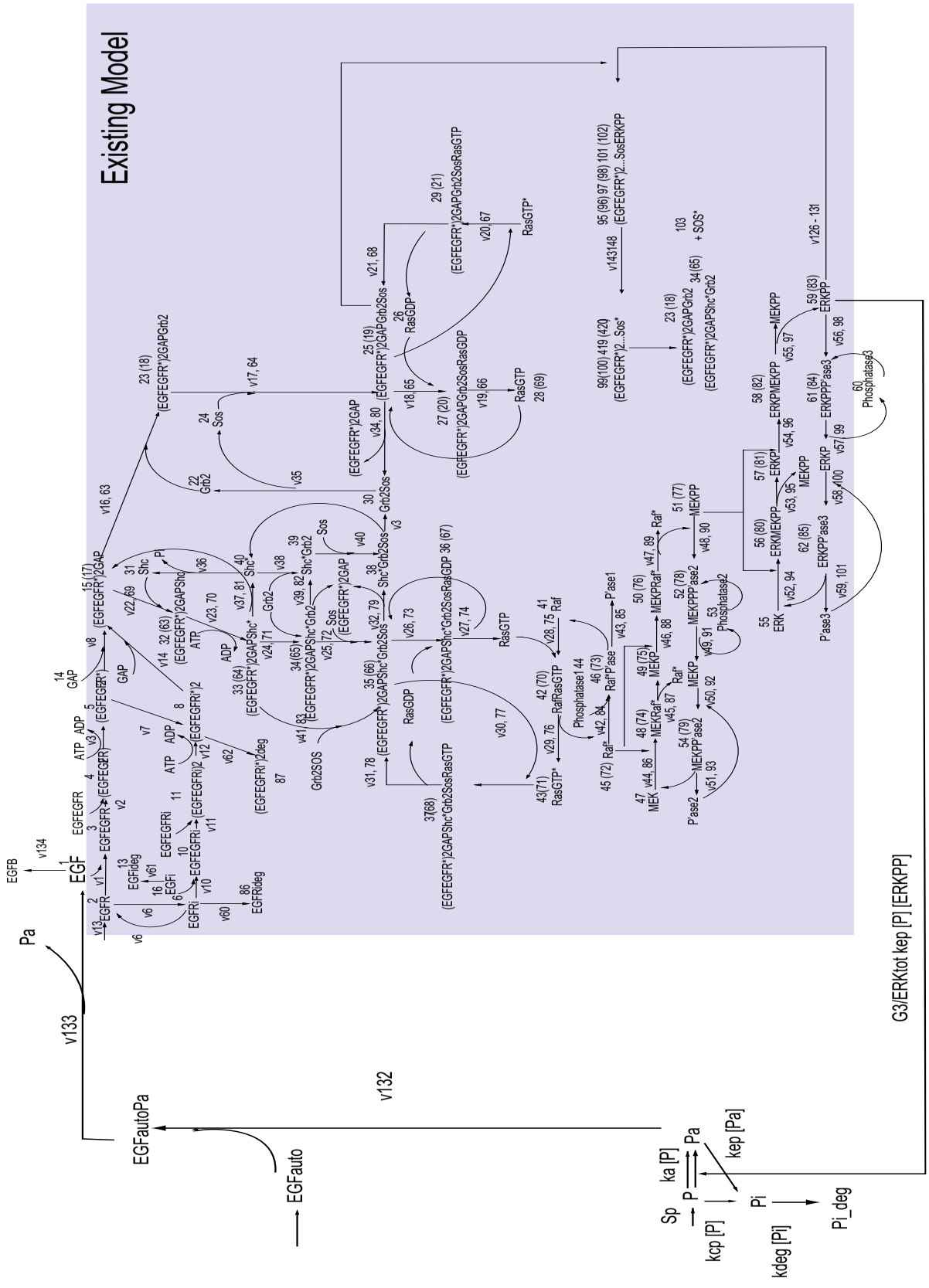

Fig. 3.16: Addition of the autocrine loop to the biochemical reaction network of the EGF induced MAP kinase cascade

.

Tab. 3.2: Kinetic Reactions v132 and v133

Reaction Number	Equation	Kinetic Parameter
v132	[EGFauto] + [Pa] $\leftrightarrow$[EGFauto-Pa]	k_{132}=1e4; k_{-132}=0.1
v133	[EGFauto-Pa]$\rightarrow$[EGF] + [Pa]	k_{-133}=5e-4

prolonged secondary activations (90-240min). Primary and secondary activation of the EGFR is abolished by molecular inhibition of EGFR function. The primary and secondary activation of the MAPK pathway is abolished by molecular inhibition of either EGFR or Ras function [26]. The latter supports the idea that radiation as well as EGF trigger the same pathways. If both trigger the same pathways we should obtain similar results by stimulating the cells with irradiation or an EGF pulse. In Figure 3.19 the black dots represent the experimental data points measured by Dent et. al. for A431 cells.

From an initial experiment we know that the desensitization effect also occurs in A431 cells. As already shown in Figure 3.14, it takes about 36hrs for A431 to reach their initial state and to be able to fully phosphorylate ERK again, which means that the same amount of ERK gets phosphorylated in the second stimulation as in the first one. As can be seen in Figure 3.14 the cells are desensitized after the first impulse-like stimulation and recover slowly. Only after 24 - 36hrs the cells are again able to respond maximally to a stimulus. Comparing the simulation results (black line) with the experimentally determined amount of phosphorylated ERK for different time points, the second stimulation can be described effectively by adjusting the GAP synthesis rate. In the model presented here, GAP is the limiting molecule. However, from the experiment shown in Figure 3.14 it is obvious that receptor downregulation does not affect desensitization as the receptor numbers on A431 are around 500000 and remain quite high after the initial stimulation (still significantly higher than the initial receptor number on HeLa cells).

Control experiments for low EGF concentrations and A431 cells are stimulated with 0.5ng/ml and the time course of ERK phosphorylation after a second stimulation with 50ng/ml during a time period of 6hrs is measured. As shown in Figure 3.17, after the release of autocrine EGF a second, higher peak of activated EGF receptor (EGF-EGFR*)2 is observable. At this concentration receptor synthesis and degradation are almost even and (EGF-EGFR*)2 decreases only a little. This second peak can also be found for ERK-PP due to the release of autocrine EGF. It

Tab. 3.3: Kinetic parameters applied in the model compared to the published parameters by S. Shvartsman.

Kinetic Parameter	Value	Value in [131]
S_P	0.0022 [Protease/s]	0.0022 [Protease/s]
kdeg	6.5e-3	6.5e-3
r_{cell}	5e-4 [cm]	5e-4 [cm]
G	0.0001	1
D	1e-6 [cm2/s]	1e-6 [cm2/s]
Q	83.3 [molecules/(cell x s)]	83.3 [molecules/(cell x s)]
k_{cp}	3.33e-6 [1/s]	3.33e-4 [1/s]
k_{ap}	1.67e-9 [1/s]	1.67e-5 [1/s]
k_{ep}	1.66e-5;[1/s]	1.67e-3 [1/s]
A	$4\pi r^2$	
Au	(Qr1000)/(ADkd1/k16e23)	
Da	(k1rk131000)/(k5 DA6e23)	

can be observed around 2hrs after the initial stimulation, though it is significantly smaller than the initial ERK-PP peak. The reason why the second peak is lower might be due to a low ligand concentration. However, this is not in accordance with observations described by Dent. From these findings desensitization might have its origin in the negative feedback loop from ERK-PP to SOS or adapter protein degradation.

From the results shown in Figure 3.17, it seems that a second stimulation is able to trigger a second ERK-PP peak if the initial concentration is low. Therefore we stimulate the cells with an initial impulse of 5min and 0.5ng/ml and a second time at the indicated times with 50ng/ml. As shown in Figure 3.18 under these conditions a second ERK-PP peak is observable (filled black dots and lines). For completion we show the experimental data of an experiment where A431 cells were stimulated twice with 50ng/ml. if the cells get stimulated the first time with 50ng/ml EGF no second ERK-PP response triggered by the second stimluation is observable. Due to the negative feedback from ERK-PP to SOS we see only a small second peak in the simulation at around 80min as at this time there is still enough ERK-PP to phosphorylate available SOS because of the prior ERK activation by autocrine EGF. However, from these results we can

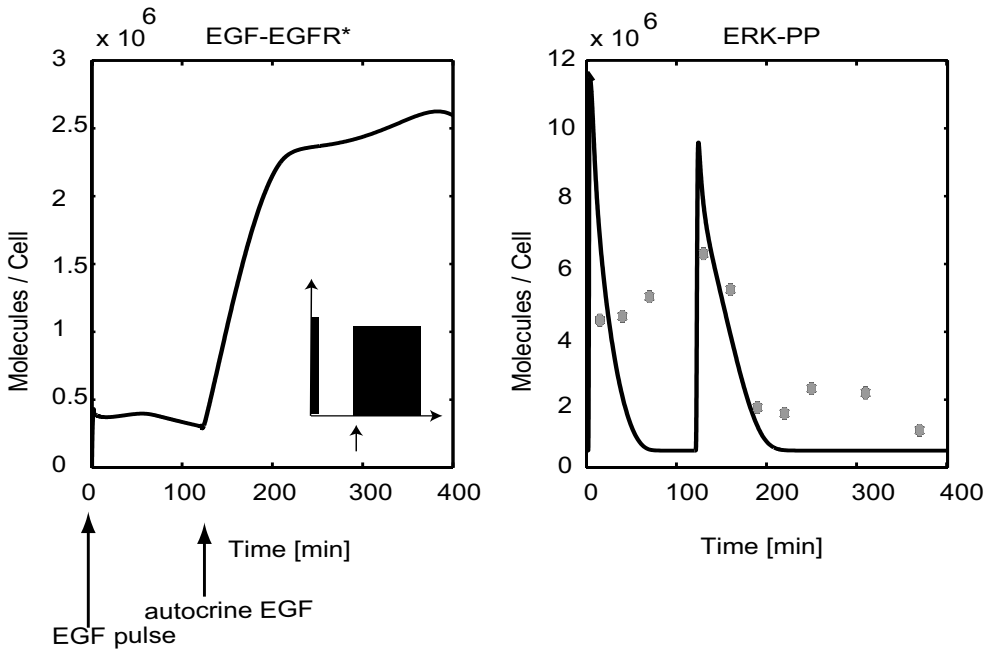

Fig. 3.17: Stimulation of A431 cells with a low EGF concentration of 0.5ng/ml. At 120min the release of autocrine EGF becomes apparent and a second ERK-PP peak is observable: **–** simulation of impulse-like stimulation with 0.5ng/ml EGF for 5min, • experimental data.

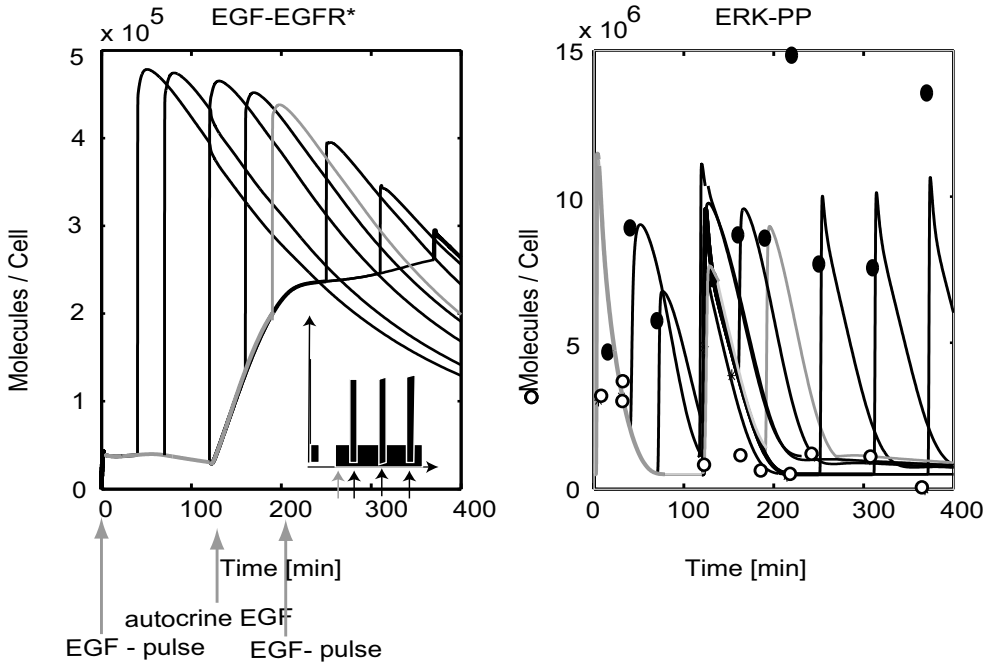

Fig. 3.18: Restimulation of A431 cells with 0.5ng/ml initial EGF impulse and 50ng/ml for the second EGF impulse **–** simulation for a 0.5ng/ml - 50ng/ml stimulation, • experimental data for a 0.5ng/ml - 50ng/ml EGF stimulation in comparison with experimental data **o** for a 50ng/ml - 50ng/ml EGF stimulation, - one example of the response pattern triggered by restimulation.

conclude that the negative feedback is not responsible for the longterm desensitization as for both concentrations 50ng/ml and 0.5ng/ml EGF the ERK activation is identical.

Therefore the effect of the negative feedback on SOS should be identical. Thus the negative feedback is not the reason for the observed desensitization effect.

To conclude, we suggest with the use of the mechanistic model and experiments that neither receptor degradation nor the negative feedback from ERK-PP to SOS is the reason for longterm desensitization of the cells to new signals. Rather, it seems that the decrease of certain key adapter molecules is the reason for the observed phenomena.

However, as shown in Figure 3.19 by the gray circles the kinetics of the second peak induced by radiation is very different from the first peak. This data was taken from [26]. The second ERK peak depicted by gray circles decreases much slower. It reaches basal level only after 200min whereas the first peak is back to its basal level already after 60min. In order to describe the published experimental data with the help of our model, the activity of phosphatases must decrease. It is widely thought that radiation may affect the phosphatase activity.

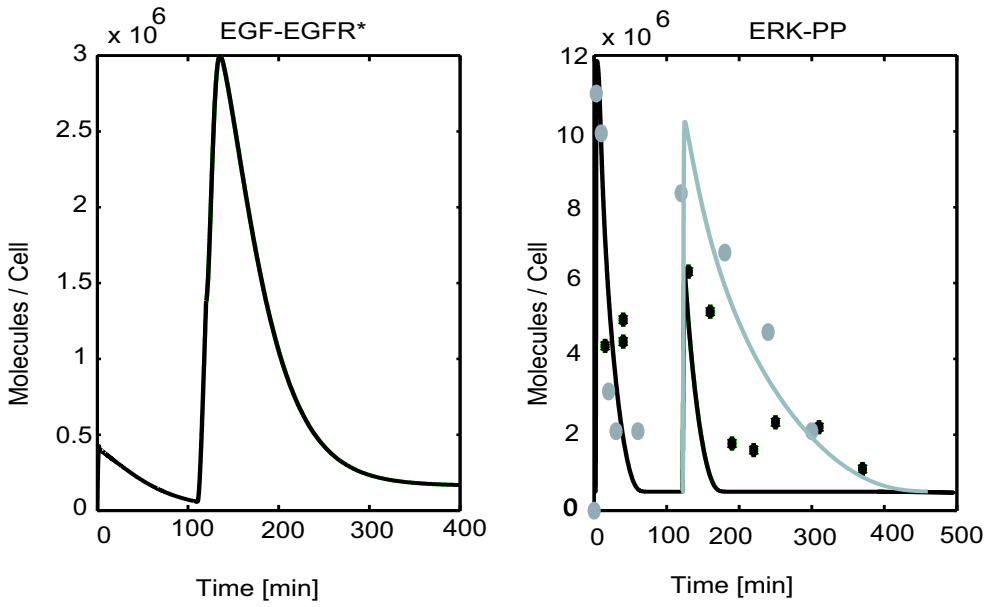

Fig. 3.19: Stimulation with 0.5ng/ml EGF: • published by Dent et. al. for a radiation induced second peak of ERK activation: • experimental data for the restimulation experiment with 0.5ng/ml-50ng/ml EGF, – simulation result assuming that radiation does not affect the phosphatase activity, - simulation result with the assumption that there is a decrease in phosphatase activity caused by radiation.

It is only possible to describe the experimental data published by Dent et. al. [26] and autocrine signaling in nature, if a stimulus does not trigger all of the EGF receptors on the cell surface

and enables thus a second stimulation. Furthermore to describe the second, much broader ERK-PP peak observed in the radiation experiments, phosphatase activity must be affected by radiation in order to obtain a second broader peak.

Tab. 3.4: Kinetic Rates used in the mathematical model of the EGF induced MAP kinase cascade part I

Reaction Number	Equation		Kinetic Parameter	References
v1	[EGFR]+[EGF]↔[EGF-EGFR]	k_1=3e7;	k_{-1}=3.8e-3	[13] [22]
v2	[EGF-EGFR]+[EGF-EGFR]↔[(EGF-EGFR)2]	k_2=1e7;	k_{-2}=0.1	[81]
v3	[(EGF-EGFR)2]↔[(EGF-EGFR*)2]	k_3=1;	k_{-3}=0.01	[81]
v4	[(EGF-EGFR*)2-GAP-Grb2]+[Prot]↔ [(EGF-EGFR*)2-GAP-Grb2-Prot]	k_4=1.73e-7 [Receptors/s]	k_{-4}=1.66e-3 [1/s]	[139]
v5	[(EGF-EGFR*)2-GAP-Grb2-Prot]→ [(EGF-EGFRi*)2-GAP-Grb2]+[Proti]	k_5=0.03 - 0.0033 [Receptors/s]		[170]
v6	[EGFR]↔ [EGFRi]	k_6=5e-5	k_{-6}=5e-3	[139]
v7	[(EGF-EGFR*)2]→ [(EGF-EGFR*i)2]]	k_7=5e-5		[139]
v8	[(EGF-EGFR*)2]+[GAP] ↔ [(EGF-EGFR*)2-GAP]	k_8=1e6	k_{-8}=0.2	Estimation
v9	[(EGF-EGFR*)2-GAP]]→ [(EGF-EGFRi*)2-GAP]]	k_9=5e-5		[139]
v10	[EGFRi]+[EGFi] ↔ [EGF-EGFRi]	k_{10}=1.4e5	k_{-10}=0.011	[139]
v11	[EGF-EGFRi]+[EGF-EGFRi]↔[(EGF-EGFRi)2]	k_{11}=1e7;	k_{-11}=0.1	[81]
v12	[(EGF-EGFRi)2]↔[(EGF-EGFRi*)2]	k_{12}=1;	k_{-12}=0.01	[81]
v13	→ [EGFR]	k_{13}=2.17 [Receptors/s];		[139]
v14	[(EGF-EGFRi*)2]+[GAP] ↔ [(EGF-EGFRi*)2-GAP]	k_8=1e6	k_{-8}=0.2	Estimation
v15	[Prot] → [Proti]	k_{15}=1e4		[139]
v16, 63	[(EGF-EGFR*)2-GAP]+[Grb2] ↔[(EGF-EGFR*)2-GAP-Grb2]	k_{16}=1e7;	k_{-16}=0.055	k_{16}= k_{24} k_{-16}=k_{-24}*0.5
v17, 64	[(EGF-EGFR*)2-GAP-Grb2] + [Sos] ↔ [(EGF-EGFR*)2-GAP-Grb2-Sos]	k_{17}=1e7;	k_{-17}=0.06	[81]
v18, 65	[(EGF-EGFR*)2-GAP-Grb2-Sos] +[Ras-GDP] ↔ [(EGF-EGFR*)2-GAP-Grb2-Sos-Ras-GDP]	k_{18}=1.5e7;	k_{-17}=1.3	Estimation
v19, 66	[(EGF-EGFR*)2-GAP-Grb2-Sos-Ras-GDP] → [(EGF-EGFR*)2-GAP-Grb2-Sos]+[Ras-GTP]	k_{19}=0.5	k_{-19}=1e5	[129]
v20, 67	[Ras-GTP*]+[(EGF-EGFR*)2-GAP-Grb2-Sos]↔[(EGF-EGFR*)2-GAP-Grb2-Sos-Ras-GTP]	k_{20}=2.1e6	k_{-20}=0.4	Estimation
v21, 68	[(EGF-EGFR*)2-GAP-Grb2-Sos-Ras-GTP] ↔ [(EGF-EGFR*)2-GAP-Grb2-Sos]+[Ras-GDP]	k_{21}=0.023	k_{-21}=2.2e5	Estimation
v22, 69	[(EGF-EGFR*)2-GAP]+[Shc]↔ [(EGF-EGFR*)2-GAP-Shc]	k_{22}=2.1e7	k_{-22}=0.1	[109]
v23,70	[(EGF-EGFR*)2-GAP-Shc]↔ [(EGF-EGFR*)2-GAP-Shc*]	k_{23}=6	k_{-22}=0.6	[109] [81]
v24,71	[(EGF-EGFR*)2-GAP-Shc*]+[Grb2]↔[(EGF-EGFR*)2-GAP-Shc*-Grb2]	k_{24}=1e7	k_{-24}=0.55	[12]
v25, 72	[(EGF-EGFR*)2-GAP-Shc*-Grb2]+[Sos]↔ [(EGF-EGFR*)2-GAP-Shc*-Grb2-Sos]	k_{25}=1e7	k_{-25}=0.0214	[81]
v26, 73	[(EGF-EGFR*)2-GAP-Shc*-Grb2-Sos]+[Ras-GDP]↔ [(EGF-EGFR*)2-GAP-Shc*-Grb2-Sos-Ras-GDP]	k_{26}=1.5e7	k_{-26}=1.3	as k_{18}, k_{-18}
v27, 74	[(EGF-EGFR*)2-GAP-Shc*-Grb2-Sos-Ras-GDP] ↔ [(EGF-EGFR*)2-GAP-Shc*-Grb2-Sos]+[Ras-GTP]	k_{27}=0.5	k_{-27}=1e-5	as k_{19}, k_{-19}
v28, 75	[Raf]+[Ras-GTP] ↔ [Raf-Ras-GTP]	k_{28}=1e6	k_{-28}=0.0053	[144]
v29,76	[Raf-Ras-GTP] ↔ [Raf*]+[Ras-GTP*]	k_{29}=1	k_{-29}=7e5	[144]
v30, 77	[Ras-GTP*] + [(EGF-EGFR*)2-GAP-Shc*-Grb2-Sos] ↔ [(EGF-EGFR*)2-GAP-Shc*-Grb2-Sos-Ras-GTP]	k_{30}=7.9e6	k_{-30}=0.3	as k_{20}, k_{-20}

Michaelis Menten constants are given in [nM], first order constants in 1/s and second order rate constants in [M^{-1} s^{-1}].

v106, v109, v112, v115, v121, v124 are aquivalent to k4; v102, v103, v104, v105, v108, v111, v114, v117, v120, v123 are aquivalent to k6 v107, v110, v113, v116, v119, v122, v125 are aquivalent to k5;

Tab. 3.5: Kinetic Rates used in the mathematical model of the EGF induced MAP kinase cascade part II

Reaction Number	Equation		Kinetic Parameter	References
v31, 78	[(EGF-EGFR*)2-GAP-Shc*-Grb2-Sos-Ras-GTP]↔ [(EGF-EGFR*)2-GAP-Shc*-Grb2-Sos] + [Ras-GDP]	k_{31}=0.023	k_{-31}=2.2e5	as k_{21}, k_{-21}
v32, 79	[(EGF-EGFR*)2-GAP-Shc*-Grb2-Sos]↔ [(EGF-EGFR*)2-GAP]+[Shc*-Grb2-Sos]	k_{32}=0.1	k_{-32}=2.45e5	Estimation
v33, 80	[Shc*-Grb2-Sos]↔ [Grb2-Sos] + [Shc*]	k_{33}=0.2	k_{-33}=2.1e7	[81]
v34, 81	[(EGF-EGFR*)2-GAP-Grb2-Sos]↔ [(EGF-EGFR*)2-GAP]+[Grb2-Sos]	k_{34}=0.03	k_{-34}=4.5e6	[81]
v35, 82	[Grb2-Sos] ↔ [Grb2]+[Sos]	k_{35}=0.0015	k_{-35}=4.5e6	[81]
v36	[Shc*] → [Shc]	$Vmax_{36}$=1.7	Km_{36}=340	[81]
v37, 81	[(EGF-EGFR*)2-GAP-Shc*] ↔ [(EGF-EGFR*)2-GAP]+[Shc*]	k_{37}=0.3	k_{-37}=9e5	[81]
v38	[Shc*] + [Grb2] ↔ [Shc*-Grb2]	k_{38}=3e7	k_{-38}=0.055	as k_{24}, k_{-24}
v39, 82	[(EGF-EGFR*)2-GAP-Shc*-Grb2] ↔[(EGF-EGFR*)2-GAP]+ [Shc*-Grb2]	k_{39}=0.3	k_{-37}=9e5	as k_{37}, k_{-37}
v40	[Shc*-Grb2]+[Sos]↔[Shc*-Grb2-Sos]	k_{40}=3e7	k_{-40}=0.064	[81]
v41,83	[(EGF-EGFR*)2-GAP-Shc*]+[Grb2-Sos] ↔ [(EGF-EGFR*)2-GAP-Shc*-Grb2-Sos]	k_{41}=3e7	k_{-41}=0.0429	Estimation
v42, 84	[Raf*]+[Phosphatase1]↔[Raf*-Phosphatase1]	k_{42}=7.17e7	k_{-42}=0.2	[71]
v43, 85	[Raf*-Phosphatase1] →[Raf]+[Phosphatase1]	k_{43}=1 [1/s]		[71]
v44, 86	[MEK] +[Raf*] ↔ [MEK-Raf*]	k_{44}=1.1e7	k_{-41}=0.001833	[36], [71]
v45, 87	[MEK-Raf*] → [MEK-P] + [Raf*]	k_{45}=1 [1/s]		[36], [71]
v46, 88	[MEK-P] +[Raf*] ↔ [MEK-P-Raf*]	k_{46}=1.1e7	k_{-46}=0.001833	[36], [71]
v47, 89	[MEK-P-Raf*] → [MEK-PP] + [Raf*]	k_{47}=2.9 [1/s]		[36], [71]
v48, 90	[MEK-PP]+[Phosphatase2]↔[MEK-PP-Phosphatase2]	k_{48}=1.43e7	k_{-48}=0.8	[71]
v49, 91	[MEK-PP-Phosphatase2] → [MEK-P]+[Phosphatase2]	k_{49}=0.058		[71]
v50, 92	[MEK-P]+[Phosphatase2]↔[MEK-P-Phosphatase2]	k_{50}=2.5e5	k_{-50}=0.5	[71]
v51, 93	[MEK-P-Phosphatase2] → [MEK]+[Phosphatase2]	k_{51}=0.058		[71]
v52, 94	[ERK]+[MEK-PP] ↔ [ERK-MEK-PP]	k_{52}=1.1e5	k_{-52}=0.033	[36], [71]
v53, 95	[ERK-MEK-PP] → [ERK-P]+[MEK-PP]	k_{53}=16		[71]
v54, 96	[ERK-P]+[MEK-PP] ↔ [ERK-P-MEK-PP]	k_{54}=1.1e5	k_{-54}=0.033	[36], [71]
v55, 97	[ERK-P-MEK-PP] → [ERK-PP]+[MEK-PP]	k_{55}=6.7		[71]
v56, 98	[ERK-PP]+[Phosphatase3]↔ [ERK-PP-Phosphatase3]	k_{56}=1.45e7	k_{-56}=0.6	[71]
v57, 99	[ERK-PP-Phosphatase3] → [ERK-P]+[Phosphatase3]	k_{57}=0.27 [1/s]		[71]
v58, 100	[ERK-P]+[Phosphatase3]↔ [ERK-P-Phosphatase3]	k_{58}=5e6	k_{-58}=0.5	[71]
v59, 101	[ERK-P-Phosphatase3] → [ERK]+[Phosphatase3]	k_{59}=0.3 [1/s]		[71]
v60	[EGF-Ri] → [EGF-Rideg]	k_{60}=6.67e-4 [1/s]		[139]
v61	[EGFi] → [EGFideg]	k_{61}=1.67e-4 [1/s]		[139]
v62	[(EGF-EGFRi*)2] → [(EGF-EGFRi*)2deg]	k_{62}=6.67e-4 [1/s]		[139], as k_{62}

Michaelis Menten constants are given in [nM], first order constants in 1/s and second order rate constants in [M^{-1} s^{-1}].

v106, v109, v112, v115, v121, v124 are aquivalent to k4; v102, v103, v104, v105, v108, v111, v114, v117, v120, v123 are aquivalent to k6 v107, v110, v113, v116, v119, v122, v125 are aquivalent to k5;

3.3 Investigation of Virtual Inhibitors of the MAP Kinase Cascade

Receptor Kinase Inhibition

Growth factors such as the epidermal growth factor play an important role in cell proliferation. Their absence can inhibit or arrest cell cycle progression, or cause cells to undergo apoptosis [1]. The importance of growth factors for tumor cell growth has been extensively shown. Clinical studies indicate that overexpression of growth factor receptors, which occurs commonly in human tumors, often correlates with poorer prognosis in primary breast cancers [155]. Due to these facts, inhibitors against the human EGF receptor have been developed [40]. Constitutive activation of the MAPK cascade may contribute to malignant progression of many human cancers [97]. Although the causes of MAPK activation differ among tumors, constitutive signaling from cell surface tyrosine kinase receptors contributes in many cancers to activation of the Ras-Raf-MEK-MAPK pathway. For example, the epidermal growth factor receptor is overexpressed up to 20% in breast cancer cells [32]. Moreover, HER2/c-ErbB-2, which activates the Ras-MAPK pathway as well, is overexpressed up to 30% in breast cancer cells [32].

It is widely anticipated that cells encode external information in terms of the temporal and spatial pattern of the activation of signaling proteins. As mentioned above, the temporal pattern of ERK activation determines in many cell types the fate of the cell. A reason for this could be e. g. that sustained ERK activation causes ERK to translocate to the nucleus, whereas a transient ERK activation does not show massive translocation to the nucleus [82]. This might correspond with the observations made for p27, which is activated by mitogenic signal transduction pathways, including Ras-dependent activation of the MAPK pathway. The protein p27 is known as a G_1 to S phase regulator. During G_o and early G_1 p27 binds tightly and inhibits cyclin E1-cdk2. During G_1 to S phase progression, proteolysis of p27 increases, leading to p27 protein loss as cells enter S phase. Proteolysis is regulated by phosphorylation of p27. In many cancers, p27 degradation is increased [32]. It is known that MAPK can phosphorylate p27 *in vitro* and reduce the ability of recombinant p27 to bind and inhibit cdk2 *in vitro* [79]. For human breast cancer cells it could be shown that constitutive MEK/MAPK activation alters p27 phosphorylation and reduces p27 protein levels, which in turn stimulates tumor growth [32].

Due to these facts there is a strong rationale supporting the continued development of

MEK/MAPK inhibitory drugs. The mathematical model describing the EGF induced MAP kinase cascade, as presented here, offers the possibility to test virtual inhibitors and reveal the most efficient target proteins within the presented pathway.

In the following we will show simulation studies, where virtual inhibitors against the EGF receptor have been applied and their inhibitory effect has been simulated. We will discuss the effect of different affinities, the effect of receptor synthesis and discuss how a receptor kinase inhibitor can affect the dynamics of the ERK signal. The gray arrows in the biochemical reaction scheme in Figure 3.2 indicate the additional biochemical reactions of the evaluated inhibitors on the level of the EGF receptor, Grb2 and MEK respectively.

Figure 3.20 represents the effect of EGF receptor inhibition on receptor complex formation as well as on the signal pattern.

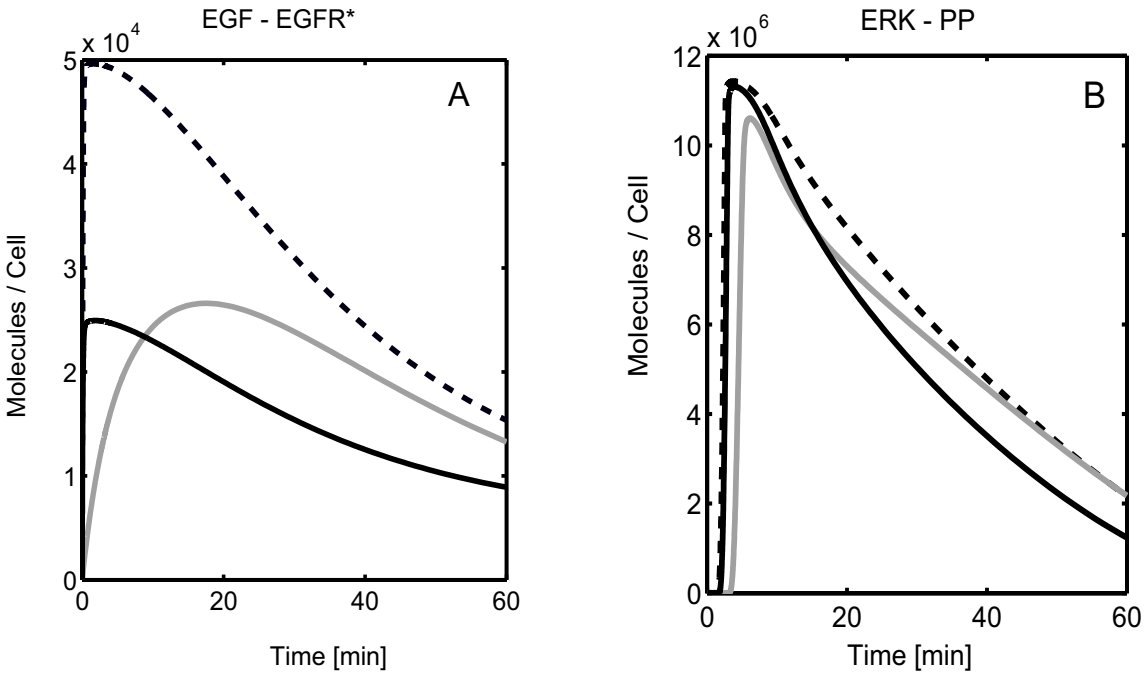

Fig. 3.20: Simulation of receptor kinase inhibition: - - in the absence of inhibitor, – in the presence of a reversible inhibitor and in the presence of an irreversible inhibitor **-**.

As depicted in Figure 3.20A, the simulated lines represent the dynamics of receptor complex formation after EGF stimulation, in the presence and absence of a receptor kinase inhibitor. In the presence of an inhibitor, which is assumed to bind competitively with EGF to the EGF receptor, the pattern of receptor complex formation strongly depends on the affinity of the receptor. The gray solid line shows the inhibitory effect of a reversible inhibitor with a KD of 40nM

whereas the black line describes the inhibitory effect of an irreversible inhibitor.

As mentioned above, the dynamic pattern of ERK activation seems to determine the cell fate: a sustained ERK-PP signal leads to cell proliferation whereas a differentiated ERK activation triggers cell differentiation or cell survival [98]. In this respect it seems to be very important in which way the inhibitor effects the dynamics of the ERK signal, which in turn activates different transcription factors like c-fos and c-jun.

As described in Figure 3.20B the irreversible inhibitor in fact reduces the number of available receptors, whereas the reversible inhibitor dilutes the EGF solution and the ERK signal is comparable with the pattern of a lower EGF concentration (Compare Figure 3.5). Due to this fact we will not measure the inhibitory effect I by the maxima but will compare the integral of the function f_I describing the ERK activation in the presence of an inhibitor and the integral of the function f_o, which describes ERK activation in the absence of an inhibitor. After 90min the ERK activation has reached again its basal level and perfect adaptation has occurred. Therefore, we integrate from t=0 to 90min. Likewise the inhibitory effect I in [%] can be derived as follows:

$$I[\%] = (1 - \frac{\int_0^{90min} f_I dt}{\int_0^{90min} f_o dt})100. \tag{3.23}$$

In Figure 3.25 the dose response curves for different inhibitors are presented. In this simulation the inhibitory effect of an irreversible inhibitor and an inhibitor with a KD of 40nM have been examined. In the upper graph the inhibition of the receptor kinase over time and in the lower graph the ERK inhibition over time is presented. For all affinities the amplifying effect of the MAP kinase cascade is obvious. An inhibition of 80% of the receptor complex formation results in an inhibition of the ERK phosphorylation of about 40 - 50%. This is consistent with the concentration studies of ERK activation shown before in Figure 3.5. As we compare the integrals of the signals and not the peak of ERK phosphorylation, the effective inhibitory effect is bigger due to the time shift of the ERK signal by examining the maximum of ERK activation, a receptor inhibition of 80% results in a 30% reduction of maximal ERK activation.

These results might serve for an explanation why the inhibition of the receptor tyrosine kinase often fails to suppress tumor formation [117], though in respect of receptor inhibition the inhibitor seems to be quite efficient. Surprisingly, a small fraction of phosphorylated EGF receptors is

sufficient to trigger at least 50% of the maximal ERK activation. For this example, mathematical models can serve as a useful tool to identify target molecules and explain experimental findings like the discrepancy of the complete inhibition of the receptor kinase in the pM range of inhibitor concentration *in vitro* [44] and the inhibition of cell proliferation in the μM range of inhibitor application [15]. Possible reasons for this discrepancy will be discussed later in this chapter.

Figure 3.25 shows a plateau for the dose response curve of ERK-PP inhibition, where about 50% of the maximal ERK activation is inhibited. This plateau of ERK-PP inhibition is characterized by a larger ERK inhibition as the affinity of the inhibitor increases. Setting the rate of receptor synthesis to zero, the plateau of ERK inhibition disappears as shown in Figure 3.25. Likewise, the continuous synthesis of new receptors complicates a successful inhibition of receptor signaling on the level of the receptor itself.

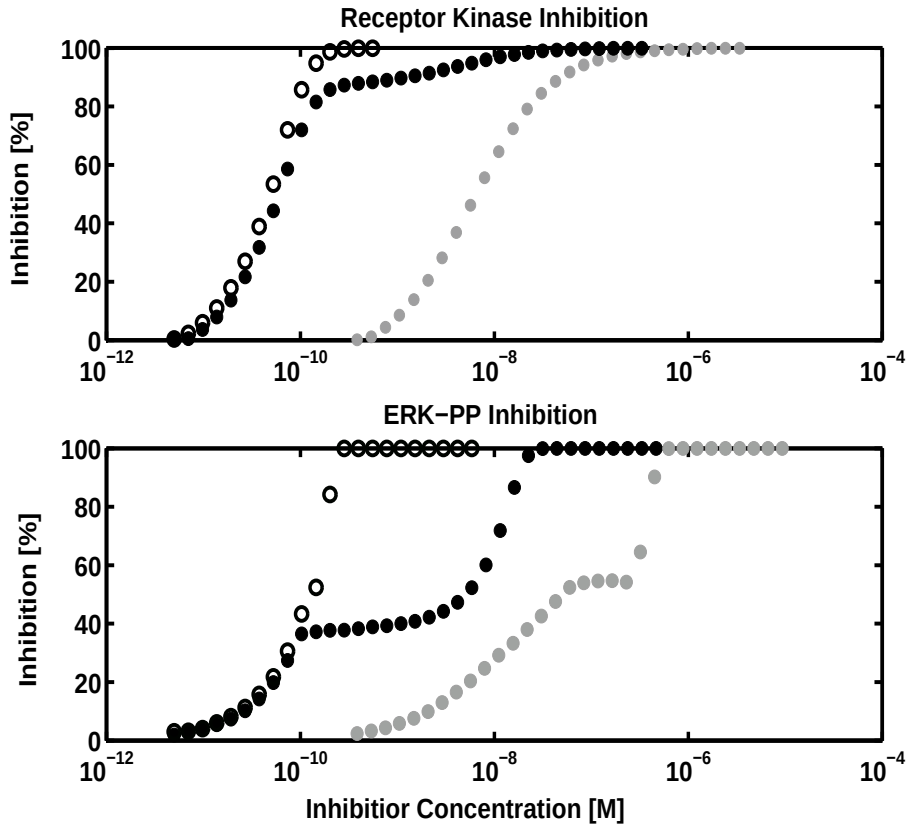

Fig. 3.21: Dose response curve of reversible and irreversible receptor kinase inhibition with and without receptor synthesis: ● reversible receptor kinase inhibition KD = 40nM, ● irreversible receptor kinase inhibition with receptor synthesis and ○ receptor synthesis rate k_{13} =0.

In biological experiments inhibitor studies are usually done by preincubating the cells with in-

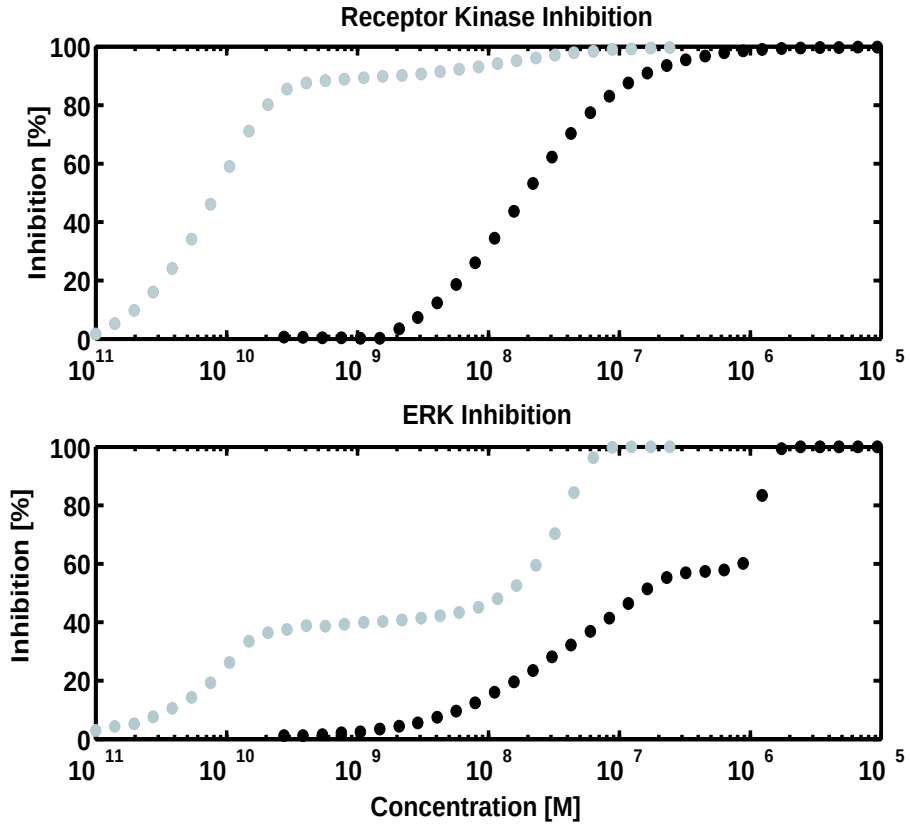

Fig. 3.22: Dose response curve of irreversible receptor inhibition with and without preincubation: ● with preincubation, ● without preincubation with inhibitor.

hibitor for a certain amount of time. This ensures that the inhibitor has diffused into the cell and has already reached steady state, when the stimulus is added. Therefore, we are interested, if it is possible to simulate the effect of preincubation of cells with a receptor inhibitor of ERK-PP inhibition. In Figure 3.22 the black dots represent the simultaneous addition of EGF and inhibitor and the gray dots show the inhibitory effect if the cells are preincubated long enough that the receptors are saturated. Obviously preincubation improves the performance of the inhibitor enormously. The comparison of the amount of inhibitor which is necessary to lead to a 100% inhibition of ERK-PP is 10 fold less when cells are preincubated.

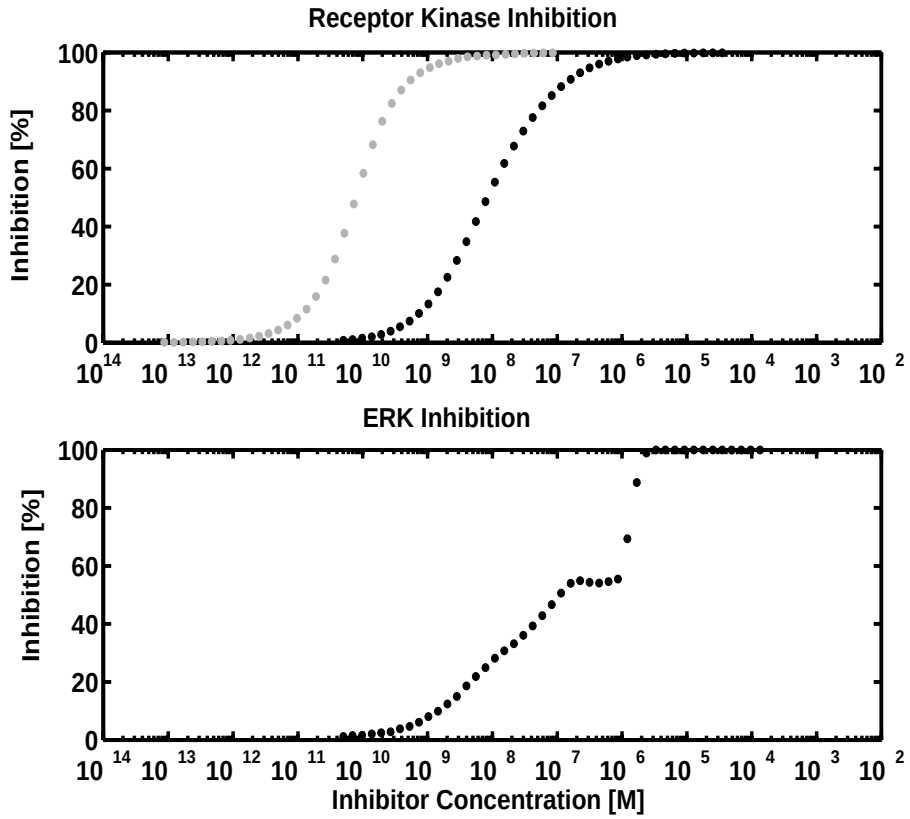

Fig. 3.23: Competition of ATP and inhibitor for the same binding domain: Explanation of the discrepancy between *in vivo* and *in vitro* studies ● without ATP ● without ATP.

In the simulation studies described above an inhibitor that competes with EGF for its binding domain has been studied. In the following the inhibitor PD153035 will be discussed, which is known to inhibit the epidermal growth factor kinase with a 5pM inhibition constant [44]. *In vitro*, PD153035 inhibits the EGF receptor tyrosine kinase by 50% at a concentration of 29pM [44]. In contrast to the *in vitro* studies, PD153035 was found to inhibit receptor phosphorylation

completely *in vivo* at dose levels of 350nM or higher [15]. As indicated in Figure 3.23 this corresponds well with the simulation results. The gray dots representing the simulation of receptor kinase inhibition without ATP where 50% inhibition is achieved at 35pM. Whereas if ATP and the inhibitor are competing for the same binding domain, total inhibition is obtained at 1μM. It has been hypothesized, that the differences between the *in vitro* studies and the inhibition of the receptor phosphorylation that was observed in actual cell lines might be due to PD153035 being competitive with ATP [44]. This hypothesis is supported by the simulation results shown. The *in vitro* experiments use about 10μM ATP which is a very small concentration of ATP compared to the amounts that can usually be found in cells e.g. for HeLa cells in the order of 10mM [176], [100].

Besides the inhibition of the receptor tyrosine phosphorylation, PD153035 was found to inhibit EGF dependent mitogenesis by 50% at a concentration of 0.08μM, which results in a receptor phosphorylation inhibition by 95% and a corresponding ERK inhibition of 55%. It seems that the integral of the ERK signal is related to the antiproliferative effects of the inhibitor. This correlation can also be found for the ZD1839 inhibitor [3], which is like PD153035 a small molecule inhibitor. In the paper describing the receptor kinase inhibition by ZD1839 the prediction of the simulation results are validated by the experimental findings described by Anderson et. al. [3]. For MDA-MB-231 cells an almost complete inhibition with 1μM of inhibitor is found, but despite that, still noticeable amounts of ERK get phosphorylated. These results support the model predictions that even a small amount in the order of 20% of activated receptors is sufficient to trigger a 70% ERK activation, which may still be sufficient to induce cellular responses.

Grb2 inhibition by its SH2 and SH3 domain

Given the key role of Ras in the mitogenic signaling by receptor tyrosine kinases, several targets upstream of Ras may prove to be excellent targets for drugs in the treatment of cancer caused by oncongenic tyrosine kinases. In the following we will discuss the possibility of preventing Ras dysfunction by the inhibition of Grb2. The adaptor protein Grb2 is comprised of one SH2 surrounded by two SH3 domains and interacts by the means of Src homology (SH2) with the phosphotyrosine residues of target molecules such as the EGF receptor or the adapter protein Shc. Grb2 recognizes proline-rich sequences of Sos via its SH3 domains and this leads to Ras activation. Inhibitors of SH2 and SH3 domains were designed with the aim of interrupting Grb2

recognition [46].

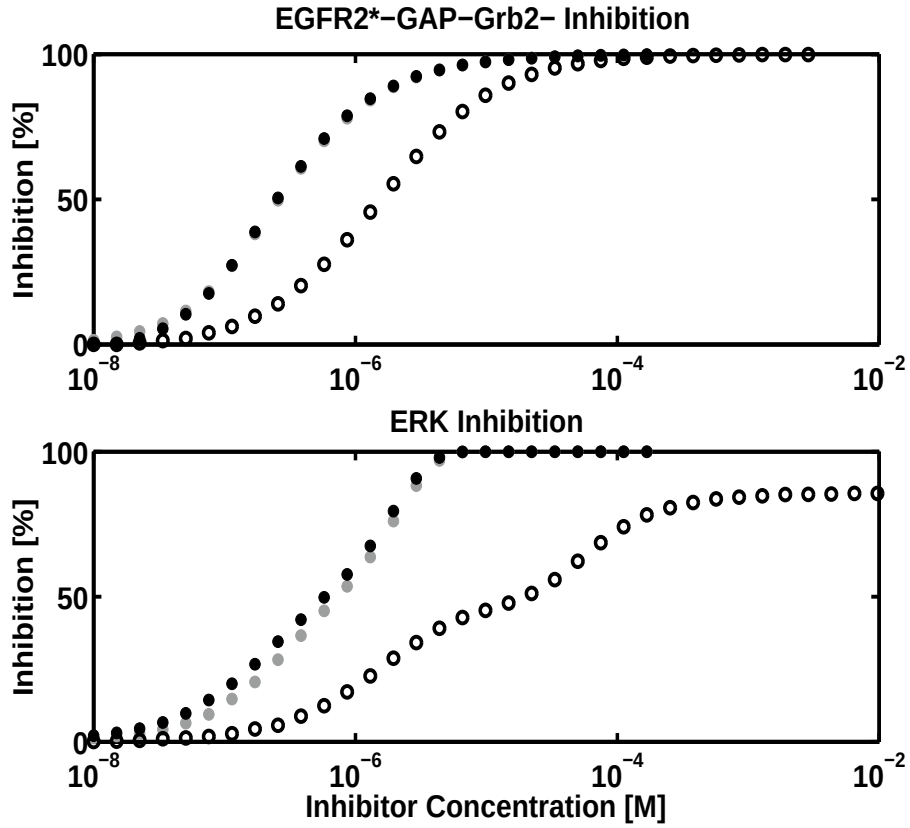

Fig. 3.24: Inhibition of ERK phosphorylation by Grb2: ○ inhibition of its SH3 domain, ● inhibition of its SH2 domain ● and inhibition of its SH2 and its SH3 domain.

In our model we include SH2 and SH3 domain inhibitors in order to evaluate the inhibition of the MAP kinase pathway on the level of the adapter molecule Grb2. We analyze the inhibitory effect for each of the domains selectively, assuming that they are characterized by the same inhibitory constant of K_i=40nM. In Figure 3.24 the upper graph shows the inhibition of the receptor complex formation and the lower graph presents the related ERK inhibition. SH3 inhibition shown in black circles is much less efficient than SH2 domain inhibition depicted by gray dots. At 5μM the SH2 inhibitor blocks ERK activation completely whereas the SH3 domain inhibitor only shows a 50% inhibition of ERK phosphorylation at this concentration.

The simulation studies reveal that the inhibition of the SH2 and SH3 domain is dominated by the SH2 inhibition.

MEK inhibition

Another target molecule in the MAPK cascade is MEK. There is a number of MEK inhibitors on the market like the PD098059, which has an inhibitor constant of K_i= 3 - 14μM. PD098059 displays potent binding to the inactivated and activated MEK-1 form [41]. In respect to clinical applications, a number of MEK inhibitors have shown good oral bioavailability and efficacy in preclinical trials [128].

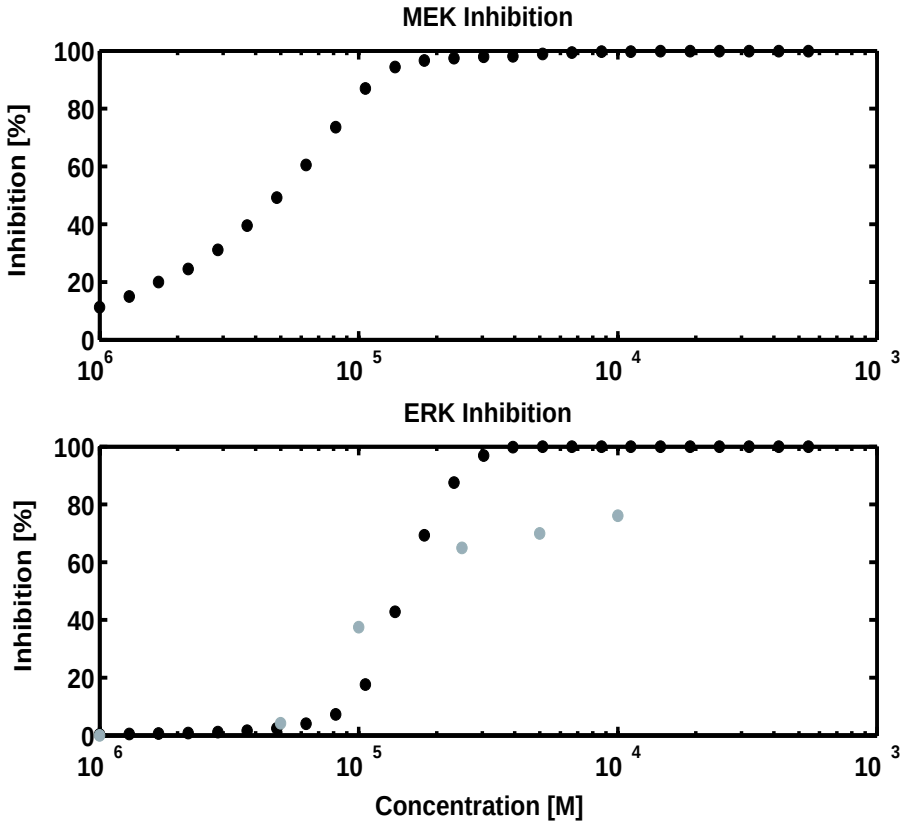

Fig. 3.25: Simulated MEK inhibition in comparison with experimental data: • Simulation of ERK inhibition by a MEK inhibitor using the PD098059 as an example, • experimental data.

Figure 3.25 displays the comparison between experimental data and the simulation of MEK inhibition. In the upper graph the dose response curve of the MEK inhibition and in the lower graph ERK inhibition is represented. The black dots represent the simulation results and the gray dots stand for the experimentally identified ERK inhibition by a MEK inhibitor. Experimentally, the ERK activation has been determined by immunoblotting and has been quantified as described in the appendix. It can be observed that for a concentration range of 1μM to 15μM,

the simulation predicts well the experimentally observed ERK activation without changing any of the kinetic parameters of the model. Full ERK inhibition is only achieved at very high EGF concentrations in the experiment, which is in contradiction to the simulation results. This may be due to the fact that the inhibitor crystallizes at these high concentrations (own observations) and can thus not penetrate into the cells.

Assuming that all the receptor, MEK and ERK inhibitors have the same inhibitory constant of K_i = 40nM, inhibition of ERK activation is most efficient when targeting Grb2. A comparison of the different simulation results reveals that a complete ERK inhibition can be observed at 5μM using a Grb2 inhibitor, whereas total ERK inhibition at the receptor level needs 50μM inhibitor and total ERK inhibition when targeting MEK (data not shown) also requires at least 20μM of inhibitor.

Simultaneous application of two inhibitors

After analyzing different inhibitors selectively, we examine the inhibitory effect of two inhibitors applied simultaneously. We discuss the simultaneous inhibition of EGF receptor and Grb2, EGF receptor and MEK as well as MEK and Grb2, assuming a K_i of 40nM for each inhibitor. As they are efficient at different concentrations we use as initial concentration, the concentration when the inhibitor starts to excite its inhibitory effect. At each concentration we increase the concentration of the second inhibitor continously until it results in a 100% inhibition of ERK activation. In the next step we increase the concentration of the first inhibitor. Likewise we obtain the information about the ERK inhibition for each combination of the two inhibitors in a concentration range of interest. As a result we obtain contour plots as depicted in Figure 3.26, where the color indicates the inhibitory effect. The color white equals a 100% inhibition. The striped area indicates where the combination of the drugs is more beneficial than a single drug to achieve 100 inhibitors can be synergistic in comparison to only one inhibitor.

Comparing the three plots for the combinations of EGF receptor and Grb2, EGF receptor and MEK as well as MEK and Grb2, only the combination of EGF receptor and Grb2 inhibition shows an improved inhibition as shown in Figure 3.26 A, which means in order to obtain a 100% inhibition a smaller amount of each of the inhibitors is necessary. In Figure 3.27 the contour plot is resolved for the inhibitory effect of 50% and a 100% for the combination of a receptor kinase inhibitor and a Grb2 inhibitor. The black circles represent 100% ERK inhibition

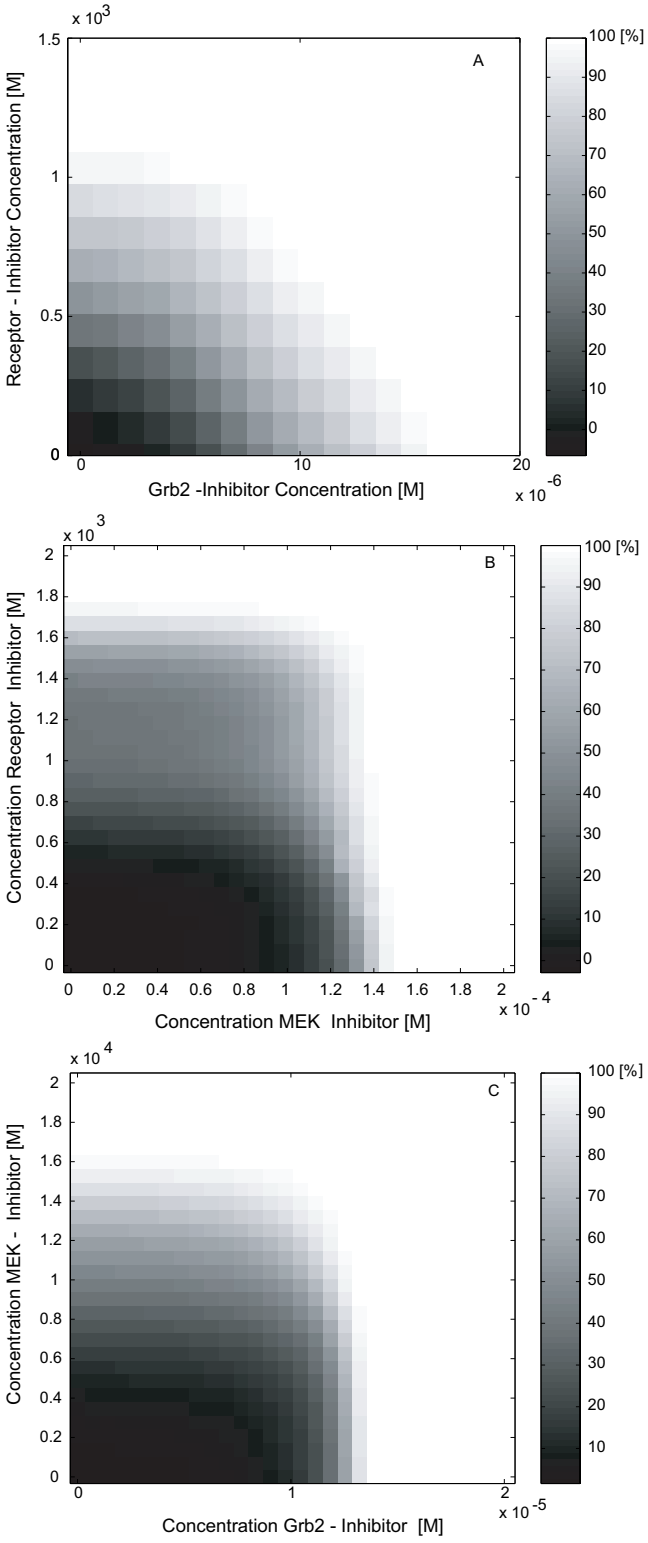

Fig. 3.26: Simultaneous inhibition of two signaling proteins represented in a contour plot: **A** Inhibition of Grb2 and EGFR, **B** Inhibition of MEK and EGFR and **C** Inhibition of MEK and Grb2.

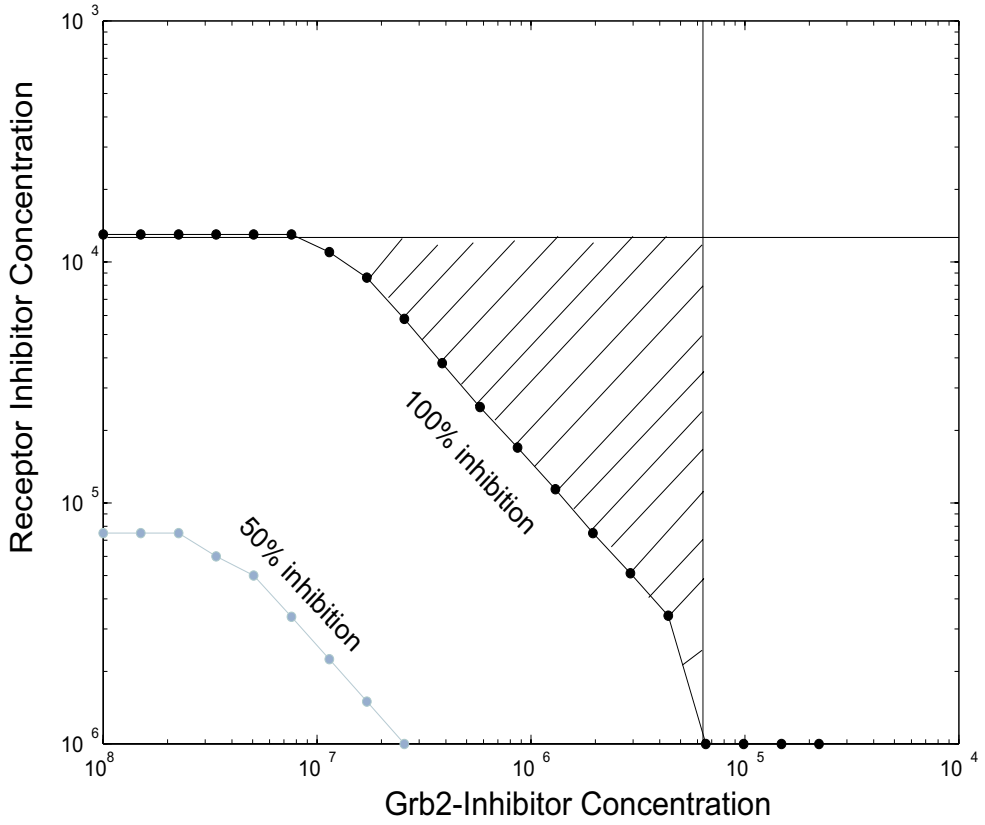

Fig. 3.27: Dose response curve of receptor inhibition and Grb2 inhibition: -●- 100% ERK inhibition, -●- 50 % ERK inhibition. The striped area indicates where the combination of the drugs is more beneficial than a single drug to achieve 100 % inhibition.

and the gray circles represent 50% ERK inhibition. The black lines indicate the concentration of each inhibitor, which is required in order to inhibit ERK activation selectively by one of the inhibitors. The area marked between the asymptotes and the black circles characterizes the area were the combination of two inhibitors leading to a 100% ERK inhibition is most effective.

Chapter 4

System Analysis

In this section we analyze the robustness of the presented mathematical models using the example of the model of the EGF induced MAP kinase cascade. A robust system tracks its desired behavior independently of noise or variation of the system's parameters. In engineering sciences one possibility to achieve robustness is using integral feedback control. This feeds the time integral of the system error, which is usually the difference between the actual output and the desired steady state output, back into the system. This type of control structure ensures that the steady state error approaches zero despite fluctuations in the input or in the system's parameters. The only required condition is the stability of the closed loop.

The degree of robustness in many biochemical networks can be quantitatively investigated. This can be achieved by characterizing a behavioral, a physical or biochemical property while varying systematically the expression level and the rate constants of the network's components. In the following the variation of single parameters and the influence in changes of the expression level of proteins are analyzed. Robust systems allow variations of the values of the biochemical rate constants without changing the systems behavior.

Hence, it should be possible to analyze the subsystems separately. Using the example of the system's behavior of the different steps of the EGF induced MAP kinase cascade we discuss if each step can be treated as a functional unit. Furthermore we compare the system's behavior of the "module" MAP kinase cascade with the "module" MAP kinase cascade embedded into the EGF signal transduction pathway. B. Kholodenko showed that a negative feedback loop combined with the ultrasensitivity of the MAPK cascade can bring about sustained oscillations in the range of minutes to hours in the module MAP kinase cascade [82]. Using the parameter set that results in sustained oscillations, the relevance of a sustained input signal vs. a rather

impulse-like input is discussed. Furthermore the oscillating module is implemented into the full model and the resulting behavior analyzed.

4.1 Evaluation of the robustness of the system

Whilst establishing the computational model and collecting experimental data on the EGF receptor cascade, a great variance in the determined parameters became apparent, with reported differences of one order of magnitude or more. Part of this variation may be attributed to cell type specific differences in expression levels of signaling molecules. However, the model suggests that the EGF receptor induced MAP kinase network is extremely stable towards apparent variations in signaling components. Within a rather wide range neither the number of intracellular signaling proteins per cell nor the rate constants of association and dissociation appear to influence the final biological outcome (ERK-1/2 activation).

Considering the high number of free kinetic parameters the question arises of whether there is only one, specific set of parameters that can describe the system's behavior of interest. In order to assess sensitivity with respect to variation of individual parameters, we took parameter sets known to produce the desired behavior and varied one parameter while holding the remaining parameters fixed. Then we analyzed how much the parameter can be varied without changing the value of ERK activation more than 1%. The results are shown in Figure 4.1. On the x-axis the parameter number which is assigned to the number of the biochemical reaction is indicated and on the y-axis the value of the association or dissociation rate is given. The bold dots indicate the upper and lower bound of a possible parameter variation. The thin horizontal line in the middle of the upper and lower bound represents the actual value used in the model. Within these bounds two or more parameters can be varied without changing the outcome.

As depicted in Figure 4.1A and B, in most cases, the model tolerates a tenfold or even larger variation of the individual parameters. However, there are also parameters where the range of variation is quite small like k_{42}, k_{48} and k_{58}. Interestingly, these are the reactions, which downregulate activation of the MAP kinase cascade components. These parameters, revealed as the most sensitive, are exactly the ones retrieved by the sensitivity analysis with respect to ERK activation as shown in Figure 4.2. Analysis of the dissociation rates, k_{48} and k_{58} as well as the Km values of the MAP kinase cascade reveal these to be most sensitive. The Km values are

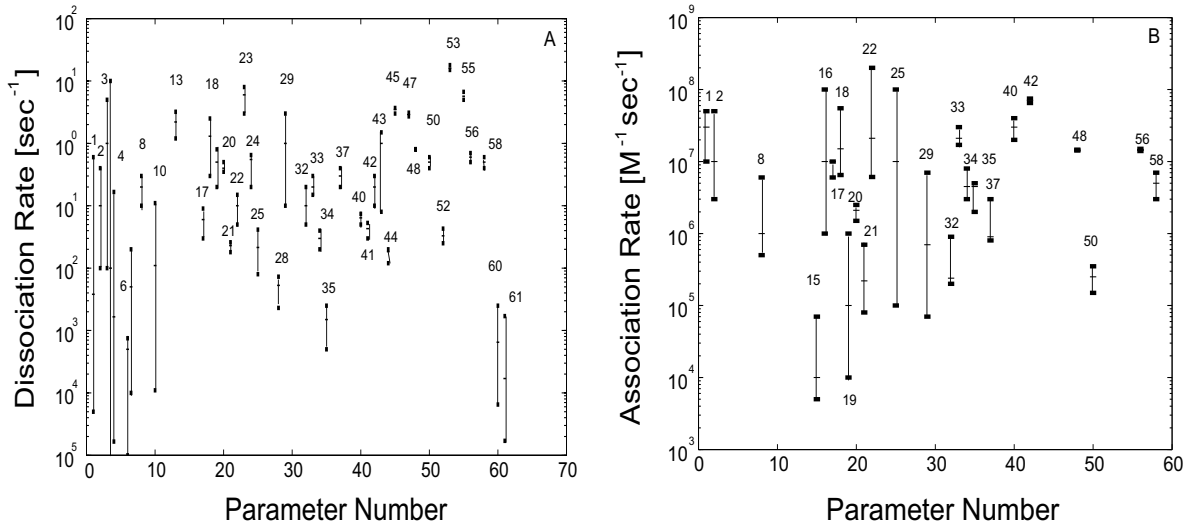

Fig. 4.1: **A** Variation of the dissociation rate k_{off} **B** variation of the association rate k_{on} while keeping the remaining kinetic parameters constant. The numbers on the y-axis represent the parameter number, which corresponds to the reaction number in the biochemical reaction scheme.

represented within Figure 4.2A by the parameter numbers 63 to 65. Regarding the association rates shown in Figure 4.2, sensitive parameters can be found already much earlier than on the level of the MAP kinase cascade like k_{20} and k_{21} which determine the conversion of Ras-GTP to Ras-GDP. From analyzing with the model, the pattern of Ras-GTP activation seems to be of great importance for the following ERK activation, which corresponds exactly with k_{20} and k_{21} being very sensitive parameters. Furthermore we find k_{42}, k_{48} to be very sensitive. These parameters determine the dephosphorylation of Raf* and MEK-PP. In accordance with the importance of the negative regulation with respect to the transient ERK activation, k_{54}, k_{56} and k_{58} show a high sensitivity as well. The latter parameters describe the phosphorylation and dephosporylation of ERK-PP.

Due to the lack of quantitative experimental data, the sensitivity of the system concerning the variation of initial values is of interest. As represented in Figure 4.3 the range of variation for the initial conditions and a fixed set of kinetic parameters is high but the system seems to be less robust to variations of the Ras, MEK and phosphatase concentrations. Therefore the question of fragility vs. robustness of the system can be addressed.

As protein concentrations in different cell lines have almost never been determined, the influence of the change in initial conditions is evaluated with regard to alterations in the system's

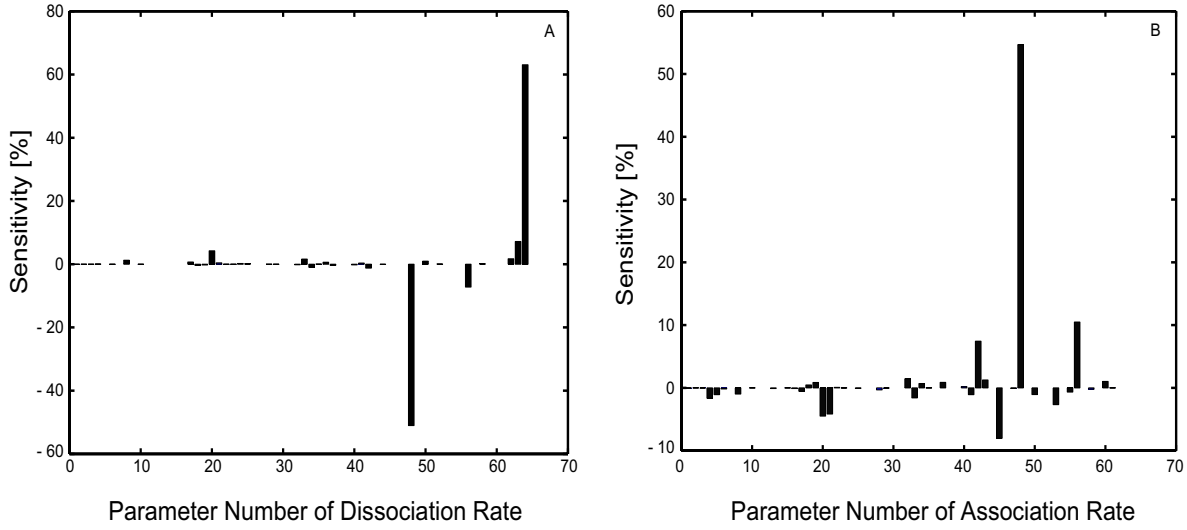

Fig. 4.2: Results of the sensitivity analysis **A** dissociation rates k_{off} **B** association rates k_{on}.

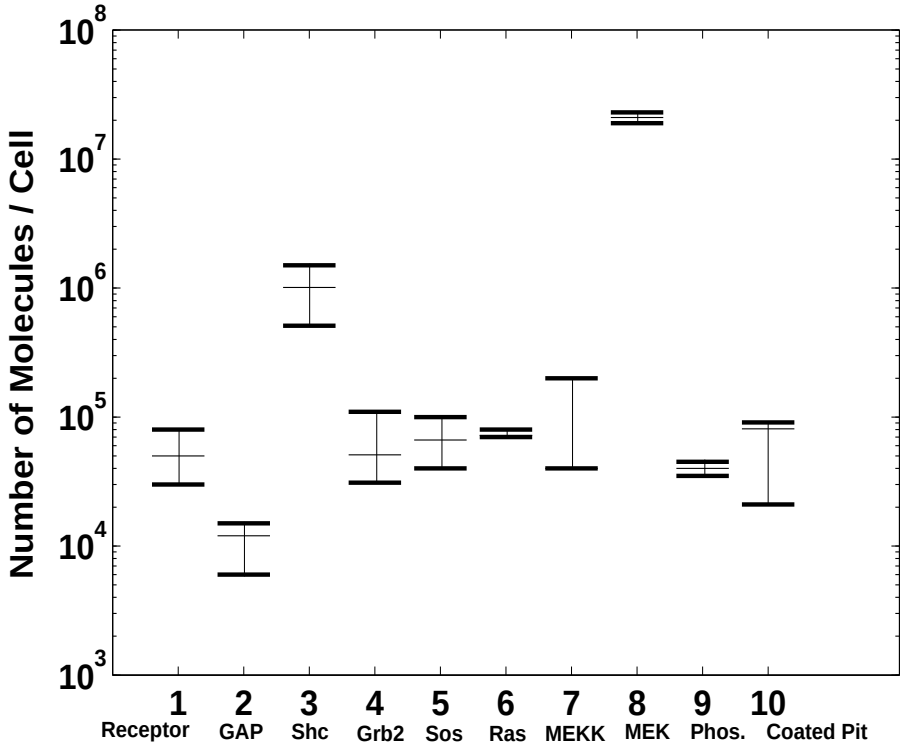

Fig. 4.3: Variation of the initial protein concentrations.

behavior. Therefore we change the initial conditions given in Table 3.1 and reduce the number of Shc molecules from 1.01 x 10^6 to 9 x 10^4, the number of Sos molecules from 6.63 x 10^4 to 2 x 10^4, the number of MEKKK molecules from 40000 to 1800, the number of MEK molecules from 2.1 x 10^7 to 7.2 x 10^5 and the number of ERK molecules from 2.2 x 10^7 to 7.2 x 10^5, the number of phosphatase molecules from 4 x 10^4 for Phosphatase 1 and Phosphatase 2 to 4 x 10^2 and for Phosphatase 3 from 10^7 to 7.2 x 10^4. The latter MAPK protein concentrations correspond to the initial conditions published by Huang and Ferrel [71] for Xenopus oocyte extracts. These concentrations are outside the lower boundary for the initial concentrations still tolerated by the same set of kinetic parameters in the presented model (compare with Figure 4.3). However, equivalent to the model presented in this work, we obtain a new set of kinetic parameters which describes the systems behavior in the same qualitative way. Hence, the gathered experimental data are insufficient to determine an unambiguous parameter set.

In the following Figure 4.4, comparison of the association and dissociation rates for each set of initial conditions is depicted. It can be observed that only a few parameters have to be changed in order to describe the systems behavior if the initial conditions differ from the current model. The parameters represented by a cross are the ones with the higher protein concentrations as initial concentrations and the parameters represented by an open circle are the ones describing the system with the lower initial concentrations. Regarding the dissociation rates the following parameters have to be changed in order to describe the experimental data: the dissociation rate of EGFi k_{10}, k_{32} , k_{33}, describing the dissociation of Shc-Grb2-Sos and Grb2-Sos, k_{43} determining the dephosphorylation of Raf*, k_{45}, k_{47}, k_{49}, k_{51} describing the phosphorylation and dephosphorylation of MEK and k_{53}, k_{54} determine the phosphorylation of ERK. For the association rates the following parameters have to be changed in order to describe the experimental data: association rate of Sos k_{17}, k_{21} in the Ras-GDP - Ras-GTP cycle , k_{28} describing the Raf phosphorylation, k_{44}, k_{46}, k_{52}, k_{54}, describing MEK and ERK phosphorylation. Hence, the change of a certain protein concentration will effect the kinetic parameters of reactions which contain this protein as product of educt. Comparing the range of the change of the parameter values, leads to the conclusion that there are multiplse solutions for different sets of initial conditions leading to the same system behavior. This phenomenon was also observed for a kinetic model describing the segment polarity network [157].

Thus the characteristics described above are intrinsic to its topology rather than to specific

quantitative tuning of kinetic parameters. Due to this fact, it is possible to use mathematical modeling to test hypotheses of possible yet unknown protein-protein interactions, which allow the description of a certain observed characteristic dynamic behavior. Specific protein-protein interactions identified by the mathematical model can consequently be verfied experimentally. Therefore it is possible to test the system's behavior by using the constraints given for protein concentrations and for the kinetic rates of protein-protein interactions, even though we lack a larger set of experimental data to exactly identify the parameters.

Hence, network topologies that embody several different solutions, which seem to be highly robust with respect to the variation of individual parameters,like the signal transduction network discussed in this work, make the system quite indifferent to changes caused by mutations or by envrionmental changes.

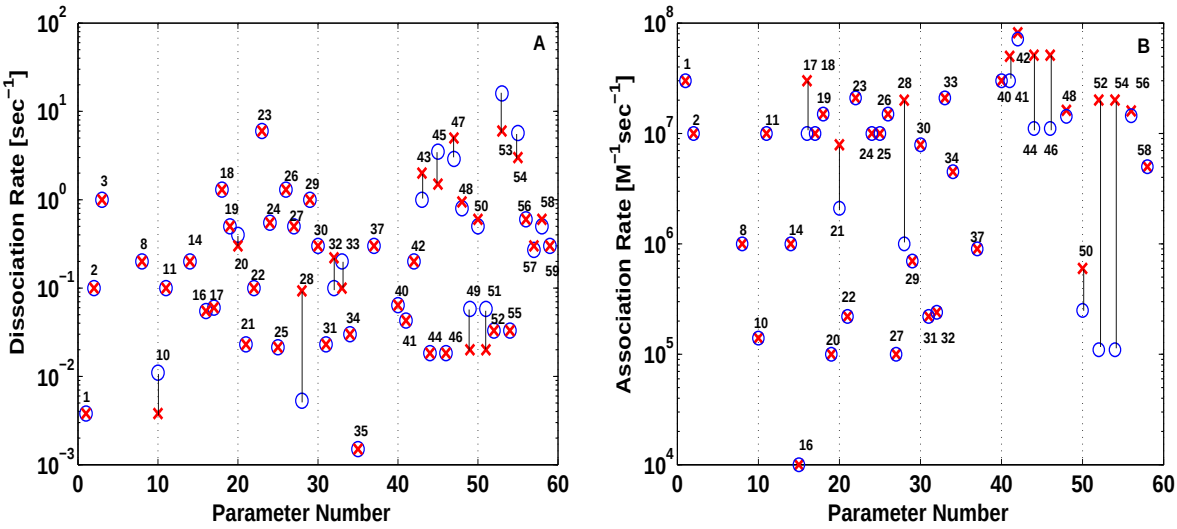

Fig. 4.4: Comparison of the dissociation k_{off} and association rates k_{on} for two different sets of initial conditions; x parameters for the high initial protein concentration as ∘ parameters describing the system with low initial protein concentrations. **A** dissociation rates and **B** association rates.

4.2 MAP Kinase Cascade

In the following we discuss the system's behavior of the MAP kinase cascade and compare the output signal as a function of the number of phosphorylation steps of the cascade as well as of the number of phosphorylation sites. Furthermore, we are interested in the influence of the quasi-steady state approximation for the intermediate complexes (Michaelis-Menten approach,

simplified model) or if we look at the detailed model without any simplification on the dose response curve.

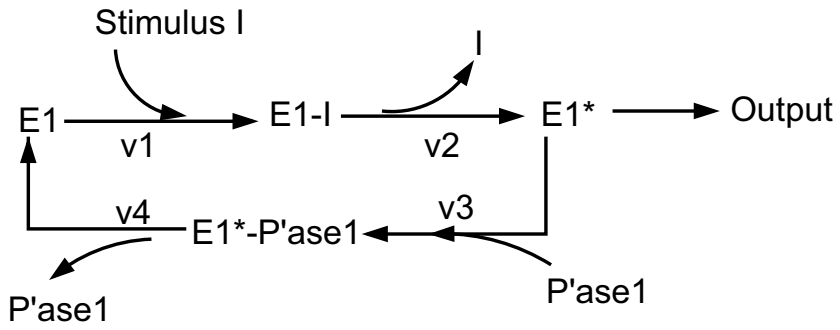

Fig. 4.5: A single step of the MAP kinase cascade with a single phosphorylation.

Stability analysis of the simplified model

On the basis of Figure 4.5 we analyze the stability of the first step of the MAP kinase cascade. The complex E1-I forms from Protein E1 and the input stimulus I, with a rate constant of k_1. E1-I can either dissociate again with rate k_{-1} into E1 and I or proceed to $E1^*$ at the rate k_2 in an irreversible reaction step. $E1^*$ is the output signal of the first step of the MAP kinase cascade, which serves as input signal for the second step. $E1^*$ can be dephosphorylated by P'ase1 and form $E1^*$-P'ase1 in a reversible reaction step with a rate constant of k_3 and k_{-3}. The complex of $E1^*$-P'ase1 proceeds then irreversibly into E1 and P'ase1 at the rate k_4.

Therefore the first step of the MAP kinase cascade can be expressed with the help of the following set of equations:

$$\frac{d[I]}{dt}(t) = -v_1 + v_2 = -k_1[E1][I] + k_{-1}[E1 - I] + k_2[E1 - I], \tag{4.1}$$

$$\frac{d[E1]}{dt}(t) = -v_1 + v_4 = -k_1[E1][I] + k_{-1}[E1 - I] + k_4[E1^* - P'ase1], \tag{4.2}$$

$$\frac{d[E1 - I]}{dt}(t) = v_1 - v_2 = k_1[E1][I] - k_{-1}[E1 - I] - k_2[E1 - I], \tag{4.3}$$

$$\frac{d[E1^* - P'ase1]}{dt}(t) = v_3 - v_4 = k_3[E1^*][P'ase1] - k_{-3}[E1^* - P'ase1] - k_4[E1^* - P'ase1], \tag{4.4}$$

$$\frac{d[E1^*]}{dt}(t) = v_2 - v_3 = k_2[E1 - I] - k_3[E1^*][P'ase1] - k_{-3}[E1^* - P'ase1], \tag{4.5}$$

$$\frac{d[P'ase1]}{dt}(t) = -v_3 + v_4 = -k_3[E1^*][P'ase1] + k_{-3}[E1^* - P'ase1] + k_4[E1^* - P'ase1]. \tag{4.6}$$

The number of equations can be reduced by making use of the conservation of mass. [I]$_T$, [P'ase1]$_T$ and [E1]$_T$ represent the total amount of Stimulus [I], Phosphatase [P'ase1] and Protein [E1] respectively.

Conservation of mass:

$$[I]_T = [I] + [E1 - I], \tag{4.7}$$

$$[P'ase1]_T = [P'ase1] + [E1^* - P'ase1], \tag{4.8}$$

$$[E1]_T = [E1] + [E1^* - P'ase1] + [E1 - I] + [E1^*]. \tag{4.9}$$

According to Briggs and Haldane (1925), we can assume that the rates of formation and breakdown of the complexes of [E1-I] and of [E1*-P'ase1] are essentially equal at all times and thus the change over time in the concentration of [E1-I] and [E1*-P'ase1] should be approximately zero. In quasi steady-steady state, the concentration of the complex satisfies:

$$[E1 - I] = \frac{[E1][I]_T}{\frac{k_{-1}+k_2}{k_1} + [E1]}, \tag{4.10}$$

$$[E1^* - P'ase1] = \frac{[E1^*][P'ase1]_T}{\frac{k_{-3}+k_4}{k_3} + [E1^*]}. \tag{4.11}$$

Thus, we can define the Michaelis-Menten constants as follows:

$$K1 = \frac{k_{-1} + k_2}{k_1}, \tag{4.12}$$

$$K2 = \frac{k_{-3} + k_4}{k_3}. \tag{4.13}$$

The system of ODEs (4.1-4.6) can be simplified to one ODE by the insertion of equations 4.7-4.11 into equation 4.5. Therefore one eigenvalue can be derived.

Stability analysis for nonlinear systems can only be determined in a very small region around a fixed point like the equilibrium points. As this system is nonlinear, we can investigate the nature of the equilibrium points. In order to determine the equilibrium points and the eigenvalues we used the software package Mathematica.

As the general solution of the equilibrium points of the system results in a too complicated expression. Hence, we determine the equilibrium points for the parameter set that has been

Tab. 4.1: Protein concentration [Number of molecules/cell] and kinetic parameters (first order rate constants in [1/s] and second order rate constants in [(molecules/cell)$^{-1}$s^{-1}]).

Kinetic Parameters	Value
k1	2e7/a/Vz
kd1	0.53
k2	1
k3	7.1e6/a/Vz
kd3	0.2
k4	1
Protein Concentration	**Value**
I_T	20000
$E1_T$	40000
$P'ase1_T$	40000

used in the simulation shown in Figure 4.6. The kinetic parameters are depicted in Table 4.1. Furthermore we determine the eigenvalues at the equilibrium points of the system and discuss the system's local stability properties.

The resulting 4 equilibrium points of the system are:

Solution1: $[E1]^*$=-0.00004899; [E1]=-1.27729;

Solution2: $[E1]^*$=-0.0000244952; [E1]=-0.0000407872;

Solution3: $[E1]^*$=-0.00004899; [E1]=1.27727;

Solution4: $[E1]^*$=20000; [E1]=4.3664e^6;

In order to analyze the local stability of the reduced system at an equilibrium point, it is necessary to examine its linear approximation. Suppose a system has an equilibrium point x=x_{eq} and the system is perturbed with x=x_{eq} +ζ, where ζ is assumed to be small. J is the Jacobian matrix evaluated at the equilibrium point. The linear approximation is given by:

$$\frac{d\zeta}{dt} = J\zeta. \tag{4.14}$$

In order to deterime the eigenvalues of the ordinary differential equation obtained from equation 4.5, it is necessary to solve the characteristic equation for the equilibrium point under consideration:

$$det|\lambda I - J| = 0. \tag{4.15}$$

Where J represents the Jacobian matrix describing the biochemical reactions, I represents the identity matrix of order n and λ are the eigenvalues. A linear system is assymptotically stable if Re$\lambda_i < 0$ for i=1,2....,n. The system is stable if Re$\lambda_i \leq 0$ and there is no repeated zero eigenvalue. If Reλ_i 0 for any i, the solution is unstable.

Only solution 3 makes biochemically sense as there is a positive amount of [E1]. Therefore, the solution of the characteristic equation at the equilibrium point of solution 3 results in the following eigenvalue:

$$\lambda = -2.12e^8 1/s. \tag{4.16}$$

As λ is negative the system is asssymptotically stable.

Stability analysis of the detailed model

Without the quasi-steady state approximation and under consideration of conservation of moieties, the following ODEs can be derived:

$$\frac{d[I]}{dt}(t) = v2 - v1 = -k_1[I][E1] + k_{-1}[E1 - I] + k_2[E1 - I], \tag{4.17}$$

$$\frac{d[E1^*]}{dt}(t) = v2 - v3 = k = v2 - v3 = k_2[E1 - I] - k_3[E1^*][P'ase1] + k_{-3}[E1^* - P'ase1], \tag{4.18}$$

$$\frac{d[P'ase1]}{dt}(t) = -v3 + v4 = -k_3[E1^*][P'ase1] + k_{-3}[E1^* - P'ase1] + k_4[E1^* - Pase1]. \tag{4.19}$$

Conservation of mass:

$$[I_T] = [I] + [E1 - I], \tag{4.20}$$

$$[E1_T] = [E1] + [E1 - I] + [E1^*] + [P'ase1 - E1^*], \tag{4.21}$$

$$[Pase1]_T] = [P'ase1] + [P'ase1 - E1^*]. \tag{4.22}$$

Applying conservation of mass the equations 4.17-4.19 can be transformed into:

$$\begin{aligned}\frac{d[I]}{dt}(t) = v2 - v1 \quad &= \quad -k_1[I]([E1]_T - ([I]_T - [I]) - [E1^*] \\ &\quad -([P'ase1]_T - [P'ase1])) + k_{-1}([I]_T - [I]) \\ &\quad +k_2([I]_T - [I]),\end{aligned} \tag{4.23}$$

$$\frac{d[E1^*]}{dt}(t) = v2 - v3 = k_2([I]_T - [I]) - k_3[E1^*][P'ase1] + k_{-3}([P'ase1]_T - [P'ase1]), \tag{4.24}$$

$$\frac{d[P'ase1]}{dt}(t) = -v3 + v4 = -k_3[E1^*][P'ase1] + (k_{-3} + k_4)([P'ase]_T - [P'ase1]). \tag{4.25}$$

The resulting 3 equilibrium points of the system are:

Solution1: [E1]*=-40000; [Pase1]=-0.0000244; [I]=-20000;

Solution2: [E1]*=0.00002449; [Pase1]=20000; [I]=0.63867;

Solution3: [E1]*=0.00002449; [Pase1]=19999.4; [I]=-0.63867;

Only solution 2 is a biochemically possible solution. In the case of the detailed model as well as in the model using Michaelis Menten kinetics we find the same biochemically possible equilibrium points. In the following we will analyze the system on the basis of solution 2.

The corresponding Jacobian Matrix of 4.23-4.25 is equal to:

$$J = \begin{vmatrix} -k_2 - k_{-1} - k_1[I] - k_1(-[E1^*] + [E1]_T + [P'ase1] - [P'ase1]_T + [I] - [I]_T) & k_1[I] & -k_1[I] \\ -k_2 & -k_3[P'ase1] & -[E1^*]k_3 - k_{-3} \\ 0 & -k_3[P'ase1] & -[E1^*]k_3 - k_4 - k_{-3} \end{vmatrix}. \tag{4.26}$$

The solution of the characteristic equation delivers the following eigenvalues λ_i at the equilibrium point of Solution2 of the system:

λ_1=-9.8e^8 1/s, λ_2=-47913.5e^8 1/s and λ_3=-1.5 1/s

All λ_i are all $\lambda < 0$, therfore the system is assymptotically stable.

One or two phosphorylation sites - detailed vs. simplified model

- Single phosphorylation and a single step

Next we analyze the steady state behavior of both approaches. We obtain only slightly different characteristic dose response curves as shown in the following Figure 4.6, depending on whether the steady state approximation is made or not. From the stability analysis and the analysis of the dose response curve, the approximation using Michaelis Menten kinetics within the MAP kinase cascade is a valid simplification to make. It does not change the system's properties in the case discussed here.

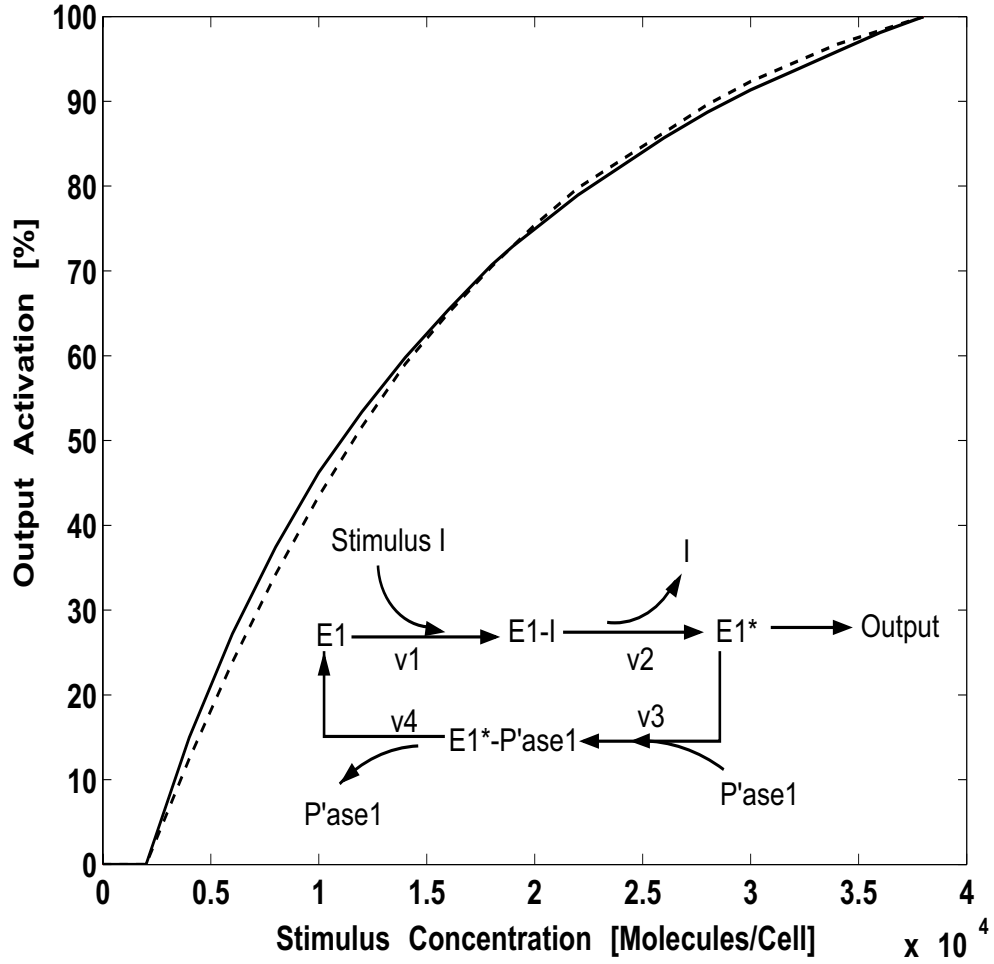

Fig. 4.6: Comparison of the dose response curves of E1* bf - simplified vs. **- -** detailed model.

- Single phosphorylation and a three step cascade

Furthermore, the impact of three amplification steps on the dose response curve is of interest. As depicted in Figure 4.7, the strong amplification, due to the three steps, can be seen.

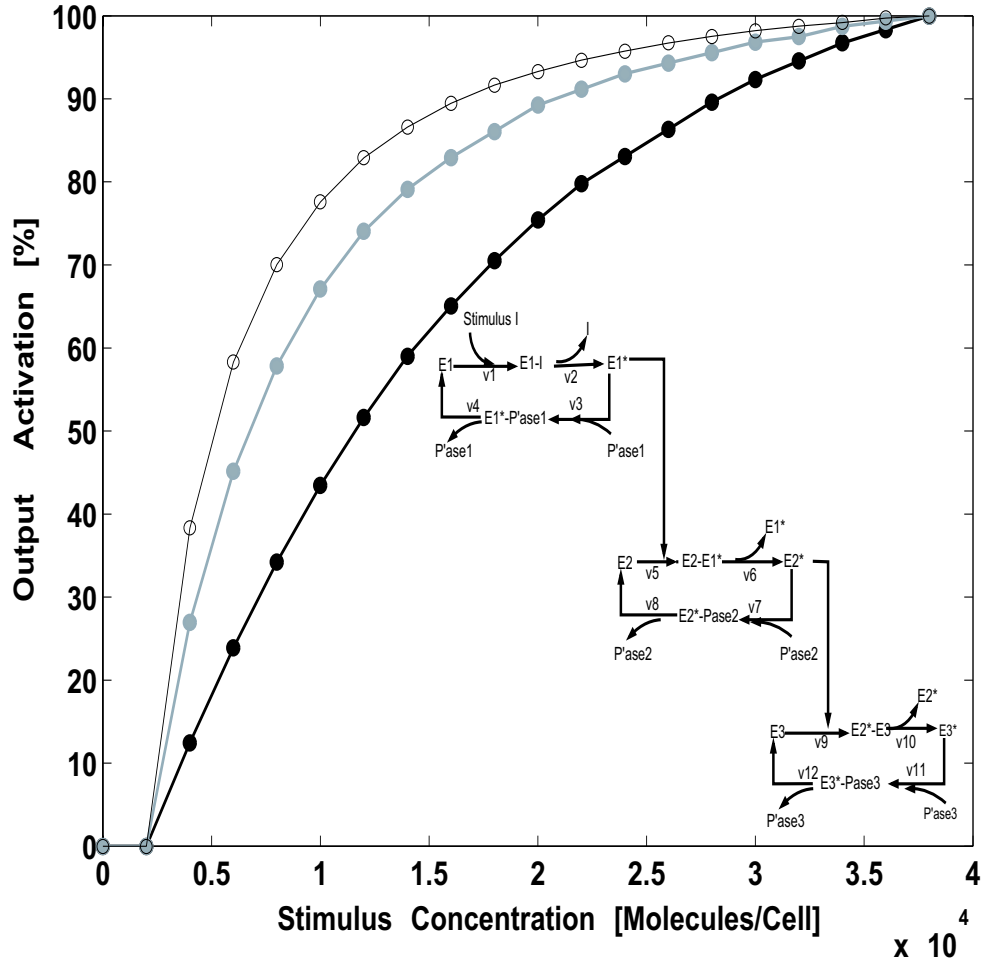

Fig. 4.7: Comparison of the dose response curves for a three step phosphorylation cascade and a single phosphorylation site: -●- dose response of a single step E1*, -●- of a two step cascade E2* and -○- of a three step cascade E3*.

If the question of the autonomy of each of the phosphorylation steps is raised, the simulation results lead to the conclusion that each single step can be treated separately, which means there is no difference between the output behavior of the first step in a single step cascade and the output behavior of the first step in a multi-step cascade.

- *Double phosphorylation and a single step*

Beyond the phosphorylation of a single site the effect of a two fold phosphorylation of a compound on the dose response curve is of interest. In the following Figure 4.8 the dose response curve of a twofold phosphorylation under consideration of the steady state approximation and the dose response curve of the detailed model are shown in comparison. If these curves are compared with the results of the single phosphorylation site, the significant sigmoidal behavior of the double phosphorylation can be recognized. Comparing the sigmoidal behavior and the dose response curve of two phosphorylation sites, the dose response is much less steep though the same kinetic parameters have been used. Again, the detailed model delivers only a slightly stronger amplification.

- *Double Phosphorylation and a three step cascade* The following Figure 4.9 shows the alignment of three steps with two phosphorylation sites per step. The sigmoidal behavior that could already be observed for a single step with two phosphorylation sites is observable again. For low concentrations an amplification of the signal can be achieved by the combination of three steps. However, in order to achieve the switch-like behavior that is attributed to the MAP kinase cascade a combination of steps with only a single phosphorylation site and steps with two phosphorylation sites is necessary, as depicted in Figure 4.10.

In Figure 4.10 the dose response curve for different combinations of steps containing one single phosphorylation site and steps with two phosphorylation sites are depicted. As can be seen in Figure 4.10 three steps with two phosphorylation sites lead to a less steep dose response curve than one step with only a single phosphorylation and two steps with two phosphorylation sites each. The dashed line represents the combination of two steps with a single phosphorylation and one step with two phosphorylation sites. As can be seen in Figure 4.10 this does not lead to a steeper dose response curve, it only shifts the dose response curve to lower concentrations. Hence, by the combination of single and double phosphorylation sites in a cascade nature we obtained a switch-like, sigmoidal dose response curve.

Further analysis revealed that the order of the different steps is not relevant for the final signal

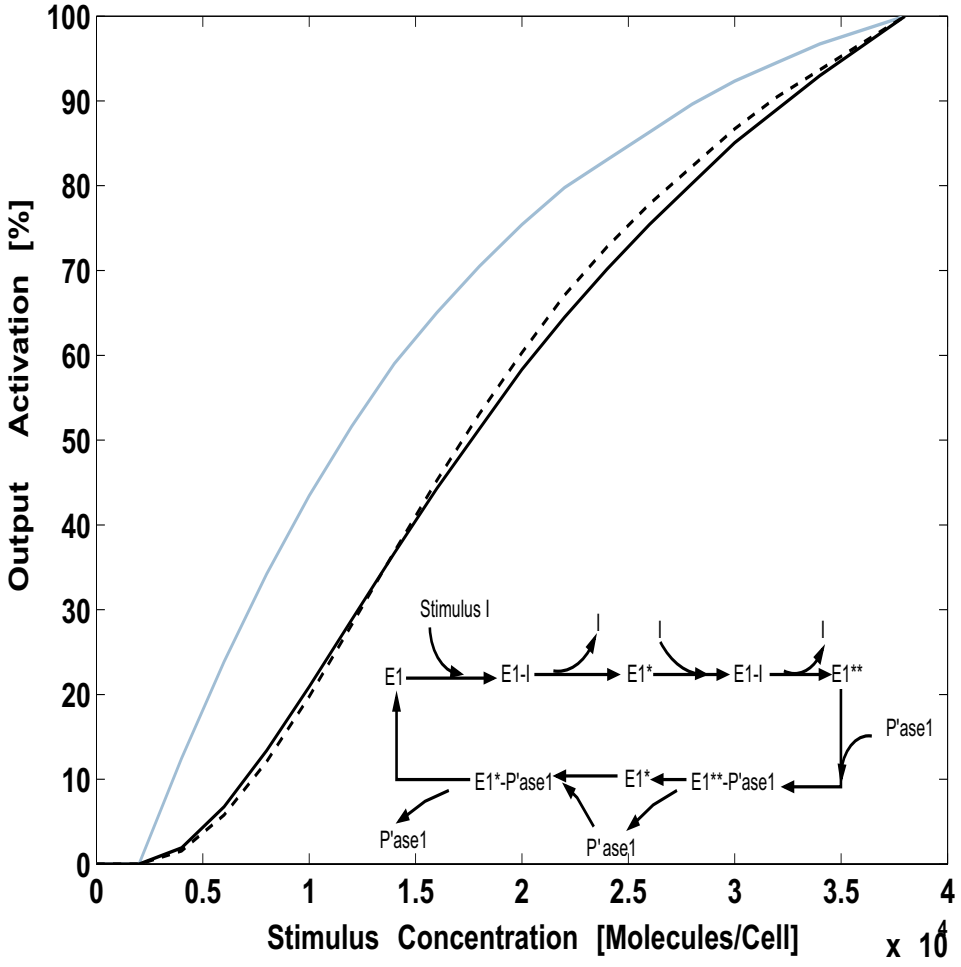

Fig. 4.8: Comparison of the dose response curves a one step phosphorylation cascade: a single phosphorylation site vs. two phosphorylation sites: **- -** detailed model, **-** simplified model of two phosphorylation sites $E1^{**}$, **-** single phosphorylation site $E1^{*}$.

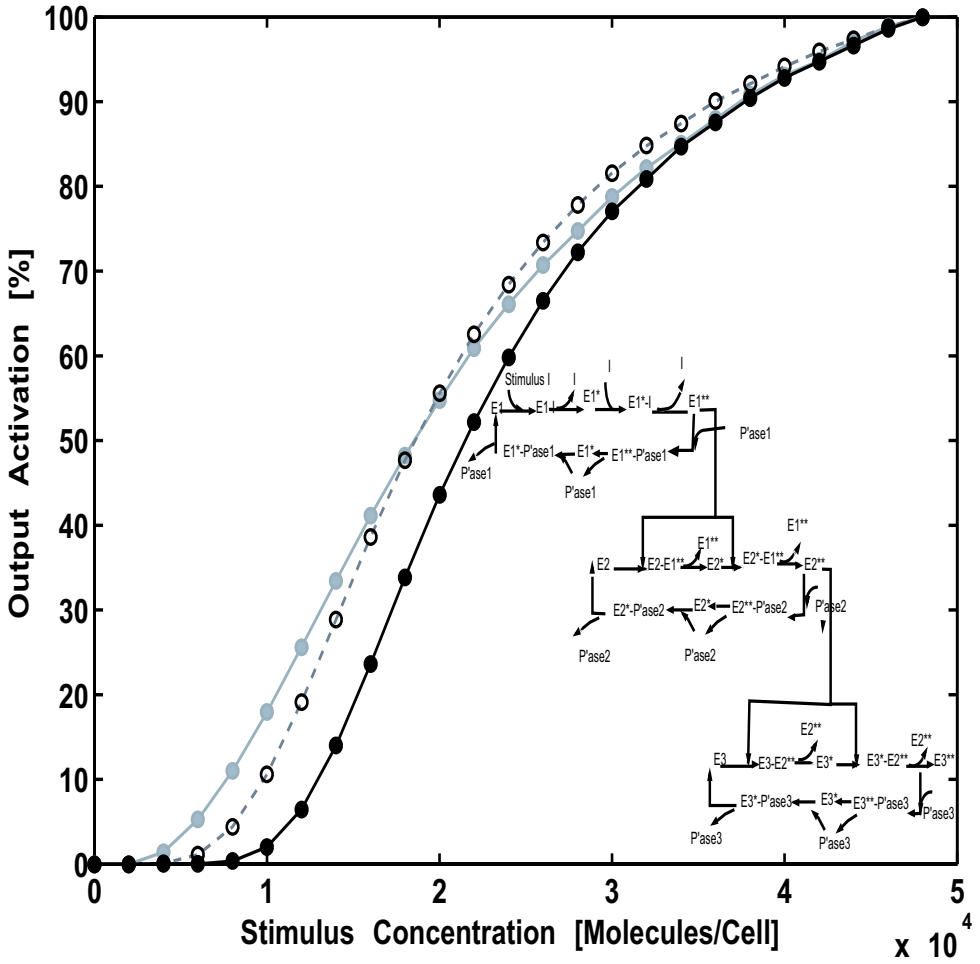

Fig. 4.9: Comparison of the dose response curves for a three step phosphorylation cascade and two phosphorylation sites: -●- first step E1** , -○- second step E2** and -●- third step E3**.

output (data not shown).

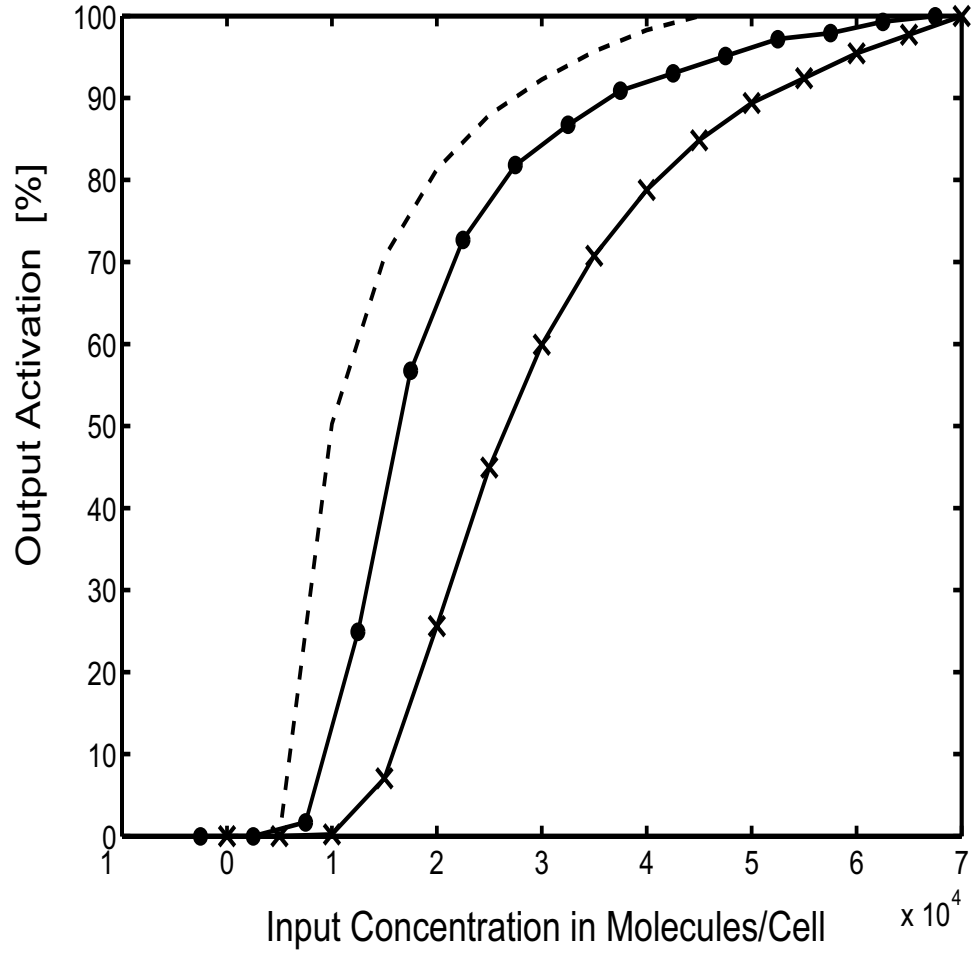

Fig. 4.10: Different combinations of steps with a single phosphorylation site and steps with two phosphorylation sites: **- -** two single phosphorylation steps and one double phosphorylation, **-●-** one single phosphorylation step and two double phosphorylation steps and **-x-** three step phosphorylation cascade with two phosphorylation sites.

Besides the behavior of the module MAP kinase cascade, the behavior of the dose response of the MAP kinase cascade within the signaling cascade is of interest. In Figure 4.11 the dose response curve of the ERK phosphorylation triggered by external and internalized receptors as well as the contribution of receptors, remaining on the cell surface and internalized receptors, to the dose response curve is shown. Comparing the dose response curve of the ERK phosphorylation, it fits the experimental data very well. Thus, the MAP kinase cascade in HeLa cells is not a pure on and off switch. Within more than a decimal power ERK transforms from the non phosphorylated state to the totally phosphorylated state.

Furthermore, the signal amplification by the internalized receptors is revealed in Figure 4.11. At very low EGF concentrations (in the pM range) the internalized receptors trigger most of the ERK phosphorylation. With increasing EGF concentration the contribution of the internalized receptors to the ERK phosphorylation decreases and the receptors remaining on the cell surface trigger most of the ERK phosphorylation.

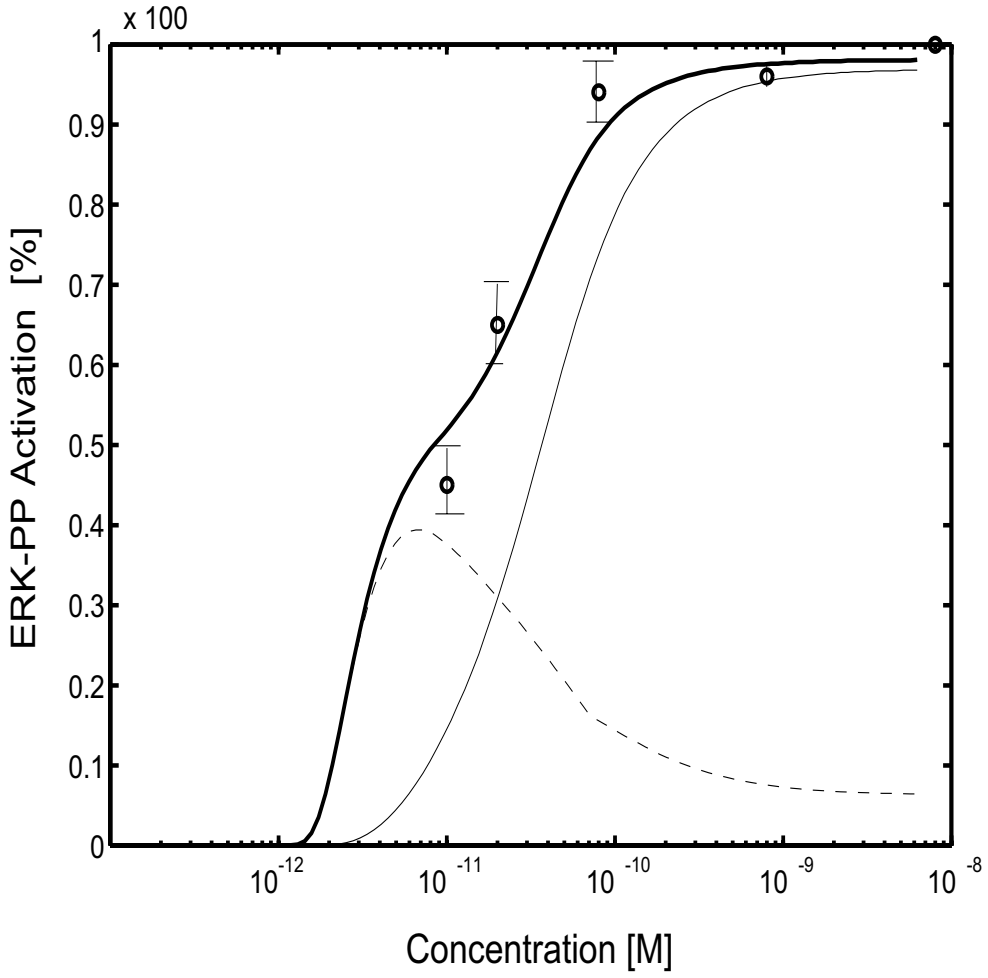

Fig. 4.11: Dose response curve of ERK activation simulated with the full model: **–** total ERK activation, - ERK activation by external receptors and - - ERK activation by internalized receptors.

Instability of the MAP Kinase Cascade through Negative Feedback

In a variety of cell types the MAP kinase cascade is embedded in feedback loops, positive or negative, depending on whether the terminal kinase stimulates or inhibits the activation of the initial level. In the following we show that a negative feedback loop can bring about sustained oscillations.

Oscillations in cellular biochemical pathways were discovered more than 30 years ago in cell-free extracts and in suspensions of intact yeast cells [67], [14]. In many pathways, the major source or oscillations is a negative feedback loop due to time delays in feedback circuits [153].

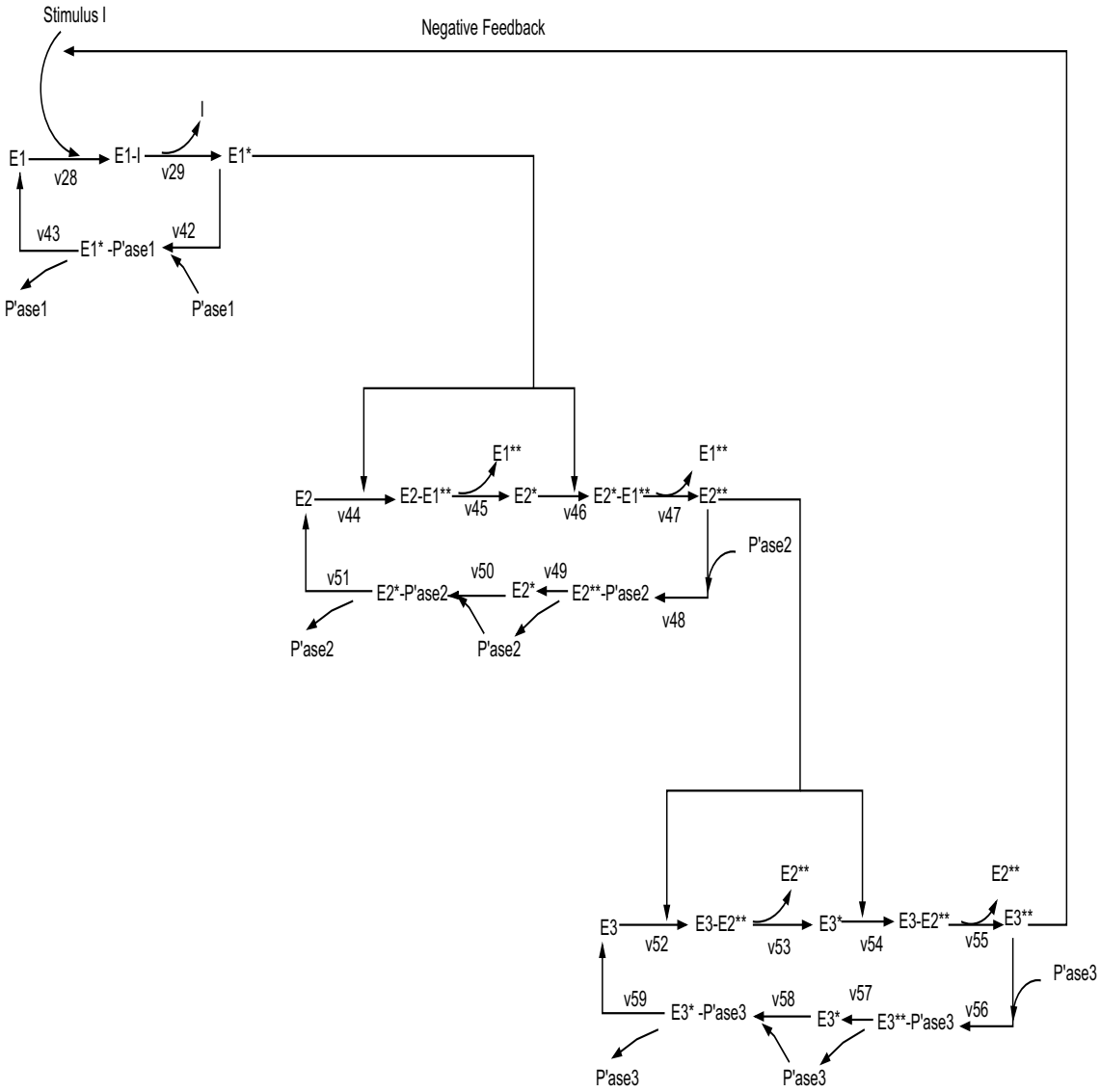

Fig. 4.12: Schematic representation of the MAP kinase cascade including the negative feedback loop from E3** to reaction v28.

According to the model developed by Kholodenko [82] stable oscillations can occur in a MAP kinase cascade as shown in Figure 4.13 due to the negative feedback from ERK to the input stimulus. This model shows stable oscillations over a wide range of Km values as long as the kinase concentrations are larger than the Km values. When the ratio is substantially decreased

Tab. 4.2: Reaction rates and kinetic parameters (first order rate constants in [1/s] and second order rate constants in [$M^{-1}s^{-1}$]) of a MAPK cascade showing sustained oscillations.

Reaction Number	Reaction	Kinetic Parameters
v28	(k28*c(28)*c(41)-kd28*c(42))/(1+c(59))^n	
v29	k29*c(42)-kd29*c(28)*c(45)	k29=1e7 ; kd29=0.0053
v42	k42*c(44)*c(45)-kd42*c(46)	k42=1e6 ; kd42=0.1
v43	k43*c(46)	k43 =1
v44	k44*c(47)*c(45)-kd52*c(48)	k44=1.2e7 ; kd44=0.55
v45	k45*c(48)	k45 =3
v46	k44*c(49)*c(45)-kd52*c(50)	k44=1.2e7 ; kd52=0.5
v47	k47*c(50)	k47 = 16
v48	k48*c(51)*c(53)-kd48*c(52)	k48=2e7 ; kd48=0.5
v49	k49*c(52)	k49 =0.5
v50	k50*c(53)*c(49)-kd50*c(54)	k50=5e6 ; kd50=0.5
v51	k49*c(54)	k49 =0.5
v52	k52*c(55)*c(51)-kd44*c(56)	k52=1.2e7 ; kd44=0.5
v53	k53*c(56)	k53 = 3
v54	k52*c(51)*c(57)-kd44*c(58)	k52=1.2e7 ; kd44=0.5
v55	k55*c(58)	k55 = 5
v56	k56*c(59)*c(60)-kd56*c(61)	k56=3e7 ; kd56=0.5
v57	k57*c(61)	k57 = 2.5
v58	k58*c(60)*c(57)-kd58*c(62)	k58=1e7 ; kd58=0.5
v59	k57*c(62);	k57 = 2.5

the oscillations dissappear. The model published by Kholodenko [82] describes the negative feedback loop from ERK as noncompetitive inhibition of MKKK (Raf). It could be shown that the dual serine/threonine phosphorylation of SOS by ERK is roughly equivalent to n=2. Hence v28 under consideration of the feedback loop is equal to v28/(1+ (ERK-PP))^n). In Table 4.2 the single reactions with the corresponding kinetic rates are displayed.

In contrast to the model published by Kholodenko, the model presented here, is not based on Michaelis-Menten type kinetics but on elementary biochemical reactions. In the following we discuss the possibility of oscillations in the full EGF model and why in experimental studies such oscillatory behavior has never been observed.

Using the kinetic parameters, shown in Table 4.2 and stimulating the system with a a constant input signal of 50000 Ras-GTP molecules per cell, leads to sustained oscillations of ERK-PP as shown in Figure 4.13. This phenomenon is also known as Hopf bifurcation. Looking at the system's behavior of the module MAPK cascade, the question arises of whether a MAPK module showing stable oscillations will show these as well if it is embedded into a signaling

cascade and whether those oscillations occur also in living cells. In the following we will address this question by looking at the system's response due to a sustained or an impulse-like stimulus and furthermore by embedding the module that shows oscillations into the full EGF model.

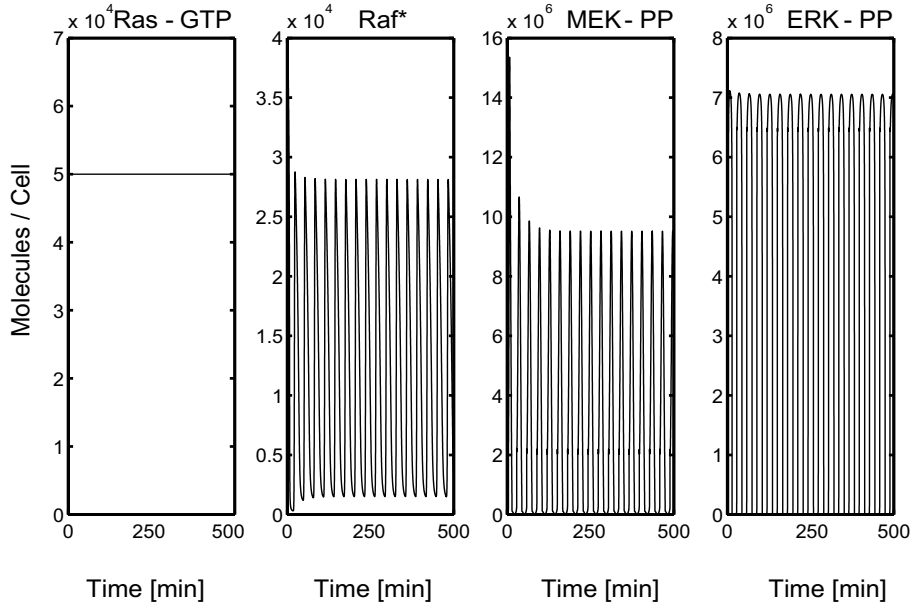

Fig. 4.13: Oscillations due to negative feedback loop in the MAP kinase cascade - sustained input signal.

Using the same amount of Ras-GTP (20000 Ras-GTP molecules/cell) as stimulus signal as in the full model we obtain damped oscillations for this parameter set as shown in Figure 4.14. Comparing the graphs for Raf-P, MEK-PP and ERK-PP the switch-like behavior of the MAP Kinase cascade can be observed. In the case of Raf-P a gradual dampening of the oscillations can be observed, whereas in the case of ERK-PP a very sudden dampening occurs.

In Figure 3.5 the dynamic pattern of several proteins involved in the EGF induced MAP kinase cascade are shown. Analysis of this example reveals that the input signal into the MAP kinase cascade is not a sustained input but rather a very transient Ras-GTP signal, which resembles more of an impulse-like stimulation of the system. In the following Figure 4.15, the system is triggered with a 1min pulse of Ras-GTP. Due to this very short stimulation the oscillations dissappear and instead a single very sharp ERK-PP peak is obtained. In Figure 4.16 the system is stimulated for 100min with Ras-GTP and only during this time frame oscillations can be observed.

From the results discussed above, is seems likely that in this particular case nature applies

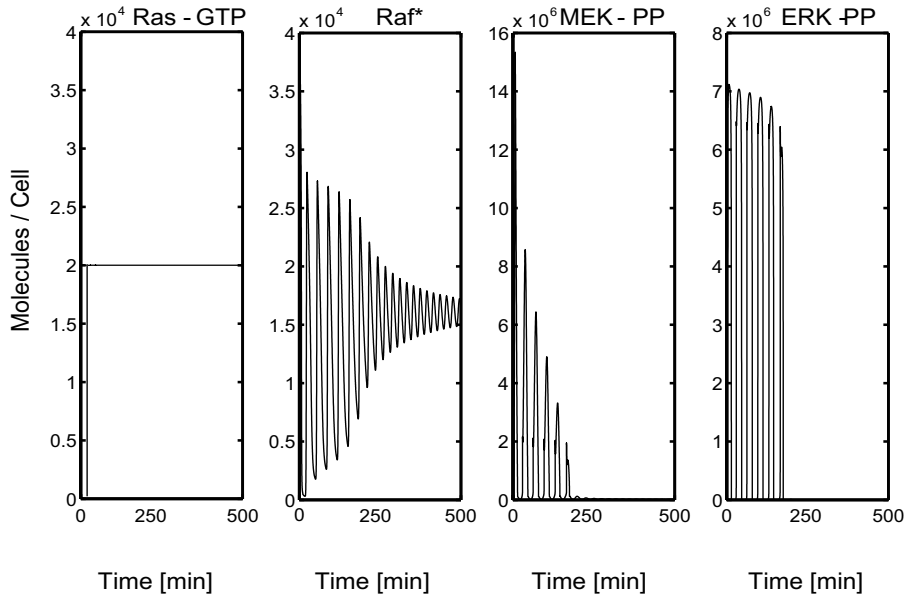

Fig. 4.14: Oscillations due to negative feedback loop in the MAP kinase cascade - sustained input signal, which equals the amount in of Ras-GTP in the full model.

certain mechanisms to stabilize the system.

In the following we discuss whether oscillations can also be observed in the full model, including the module MAP kinase cascade which we have analyzed in the paragraphs above. In Figure 4.17 the simulation results are displayed. The Ras-GTP signal resembles the impulse-like stimulation shown in Figure 4.15. The difference between the two models is that in the full model also internalization of the receptors and their degradation is taken into consideration. Due to the fact that the signal of internalized vs. external receptors is shifted in time prevents oscillations as well. From these analyzes it seems that the probability of observing experimentally oscillations of MAP kinase cascades is quite unlikely.

In this chapter we have analyzed the model of the MAP kinase cascades in several aspects. First, we show that the system is robust to variations of the kinetic parameters, though there are a few very sensitive ones e.g. the kinetic parameters related to the phosphatases. The same holds true for the variation of the initial protein concentrations. As shown in Figure 4.1 and Figure 4.2 the phosphatases play an important role in modulating the signal. We discuss and analyze the differences between a detailed model of the first step of the MAP kinase cascade and a model using Michaelis Menten kinetics. We show that both systems are stable for the parameter set used in the large model. We also show that there are only little differences in

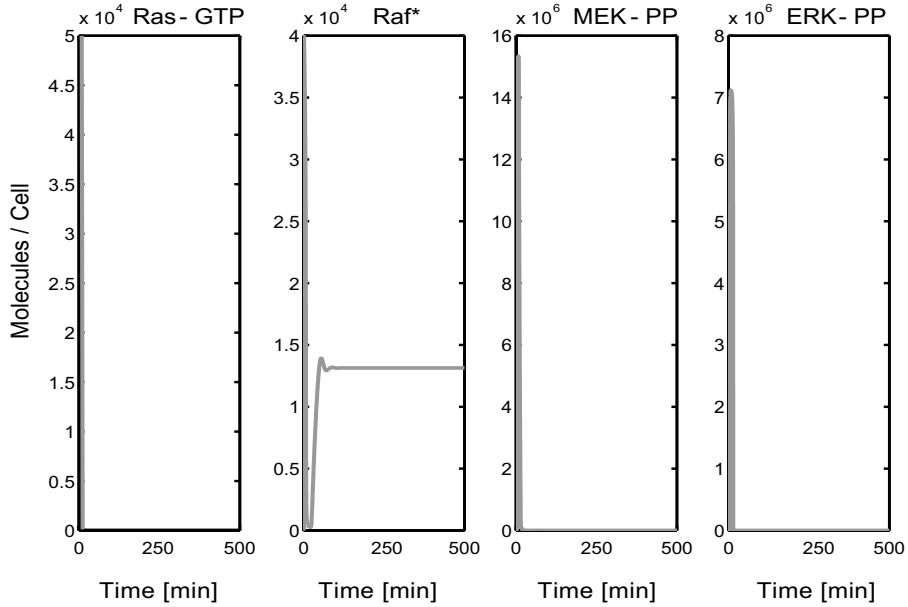

Fig. 4.15: Damped oscillations due to negative feedback in the MAP kinase cascade - 1min impulse-like input signal of Ras-GTP.

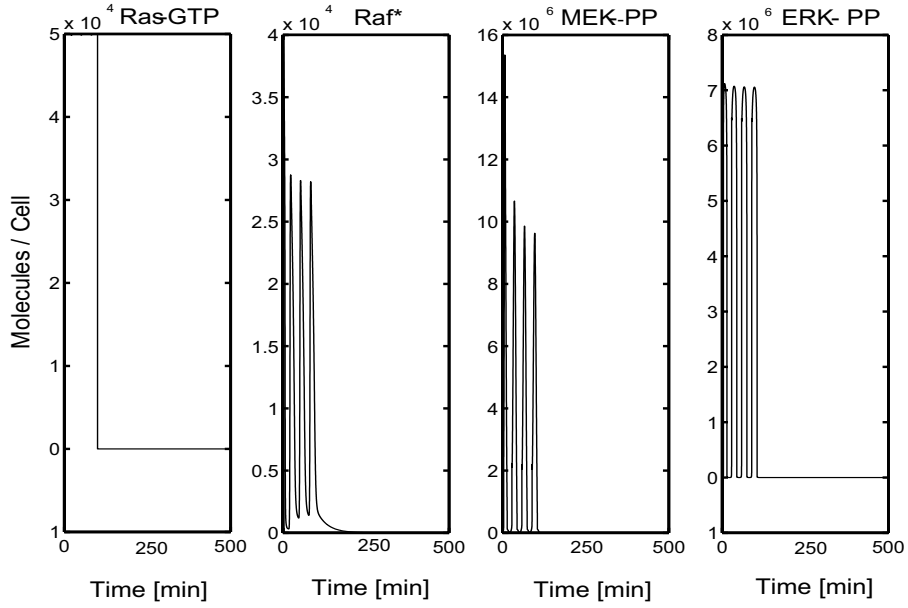

Fig. 4.16: Damped oscillations due to negative feedback in the MAP kinase cascade - impulse-like signal (Ras-GTP).

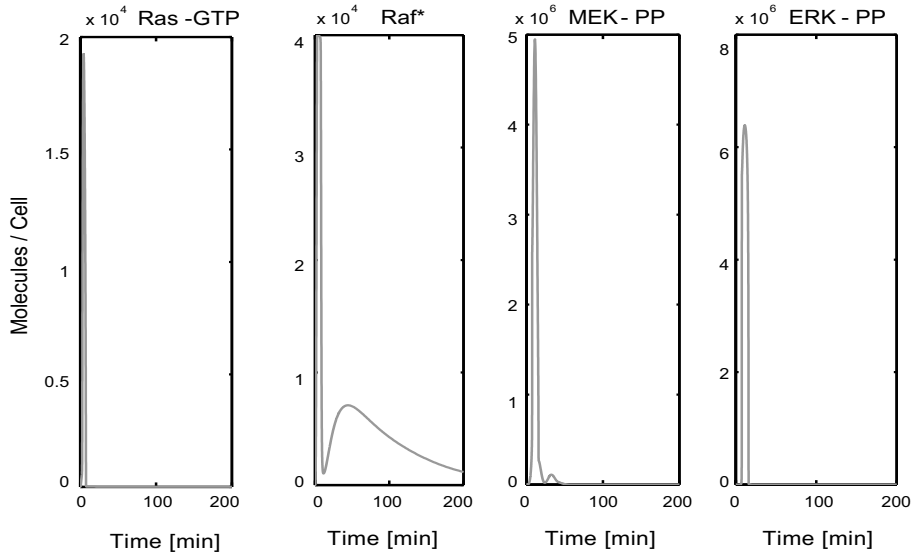

Fig. 4.17: Oscillations due to negative feedback in the MAP kinase cascade - full model.

the dose response curve and that we find the same biochemically possible equilibrium points solving both models. Therefore, it seems like for the kinetic parameters used here, a Michaelis Menten approach is a valid approach, which also implies the independency of the steps of the MAP kinase cascade. Thus, the single steps of the MAP kinase cascade can be treated separately.

Furthermore, we show that the combination of single and double phosphorylation sites in a cascade nature obtained a switch-like, sigmoidal dose response curve. We also found that the order of a step with a single or double phosphorylation site does not matter.

We also discuss the phenomenon of oscillations of the MAP kinase cascade module. They can be observed over a wide range of Ras-GTP. We showed that they occure more likely with a sustained input signal, whereas an impulse-like signal, results in damped oscillations. Furthermore, we show that oscillations, that can be observed for the module, can not be observed in the full model due to the network structure.

Chapter 5

A Mathematical Model of TNF Receptor Interaction

5.1 The TNF Signal Transduction Network

In the 1970's, lymphotoxin (LT) and tumor necrosis factor (TNF) were identified as products of lymphocytes and macrophages that caused the lysis of certain cells, expecially tumor cells. TNF is the prototypic member of a large family of cytokines that interact with a large number of receptors. The pleiotropic actions of TNF range from proliferative responses such as cell growth and differentiation to inflammatory effects and mediation of immune responses, to destructive cellular processes such as apoptotic and necrotic cell death mechanisms. Apoptosis (programmed cell death) is an important regulatory mechanism to eliminate unwanted cells in development or irreversibly damaged cells in infection.

TNF exerts its diverse biological functions by binding to and activating two distinct cell surface receptors, TNF-R1 also known as CD120a or p55 and TNF-R2 also known as CD120b or p75 [6]. Activation of TNF-Rs occurs by oligomerization through the trimeric ligand TNF [75]. In recent years a large number of proteins has been identified that associates directly or indirectly with the cytoplasmic domains of the two receptors. Among these, two groups of signal transduction molecules have been identified, the so called death domain (DD) proteins like TRADD and FADD and the TNF receptor associated factor (TRAF) family. Overexpression of death domain containing molecules leads to the induction of apoptosis. The cytoplasmic part of TNF-R1, but not TNF-R2, carries a death domain and is thus capable of binding other death domain proteins.

Following ligand binding, the DD containing adapter molecule TRADD binds through its death

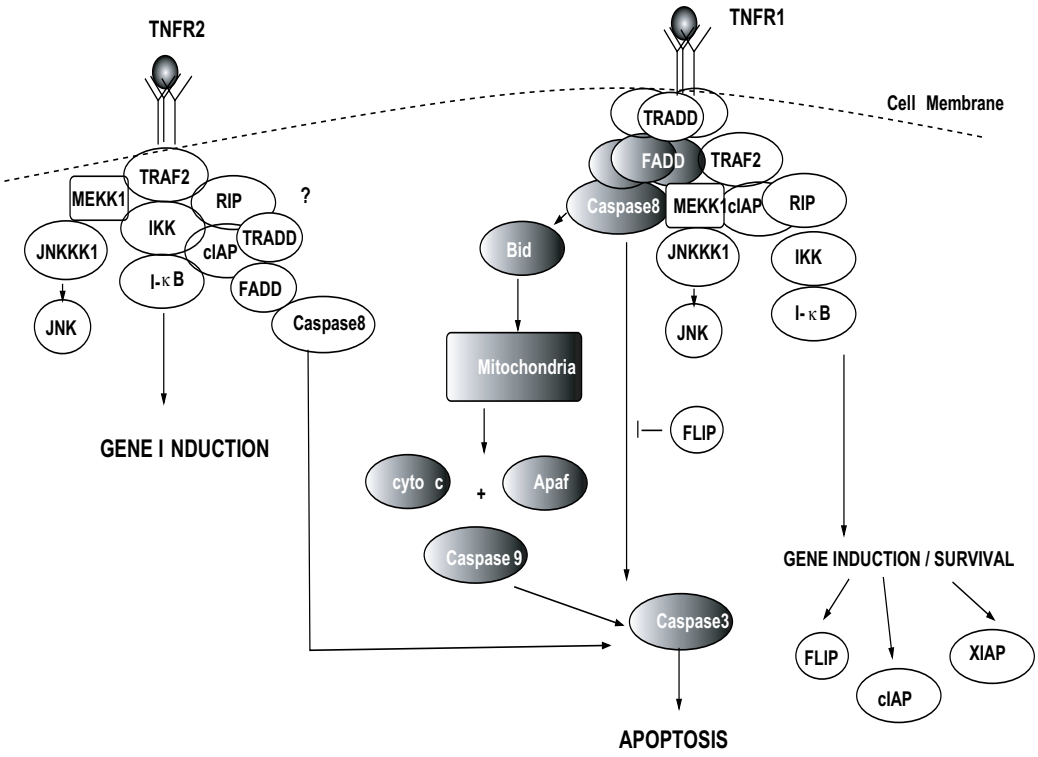

Fig. 5.1: Schematic representation of TNF-R1 and TNF-R2 signaling pathways.

domain to TNF-R1, thereby forming a platform for the initiation of both, the apoptotic pathway or, alternatively, the survival pathway as depicted in Figure 5.1. Regarding the apoptotic pathway, FADD binds to TRADD and induces the caspase cascade via procaspase-8 binding and proteolytic activation. Thus, caspase-8 is the initiating caspase, whereas caspase-3 and -7 represent major executional caspases which cleave protein targets leading to apoptosis. At least two caspase-8 molecules must be recruited to the TNF-R1 complex in order to achieve caspase-8 activation [106]. Besides this direct caspase activation pathway, there is an alternative pathway leading to the mitochondria, which can also be activated by many stimuli besides death receptors. In death receptor signaling the mitochondrial pathway has been proposed to function as an amplifier of caspase activation [125]. To initiate this pathway, activated caspase-8 cleaves Bid into tBid, which induces oligomerization of Bax [165], [112] and results in a mitochondrial dysfunction leading to the release of cytochrome c. Cytoplasmic cytochrome c then binds to a docking protein called Apaf-1 that facilitates binding and activation of caspase-9 [125], [176], [16]. Activated caspase-9 in turn cleaves procaspase-3 which leads to DNA fragmentation.

Regarding the survival pathway, binding of TRAF2 and RIP to the TNF-R1-TRADD complex

is essential to induce strong NF-κB activation [149], [68], [70] via IKK [24]. In unstimulated cells, the transcription factor NF-κB is sequestered in the cytoplasm by binding to I-κB proteins [10]. After stimulation, N-terminal serine residues of I-κBs are phosphorylated, which lead to ubiquination and subsequent degradation via a 26-S proteasome pathway [156]. Likewise, liberated NF-κB molecules are translocated into the nucleus in order to activate transcription of gene targets. It has been shown that the I-κB kinase (IKK) complex is responsible for the phosphorylation. The IKK complex consists of three subunits IKKα, IKKβ and IKKγ. It still needs to be clarified, how these three units act in concert, therfore we will treat the IKK complex as one component IKK, which represents all three subunits in the model as shown in Figure 5.1.

NF-κB activation was shown to induce the expression of survival proteins like c-IAPs, XIAP or FLIP that prevent apoptosis [160], [101]. These antiapoptotic proteins inhibit caspase activation at different levels within the signal transduction network. Cellular FLIP structurally resembles caspase-8 except that it lacks proteolytic activity. FLIP is highly expressed in tumor cells. It interacts with both FADD and caspase-8 to inhibit the apoptotic signal of death receptors. FLIP inhibits caspase-8 activation through the recruitment of FLIP to the DISC [151].

Although other proteins have been identified which inhibit upstream caspases, only the IAPs have been demonstrated to be endogenous repressors of the terminal caspase cascade. The X-linked Inhibitor of Apoptosis, XIAP, is a key member of the newly discovered family of intrinsic inhibitors of apoptosis (IAP) proteins. IAPs block cell death both *in vitro* and *in vivo* by inhibition of distinct caspases. It could be shown that XIAP, c-IAP1 and c-IAP2 can prevent the proteolytic processing of procaspase-3, -6 and -7 by blocking the cytochrome c induced activation of procaspase-9 [28]. Furthermore, it was shown that IAPs inhibit the cleaved caspase-3 directly, and thus block downstream events. Whereas one inhibitory effect of c-IAP-2 on caspase-3 activation is weaker than that of XIAP [28]. For U937 cells it could be demonstrated that c-IAPs block TNF initiated signaling upstream of caspase-8 and the mitochondria [38]. It remains to be elucidated whether and how c-IAPs act upstream of caspase-8.

Much less is known about the signal transduction pathways of TNF-R2. It has been observed that TNF-R2 can potentiate the apoptotic response to TNF [167]. It has been postulated that TNF-R2 can modulate the signal of TNF-R1 to enhance apoptosis for example throughout the so called Ligand Passing Phenomenon and common intermediates like TRAF1 and TRAF2 [167], [21]. Ligand Passing takes place on the cell surface. It has been hypothesized that TNF-

R2 bound ligand may be passed over to TNF-R1 to enhance TNF-R1 signaling [146].

TRAF2 can directly associate with TNF-R2 and activate NF-κB and N-terminal c-Jun kinase (JNK). However, TNF-R2 has been shown to enhance TNF-R1 induced apoptosis in many cellular systems. TRAF2 depletion has been proposed by several groups [167], [166], [21] as a likely mechanism to shift the fragile balance between survival and apoptosis towards apoptosis. It could be shown for transfected Jurkat cells that RIP can interact with both receptors. According to these data, TNF-R2 triggers caspase activation via RIP and TRADD [113]. Concerning survival proteins, c-IAP1 and c-IAP2 have been identified as part of the TNF-R2 signaling complex. The c-IAPs associate indirectly to TNF-R2 via a TRAF1-TRAF2 heterocomplex [118].

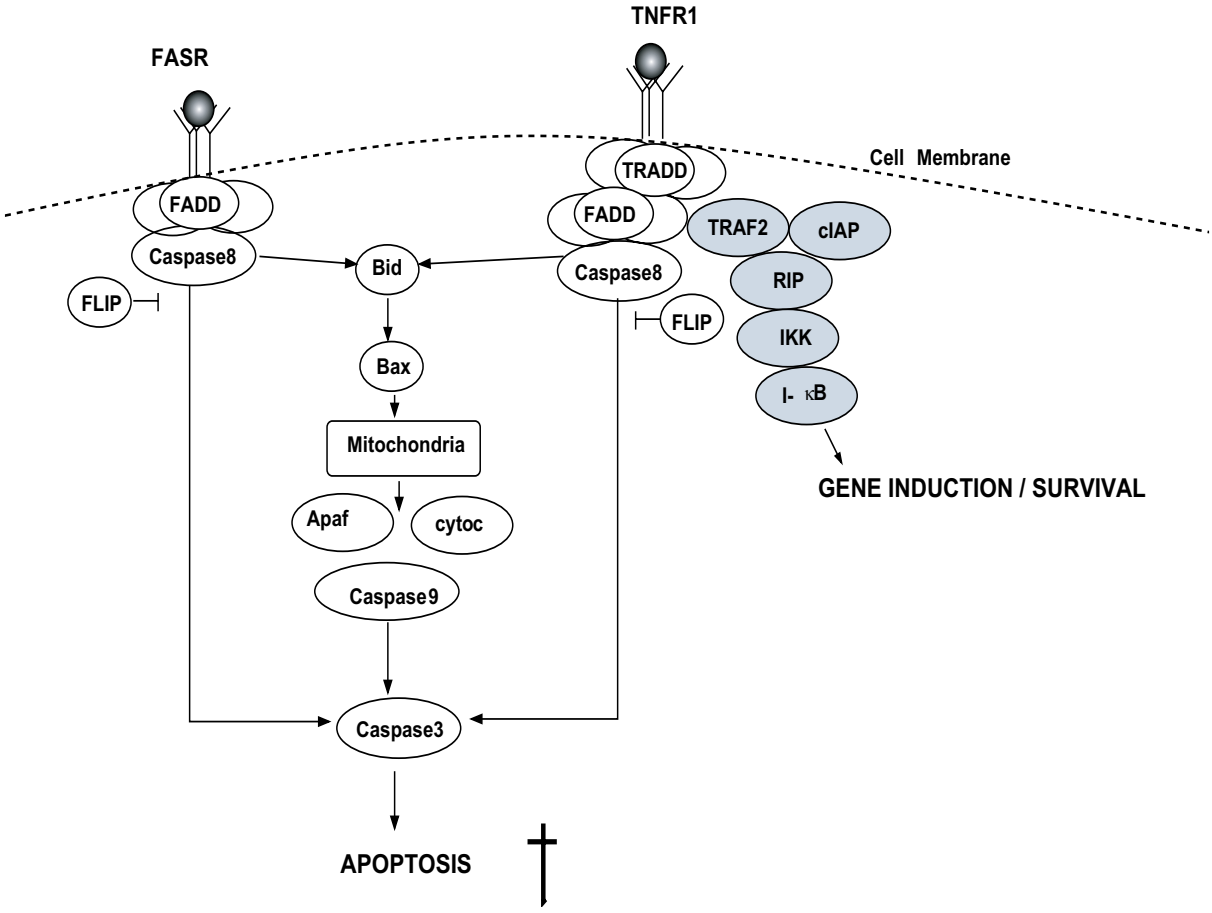

Fig. 5.2: Comparison of TNF-R1 and Fas-L signal transduction pathways.

In this work the hypotheses of the Ligand Passing phenomenon and TRAF2 as key regulatory molecule of TNF-R1 / TNF-R2 crosstalk are tested with the help of computational modeling.

As Fas-R and TNF-R1 belong to the same receptor family and the apoptotic pathways of Fas

and TNF are almost identical, we started with the development of a mathematical model describing the Fas induced caspase activation. Therefore, initially, we have developed a model that is less complex and serves as a basis for the TNF model development.

Fas is a cysteine-rich transmembrane protein of 335 amino acids, which was originally defined by a mouse monoclonal antibody [174]. This trimeric receptor, which is also called CD95 or TNF-RSF6, is expressed on cells of the lymphoid system, organs such as the heart, and in various places throughout embryonic and adult life. It is a member of the tumor-necrosis factor (TNF) receptor superfamily of molecules [158], [84]. Engagement of this receptor on the cell surface by its natural ligand (FasL; also known as CD95L or TNF-SF6) results in apoptotic death of the cell. FasL is the membrane-bound ligand for Fas. This 278 amino-acid protein also belongs to the TNF superfamily. FasL was initially thought to be expressed primarily on activated T cells. However, recent studies have shown that it is expressed constitutively in the eye, testis, and several other places during neonatal and adult life. Like TNF, when FasL binds to Fas, it oligomerizes the receptor, which results in the recruitment of the death-inducing signal complex [134].

Based on this initial Fas model, we have developed a mathematical model that describes the TNF-R1 signal transduction network. In contrast to TNF-R1, Fas-R triggers mainly apoptosis. However, the apoptotic signal transduction pathways of Fas-R and TNF-R1 are almost identical. The only difference is that in the case of Fas-R, FADD directly binds to FAS-R and in the case of TNF-R1, FADD can only associate via TRADD to TNF-R1 as shown in Figure 5.2. Analyzing both models, we will discuss the influence of several adapter molecules consecutively binding to the receptor, which is secondary to the phosphorylation cascades as a main mechanism found in signal transduction.

The single biochemical reactions that have only been roughly described above will be explained below in more detail along with explanations about the implementation of the biological knowledge into the model.

5.2 Derivation of a Mechanistic Model of TNF Receptor Interaction

The mathematical model of TNF receptor interaction presented in the following is certainly not complete but may serve as a basis for further model development and covers the currently

known main protein-protein interactions. The goal of this work is to analyze and explain the different time courses of caspase activation of pre-, co- and TNF-R1 selective stimulation with the help of the mathematical model.

The model has been developed for transfected HeLa cells, which express about 30,000 TNF-R2 and 3,000 TNF-R1. With the help of the model presented in this work, it is possible to explain some characteristics of TNF receptor signaling and to make predictions about the system's behavior, which in turn lead to new biological knowledge.

In the following paragraphs, we focus on the TNF receptor crosstalk. TNF-R1 and TNF-R2 share several adapter molecules within the TNF receptor (TNF-R) signalosome, which are involved in the initiation of nuclear factor-κB (NF-κB) activation, which is essential for cell survival or apoptosis.

At least three different mechanisms of regulation can be distinguished:

- NF-κB-mediated induction of proteins of the TNF-R complex;

- NF-κB-independent protection against apoptosis by the TNF-R-associating factor 2 (TRAF2)-mediated recruitment of survival proteins;

- amplification of the death signal by proteolytic inactivation of signaling proteins that are involved in NF-κB activation or cell survival;

The above mentioned mechanisms of regulations are discussed on the basis of simulation studies in the context of caspase activation under three distinct stimulation conditions: First, costimulation of TNF-R1 and TNF-R2; second, prestimulation of TNF-R2 for 6 hours and third, the selective stimulation of TNF-R1. The prestimulation protocol results in an almost maximal caspase activation, costimulation results in a half maximal caspase activation whereas selective TNF-R1 stimulation only leads to a caspase activation of around 30%. Maximal caspase activation, as observed for the prestimulation protocol, can be explained by the almost complete depletion of TRAF2 after 6 hours of TNF-R2 selective stimulation [43]. As shown in Figure 5.2, the depletion of TRAF2 leads to a "Fas-like" signal transduction pathway. In fact, caspase activation triggered by Fas-L and in TRAF2 depleted cells is the same [43]. In the absence of TRAF2 no gene induction of antiapoptotic proteins can take place. As shown in Chapter 5.3 the induction of antiapoptotic proteins is an important regulatory mechanism.

In this work, we present a computational model that can describe the experimental data of the three experimental protocols. The model is used to test existing hypotheses e.g. TRAF2

being the critical molecule by which the crosstalk is regulated or to make predictions about the system's behavior. Perturbations of known outcome are used to validate the model. These experiments have already been described in the literature but have not been incorporated into the model a priori. For example, we discuss the influence of overexpression of certain proteins like TNF-R2 or antiapoptotic proteins on caspase activation. Finally, we discuss the role of the feedforward and feedback pathways observed in caspase activation module.

A biological scheme of the TNF signal transduction pathways, which have been included into the model, is shown in Figure 5.1 and these core pathways have been introduced roughly in Chapter 5.1. In Figure 5.3, Figure 5.4 and Figure 5.5 the detailed biochemical reaction schemes for TNF-R1 and TNF-R2 are displayed. However, the network representation in the detailed biochemical reaction schemes lacks transperancy which is achieved effectively by representing the system according to the Modular Modeling Concept [85]. In Figure 5.6 the signaling pathway of TNF-R1 according to the Modular Modeling concept is depicted.

As mentioned above, all biochemical reactions, that have been included into the model are represented in the biochemical reaction schemes. The system consists of n=651 biochemical reactions and m=391 components. The different components (=state variables) are indicated with numbers 1...m and the different reactions with v1...n in accordance to the model of the EGF induced MAP kinase cascade. Similar to the EGF receptor model, receptor internalization and degradation have been included into the model. As mechanisms of internalization the clathrin-coated pit path as well as the direct internalization of the receptor (v74) have been considered. The mechanisms of TNF receptor internalization remain to be elucidated and the possibilities presented above have been included into the model, as internalization could be shown for TNF-R1 and TNF-R2 [8], [P. Scheurich personal communtication]. In the biochemical reaction networks displayed in Figure 5.3, Figure 5.4 and Figure 5.5, three numbers specify each compound. The first number indicates the receptor complex signaling from the cell surface, the second number represents the receptor complex associated with the coated pit protein and the third number stands for the internalized receptor complex. In order to keep the biochemical reaction network as transparent as possible, the complexes that form with TNF-R1-TRADD-TRAF2-c-IAP and caspase-3*, caspase-9 and caspase-8 are combined within the pathways showing the c-IAP TNF-R1 interaction. The last two numbers in the biochemical reaction scheme in Figure 5.3 indicate the TNF-R1-TRADD-TRAF2-c-IAP complexes formed with

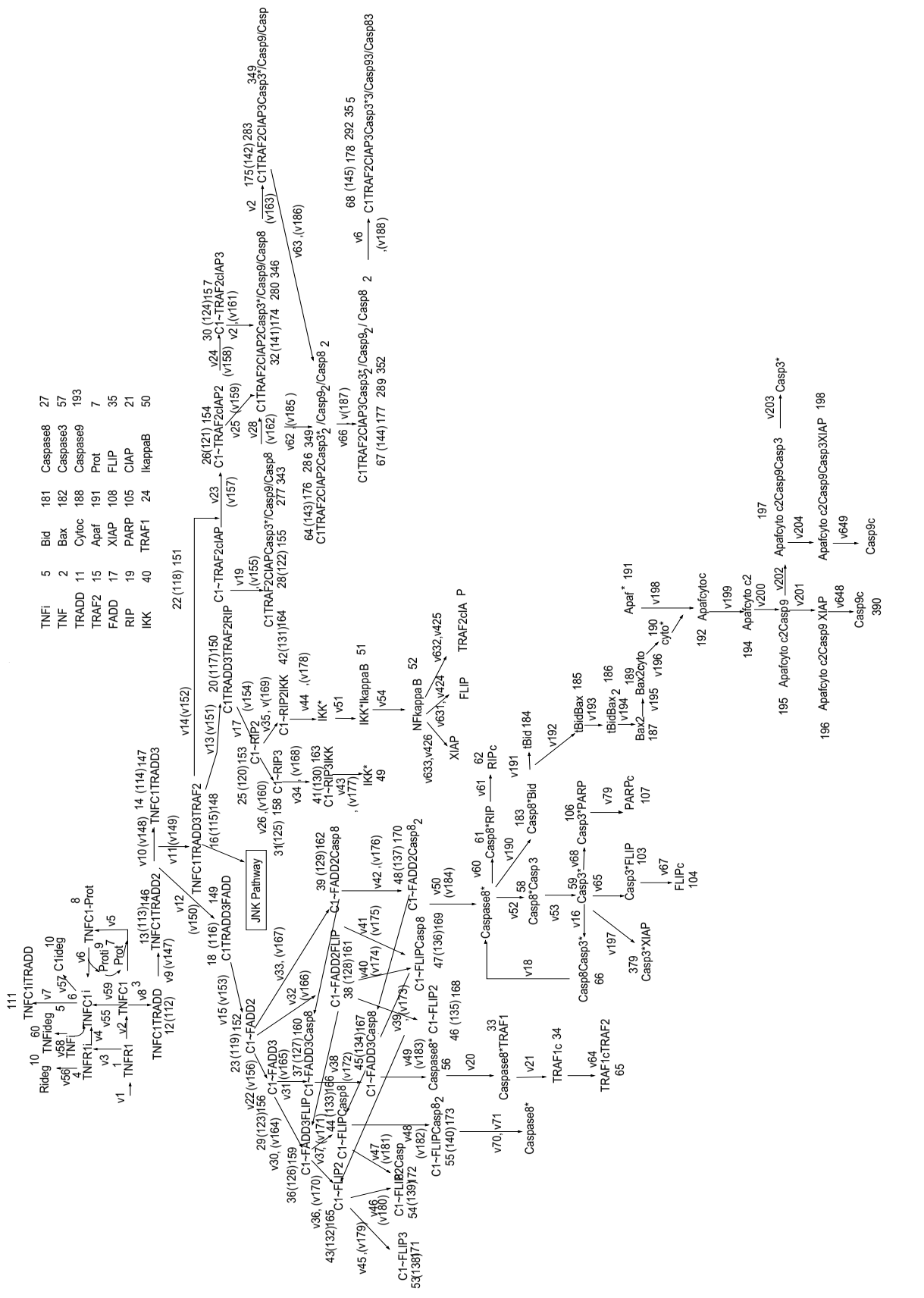

Fig. 5.3: Biochemical reaction scheme of TNF-R1.

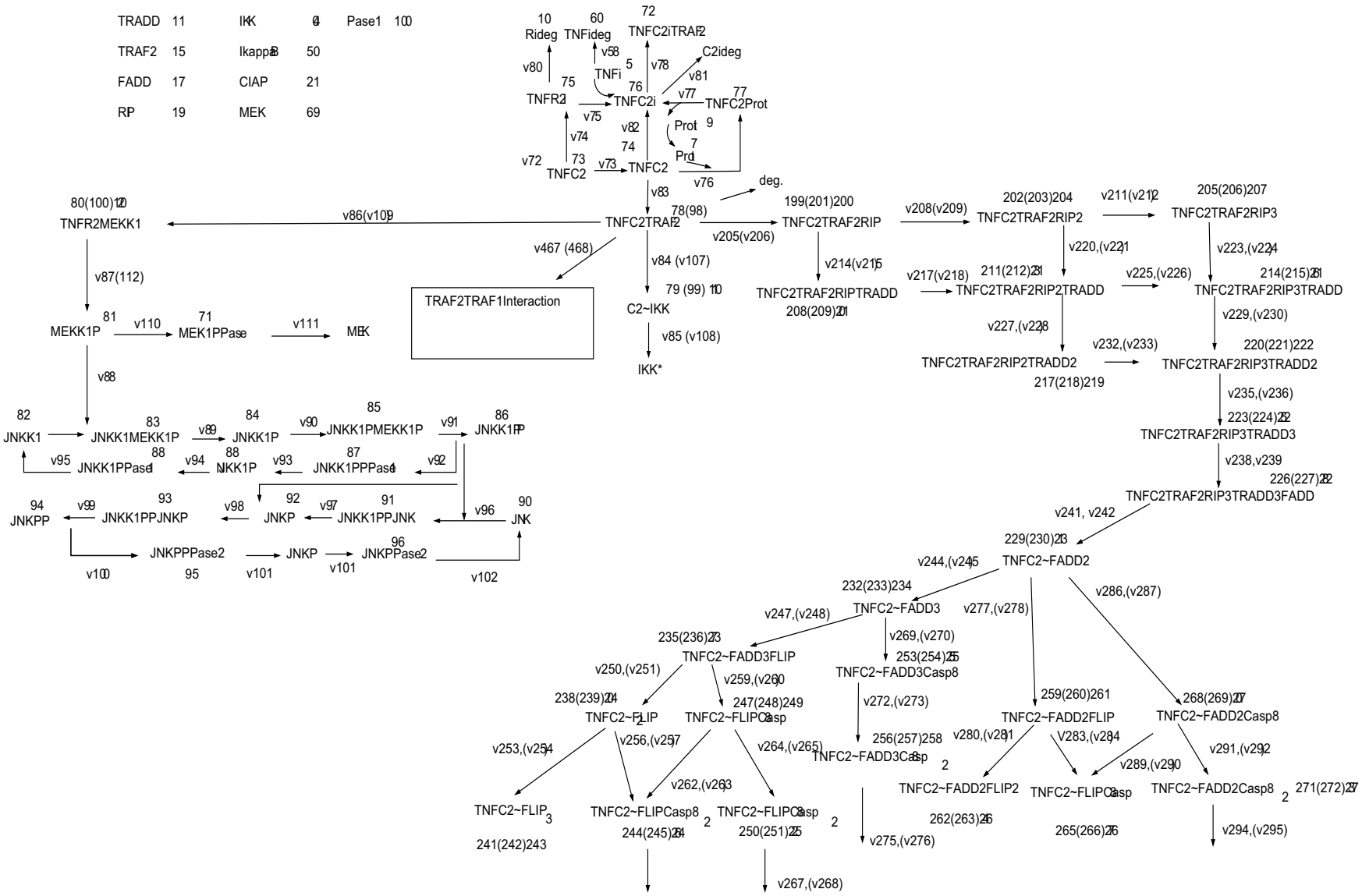

Fig. 5.4: Biochemical reaction scheme of TNF-R2.

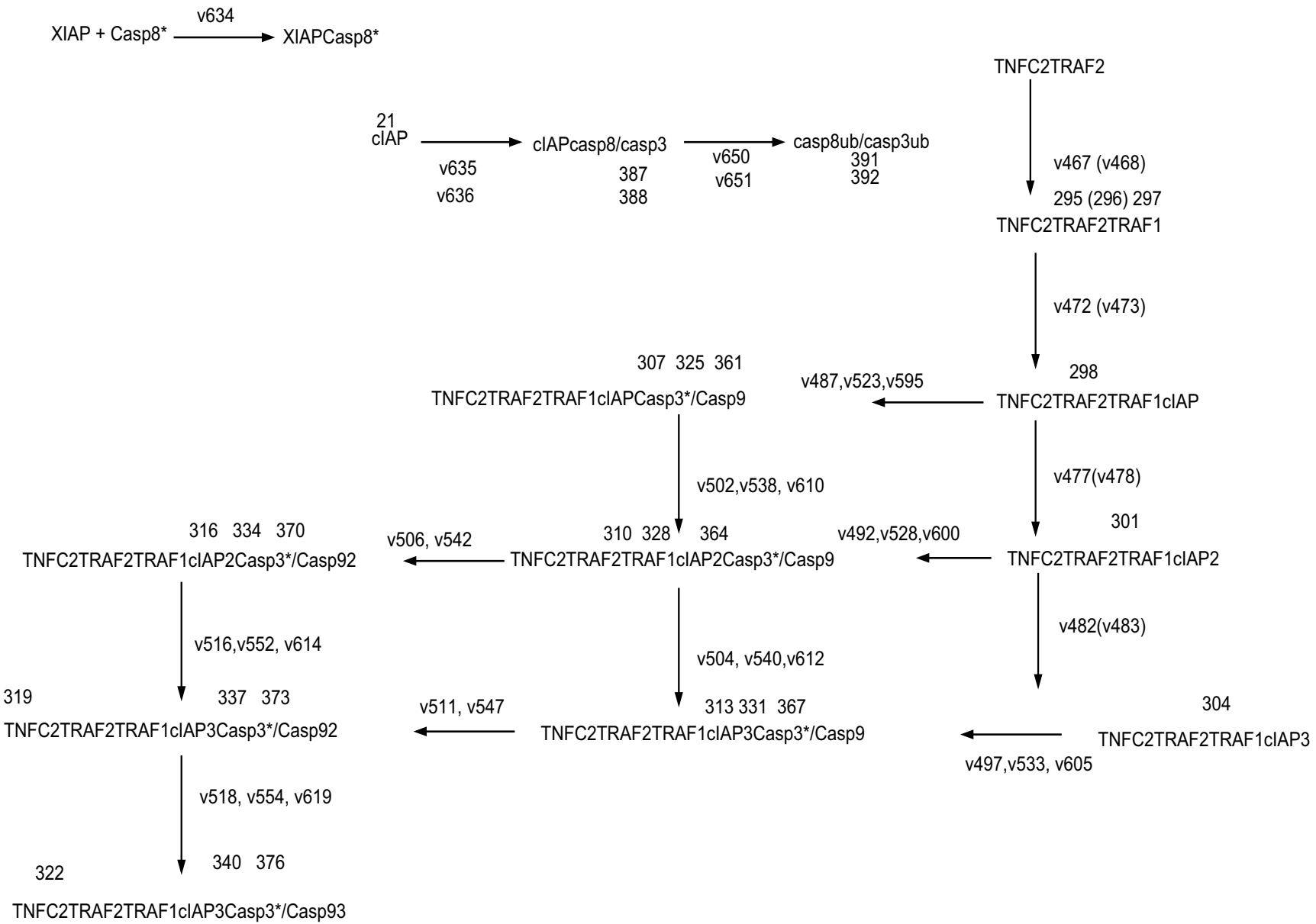

Fig. 5.5: Biochemical reaction scheme of TRAF2, TRAF1 and cIAP binding to TNF-R2.

caspase-3* and caspase-9. In order to keep the number of compounds in the biochemical reaction networks low, the last two numbers indicate only the extracellular receptor complex of caspase-3* and caspase-9. In Table 5.1 the initial protein concentrations used in the model are displayed. Some key proteins have been quantified with the help of purified GFP proteins as explained at the example of TRAF2 in the Appendix. The kinetic parameters were estimated based on the average concentrations for TRAF2, FADD and RIP. If the TRAF2 concentration reaches its upper limit of 84000 molecules/cell and FADD its lower limit of 31000 molecules/cell the onset of caspase-8 and caspase-3 activation is about 20min delayed. In the reverse situation if TRAF2 reaches its lower limit and FADD its upper limit the onset of caspase activation is about 30min early.The assumption that TRAF2 and FADD compete for TRADD leads to the observed differences in caspase activation in the simulation results. The competition takes place on the level of TRADD, the actual concentration of RIP does not affect the onset caspase activation as long as it is not limiting.

As can be seen in the biochemical reaction scheme in Figure 5.3 and in Figure 5.4 the trimeric structure of the TNF receptor has been taken into consideration in the model building process. Therefore, after TNF forms a complex with its receptor, three TRADD molecules bind to TNF-R1. TRADD forms the platform for the apoptotic and survival pathways triggered by TNF-R1. The survival pathway is initiated by the binding of TRAF2 (indicated by v11 and v149). The biochemical quantification of TRAF2 revealed 62000 single molecules. However, TRAF2 is known to be a trimer itself and binds in a 1:1 stoichiometry to the receptor. The initial concentration of TRAF2 in the model is set to 20700, as TRAF2 is known to be already trimerized in the cytosol [114]. There is no evidence yet, that TRAF2 and FADD can exist in the same receptor complex. Therefore, we assume that FADD and TRAF2 bind to TNF-R1 competitively. This assumption reduces the number of possible protein complexes significantly as well as the complexity of the model.

Downstream of the binding of TRAF2, we assume that RIP and c-IAP compete for the TNF-R1-TRADD-TRAF2 complex (v13,v14, v151, v152). This assumption is made because c-IAP was found to bind to molecules of the TRAF family in Drosophila [175] and was also shown to bind to TNF-R2 via TRAF2 in mammalian cells [118]. Therefore it seems more than likely that c-IAP

Tab. 5.1: Signaling protein levels

Protein	Concentration [nM]	Number of Molecules/Cell [ ]	References
TNF-R1		3000	Biochemical Quantification
TNF-R2		30000	Biochemical Quantification
TRADD	91.7	55000	Estimation
FADD	96.7	58000 $\pm$ 2.7e4	Biochemical Quantification
RIP	63.3	38000 $\pm$ 0.7e4	Biochemical Quantification
TRAF2	103.3	62000 $\pm$ 2.2e4	Biochemical Quantification
TRAF1	75	45000	Estimation
caspase-8	216.7	130000 $\pm$ 6e4	Biochemical Quantification
caspase-3	250	150000	Estimation
caspase-9	66.7	40000	[141]
IKK	166.7	100000	Estimation
I-κB	200	120000	Estimation
Coated Pit Protein 1		81000	[139]
c-IAP1(Prot2)	33.3	20000	Estimation
bid	25	15000	Estimation
bax	83.3	50000	Estimation
c-Flip	0.2	120	[125]
XIAP	8.33	5000	Estimation
c-IAP	5	3000	Estimation
PARP	26.7	16000	Estimation
cytochrome c	1000	600000	[100]
Apaf	16.7	10000	Estimation
MEKK1	25	15000	Estimation
JNKK1	36667	22000000	According to EGF Model
JNK	36667	21000000	According to EGF Model
Phosphatase 1	66.7	40 000	According to EGF Model
Phosphatase 2	66.7	40000	According to EGF Model
Phosphatase 3	16667	10000000	According to EGF Model

also binds to TNF-R1 via TRAF2. Whether RIP and c-IAP compete or can exist in the same complex though they bind to different binding domains remains to be elucidated.

It was shown that TNF-R1-mediated IKK activation requires both RIP and TRAF2 proteins [29]. Although TRAF2 or RIP can be independently recruited to the TNF-R1 complex, neither one of them by itself is capable of transducing the TNF signal that leads to IKK activation. It was demonstrated that IKK is recruited to the TNF-R1 complex through TRAF2 upon TNF treatment and that IKK activation requires the presence of RIP in the same complex [29]. Activated IKK leads to I-κB degradation, which frees NF-κB to translocate into the nucleus and to activate the transcription of its target genes [120]. c-FLIP [87], XIAP, TRAF1 (TNF-R-associated factor 1), TRAF2, and the inhibitor-of-apoptosis (IAP) proteins c-IAP1 and c-IAP2 have been identified as gene targets of NF-κB transcriptional activity [160]. In cells in which NF-κB is inactive, all of these proteins are required to fully suppress TNF-induced apoptosis [160]. c-IAPs have been found to inhibit active caspase-3 directly by ubiquitination [72], which implies an anti-apoptotic mechanism in addition to enzymatic inhibition. Furthermore c-IAPs were also found to inhibit caspase-9 activation by binding of procaspase-9. [28]. For U937 cells it was shown that c-IAPs inhibit TNF signaling at a level that controls activation of caspase-8 [38]. Therefore we assume that c-IAPs also ubiquitinate caspase-8 (v635, v650). In fact, we have to make this assumption in order to describe the different levels of caspase cleavage, which have been observed experimentally for the three different experimental conditions.

Structure and function analysis of XIAP revealed two distinct domains in XIAP that can suppress caspase activity [27]. The BIR3 domain binds directly to the small subunit of caspase-9. The cleavage of caspase-9 is not required for activation [141], but seems to be required for inactivation implemented by v648, v649 into the model. The crystallographic resolution of XIAP bound to caspase-3, shows that the interaction lies in a segment, which is amino-terminal to BIR2 [73]. This domain functions by a reversible, high affinity binding to caspase-3, with a dissociation constant K_D of 0.7nM for caspase-3 [123]. This high affinity interaction is implemented by reaction v197 into the model. The binding of caspase-8 to XIAP is much weaker and characterized by an affinity which result in a dissociation constant K_D higher than 10μM [123] (v634).

Looking at the apoptotic pathway, three molecules of FADD can bind to the TNF-R1-TRADD complex [70]. After the binding of FADD, c-FLIP and caspase-8 compete for binding to FADD

in the receptor complex. The binding of c-FLIP leads the apoptotic pathway into a dead end. In order to obtain activated caspase-8 two molecules of procaspase-8 have to bind to the receptor complex [106]. Caspase-8 was shown to activate caspase-3 directly [84] but also cleaves Bid into tBid which translocates from the cytosol to the mitochondria to induce the oligomerization of BAX or BAK, resulting in the release of cytochrome c (Cyto c) [53], [37]. This step is simplified by an activation step of cytochrome c by Bax, (v190 and v195) as displayed in Figure 5.3. During apoptosis, release of cytochrome c initiates dATP-dependent oligomerization of Apaf-1 and formation of the apoptosome. It could be shown, that the apoptosome binds processed and unprocessed caspase-9 and consequently recruits caspase-3. Next to caspase-3 activation it also recruits the antiapoptotic protein XIAP into the complex [16]. Cleaved caspase-3 leads to the cleavage of PARP, FLIP and XIAP [116], but can also activate caspase-8. Activated caspase-8 leads to the cleavage of TRAF1 into two fragments indicated by TRAF1c in the biochemical reaction network [76] and to the cleavage of RIP [95] indicated by RIPc in the biochemical reaction network (v21, v64). It was found that the cleavage product of TRAF1 coimmunoprecipitates with TRAF2. These results indicate that caspase-dependent cleavage of TRAF1 generates TRAF1-c fragments that are able to bind TRAF2, and then sequester TRAF2 from the TNF-R1 complex [76] and thus elicit an apoptotic effect (v64).

In order to study TNF receptor crosstalk a model of the TNF-R2 receptor needs to be included. TNF-R2 was fully cloned after TNF-R1 and its structural and functional characterization is less well understood than of its sister receptor. Part of the reason for the relative lack of knowledge about its signaling properties is that it can not be fully activated by soluble TNF, only the membrane bound form of TNF (mTNF) is capable of triggering TNF-R2 related signals [51]. TNF-R1 is equally well activated by soluble TNF and mTNF. The studies performed here were carried out with a mTNF like stimulus (details are described in the Appendix). TNF-R2 does not contain a death domain motif but was shown to recruit adapter molecules. In fact, TRAF1 and TRAF2 association was first discovered for TNF-R2 [119]. It was found that TNF-R2 induces NF-κB and JNK activation. Recent work showed that RIP is also capable of binding to TNF-R2. Little evidence indicates that TNF-R2 might trigger caspase activation in the presence of RIP in some cell lines [113]. The role of TNF-R2 in caspase activation remains to be elucidated.

As indicated in the biochemical reaction scheme in Figure 5.4 and Figure 5.5 the model contains receptor ligand binding, internalization and degradation of the TNF-R2 receptor. In the

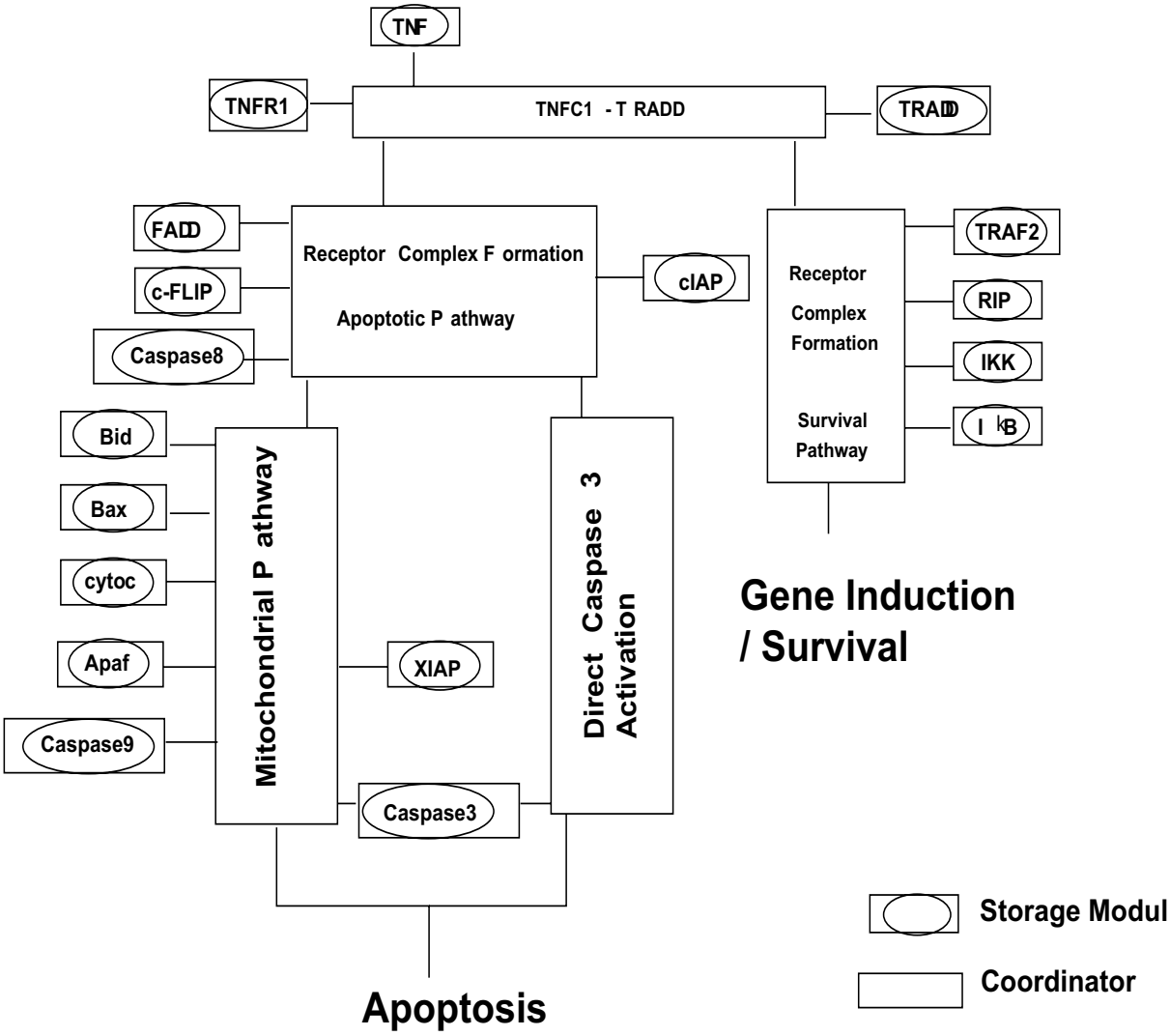

Fig. 5.6: Representation of TNF-R1 signal transduction network according to the Modular Modeling Concept.

mathematical model we incorporated JNK activation (v86 and v109), binding of TRAF2, TRAF1 and c-IAP to TNF-R2, which is shown in more detail in Figure 5.5. Furthermore IKK activation and therefore NF-κB activation (v84 and v107) have been included into the model. In order to analyze the possible role of RIP mediated caspase activation, the binding of RIP and TRADD to the TNF-R2-TRAF2 complex is taken into account, indicated by the reactions v205 and v206 in the biochemical scheme.

Experimental results show that TNF-R2 enhances TNF-R1 induced cell death via TNF-R2 induced TRAF2 depletion [166]. In the following, we discuss this hypothesis on the basis of the presented mathematical model. TRAFs mediate signal transduction from many members of the TNF receptor superfamily. In contrast to TNF-R2, TNF-R1 binds TRAF2 indirectly through the adapter protein TRADD [70]. The indirect TRAF2 recruitment by TRADD triggers the survival pathway. Alternatively the adapter molecule FADD initiates the survival pathway by binding to TRADD. As TRAF2 and FADD compete for TRADD, TNF-R1 might alternatively form pro- or antiapoptotic complexes using the available adapter molecules. It seems therefore probable that the recruitment of TRAF2 to TNF-R2 affects the pro- and antiapoptotic balance of TNF-R1 signaling. It was found that the interaction between TRADD and TRAF2 is significantly stronger (K_D=7.8μM) [110] than the direct interaction of TNF-R2 and TRAF2 (K_D=40μM - 1mM) [173], which is weak compared to other protein interactions.

As already mentioned, it has been found that costimulation of TNF-R2 enhances TNF-R1 induced apoptosis. Depletion of endogenous TRAF2 from the cytoplasmic fraction has been observed, when TNF-R2 is stimulated for prolonged times [69], [33]. Recent findings indicate that TRAF2 is recruited into endosomes after TNF-R2 stimulation [43] and finally becomes degraded. Only very recently it has been shown that binding of TNF to TNF-R2 induces ubiquitination and proteasomal degradation of TRAF2. Although c-IAP1 binds TRAF2 and TRAF1 *in vitro*, it ubiquitinates only TRAF2 [94]. In order to analyze the role of TRAF2 depletion in TNF receptor crosstalk in apoptosis we applied mathematical modeling.

In the case of TNF-R2 prestimulation, the initial TRAF2 concentration is set to zero in the model, which is consistent with the experimental data that show complete TRAF2 depletion after 6 hours of prestimulation. Due to the similarity between Fas and the apoptotic pathway, we test whether the additional binding of TRADD to the receptor would have any influence on caspase activation. The simulation and the experimental data [43] show no difference in the

caspase activation pattern. Therefore, a possible reason for the binding of TRADD to TNF-R1 is that it provides an increased binding surface and TNF-R1 can bind a larger number of additional adapter molecules rather than delaying the signaling process by the binding of additional adapter molecules.

Initially, we included the caspase activating pathway by TNF-R2 (v205, v206). During the process of parameter estimation it has become evident that TNF-R2 seems not to induce caspase activation or only to a very small extent. If we include this pathway into the model, depletion of caspase molecules through TNF-R2 occurs, which results in a much lower caspase activation by the costimulation protocol versus the experimentally observed activation. Due to these findings the reaction rates starting off at v205, v206 in Figure 5.4 are set to zero in the following.

In the literature it is shown that there is a stronger association between TRAF2 and c-IAPs in the presence of TRAF1 [118]. Therefore, we include into the model that once TRAF1 is bound to TNF-R2 its affinity for c-IAP is higher than in the TNF-R1-TRAF2-c-IAP complex.

After the detailed description of the implementation of the TNF signal transduction pathways, we discuss the simulation results for the three experimental protocols. It is important to note, that these simulation results describe the behavior of a cell population and not of a single cell, as the experimental data for caspase activation were derived from a cell population as well. In Figure 5.7 some selected time courses are shown in the graphs A-H for the stimulation with 10ng/ml TNF for the three distinct conditions. The thick black line represents the simulation results of TNF-R2 prestimulation, the gray line TNF-R1 and TNF-R2 costimulation and the thin black line selective TNF-R1 stimulation.

In the graphs A and B the time courses of the total number of receptor complexes of TNF-R1 and TNF-R2, including both external and internalized receptors, are shown. The decrease in the number of complexes is due to receptor degradation following receptor internalization, which corresponds well with literature data [9], [111]. In graph C TRAF2 depletion is depicted with a half life time of about 30min, which is consistent with experimental observation [43]. Binding of TRAF2 to TNF-R2 and the degradation of TNF-R2 itself does not lead to the observed strong TRAF2 depletion. Therefore, we assume in the model that TRAF2 interacts with an ärtificalprötein Prot2, which is only active in the presence of TNF-R2. The introduction of Prot2 leads to a TRAF2 depletion, which is consistent with the experimental data (data not shown). Interestingly only very recently c-IAP1 has been identified as this protein Prot2 by [94]. It was

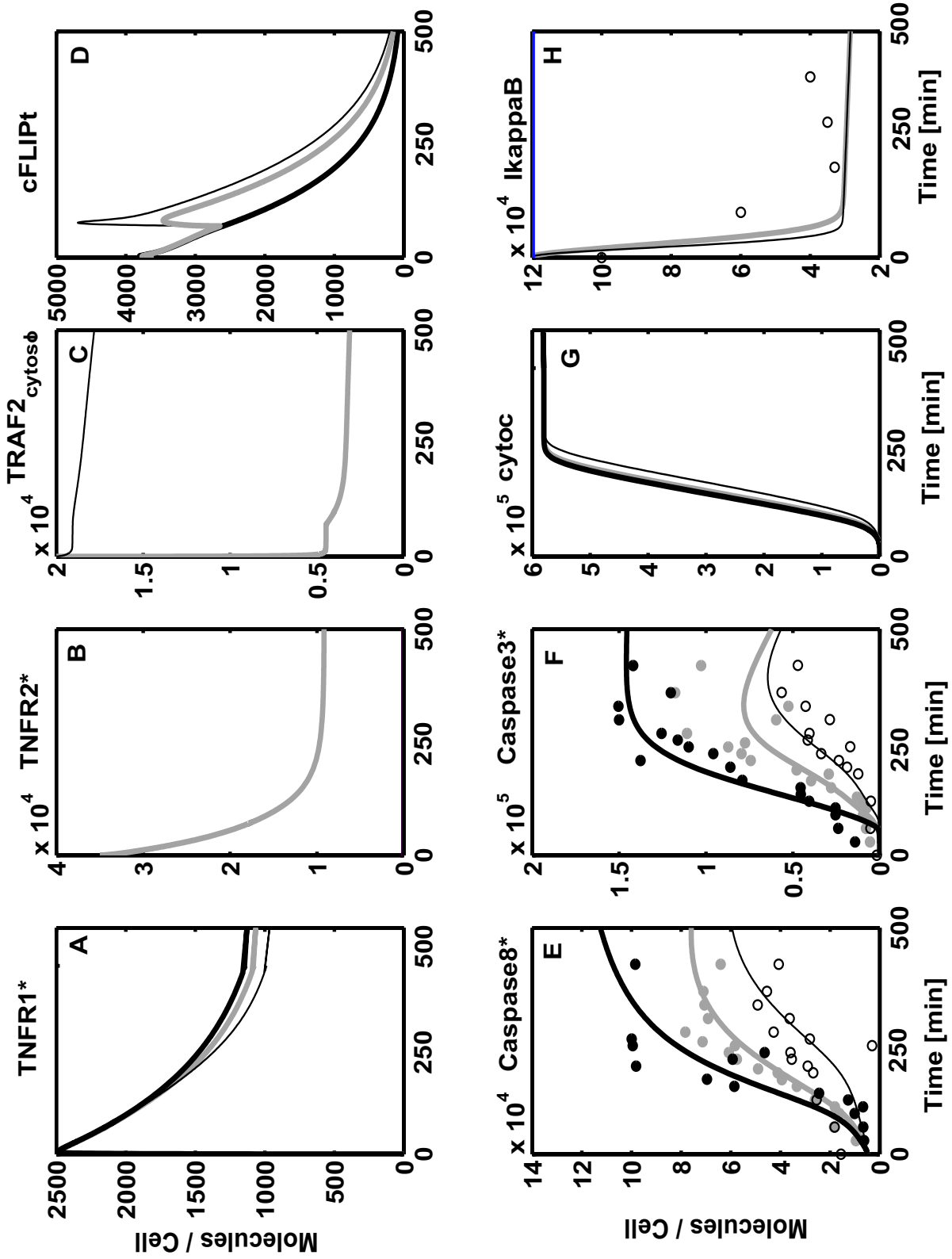

Fig. 5.7: Selective time courses of TNF-R1/TNF-R2 crosstalk under three distinct experimental conditions and 10ng/ml TNF. Simulation results: – Prestimulation of TNF-R2, – Costimulation of TNF-R1 and TNF-R2, – TNF-R1 selective stimulation. Experimental data: • Prestimulation of TNF-R2, • Costimulation of TNF-R1 and TNF-R2, ○ TNF-R1 selective stimulation.

shown that binding of TNF to TNF-R2 induces ubiquitination and proteasomal degradation of TRAF2. Although c-IAP1 binds TRAF2 and TRAF1 in vitro, it ubiquitinated only TRAF2. Graph D shows the time course of c-FLIP, a potent inhibitory molecule acting as a competitor for caspase-8. The initial concentration of c-FLIP in CHX pretreated cells is very low and the caspase-8/c-FLIP ratio was found to be 100:1 in T cells and other apoptosis sensitive cell lines [125], making it ineffective for caspase inhibition. The increase of c-FLIP after 100min is due to NF-κB induced gene induction, which was observed experimentally [87]. The decrease of the total amount of c-FLIP is caused by the cleavage of c-FLIP by active caspase-3. The selective stimulation of TNF-R1 shows a higher amount of total c-FLIP. The reason is, that there is less active caspase-3 available, which cleaves c-FLIP and leads to a decrease of c-FLIP. The cytochrome c release of the mitochondria is shown in graph G. Graph H depicts the TNF-R1 induced I-κB degradation, which then leads to NF-κB activation. It is recognizable that I-κB is already completely degraded after 12min, which is consistent with observations of NF-κB activation described in the literature [68]. The time courses of caspase-8 and caspase-3 activation are represented in the graphs E and F.

Thus, from the analysis of the current model we find, that the TNF-R1/TNF-R2 crosstalk is regulated by TRAF2, TRAF1 and c-IAP. TRAF2 is part of the crosstalk but is not the limiting molecule. The presence of TRAF2 lowers the level of caspase activation to the degree found in the costimulation experiment. A decreased level of caspase activation is equicalent with less cells going into apoptosis. If TRAF2 is the only crosstalk protein we find a slightly delayed caspase activation but no difference in the level of caspase activation. The difference in the observed lag phase between costimulation and the TNF-R1 selective stimulation appears to be due to TRAF1. The binding of TRAF1 to TNF-R2 leads to less available TRAF1 for the cleavage of active caspase-8, thus the lag phase of active caspase-8 and -3 activation is shorter as shown in Figure 5.7. Therefore, the difference in timeshift for costimulation and TNF-R1 selective stimulation seems to be regulated by TRAF1 and TRAF2. The onset of caspase-3 cleavage depends directly on the amount of activated caspase-8, which is regulated by the amount of TRAF2 binding to TNF-R1. In Chapter 5.3 we will discuss the lag phase in more detail. However, the analysis of the model reveals that the level of caspase activation is regulated by the IAPs. Due to c-IAP binding to TNF-R2, c-IAP is depleted in the cytoplasm, which results in a higher amount of caspase activation by TNF-R1 as in the case of costimulation. As the c-IAP

caspase interaction is rather weak the positive feedback from caspase-3 to caspase-8 must be very weak or does not exist. Thus, it remains to be elucidated whether an interaction between c-IAP and caspase-8 really exists or what mechanism protects the cells from apoptosis and finally defines the level of caspase activation within a population.

5.3 System Analysis - Identification of Key Proteins

The complexity of the TNF signal transduction network makes it impossible to determine the key proteins of regulation by intuition alone. In the following, we discuss the influence of TNF concentration, the number of TNF-R2 as well as influence of the concentration of certain signaling proteins on signal output. We analyze the signal output resulting from caspase-8 and -3 activation as well as I-κB degradation.

First, we discuss the influence of TNF concentration on caspase activation and I-κB degradation. Interestingly, the survival output, I-κB degradation, is much less sensitive to the TNF concentration than caspase activation. In Figure 5.8 the simulation results are shown for two concentrations of 10ng/ml and 1ng/ml TNF. The solid lines represent 10ng/ml TNF and the dashed lines stand for 1ng/ml TNF. The simulation results reveal for all three experimental protocols with 1ng/ml TNF, a significant delay in caspase activation. The increase in lagtime, which is most significant for the TNF-R1 selective stimulation, causes active caspase-8* to become more apparent after 400min which is equal to an additional delay of caspase activation of 200min compared to the 10ng/ml TNF stimulation. This finding is in contrast to the costimulation and prestimulation protocol, where the observed increase is about 100min. Therefore the selective stimulation of TNF-R1 seems to be the most sensitive to a decrease in TNF concentration. Despite the low TNF concentration all three protocols reach the same level of caspase activation after a certain time as depicted in Figure 5.8 though they do not reach the same maximum as can be seen for the TNF-R1 selective stimulation and the costimulation.

In contrast to the apoptotic output signal, caspase activation, the dose response of the survival output, I-κB degradation, reveals only a tiny time shift in the simulation. Hence, compared to caspase activation, the dose response of I-κB degradation shows almost no dependence on the stimulation protocol and the actual TNF concentration. One could speculate that this is due to a higher TRAF2 concentration, which shifts the life/death balance towards the survival pathway.

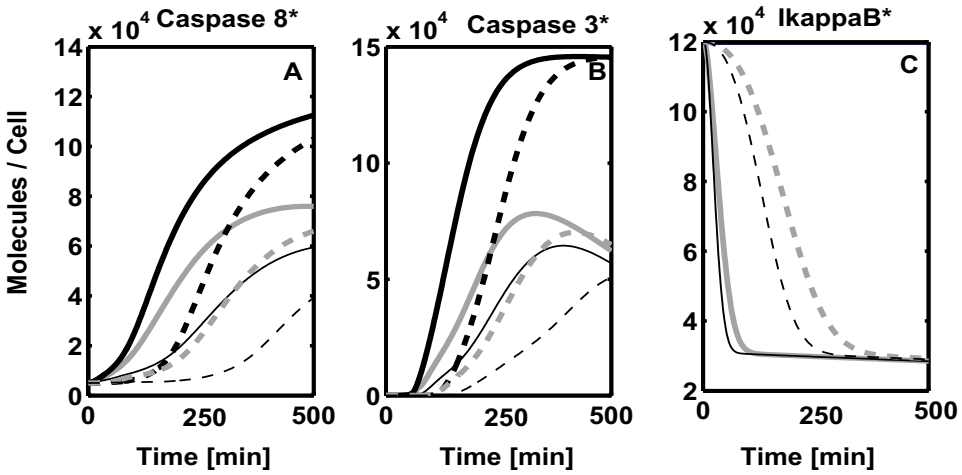

Fig. 5.8: Comparison of selective time courses of TNF-R1/TNF-R2 crosstalk for 10ng/ml and 1ng/ml for the three distinct experimental conditions. Solid lines 10ng/ml TNF; dashed lines 1ng/ml TNF (– Prestimulation of TNF-R2, – costimulation of TNF-R1 and TNF-R2 and – TNF-R1 selective stimulation).

From the measured protein concentrations of TRAF2 and FADD we know that these are about the same as shown in Table 5.1. The observed fast I-κB degradation is a result of fast kinetics downstream of TRAF2 and RIP. These results are consistent with observations described in the literature. In HeLa cells it was shown that within 30min, maximal NF-κB activation can still be observed even for TNF concentrations in the pM range [68].

Second, we investigate the influence of TNF-R2 expression on caspase-3 activation. From the simulation studies for the three experimental protocols the increase in the TNF-R2 receptor number from zero in the TNF-R1 selective stimulation protocol to 30,000 TNF-R2 receptors in the costimulation protocol indicates a significant increase in caspase activation. In Figure 5.9 the surface plot displays caspase activation as a function of time and TNF-R2 number. On the x-axis the number of TNF-R2 and on the y-axis the time in minutes is displayed. Caspase activation is indicated by the color. Black stands for 0% and white for 60% cleaved caspase-3, based on the total number of caspase-3 molecules in the cell.

As shown in Figure 5.9 even a small number of TNF-R2 receptors of about 2,000 is sufficient to increase caspase-3 activation significantly. The increase from 5,000 to 100,000 TNF-R2 results only in a small augmentation of active caspase-3. However, a further increase in TNF-R2 does not deliver a “Fas-like” caspase activation. The higher affinity of TRAF2 for TNF-R1 assures that still some TRAF2 molecules bind to TNF-R1, which leads to the induction of antiapoptotic

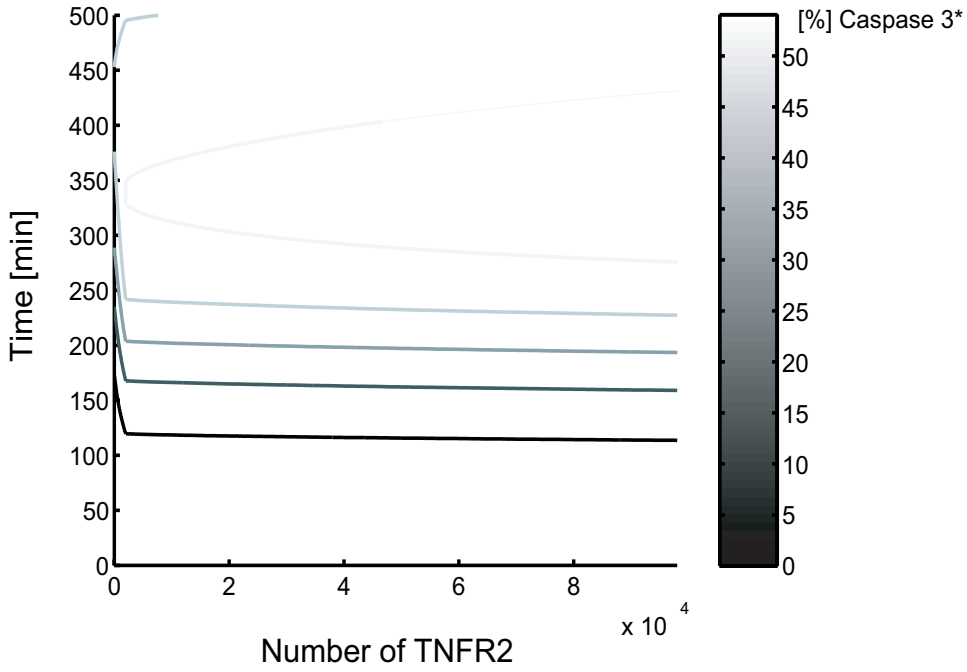

Fig. 5.9: Surface plot of caspase-3 cleavage as a function of TNF-R2 number based on the total number of caspase-3 molecules.

proteins.

Next, we analyze the influence of the overexpression of adapter molecules on caspase activation. In the following, we focus on TRAF2, TRAF1 and the antiapoptotic proteins. The overexpression of TRAF2 shifts the fragile balance between the survival pathway and the apoptotic pathway towards the survival pathway as shown in Figure 5.10. Here, the influence of TRAF2 overexpression is shown in a surface plot. As in Figure 5.9 the number of TRAF2 molecules is depicted on the x-axis and the time in minutes on the y-axis. The activation of caspase-3 in % based on the total number of receptors is indicated by the color. Black stands for 0% and white for 100% of active caspase-3, based on the total number of molecules.

As shown in Figure 5.10 the increase of TRAF2 molecules leads to a prolonged lag time as well as to a significant decrease in caspase-3 activation. In fact it could be shown experimentally that overexpression of TRAF2 and of a TRAF2 mutant, deficient in nuclear factor-kappaB activation, selectively desensitized and enhanced, respectively, TNF-R1-induced cell death in HeLa cells [166]. Once the concentration of TRAF2 exceeds the number of FADD molecules caspase-3 activation is completely abolished, as depicted in Figure 5.10. Whether such a threshold can be observed in nature remains to be elucidated. Thus, the overexpression shifts the balance

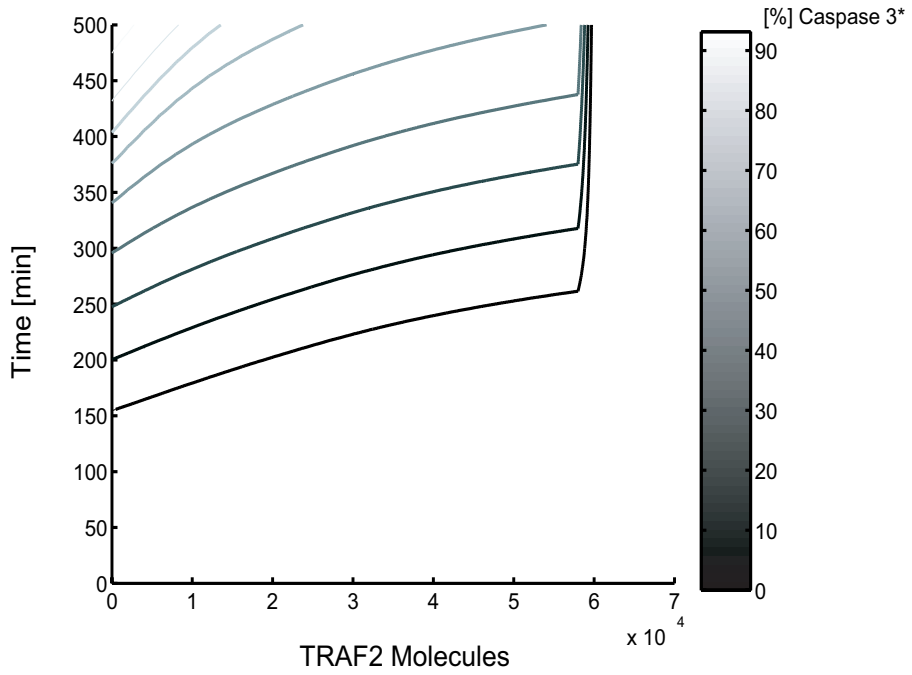

Fig. 5.10: Surface plot of caspase-3 cleavage as function of TRAF2 molecules based on the total number of caspase-3 molecules.

between the apoptotic and survival pathway clearly towards the survival pathway.

Furthermore, we are interested in the the possible role of TRAF1 overexpression and the influence of gene induction. In Figure 5.11 the solid lines represent the simulation of caspase activation stimulated by 10ng/ml TNF for the three protocols. The dashed lines represent a tenfold TRAF1 overexpression. As depicted in Figure 5.11 the combination of NF-κB induced antiapoptotic proteins and TRAF1 overexpression leads to a complete loss of free active caspase-8 for the TNF-R1 selective stimulation protocol. However, there is still some caspase-3 cleavage observable. As these results represent the behavior of a cell population, there are still cells which enter apoptosis. To conclude, TRAF1 overexpression itself is not sufficient to suppress caspase activation but in combination with gene induction it is very potent. However, a complete suppression of apoptosis is only possible in combination with an overexpression of TRAF2 and/or c-IAPs. These results are consistent with literature data, as it could be shown that TRAF1 overexpression prevents cells death only in combination with c-IAP and TRAF2 [160].

In the case of the pre- and costimulation protocol shown in Figure 5.11 by the dashed black and gray line, the overexpression of TRAF1 leads to a significant time shift of caspase activation. The simulation results depict that in the case of the TNF dose response study the same level

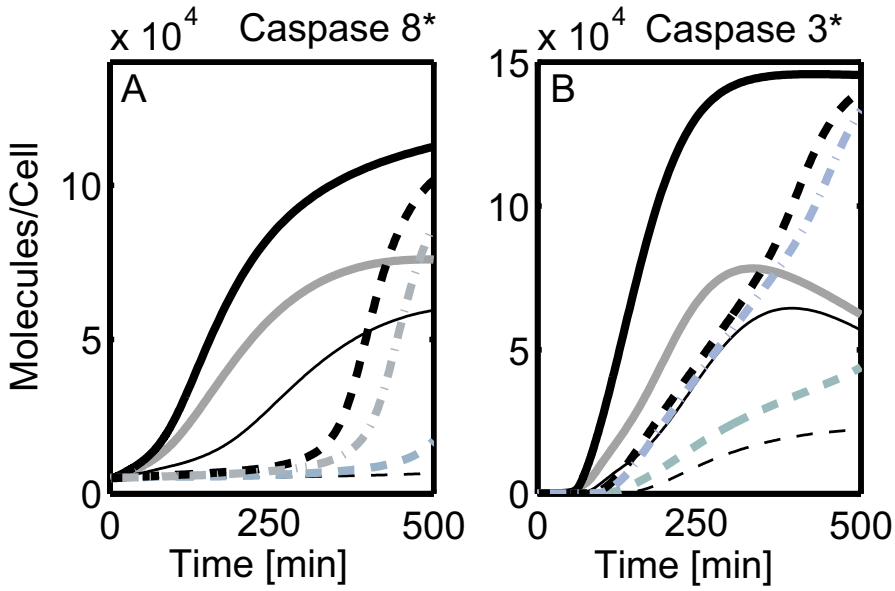

Fig. 5.11: Simulation study for the overexpression of TRAF1 in the presence and absence of gene induction of antiapoptotic proteins at 10ng/ml TNF: – Prestimualtion of TNF-R2, – costimulation, – TNF-R1 selective stimulation, original model. Dashed lines: 10 fold TRAF1 overexpression in the presence of gene induction; dashed-dotted lines: 10 fold TRAF1 overexpression in the absence of gene induction.

of caspase activation is reached despite the TRAF1 overexpression. The inhibition of gene induction, depicted by the dashed-dotted gray line for the prestimulation protocol reveals a delay in caspase activation but at steady state the system reaches the same level of caspase activation as found in the prestimulation protocol.

Taken together these results indicate that the ratio between TRAF1 and TRAF2 as well as whether these molecules can replace each other in this signal transduction network, seems to be of great importance. However, the results discussed above, indicate that the level of caspase activation is not determined by TRAF1 alone. A TRAF1-c-IAP complex in the cytosol which binds cleaved caspase-3, would result in a significantly lower caspase activation if TRAF1 is overexpressed. However, TRAF1 is not shared by the two receptors TNF-R1 and TNF-R2 to a large extend and is therefore not subject to receptor crosstalk. In contrast to TRAF1, TRAF2 plays an important role in both signaling networks and can therefore modulate the crosstalk together with c-IAP and TRAF1. Changes in the level of caspase activation provide indirect evidence of the existence of cytosolic TRAF2-TRAF1-c-IAP complexes.

Furthermore, we address the question of whether the overexpression of XIAP, c-FLIP and c-

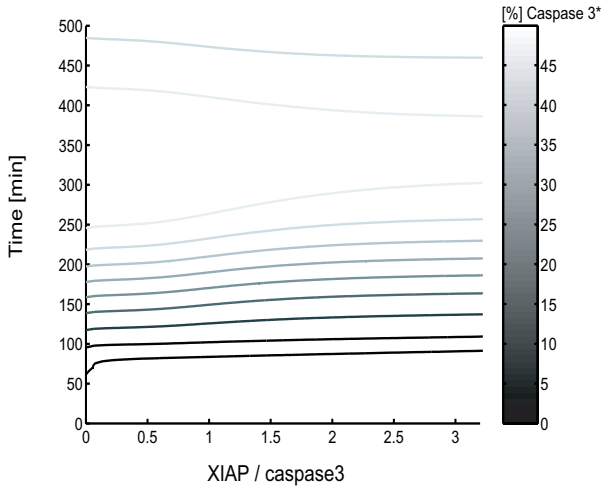

Fig. 5.12: Surface plot of caspase-3 cleavage as function of XIAP molecules per cell based on the total number of caspase-3 molecules.

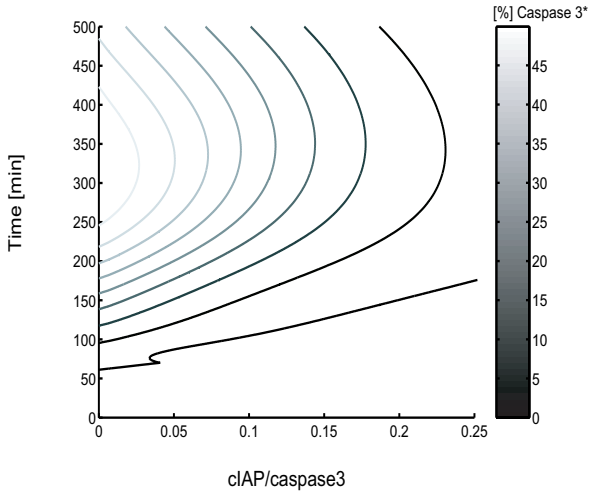

Fig. 5.13: Surface plot of caspase-3 cleavage as function of c-IAP molecules per cell based on the total number of caspase-3 molecules.

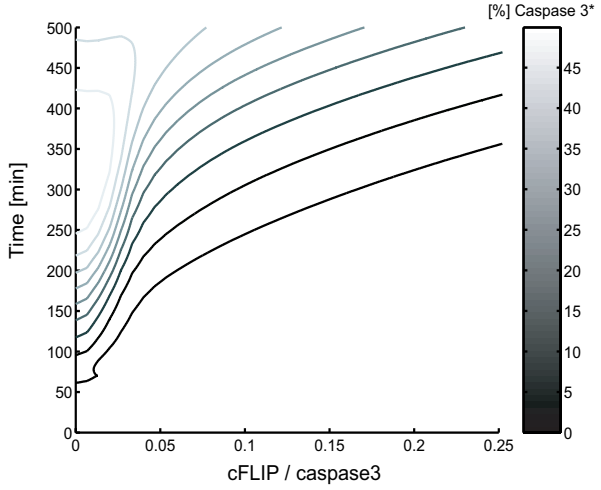

Fig. 5.14: Surface plot of caspase-3 cleavage as function of c-FLIP molecules per cell based on the total number of caspase-3 molecules.

IAP can protect the cells from apoptosis. In the following simulation studies we set two of the three antiapoptotic proteins to zero and increase the concentration of the third from zero on. In Figure 5.12 the influence of XIAP on caspase-3 cleavage is shown. All these studies have been done for the TNF-R1 selective stimulation protocol and 50ng/ml TNF. On the x-axis the ratio of XIAP to caspase-3 is depicted and on the y-axis the time in minutes. The color indicates caspase-3 cleavage. White stands for 50% caspase-3 cleavage and black for 0%. As can be seen from Figure 5.12 XIAP influences the lag phase of caspase activation only slightly, whereas it acts more on the decrease in caspase-3 activation. In general XIAP does not seem to be very potent.

The according simulation study for c-IAP reveals a different picture, as shown in Figure 5.13. First, c-IAP is much more effective than XIAP. Compared to the XIAP concentrations, much less c-IAP molecules influence caspase-3 cleavage significantly. C-IAP increases the lag time of caspase activation but it mainly decreases caspase-3 cleavage. Indeed, the prevention of apoptotsis by overexpression of c-IAP in combination with TRAF2 is shown in the literature [160]. A complete inhibition of caspase-3 cleavage soley by c-IAP overexpression is not possible as depicted in Figure 5.13.

In Figure 5.14 the effect of c-FLIP on caspase-3 activation is displayed. From the simulation study, c-FLIP seems to influence caspase activation by increasing the lagtime significantly. Comparing Figure 5.12 and Figure 5.13 to Figure 5.14, c-FLIP is observed to be the most potent protein of the three antiapoptotic proteins discussed here.

As a consequence, the following hierarchy within the mentioned antiapoptotic proteins can be found:

$$\textbf{cFLIP} \gg \textbf{c-IAP} \gg \textbf{XIAP}$$
$$\Longrightarrow \text{decrease in antiapoptotic potency}$$

5.4 Analysis of the Caspase activating Pathways

Scaffidi et. al. showed that there exist at least two different ways to stimulate caspase activation [125]. So called type I cells induce apoptosis directly by large amounts of activated caspase-8

that is triggered by the receptor complex. In contrast, in type II cells very little initial caspase-8 activation can be observed but caspase-8 activation is amplified by the mitochondrial pathway [125], which leads to a significant caspase-3 activation.

In Figure 5.15 a simplified scheme of caspase activating pathways is shown. As mentioned in the section before, the prestimulation of TNF-R2 leads to an almost complete depletion of TRAF2 in the cytosol. Likewise it is possible to shut off pathway A in Figure 5.15. In Figure 5.7 the experimental and simulation results reveal the strong protecting function of the survival pathway via TRAF2. In the following, we analyze the influence of the mitochondrial pathway, indicated in Figure 5.15 by B, of the positive feedback from cleaved caspase-3 to caspase-8, indicated by C and the direct cleavage of caspase-3 by caspase-8 indicated by D on caspase-3 cleavage.

Our biological system, the HeLa cell, is well known to be a so called type II cell in the case of Fas stimulation [50]. The model contains the mitochondrial pathway. To validate the model, we test if the simulation confirms the experimental result of HeLa cells being type II cells. Therefore, a complete abolishment of caspase activation if the mitochondrial pathway is inhibited should be observed. Blocking the mitochondrial pathway and testing the three experimental protocols of receptor stimulation leads to three distinct patterns of caspase-3 cleavage, which are depicted in Figure 5.16. As shown by the dashed lines the model predicts that the mitochondrial pathway leads to a complete loss of caspase activation for the TNF-R1 selective stimulation, which is consistent with experimental data of bcl-2 overexpressing cells (P. Scheurich personal communication). For the costimulation of TNF-R1 and TNF-R2 a significant decrease in caspase activation is predicted by the model. However, for the prestimulation protocol the influence of inhibiting the mitochondrial pathway shows only a slight effect on caspase activation. Taken together, the mitochondrial pathway seems to amplify caspase cleavage in the case of TNF-R1 costimulation protocol and in the case of TNF-R1 selective stimulation. In contrast, the mitochondrial pathway hardly affects caspase activation, when TNF-R2 has been prestimulated.

These predictions are difficult to evaluate experimentally, but may give an idea of the functional role of the mitochondrial pathway. In fact, preliminary experiments of bcl-2 overexpressing cells show a complete loss of caspase-3 activation for the TNF-R1 selective stimulation but for the costimulation protocol still some caspase cleavage (P. Scheurich personal communication).

In Figure 5.17 and in Figure 5.18 the surface plots of the dose responses for caspase-3 cleav-

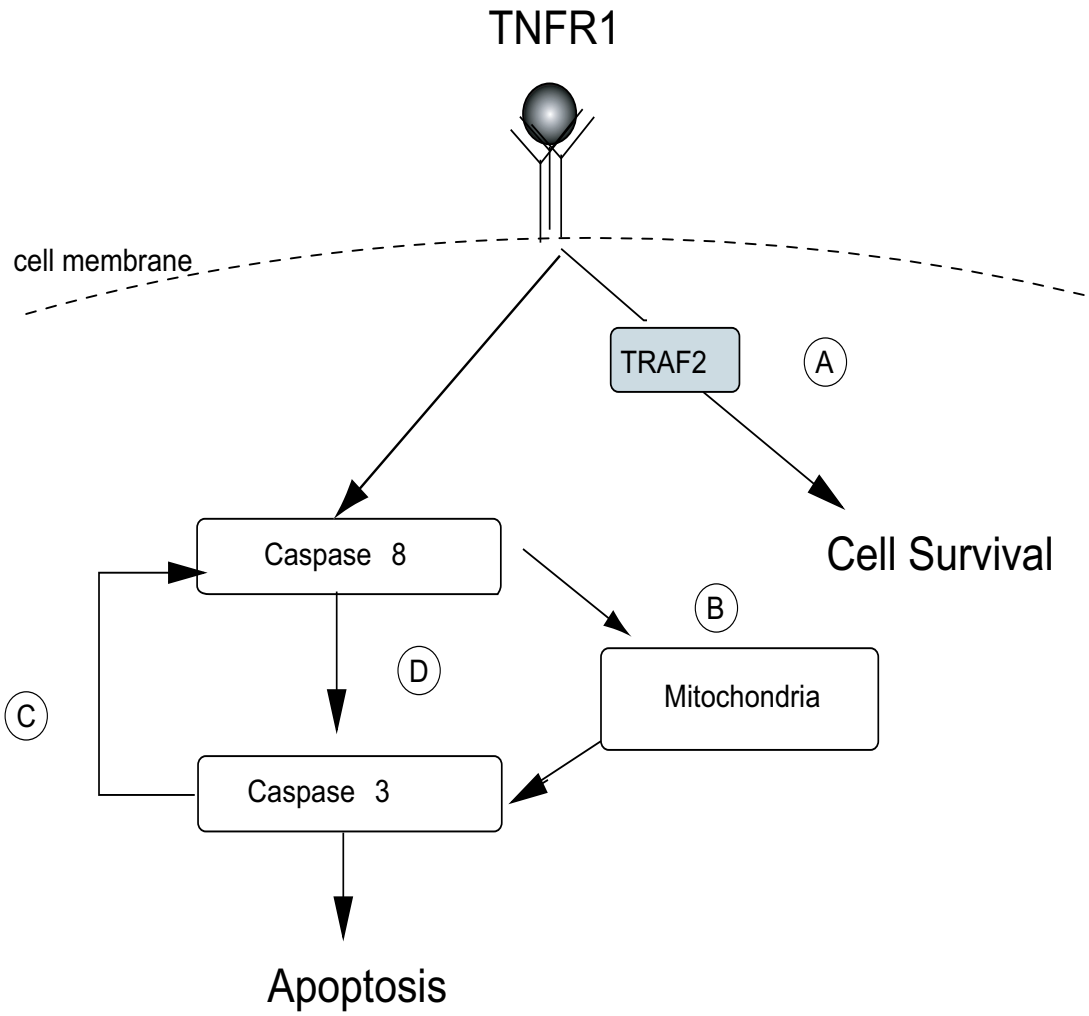

Fig. 5.15: Scheme of the different caspase activating pathways. A TNF induced survival pathway, B mitochondrial pathway, C positive feedback, caspase-3 cleaves caspase-8 and D caspase-8 cleaves caspase-3.

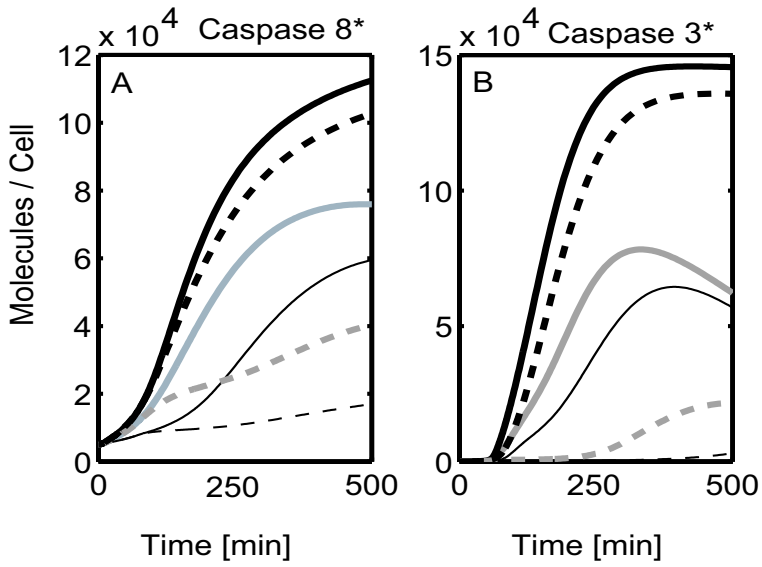

Fig. 5.16: Influence of the mitochondrial pathway in caspase activation. Solid lines: – Prestimulation, – Costimulation, – TNF-R1 selective stimulation; Dashed lines: Caspase activation without the mitochondrial pathway.

age are displayed. In both figures cleaved caspase 3 as a function of TNF concentration is shown. On the x-axis the TNF concentration and on the y axis the time is depicted. In Figure 5.17 the TNF-R1 selective caspase-3 cleavage is presented. In comparison to Figure 5.17, Figure 5.18 shows the surface plot of caspase-3 activation if the mitochondrial pathway is inhibited. Just by comparing the scales of the two plots, the amplifying effect of the mitochondrial pathway becomes obvious. In Figure 5.18 the maximal caspase-3 activation is 9% compared to 40% in Figure 5.17. From Figure 5.18 it can be seen that even at longer times the positive feedback from caspase-3 to caspase-8 does not lead to a maximal caspase-3 activation.

Therefore, the inhibition of the positive feedback from cleaved caspase-3 to caspase-8 (indicated in Figure 5.15 by C) influences the caspase activation only slightly. In order to assess the contribution of the different pathways to caspase activation, we analyze the dynamics of the reaction rates leading to caspase activation via the presented pathways. Caspase-8* cleaves caspase-3 directly via reaction v53, caspase-9* cleaves caspase-3 via the mitochondrial pathway, represented by reaction v203 and reaction v18 stands for the consumption of caspase-3* by the positive feedback from caspase-3* to caspase-8. In Figure 5.19 the time courses of v53, v203 and v18 are depicted. As can be seen in Figure 5.19A if TNF-R1 is stimulated selectively the initial caspase-3 cleavage is caused directly by caspase-8* (pathway D) but soon

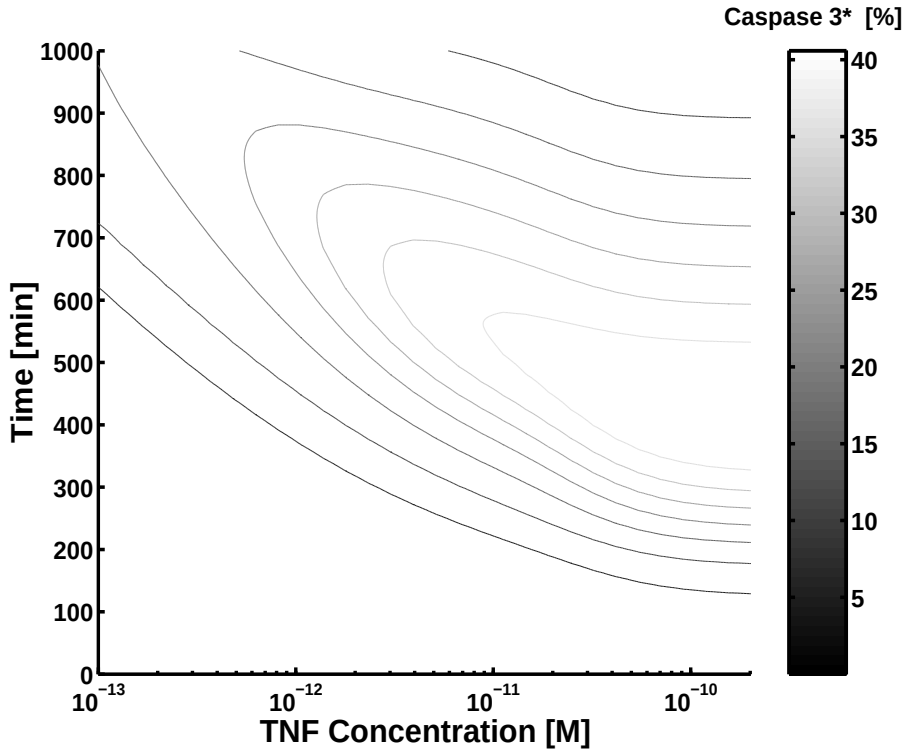

Fig. 5.17: Surface plot for caspase-3 cleavage as a function of TNF concentration.

the mitochondrial pathway becomes dominant. In Figure 5.19 B caspase-3 cleavage for the costimulation of TNF-R1 and TNF-R2 is shown. In comparison to graph A, in graph B the mitochondrial pathway is less influential. In fact, blocking v53 in the case of pre- or costimulation protocol leads to caspase activation patterns that are very similar to TNF-R1 selective stimulation and for the TNF-R1 selective stimulation caspase-3 activation is decreased and delayed. From this, we can conclude that caspase-3 cleavage is dominated in all cases according to Figure 5.15 by pathway B and D. The influence of the mitochondrial pathway is most significant for the TNF-R1 selective stimulation.

5.5 The Ligand Passing Phenomenon

In this section the so called Ligand Passing phenomenon is studied. The basis of Ligand Passing is that the 75-kDa tumor necrosis factor (TNF) receptor recruits TNF for signaling by the 55-kDa TNF receptor. It was discovered by Tartaglia et. al. in 1993 on U937 cells at 0^{o}C [146]. They found that the number of complexes measured under costimulation conditions is much

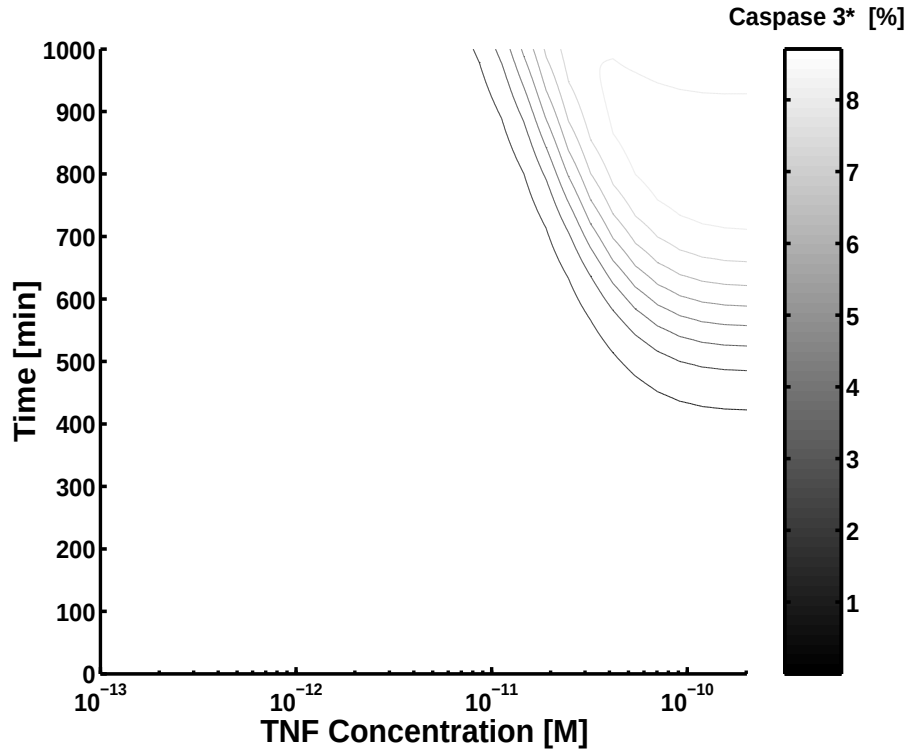

Fig. 5.18: Surface plot for caspase-3 cleavage as a function of TNF concentration while the mitochondrial pathway is inhibited.

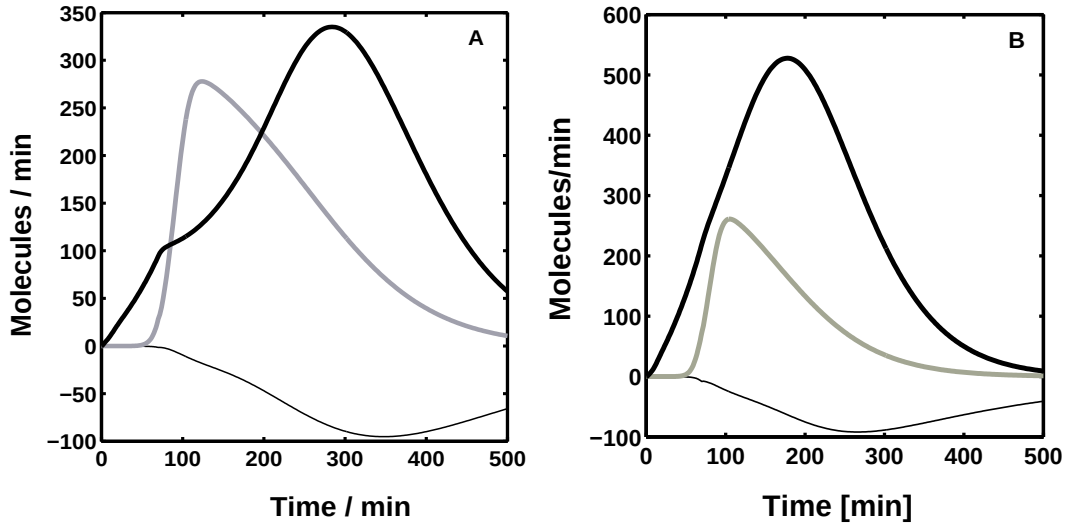

Fig. 5.19: Dynamics of the reaction rates leading to caspase 3 activation: **–** direct activation of caspase-3 by caspase-8* (v53), – caspase-3 cleavage via the mitochondrial pathway (v203) and – positive feedback from caspase-3* to caspase-8 (v16): **A** TNF-R1 selective stimulation **B** TNF-R1/TNF-R2 costimulation.

bigger than the selective stimulation of TNF-R1 and TNF-R2. Here, we investigate if this phenomenon, which Tartaglia called “Ligand Passing” is observable at 37^{o}C as well and whether it influences the intracellular signaling. Initially, we deterimine the binding rates for each of the receptors on the two cell lines under investigation: U937 and transfected HeLa cells. In the next step both receptors are costimulated and in order to asses Ligand Passing, we compare the simulation results with experimental data. As a result we find for low TNF concentrations a higher number of TNF receptor complexes then expected with the kinetic rates describing the complex formation for each receptor type separately. The analysis of the influence of Ligand Passing on the intracellular signal transduction with respect to caspase-3 activation or I-κB degradation, reveal no significant differences.

Binding Kinetics

TNF induced signal transduction is controlled by two distinct membrane receptors, TNF-R1 and TNF-R2, which differ in their affinity. TNF-R1 was found to be the high affinity receptor [52]. This high affinity determined for TNF-R1 is mainly caused by the marked stability of its ligand-receptor complexes in contrast to the transient interaction of soluble TNF with TNF-R2. In the following section, we compare the binding kinetics determined with the help of a Matlab routine for the three human cancer cell lines U937, KYM and HeLa80. The Matlab routine fits the association and dissociation rates, under consideration of depletion in the solute, to experimental data. We chose the U937 cells because Tartaglia et. al [146] observed the Ligand Passing phenomenon in these cells at 0^{o}C. The U937 have the advantage of expressing TNF-R1 and TNF-R2 in the same range. Furthermore, we chose transfected HeLa cells as the model for the intracellular signaling that has been developed for this cell line. Comparing the receptor expression levels of the different cell lines, on the U937 both receptor types are present with average numbers of 1000 TNF-R1 and 2000 TNF-R2 whereas the transfected HeLa cells express about 3000 TNF-R1 and 30000 TNF-R2. For the binding studies one receptor type is blocked in order to measure the number of complexes formed with the second receptor type at 37^{o}C and soluble TNF. The routine is based on the following equations and the number of receptors is assumed to be constant. L(t) indicates the ligand concentration TNF in [M], R_1(t) for TNF-R1, R_2(t) for TNF-R2, and C_1(t), C_2(t) for the number of complexes formed with TNF-R1 and TNF-R2 respectively.

$$L + R_1 \rightleftharpoons C_1 \tag{5.1}$$

$$L + R_2 \rightleftharpoons C_2 \tag{5.2}$$

$$\frac{dC_1}{dt}(t) = k_{on1}L(t)R_1(t) - k_{off1}C_1(t), \tag{5.3}$$

$$\frac{dC_2}{dt}(t) = k_{on2}L(t)R_2(t) - k_{off2}C_2(t). \tag{5.4}$$

Mass Balance:

$$R_1 = R_{T1} - C_1, \tag{5.5}$$

$$R_2 = R_{T2} - C_2, \tag{5.6}$$

$$L = LT - (C_1 - C_2) * Z/(VNav). \tag{5.7}$$

Where Z=1.2x10^6 represents the number of cells per well, V=100μl the volume of solute and N_{AV} Avogadro's Number. In the following table the kinetic rates for the different experiments can be found.

Considering only one receptor type and its ligand the equation can be solved analytically and the number of complexes results as:

With $z = \frac{Z}{N_{AV}V}$

$$\frac{dC}{dt}(t) = k_{on1}(R_T - C(t))(L_T - C(t)z) - k_{off1}C(t), \tag{5.8}$$

$$\frac{dC}{dt}(t) = k_{on1}L_TR_T - C(t)(k_{on1}R_Tz - k_{on1}L_T - k_{off1}) + k_{on1}zC^2(t). \tag{5.9}$$

and defining a,b,c and δ as:

$c = k_{on1}L_TR_T$,

$b = -(k_{on1}R_Tz - k_{on1}L_Tz - k_{off1})$,

$a = k_{on1}z$,

$\delta = 4ac - b^2$.

$$\int_0^C \frac{dC}{aC^2 + bC + c} = \int_0^t dt. \tag{5.10}$$

Tab. 5.2: Experimental Conditions.

File	Conc. [M]	$R1_{Pb}$	$R2_{Pb}$	Cell Number	Spec. Radioact.	Volume[μl]
U937						
mappe	3.2e-11			1.2e6	49300	100
ass	4.1e-11	1394	1597	1.2e6	100000	100
gudneu	4.1e-11			1.2e6	100000	100
Gud200400	1.96e-11	330	370	1.2e6	115000	100
assjun	3.9e-11	600	960	1.5e6	92000	100
Hela80						
Hela80141100	4.1e-11	1300	25000	0.7e6	57000	150
Hela802201	4.0e-10	700	15000	0.1e6	80000	150
Hela802501	4.0e-10	2400	26000	0.1e6	80000	150

Integrated from C=0 to C and from t=0 to t and the initial conditions of C(t=0)=0 one obtains:

$$\frac{1}{\sqrt{(-\delta)}} ln(\frac{2aC+b-\sqrt{-\delta}}{2aC+b+\sqrt{-\delta}}) - ln(\frac{b-\sqrt{-\delta}}{b+\sqrt{-\delta}}) = t. \tag{5.11}$$

Solved for C reveals:

$$C(t) = \frac{(b^2+\delta)(\exp(t\sqrt{-\delta})-1)}{2a[b(1-\exp(t\sqrt{-\delta}))+\sqrt{-\delta}(1-\exp(t\sqrt{-\delta}))]}. \tag{5.12}$$

Equation 5.12 was used to fit the kinetic rates of the experimental data. In Table 5.2 the experimental conditions for each of the experiments is listed (for the exact methods see [52]:

From these results the dissociation constant K_D for TNF-R1 ranges from 0.1 - 0.4nM and for TNF-R2 from 0.01 - 0.04nM, which means TNF-R2 shows the higher affinity. The dissociation constant for TNF-R1 is consistent with the published dissociation constant for TNF-R1 on HeLa cells, which was found to be 0.25nM for solubilized receptors [135]. Comparing our K_D's with the K_D's determined by Grell et. al. [52] there is a contradiction, which has not been resolved yet. M. Grell et. al. find experimentally a very low ligand dissociation rate from TNF-R1, which is about one order of magnitude smaller then the one determined for TNF-R1 as depicted in Table 5.3. However, the experimental data assuming reasonable receptor numbers and a rather low TNF concentration can only be described by the kinetic rates determined here. The difference in the dissociation constants is due to the different dissociation rates. As the K_D's described by Grell et. al were measured *in vivo* the difference might be due to nonspecific binding of TNF to the membrane proteins.

In Table 5.3 the kinetic parameters obtained by fitting the experimental data to the equation are listed.

Ligand Passing

Tab. 5.3: Kinetic parameter for ligand receptor interaction.

File	Concentration [M]	koff1 [s]	koff2 [s]	K_D1 [M]	K_D2 [M]
U937					
Gud2004001	1.9e-11	1.9e-2	3.1e-3	3.4e-10	3.4e-11
Gud2004002	1.9e-11	2.2e-2	2.7e-3	3.7e-10	2.9e-11
Gud2004003	1.9e-11	2.3e-2	3.9e-3	3.9e-10	4.3e-11
mappe1	3.2e-11	1.03e-2	1.7e-3	1.84e-10	1.89e-11
mappe2	3.2e-11	8.5e-3	1.5e-3	1.5e-10	1.65e-11
mappe3	3.2e-11	1.3e-3	9.7e-4	2.3e-11	1.1e-11
ass1	4.1xe-11	1e-2	4E-3	4.4e-11	4.4e-11
ass2	4.1e-11	1e-2	4e-3	1.9e-10	4.4e-11
ass3	4.1e-11	9.8e-3	3.6e-3	1.75e-10	4.0e-11
assjun001	3.9e-11	8.2e-3	3.8e-3	1.46e-10	4.2e-11
assjun002	3.9e-11	8.2e-3	3.8e-3	1.46e-10	4.2e-11
assjun003	3.9e-11	9.3e-3	3.5e-3	1.66e-10	3.89e-11
gudneu1	4.5e-10	1.9e-2	2.9e-2	3.4e-10	3.19e-10
gudneu2	4.5e-10	8.6e-3	3.1e-2	1.54e-10	3.41e-10
gudneu3	4.5e-10	2.8e-2	2.8e-2	4.91e-10	3.02e-10
Hela80					
Hela80141100	3.9e-11	2.5e-2	2.7e-3	4.5e-10	3.0e-11
Hela80141100	3.9e-11	2.8e-2	2.4e-3	5e-10	2.64e-11
Hela80141100	3.9e-11	2.8e-2	2.2e-3	5e-10	2.4e-11
Hela8022011	4e-10	1.7e-2	2.7e-2	4.5e-10	3.0e-10
Hela8022012	4e-10	4.2e-2	2.4e-2	5e-10	2.64e-10
Hela8022012	4e-10	3.7e-2	1.7e-2	6.6e-10	1.87e-10
Hela802501	3.9e-11	2.2e-2	1.9e-2	3.9e-10	2.1e-11e
Hela802501	3.9e-11	3.3e-2	2.2e-2	5.9e-10	2.4e-11
Hela802501	3.9e-11	2.8e-2	2.8e-3	5e-10	3.08e-11

In section, the theory of Ligand Passing is under investigation. We apply the kinetic rate constants determined above and compare the simulated results of the binding studies for the selective stimulation of TNF-R1 and TNF-R2 and the costimulation of TNF-R1 / TNF-R2 for a high (50ng/ml) and a low (5ng/ml) concentration with experimental results. The first concentration investigated is a high TNF concentration (50ng/ml) and the second concentration is a very low TNF concentration (5ng/ml). The theory of Ligand Passing hypothesizes that TNF-R2 bound ligand might be passed over to TNF-R1 to enhance TNF-R1 signaling [146]. Assuming that at a high TNF concentration the system has already reached saturation, we do not expect any Ligand Passing to occur. In contrast as a low concentration implies low receptor occupation, the effect of Ligand Passing should become evident.

Thus, in the following figures the simulation results of a TNF-R1 selective stimulation, a TNF-R2 selective stimulation and the costimulation of TNF-R1 and TNF-R2 are presented. In order to simulate the receptor complex formation the equations 4.38 and 4.39 were used. The number of complexes, if the receptors are costimulated, results from the sum of the number of complexes of TNF-R1 and TNF-R2. In Figure 5.20 A the simulation describes well the experimental data. Thus the summation over the number of complexes formed by TNF-R1 and TNF-R2 describes without any further changes of the kinetic parameters the experimental data. In Figure 5.20 B the depletion of TNF due to ligand binding to the receptors on the cell surface is presented.

In contrast to Figure 5.20 the simulation can not describe the experimental results for 5ng/ml TNF as shown in Figure 5.21 A. The solid lines represent the conventional model not taking any cooperative effects into account. The dashed lines show the simulation results from a model assuming that TNF-R1 shows a higher affinity for TNF if TNF-R2. The thick black dashed line stands for the number of TNF-R1 complexes formed in the presence of TNF-R2 and the gray dashed line represents the number of TNF-R2 complexes respectively. Due to ligand depletion in the solute the number of TNF-R2 complexes actually decreases. Assuming a 1.5 times higher association rate of TNF-R1 enables us to describe the experimental data reasonably well. These results could be shown in several independent experiments. From these findings it seems that there is some kind of positive cooperativity occurring at the receptor level for low TNF concentrations, which could be called Ligand Passing. This only becomes obvious for low

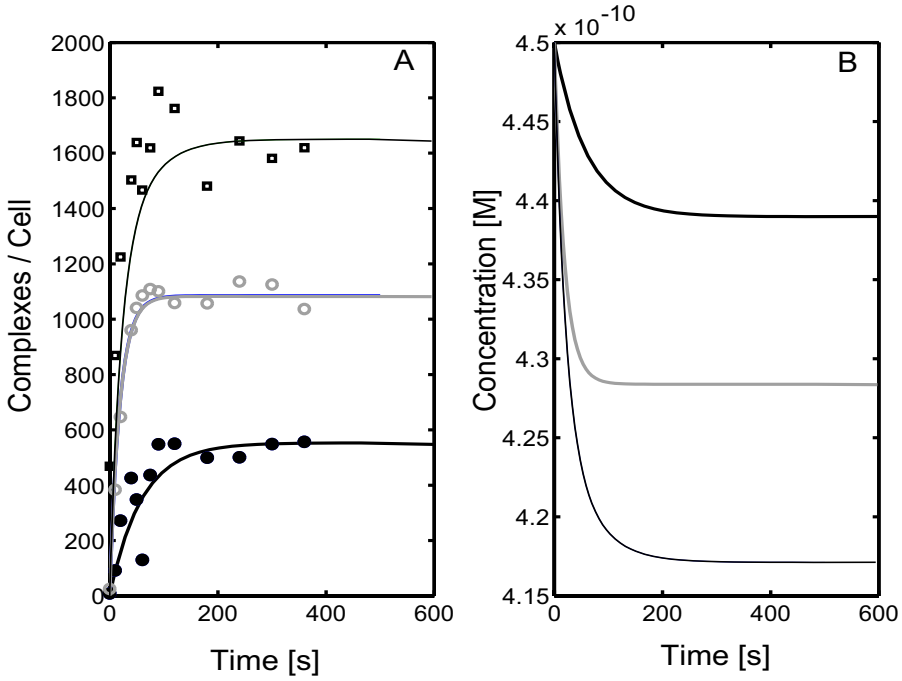

Fig. 5.20: High TNF concentration (50ng/ml): **A** TNF receptor complex formation: • TNF-R1 selective stimulation, ○ TNF-R2 selective stimulation and □ Costimulation of TNF-R1 and TNF-R2. The solid lines always indicate the simulation results. **B** TNF concentration in the solute, **–** TNF-R1 selective stimulation, – TNF-R2 selective stimulation and – costimulation of TNF-R1 and TNF-R2.

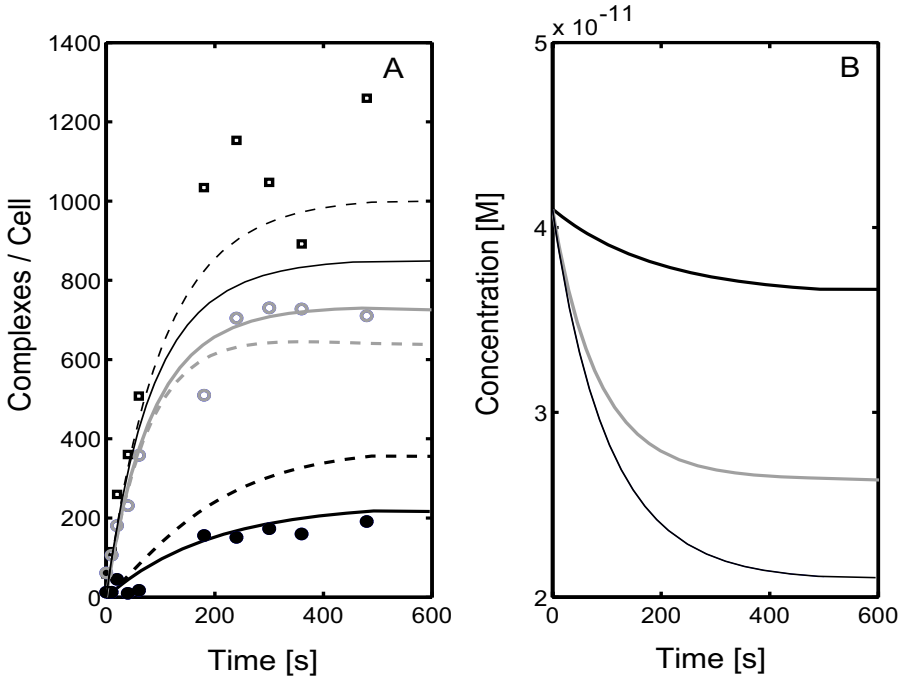

Fig. 5.21: Low TNF concentration 5ng/ml: **Solid lines A** TNF receptor complex formation: • TNF-R1 selective stimulation, • TNF-R2 selective stimulation and □ Costimulation of TNF-R1 and TNF-R2. **Dashed lines in A:** Simulation results assuming Ligand Passing
B TNF concentration in the solute, **–** TNF-R1 selective stimulation, – TNF-R2 selective stimulation and – costimulation of TNF-R1 and TNF-R2.

TNF-R1 and low TNF-R2 expression levels. In cell lines which overexpress TNF-R2 it is very hard to block all TNF-R2 and the cooperative effect is not observable as the number of TNF-R2 complexes dominates the total number of receptor complexes.

However, to assess if the phenomenon of Ligand Passing does effect intracellular signaling, we suppose that the effect should be most dominant at a low TNF concentration and in cells overexpressing TNF-R2. Thus we stimulated the transfected HeLa cells *in silico* with a low TNF concentration (5ng/ml) and determined I-κB degradation. We chose I-κB degradation as this is a very fast response, whereas caspase activation occurs much later. As can be seen in Figure 5.22 the simulation studies (solid lines) do not show a major impact of a TNF-R1 with an assumed higher affinity. The simulation results for caspase activation do not show any Ligand Passing effects as well (data not shown). The experiments support this finding as depicted in Figure 5.22 C. From these results we conclude that Ligand Passing might exist at the receptor level but does not show any impact on intracellular signaling as far we could investigate.

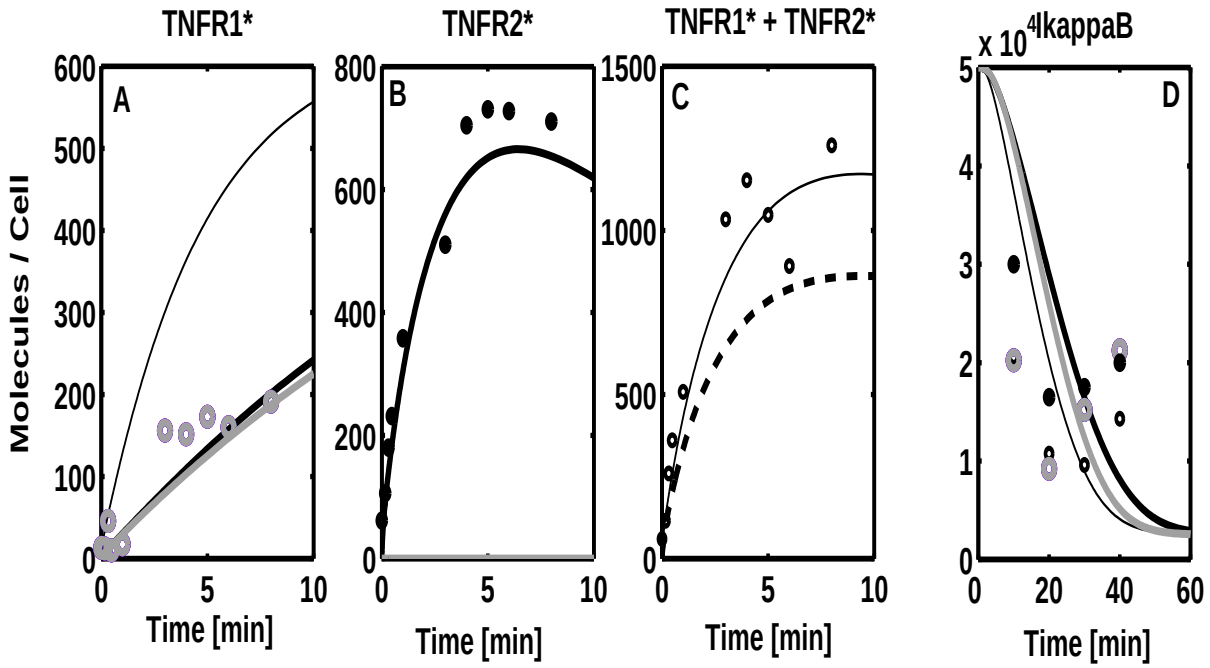

Fig. 5.22: Effect of Ligand Passing on IκB degradation, **A** – TNF-R1 selective stimulation, **B** – TNF-R2 selective stimulation, **C** – costimulation of TNF-R1 and TNF-R2 and **D** I-κB degradation. Dots represent experimental data points.

Tab. 5.4: Kinetic rate constants as used in the mathematical model of TNF-R1 part I

Reaction Number	Equation	Kinetic Parameter		References
v1	$\rightarrow$[TNFR1]	k_1=0.06 receptors/s	k_{-1}=0	
v2	[TNF-R1]+[TNF]$\leftrightarrow$[TNF-C1]	k_2=5.7e7	k_{-2}=0.0026	own experimental data
v3	[TNF-R1]$\leftrightarrow$[TNF-R1i]	k_3=0.2	k_{-3}=0.1	v55, v74, v82
v4	[TNF-R1i]+[TNFi]$\leftrightarrow$ [TNF-Ci]	k_{2b}=19.8	k_{-4}=0.0026 [1/s]	
v5	[TNF-C1] + [Prot] $\leftrightarrow$ [TNF-C1-Prot]	k_5=1.73e-7	k_{-5}=1.66e-3	v76, v104-v106, v113-v146, v207, v210, v213, v216, v219, v222 v231, v234, v237, v240, v243, v246, v249, v252, v255, v258, v261, v266, v271, v274, v279, v282, v300,v461-v466, v469 v479, v484, v489, v494, v499, v508, v513, v520, v525, v530, v535, v535, v544, v549, v556, v589-v594, v597, 602, v602, v616, v621, v628
v6	[TNF-C1-Prot] $\rightarrow$ [TNF-Ci] + [Proti]	k_6=0	k_{-6}=0.003	v77, v301-v363, v449-v454, v470, v475, v480, v485, v490, v495 v500, v509, v514, v521, v526, v531, v545, v550, v557 v577-v582, v598, v603, v608, v617, v622, v629
v7	[TNF-C1i] + [TRADD] $\leftrightarrow$ [TNF-C1i-TRADD]	k_7=1e7	k_{-7}=1.1e-4	[77], v8, v9, v10, v147, v148, v214, v215, v220 v221, v223, v224, v227-v230, v235, v236
v11	[TNF-C-TRADD]+[TRAF2] $\leftrightarrow$ [TNF-C-TRADD-TRAF2]	k_{11}=5.65e5	k_{-11}=1.3	v83, v149 [110]
v12	[TNF-C-TRADD] + [FADD] $\leftrightarrow$ [TNF-C-TRADD-FADD]	k_{12}=1e6	k_{-12}=0.2	v15, v22, v150, v153, v156, v241, v242, v244, v245, v638-v647
v13	[TNF-C1-TRADD-TRAF2]+[RIP] $\leftrightarrow$ [TNF-C1...TRAF2-RIP]	k_{13}=1e7	k_{-13}=1e-4	v17, v26, v151, v154, v160, v208, v209,v211, v212, v217, v218, v225, v226, v232, v233
v14	[TNF-C1-TRADD-TRAF2]+[cIAP2]$\leftrightarrow$[TNF-C1...TRAF2-cIAP2]	k_{14}=3e6	k_{-14}=0.002	[145] v23, v24, v28, v29, v66, v152 v157, v158, v162, v163, v187, v437-v440, v445, v446, v472 v565-v568, v573, v574, v610-v613, v624, v625, v637
v16	[Casp3*] + [Casp8] $\leftrightarrow$[Casp3*-Casp8]	k_{16}=2.8e4	k_{-16}=1	[143]
v18	[Casp3*-Casp8] $\rightarrow$ [Casp8*] + [Casp3*]	k_{18}=0	k_{-18}=0.47	[142]
v19	[TNF-C1..TRAF2-cIAP] + [Casp8*] $\leftrightarrow$ [TNF-C1...cIAP-Casp8*]	k_{19}=2.8e6	k_{-19}=0.2	[143], v25, v27, v31, v33, v37, v38, v40, v42, v46 v48, v62, v63, v69, v155, v159, v161, v165, v167, v171, v172 v174, v176, v180, v182, v185, v186, v188, v256, v257, v259, v260 v264, v265, v269, v270, v272, v273, v283, v284, v286,v287, v291 v292, v431-v436, v440-v444, v447-v448, v487, v488, v492 v493, v497, v498, v506, v507, v511, v512, v518, v519, v523 v524, v528, v529, v533, v534, v542, v543, v547, v548,v554, v555 v559-v564, v569-v572, v575, v576, v595, v596, v600, v601, v605 v606, v614,v615, v619, v620, v626, v627
v20	[Casp8*] + [TRAF1] $\leftrightarrow$ [Casp8*-TRAF1]	k_{20}=8e6	k_{-20}=0.2	
v21	[Casp8*-TRAF1] $\rightarrow$[TRAF1c] + [Casp8*]	k_{21}=0	k_{-21}=0.0005	
v30	[TNF-C1...FADD3] + [cIAP] $\leftrightarrow$ [TNF-C1...FADD3-cIAP]	k_{30}=1e7	k_{-30}=1e-4	v32, v36, v39, v41, v45, v47, v164, v166, v170, v173, v175, v179, v181, v247, v248, v250 v251, v261, v263, v277, v278, v280, v281, v289, v290
v34	[TNF-C1...RIP3] +[IKK] $\leftrightarrow$ [TNF-C1...RIP3-IKK]	k_{34}=3e7	k_{-34}=0.3	v35, v84, v107, v168, v169, v174

First order constants are given in 1/s and second order rate constants in [M^{-1} s^{-1}].

Tab. 5.5: Kinetic rate constants as used in the mathematical model of TNF-R1 part II

Reaction Number	Equation		Kinetic Parameter	References
v43	[TNF-C1...RIP3-IKK] $\rightarrow$ [IKK*]+[TNF-C1...RIP]	k_{43}=0	k_{-43}=7	v44, v85, v108, v177, v178
v49	[TNF-C1...FADD$_3$-Casp8*$_2$]$\rightarrow$[Casp8*] + [TNF-C1...FADD$_3$Casp8*]	k_{49}=0	k_{-49}=0.55	v50, v70, v71, v183, v184, v267, v268, v275, v276, v294, v295
v51	[IKK*]+[IkappaB]$\leftrightarrow$[IKK*-IkappaB]	k_{51}=3e6	k_{-51}=1.5e-3	[64]
v52	[Casp8*] + [Casp3] $\leftrightarrow$ [Casp8*-Casp3]	k_{52}=4.1e6	k_{52}=0.05	
v53	[Casp8*-Casp3]$\rightarrow$ [Casp3*] + [Casp8*]	k_{53}=0	k_{-53}=0.003	
v54	[IKK*-IkappaB]$\rightarrow$ [IKK*] + [IkappaB]	k_{54}=0	k_{-54}=1e-5	[64]
v56	[TNF-C1i]$\rightarrow$[TNF-Cideg]	k_{562}=0	k_{-562}=3.667e-5	v57, v364-v397, v430, v583-v588
v58	[TNF]$\rightarrow$ [TNFi]	k_{58}=0	k_{-58}=1.67e-4	
v59	[Proti]$\rightarrow$ [Prot]	k_{59}=1e4	k_{-59}=0	
v60	[Casp8*] + [RIP] $\leftrightarrow$ [Casp8*-RIP]	k_{60}=1e7	k_{-60}=0.1	
v61	[Casp8*-RIP] $\rightarrow$ [RIPc] +[Casp8*]	k_{61}=0	k_{-61}=0.1	
v64	[TRAF1c] + [TRAF2] $\leftrightarrow$ [TRAF1c-TRAF2]	k_{64}=1e4	k_{-64}=0.5	v78, v83 [110]
v65	[Casp3*] + [cFLIP] $\leftrightarrow$ [Casp3*-cFLIP]	k_{65}=7e6	k_{-65}=0.1	
v67	[Casp3*-cFLIP] $\rightarrow$ [Casp3*] + [cFLIPc]	k_{67}=0	k_{-67}=0.5	
v68	[Casp3*] + [PARP]$\leftrightarrow$ [Casp3*-PARP]	k_{68}=1e4	k_{-68}=0.2	[47]
v79	[Casp3*-PARP]$\leftrightarrow$ [Casp3*] + [PARPc]	k_{79}=0	k_{-79}=10	
v80	[TNF-C1i]$\rightarrow$[TNF-Cideg]	k_{56}=0	k_{-56}=6.667e-4	v81, v399-v423, v427-v428, v455-v460, v471, v476, v486 v491, v496, v501, v510, v515,v522,v527, v532, v537, v546, v551 v558, v599, v604, v609, v618, v623, v630
v190	[Casp8*] + [Bid] $\leftrightarrow$ [Casp8*-Bid]	k_{190}=7e5	$k_{-190} = 0.1$	
v191	[Casp8*-Bid] $\rightarrow$ [tBid] + [Casp8*]	k_{191}=0	k_{-191}=0.1	
v192	[tBid] + [Bax] $\leftrightarrow$ [tBid-Bax]	k_{192}=3e5	k_{-192}=0.05	
v193	[tBid-Bax] + [Bax] $\leftrightarrow$[tBid-Bax]	k_{192}=3e5	k_{-192}=0.05	
v194	[tBid-Bax$_2$] $\rightarrow$ [Bax$_2$] + [Bid]	k_{194}=0	k_{-194}=0.1	v45, v47
v195	[Bax$_2$] +[cyto c] $\leftrightarrow$ [Bax$_2$-cytoc]	k_{195}=5.1e4	k_{-195}=4e-4	[176]
v196	[Bax$_2$-cytoc] $\rightarrow$ [cytoc*]+[Bax$_2$]	k_{196}=0	k_{-196}=0.003	
v197	[Casp3*]+[XIAP] $\leftrightarrow$ [Casp3*XIAP]	k_{197}=1e7	k_{-197}=0.01	
v198	[cytoc*] + [Apaf] $\leftrightarrow$[Apaf-cytoc]	k_{195}=5.1e4	k_{-195}=4e-4	[176]
v199	[cytoc*]+[Apaf-cytoc]$\leftrightarrow$[Apaf-cytoc$_2$]	k_{195}=5.1e4	k_{-195}=4e-4	[176]
v200	[Apaf-cytoc$_2$] + [Casp9] $\leftrightarrow$ [Apaf-cytoc$_2$-Casp9]	k_{200}=8.8e6	k_{-200}=0.011	[143]
v201	[Apaf-cytoc$_2$-Casp9] + [XIAP] $\leftrightarrow$ [[Apaf-cytoc$_2$-Casp9-XIAP]	k_{201}=1e7	k_{-201}=2.4e-7	[27],v197
v202	[Apaf-cytoc$_2$-Casp9] +[Casp3] $\rightarrow$ [Apaf-cytoc$_2$-Casp9-Casp3]	k_{52}=4.1e6	k_{52}=0.05	
v203	[Apaf-cytoc$_2$-Casp9-Casp3]$\rightarrow$ [Apaf-cytoc$_2$-Casp9]+ [Casp3*]	k_{203}=0	k_{-203}=0.07	
v204	[Apaf-cytoc$_2$-Casp9-Casp3] + [XIAP] $\leftrightarrow$ [[Apaf-cytoc$_2$-Casp9-Casp3-XIAP]	k_{204}=8e7	k_{-201}=2.4e-7	

First order constants are given in 1/s and second order rate constants in [M^{-1} s^{-1}].

Tab. 5.6: Kinetic rate constants as used in the mathematical model of TNF-R2

Reaction Number	Equation		Kinetic Parameter	References
v72	→[TNF-R2]	k_{72}=2.17 receptors/s	k_{-72}=0	
v73	[TNF-R2]+[TNF]↔[TNF-C2]	k_2=1.1e8	k_{-2}=2e-3	own experimental data
v75	[TNF-R2i]+[TNFi]↔ [TNF-C2i]	k_{73b}=46.3	k_{-73}=0.002 [1/s]	
v80	[TNFR2i]]→[TNFR2ideg]	k_{80}=0	k_{-80}=6.67e-3	v81, v399-v423, v430, v481, v486, v491, v496, v501, v510 v515, v522, v527, v532, v537, v546, v551, v558, v599, v604 v609, v618, v623, v630
v86	[TNF-C2-TRAF2] + [MEKK1] ↔ [TNF-C2-TRAF2-MEKK1]	k_{86}=5e7	k_{-86}=0.064	v296, v298
v87	[TNF-C2 -TRAF2-MEKK1] → [MEKK1-P]	k_{87}=0	k_{-87}=0.5	v112, v297, v299
v88	[MEKK1-P] + [JNKK1] ↔ [MEKK1-P-JNKK1]	k_{88}=1.1e7	k_{-88}=0.01833	v109
v89	[MEKK1-P-JNKK1 → [JNKK1-P] + [MEKK1-P]	k_{89}=0	k_{-89}=3.5	[77], v8, v9, v10
v90	[MEKK1-P] + [JNKK1-P] ↔ [MEKK1-P-JNKK1-P]	k_{88}=1.1e7	k_{-88}=0.01833	
v91	[MEKK1-P-JNKK1-P] ↔ [JNKK1-PP] + [MEKK1-P]	k_{91}=0	k_{-91}=2.9	
v92	[JNKK1-PP]+[Pase1] ↔ [JNKK1-PP-Pase]	k_{92}=1.43e7	k_{-92}=0.8	
v93	[JNKK1-PP-Pase1]→[JNKK1-P] + [Pase1]	k_{93}=0	k_{-93}=0.058	
v94	[JNKK1-P]+[Pase1] ↔ [JNKK1-P-Pase]	k_{94}=2.5e5	k_{-94}=0.5	
v95	[JNKK1-P-Pase1]→[JNKK1] + [Pase1]	k_{95}=0	k_{-95}=0.058	
v96	[JNKK1-PP] + [JNK] ↔ [JNKK1-PP-JNK]	k_{96}=5.3e7	k_{-96}=0.033	
v97	[JNKK1-PP-JNK ↔ [JNK-P] + [JNKK1-PP]	k_{97}=0	k_{-97}=16	
v98	[JNK1-PP] + [JNK-P] ↔ [JNKK1-PP-JNK-P]	k_{98}=5.3e7	k_{-98}=0.033	
v99	[JNK1-PP-JNK-P] ↔ [JNK-PP] + [JNKK1-PP]	k_{99}=0	k_{-99}=5.7	
v100	[JNK-PP]+[Pase2] ↔ [JNK-PP-Pase2]	k_{100}=1.45e7	k_{-100}=0.6	
v101	[JNK-PP-Pase2]→[JNK-P] + [Pase2]	k_{101}=0	k_{-101}=0.27	
v102	[JNK-P]+[Pase2] ↔ [JNK-P-Pase2]	k_{102}=5e6	k_{-102}=0.5	v17, v26, v151, v154, v160
v103	[JNK-P-Pase2]→[JNK] + [Pase2]	k_{101}=0	k_{-101}=0.27	
v110	[MEKK1-P]+[Pase] ↔ [MEKK1-P-Pase]	k_{110}=9.7e6	k_{-110}=0.2	
v111	[MEKK1-P-Pase]→[MEKK1] + [Pase2]	k_{111}=0	k_{-111}=1	
v189	[TNFR2] + [cIAP1] ↔[TNFR2-cIAP1]	k_{189}=1e6	k_{-189}=0.0002	
v205	[TNF-C2-TRAF2] + [RIP] ↔[TNF-C2-TRAF2-RIP]	k_{k238}=0	k_{-238}=0	v206 seems not to exist according to simulation results
v467	[TNF-C2-TRAF2] + [TRAF1] ↔[TNF-C2-TRAF2-TRAF1]	k_{467}=5e7	k_{-189}=0.05	v468
v472	[TNF-C2...TRAF1] + [cIAP2] ↔[TNF-C2...TRAF1-cIAP2]	k_{14b}=1e8	k_{14b}=0.002	v473, v477, v478, v482, v483, v502-v505, v516, v517 v538-v541, v552, v553, v565-v568
v424	[NFkappaB]+[*cflip*] ↔[*NFkappaB-cflip*]	k_{424}=5e6	k_{-424}=1	for t $\geq$ 70min
v425	[NFkappaB]+[*ciap*] ↔[*NFkappaB-ciap*]	k_2=3e5	k_{-425}=1	for t $\geq$ 70min
v426	[NFkappaB]+[*xiap*] ↔[*NFkappaB-xiap*]	k_2=6.66e6	k_{-2}=1	for t $\geq$ 70min
v467	[TNF-C2-TRAF2]+[TRAF1] ↔[TNF-C2-TRAF2-TRAF1]	k_{467}=1.66e7	k_{-467}=0.1	v468
v631	[*NFkappa-cflip*] →[NFkappaB] + [c-FLIP]	k_{631}=0	k_{-631}=0.009	for t $\geq$ 70min
v632	[*NFkappa -ciap*] →[NFkappaB] + [cIAP]	k_{632}=0	k_{-632}=0.2	for t $\geq$ 70min
v633	[*NF-kappa-xiap*] →[NFkappaB] + [XIAP]	k_{633}=0	k_{-633}=0.006	for t $\geq$ 70min
v634	[Casp8*]+[XIAP] ↔[Casp8*-XIAP]	$k_{634} = 1e5$	k_{-634}=1	
v635	[TRAF2-cIAP2] + [Casp8] ↔[TRAF2-cIAP2-Casp8]	k_{635}=1e7	k_{-635}=0.001	v636
v637	[TRAF2]+[cIAP2]↔[TRAF2-cIAP2]	k_{14}=3e7	k_{-14}=0.02	
v648	[Apaf-cytoc-Casp9-XIAP] →[Casp9c] + [Apaf-cytoc-XIAP]	k_{648}=0	k_{-650}=0.1	v651
v650	[cIAP-Casp8/Casp3] →[cIAP] + [Casp8/3-ubiquit.]	k_{650}=0	k_{-650}=0.00019	v651

First order constants are given in 1/s and second order rate constants in [M^{-1} s^{-1}].

Chapter 6

Conclusions

In the field of signal transduction the number of components and known interactions is constantly increasing. Therefore, the dynamics of these networks can not be understood by intuition alone. Mathematical modeling has proven to be a valuable tool in engineering that deals effectively with complexity. Here, we apply mathematical modeling to signal transduction networks in mammalian cells. In particular, we have developed models for a survival pathway, the EGF induced MAP kinase cascade and an apoptotic signal transduction network the TNF receptor crosstalk.

The epidermal growth factor (EGF) is involved in a variety of cellular responses such as growth, differentiation, migration, metabolism, and transformation. Binding of EGF to its corresponding cell surface receptor results in the activation of the receptor's intrinsic tyrosine kinase activity, and subsequently in the activation of complex multistep signal transduction cascades.

The EGF induced MAP kinase cascade is well characterized and most interactions of the signaling components are known. In the case of EGF a lot of quantitative or semi-quantitative data like receptor numbers or protein concentrations have already been published in the literature as well as time courses of protein phosphorylation. Using these data and our own experimental data enables the estimation of the unknown kinetic parameters and hence, to obtain an operating model. This model can then be used to test the consistency of the network, to test hypotheses or to establish new hypotheses as well as to identify design principles.

In Chapter 3 we present a mathematical model of the EGF induced MAP kinase cascade in HeLa cells. Using the developed model, we have been able to make several predictions, which have been verified by own experiments or by experimental findings described in the literature, which were not included a priori into the model. First, the model predicts maximal ERK activation from 50ng/ml down to 0.5ng/ml EGF stimulation, which we have verified experimentally. This finding is in accord with the ERK activation pattern observed experimentally in tumor cells

[126]. Second, we found that the maximum of activated EGFR does not seem to be important for the ERK response as shown in the initial slope of EGF receptor phosphorylation. We also studied the signal contribution of internalized receptors and receptors remaining on the cell surface to the total ERK signal. Taken together, we find that internalization appears to play a dual role in signal transduction: at high EGF concentrations internalization seems to attenuate the response, whereas at low concentrations internalization amplifies the response. The model predicts a more sustained ERK activation due to EGF receptor overexpression which is in good agreement with experimental observations [127]. Furthermore, the model predicts well the influence of the deletion of the adapter molecule Shc on ERK activation. In wet lab experiments, Shc deficient cells show the same amount of activated ERK for high EGF concentrations and at the same time an increase of Ras-GTP activation. The increase of Ras-GTP in the mutant occurs in the simulation as well (data not shown), since more Ras is shuttled into the second pathway if the first pathway is inactivated. However, ERK activation of the wild type and the mutant cell is different for the low EGF concentration of 0.5ng/ml. At low EGF concentrations the mutant shows in experiments a significant decrease in ERK activation, which has been predicted correctly by the simulation results.

All the simulation and experimental results described above, are the result of a single, sustained stimulation. Beyond a single EGF stimulation, the question of restimulation with pulses of EGF is of interest and is discussed in Chapter 3.2. The initial model prediction is that the second stimulation does not trigger a second ERK peak after an initial stimulation. The experimental results revealed that in fact, there is no second ERK peak observable within the first hours after the initial stimulation. In the model, which was developed for the HeLa cell, this is due to receptor internalization and degradation. As in the model the receptors bound to the adapter molecules become degraded and the reason for desensitization is the decrease of adapter molecules. An experiment monitoring the ERK activation after a second stimulation shows, that it takes the cell about 36 hours to get back to its initial physiological condition. Thus, the cells possess certain mechanisms to become desensitized to endogenous signals. In order to identify possible mechanisms of desensitization, we applied the mathematical model to an autocrine system, the A431 cell line. Autocrine signaling is an example where restimulation occurs in nature and where the phenomenon of desensitization is of major interest. Autocrine loops are established, when soluble factors secreted by cells bind to and stimulate receptors on their own surfaces [137]. In the literature the phenomenon of two ERK peaks is described [26], where the fist peak is induced by radiation and the second by autocrine EGF, which is

triggered by the first radiation induced ERK peak. Using the example of the A431 cells, we discuss three possible mechanisms of desensitization; the negative feedback from phosphorylated ERK to SOS, receptor downregulation and slow dephosphorylation as well as protein degradation followed by a slow protein synthesis. With the help of the mathematical model, we have identified slow dephosphorylation steps as well as protein degradation followed by a slow protein synthesis as a possible mechanism of desensitization.

The observed high sensitivity of the MAP kinase cascade is of great importance for the development of anti-tumor agents. A mathematical model like the one presented in this work of the EGF induced MAP kinase cascade, might be used for drug target identification and drug development in the future. Using the example of a MEK inhibitor and a receptor kinase inhibitor, we demonstrate successfully the predictive potential of such mechanistic models in Chapter 3.3. The comparison of the dose response curves between the simulation results and the experimental data of ERK phosphorylation in HeLa cells treated with different concentrations of MEK inhibitor show good accordance. Furthermore, we investigated the inhibitory effect, if two inhibitors are combined. The combination of a receptor tyrosine kinase inhibitor and a Grb2 inhibitor improved the inhibitory effect significantly in comparison to the selective application of only one inhibitor.

In Chapter 4 System Analysis, we address the question of the robustness of the EGF induced MAP kinase cascade model with respect to the range in which the kinetic parameters and the initial conditions can be varied without changing the system output. We show that certain kinetic parameters as well as certain initial conditions can be varied within specific limits in order to obtain the same signal transduction behavior of the system. Interestingly the certain initial protein concentration as well as the kinetic parameters can be varied up to 5 fold. A significant change of initial conditions results in a different set of kinetic parameters, which shows, however, the same behavior of the system. Thus, biological systems seem to have more than one solution space, as could also be shown for the segment polarity network in Drosophila [157]. This is of great importance as most of the protein concentrations in cells are unknown and therefore, initial models are often developed based on estimates. Due to the lack of quanitative experimental data only some parameters can be identified, whereas others are defined by constraints or rough estimates. We could show here that the system behavior is identical even though kinetic parameters were estimated based on different initial conditions. The robustness of these signal transduction networks allows the construction of computational models despite the lack of experimental data. If the topology is captured correctly in the mathematical model, it

can already be used for qualitative predictions and for further system analysis.

We discuss and analyze the differences between a detailed model of the first step of the MAP kinase cascade and a model using Michaelis Menten kinetics. We show that both systems are stable for the parameter set used in the large model. We also show that there are only little differences in the dose response curve and that we find the same biochemically possible equilibrium points solving both models. Therefore, it seems like for the kinetic parameters used here, a Michaelis Menten approach is a valid approach, which also implies the independency of the steps of the MAP kinase cascade. Thus, the single steps of the MAP kinase cascade can be treated separately.

Furthermore, we show that the combination of single and double phosphorylation sites in a cascade nature obtained a switch-like, sigmoidal dose response curve. We also find that the order of a step with a single or double phosphorylation site does not matter.

We also discuss the phenomenon of oscillations of the MAP kinase cascade module. Using Ras-GTP as input signal, they can be observed over a wide range of Ras-GTP levels. We show that they occur more likely with a sustained input signal, than with an impulse-like signal, which results in damped oscillations. Furthermore, we show that these oscillations, that can be observed for the module, can most likely not be observed in the full model due to the network structure.

In contrast to the EGF system, the TNF receptor crosstalk is much less well understood. Here, we show that mathematical modeling can be applied to much less well understood systems as well. These mechanistic models can contribute to current research and propose certain hypotheses in order to get a better understanding of the connectivity of the system and the system as a whole.

TNF is a potent immunoregulatory cytokine that mediates its effects through two distinct receptors, TNF-R1 and TNF-R2. Following ligand binding, the DD containing adapter molecule TRADD binds through its death domain to TNF-R1, thereby forming a platform for the initiation of both, the apoptotic pathway or, alternatively, the survival pathway. While it is known that TNF-R1 on its own is capable to trigger apoptosis, the role of TNF-R2 in TNF induced cell death is still a matter of debate. Nevertheless, there exist several studies indicating that TNF-R2 overexpression enhances TNF induced apoptosis [21], [43], [167], [59]. The underlying mechanisms, however, remain largely undefined and have been investigated here in this work.

In order to gain a better understanding of TNF-R1/TNF-R2 crosstalk and the role of TNF-R2 enhancing TNF induced apoptosis, we have developed a mechanistic model. The model de-

scribes caspase activation triggered by three distinct protocols of TNF receptor stimulation. These include the selective stimulation of TNF-R1, the costimulation of TNF-R1 and TNF-R2 as well as the prestimulation of TNF-R2 for 6 hours. In the case of the prestimulation protocol, it is has been shown that the antiapoptotic adapter molecule TRAF2 is completely depleted in the cytosol after 6hrs of TNF-R2 prestimulation [43]. Therefore, after TNF-R2 prestimulation only the apoptotic signaling pathway is active. We focus on two typical cellular TNF responses, activation of NF-κB and induction of apoptosis. Experimental data for caspase-8 and -3 activation under all the three experimental protocols were collected [43]. The results derived from an iterative process between biochemical experiments and mathematical modeling finally resulted in a validated model. From the model analysis, we can conclude that TNF receptor crosstalk is regulated according to our simulation results through TRAF2, TRAF1 and c-IAP. These results are consistent with hypotheses raised in literature [43].

From further simulation studies we have revealed that overexpression of TRAF1 only in combination with TRAF2 and c-IAP prevents cell death, which is in good agreement with literature data. We also find a certain hierarchy within the antiapoptotic proteins c-IAP, c-FLIP and XIAP. c-FLIP turns out to be the most potent of the three, which corresponds to experimental data.

In order to analyze caspase activation, the dose response curves for the three experimental protocols habe been analyzed. According to the simulation studies TRAF2 deficient cells should show maximal caspase activation even at a very low TNF concentration. To assess the contribution of the mitochondrial pathway and the positive feedback from cleaved caspase-3 to caspase-8, these pathways are set to zero in the model and the dose response curves are analyzed. The mitochondrial pathway seems to be most important for the TNF-R1 selective stimulation, whereas for TRAF2 deficient cells the mitochondrial pathway does not show much impact on caspase activation. The positive feedback loop in contrast seems to affect mostly caspase-8 activation. Those hypotheses obtained by the simulation results remain to be verified experimentally. The current model of TNF signaling, which is the result of an iterative process between model development and experiments may therefore serve as a platform for further experimental and theoretical investigations.

A general finding, which we derive from both models is that they are fundamentally very robust but that there are certain key parameters which influence the system significantly. Furthermore, we find that the developed models are very sensitive to their structure, in regard to the system's behavior of the actual signal transduction pathway, and less sensitive to its kinetic parameters.

This work shows that mathematical modeling in combination with quantitative experimental

data can give new insights into the potential mechanisms of intracellular signal transduction and regulation.

Appendix

6.1 Biochemical Methods and Results

The biochemical results presented in the following, were used for the model derivation or resulted from hypotheses obtained by the mathematical model. The data were collected at the Institute of Cell Biology and Immunology at the University of Stuttgart. All the experiments related to EGF were carried out by Claudia Eichler-Jonsson, all the caspase related experiments by Mariola Fotin and the quantification of the proteins involved in the TNF signal transduction pathway was done by Thomas Eissing.

6.1.1 Cell Culture

Cells were grown and maintained in RPMI-1640 medium supplemented with 5% fetal calf serum (FCS). Cultures were maintained in an incubator at 37^{o}C in a 5% CO_2 atmosphere. When cells reached confluence, they were detached using 0.02% EDTA in PBS and replated in new plastic dishes. Stock cells were kept in FCS containing 10% DMSO and frozen at 80^{o}C or in liquid nitrogen.

6.1.2 Western Blot Technique

1. Total protein extraction

After stimulation cells were washed twice with cold PBS and lysed with 200μl (3.5cm dishes) or 750μl (10cm dishes) of cold Lysis buffer, Ripa buffer or MLB buffer containing phosphatase/protease inhibitors (1mM NaF, 1mM NaPP, 2mM sodium orthovanadate, 1mM sodium molybdate, 100mM okadaic acid, 100nM calyculin A, 1mM p-nitrophenylphosphate, 1μg leupeptin, 1μg aprotinin and 1mM PMSF). Cells were scraped from the plates, transferred to microtubes and incubated for 30min on ice. Then, lysates were clarified by centrifugation (14000rpm,

10min, 4^{o}C) and supernatants containing the cellular proteins were transferred to new microtubes. Protein concentration was determined by the Bradford method (Bradford, 1976) using a BioRad protein assay solution. Cellular protein extracts were stored at 80^{o}C until use.

2. SDS-Polyacrylamide Gel Electrophoresis (SDS-PAGE)

Equal amounts of protein were separated by SDS-PAGE (7.5% until 12.5% polyacrylamide gels depending on the size of the proteins of interest) in a vertical gel electrophoresis chamber (Phase). Polymerization of the resolving gel solution (12.5% polyacrylamide in 1x SDS buffer) was started by adding APS and TEMED (both at 0.1% final concentration). After polymerization, the resolving gel was overlaid by a 3% stacking gel and its polymerization induced as mentioned above. Cellular protein extracts (50μg/sample) were mixed with 2x Laemmli sample buffer, heated for 5min at 95^{o}C and immediately cooled on ice. Gel electrophoresis was performed at 50mA for 1.5h in SDS-PAGE running buffer.

3. Transfer of Proteins to Nitrocellulose

Membrane Proteins separated by SDS-PAGE were blotted onto a nitrocellulose membrane using a horizontal blotting chamber (Phase) at 1.5mA constant current per cm^2 of gel for 1.5 hours. For blotting, gel was layered between nitrocellulose membrane and blotting papers (Whatmann) soaked with blotting buffer.

4. Immuno Blot (Western Blot Analysis)

For the western blot analysis, the nitrocellulose membrane was incubated with 3% milk in PBS-T (0.05% Tween 20 in PBS) for 30min at RT to block unspecific binding sites. The membrane was washed 3 times for 5min in PBS-T and then incubated with an appropriate primary antibody for 2 hours at RT or overnight at 4^{o}C. All primary antibodies were diluted in PBS-T containing 0.04% azide and 0.1% BSA. Then, the membrane was washed again 3 times for 5min in PBS-T following incubation with horse radish peroxidase (a) or alkaline phosphatase (b) - conjugated secondary antibodies for 1 hour at RT. The membrane was washed 3 more times for 5min in PBS-T and finally developed either with ECL kit (Amersham) (for a) or in AP buffer (for b) containing 0.162mg/ml BCIP and 0.324mg/ml NBT. Washing the membrane with water terminated the AP staining reaction.

5. Immunoprecipitation

For the immunoprecipitations, equal amounts of cellular protein lysates (0.5-1mg/ml) were incubated with the specific antibody for 1 hour at 4^{o}C with constant agitation. After centrifugation (14000 rpm, 15min, 4^{o}C), supernatants were transferred to new microtubes and incubated with 30μl of protein A sepharose beads for 30 min at 4^{o}C. Sepharose beads were then washed

three times and resuspended in 20μl of washing buffer. After adding 20μl of 2x Laemmli sample buffer, samples were heated at 95^{o}C for 5min and immediately cooled on ice. For the kinase assays, samples were washed twice with kinase wash buffer and once with kinase reaction buffer. All washing/centrifugation steps were performed at 4^{o}C (Eppendorf Centrifuge 5403).

Determination of ERK-1/2 Activation

HeLa cells were replicated and plated at a density of 3 x 10^5 cells per 6-cm cell culture dishes in RPMI growth medium plus 5% fetal calf serum for 24 hours, and transferred to serum-free medium for another 24 hours to induce growth arrest. Cells were treated with different concentrations of human recombinant EGF (R&D Systems) for the times indicated, rinsed once with cold phosphate-buffered saline, and solubilized in 0.2ml of lysis buffer containing 1% Triton x-100, 50 mM Tris (pH 7.4), 150mM NaCl, 5mM EDTA (pH 7.4) and protease inhibitors (1μg/ml aprotinin, 1μg/ml leupeptin, 1mM sodium orthovanadate, 0.5mM phenylmethanesulfonylfluoride (PMSF), 1mM (NPP), 1mM sodium pyrophosphate and 1mM sodium molybdate). Samples were clarified by centrifugation at 14,000rpm for 15min at 4^{o}C. Samples (50μg of protein) were electrophoresed on 15% SDS polyacrylamide and electroblotted onto nitrocellulose membranes (Schleicher & Schuell, Germany). Phosphorylated forms of ERK-1/2 were detected by immunoblotting using an anti-phospho p42/p44 ERK (Thr202/Tyr204) rabbit polyclonal primary antibody (New England Biolabs) and a secondary alkaline phosphatase-conjugated anti-rabbit IgG antibody (Jackson ImmunoResearch Laboratories) for visualization.

To determine the concentration of the signaling molecules Ras, MEK, ERK for the EGF pathway and caspase-8, TRAF2 and TRADD for the TNF signaling pathway purified GST proteins were used. The purified GST proteins of MEK, ERK and ERK-PP were used for the quantification of MEK, ERK and ERK-PP and the HIs-tagged protein of c-H-Rsa for the calibration curve. Cellular lysates of HeLa cells were run on the same gel for ERK and ERK-PP. After blotting and detection of bands by the specific antibodies, the concentration of cellular proteins was calculated by a standard curve after densiometric evaluation as shown in the following graphs. The obtained concentrations are listed in Table 3.1. Each determination was performed twice with similar results.

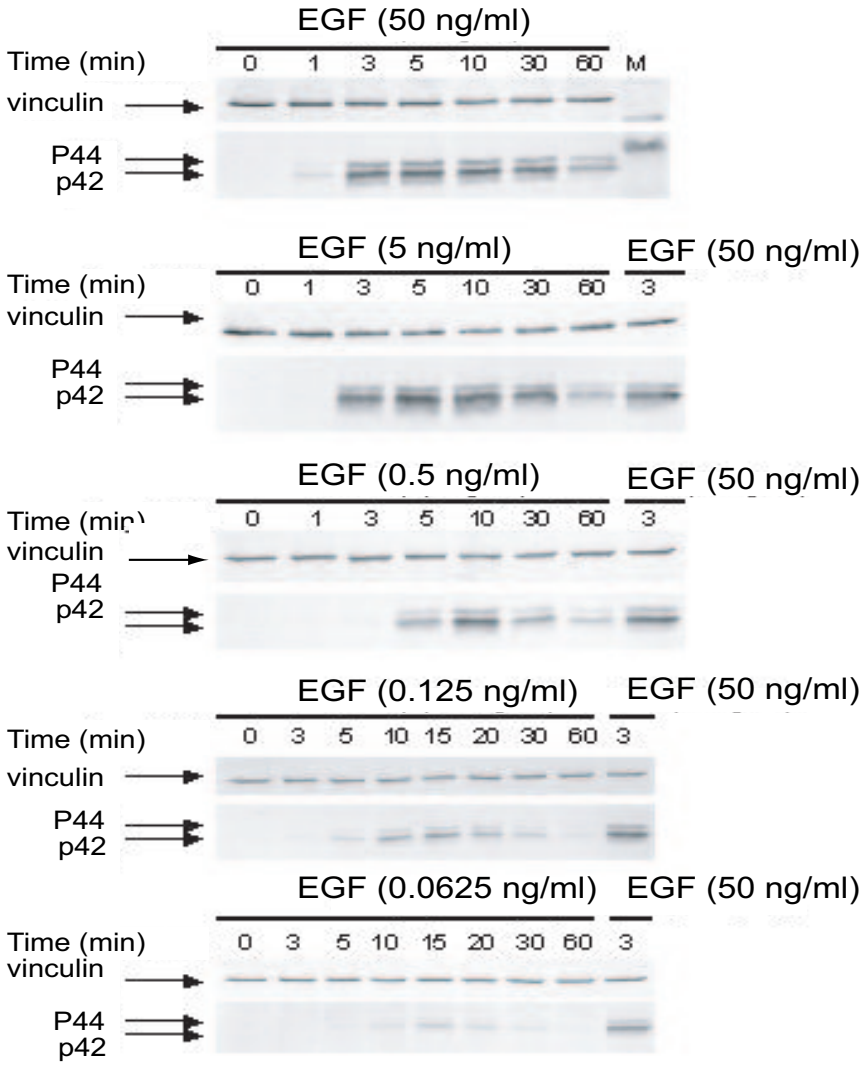

Fig. 6.1: Kinetics of ERK1/2 phosphorylation.

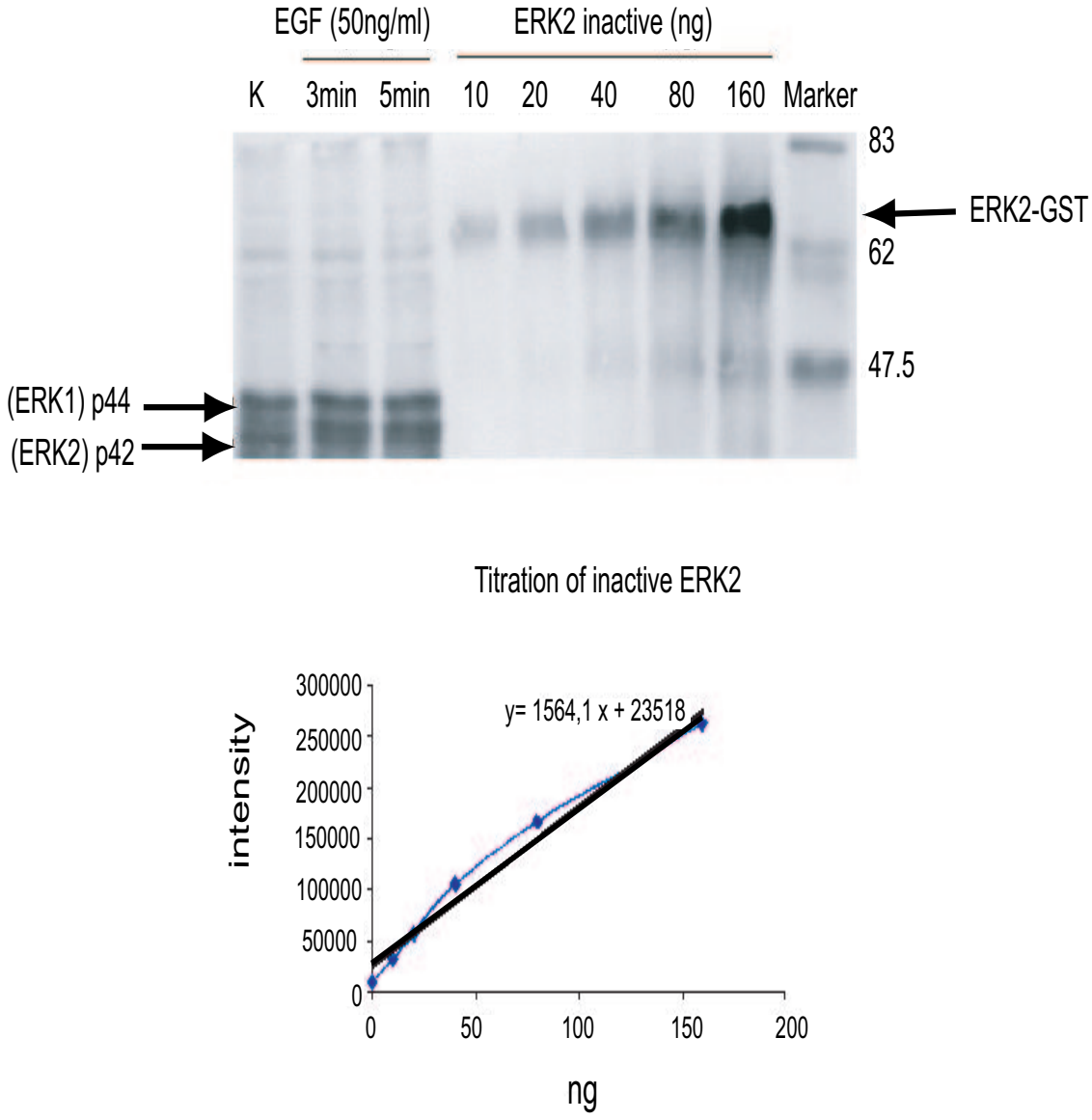

ERK2 inactive in HeLa cells: 74.15 ng/50 μg total protein

Fig. 6.2: Protein quantification of ERK in HeLa cells.

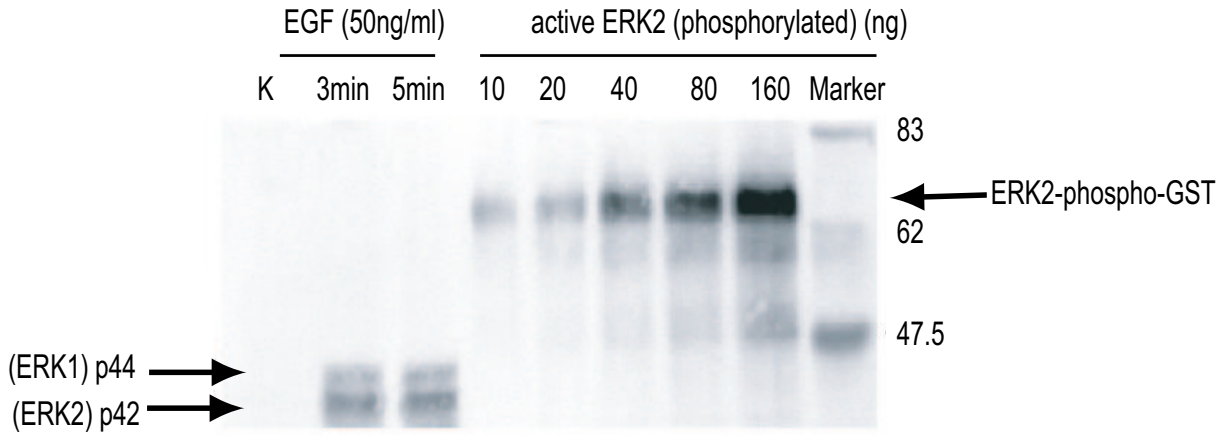

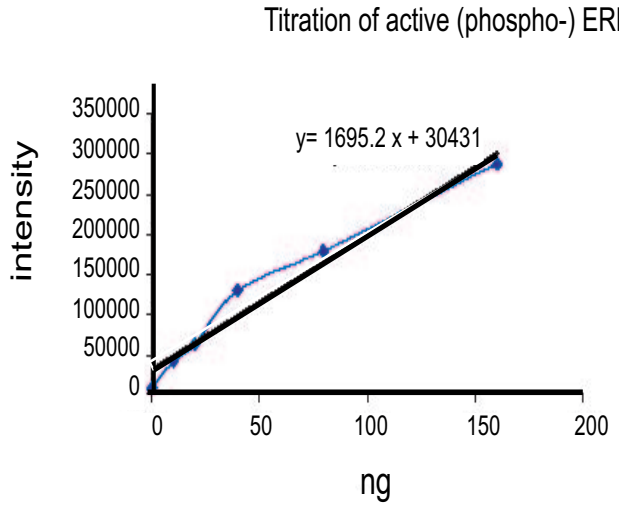

active ERK2 (phosphorylated) in HeLa cells: 38.05 ng/50 μg total protein

Fig. 6.3: Protein quantification of phosphorylated ERK in HeLa cells.

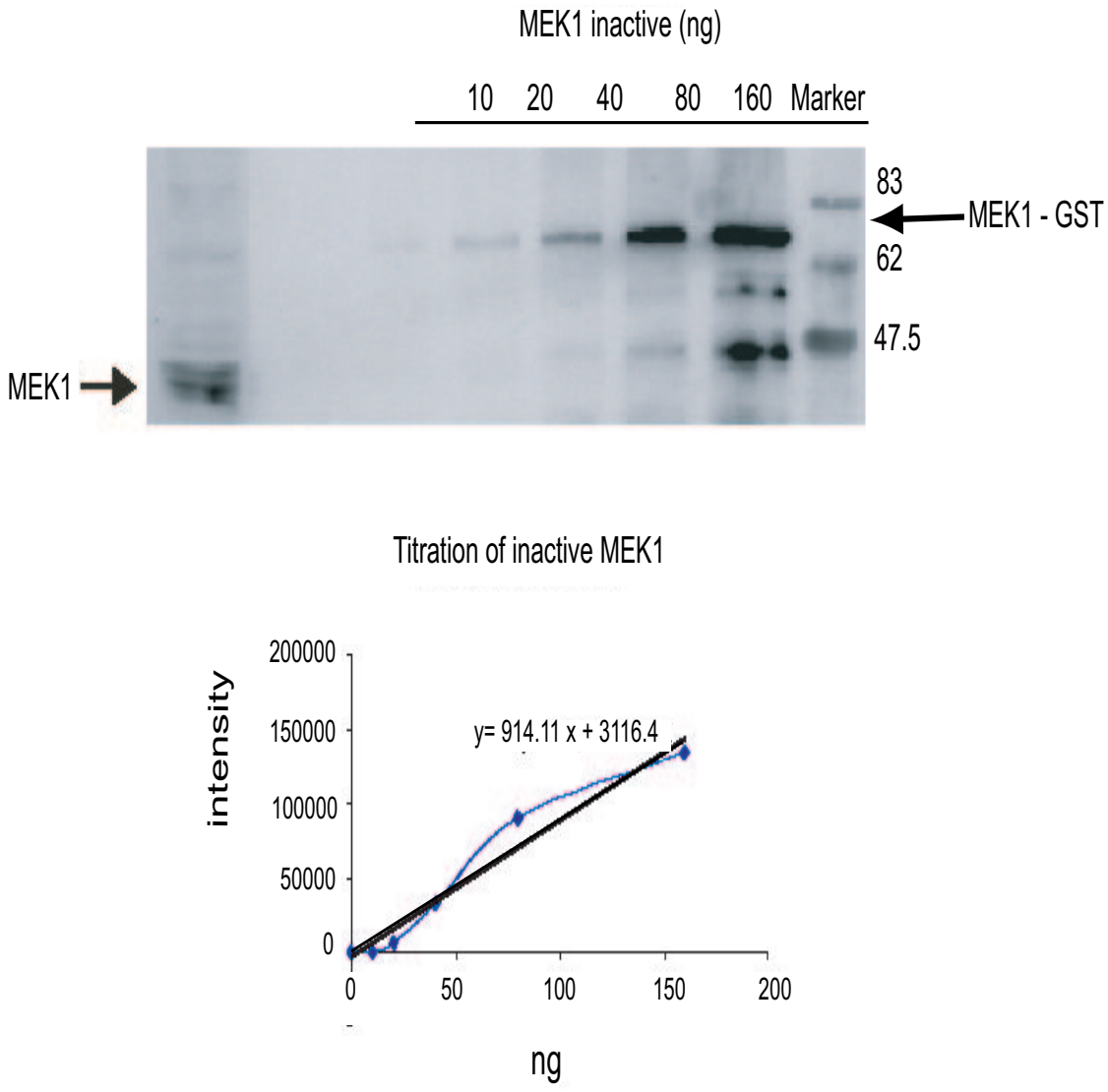

MEK1 inactive in in HeLa cells: 94.2 ng/50 μg total protein

Fig. 6.4: Protein quantification of MEK in HeLa cells.

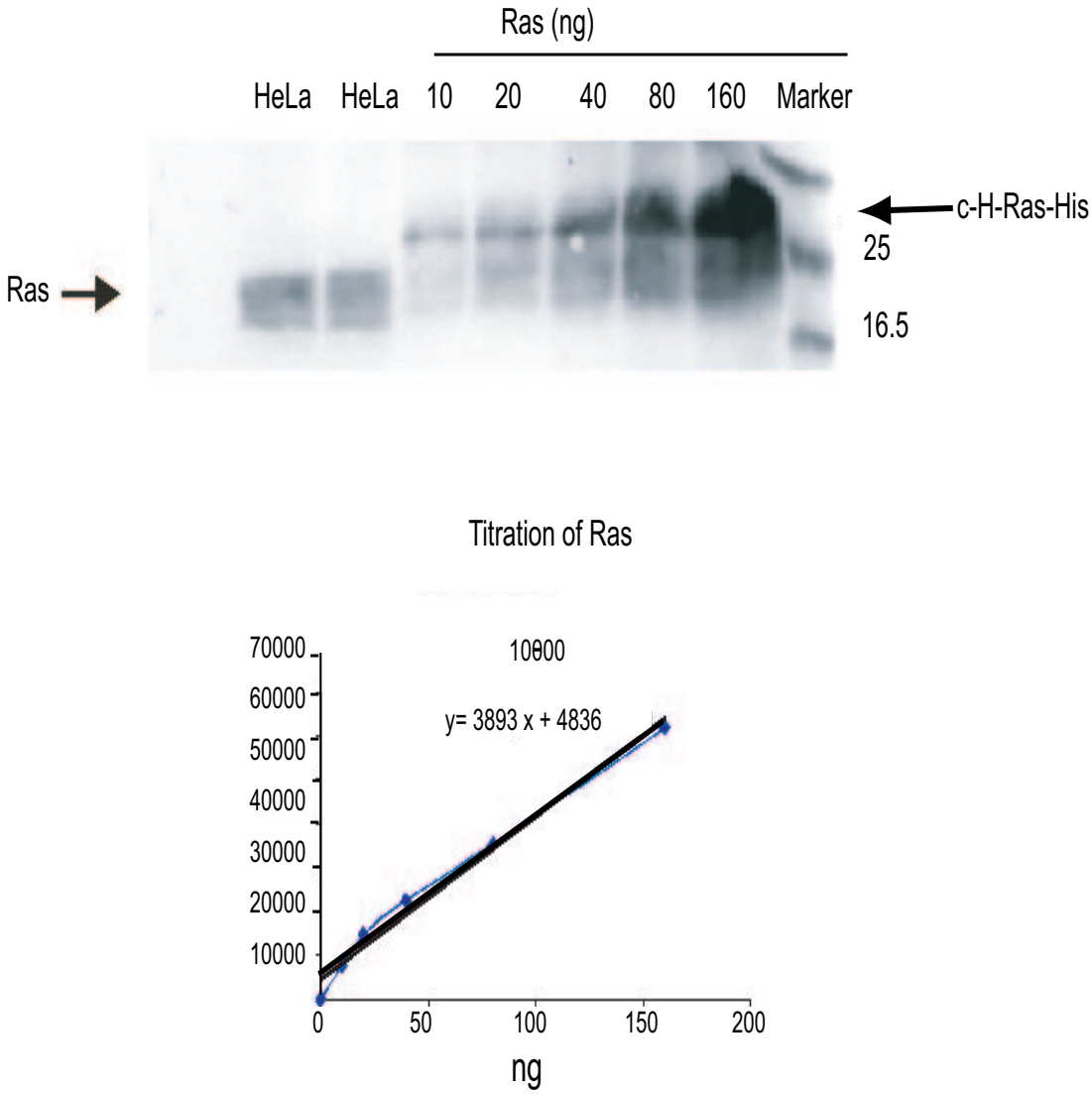

Ras in HeLa cells: 25.3 ng/50 μg total protein

Fig. 6.5: Protein quantification of Ras in HeLa cells.

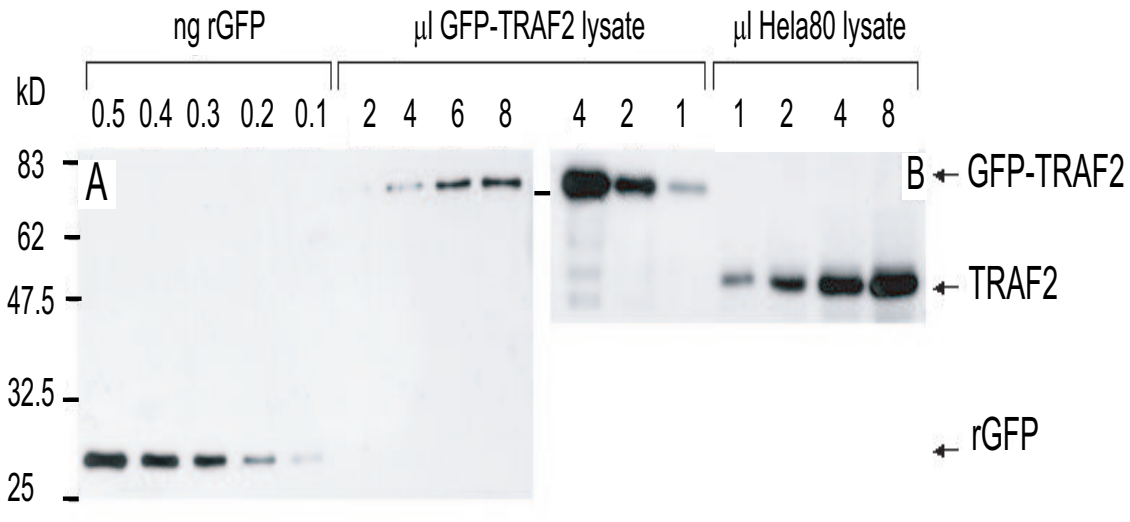

Fig. 6.6: Quantification of selected endogenous proteins at the example of TRAF2 via Western Blotting.

At the example of TRAF2 the quantification of of selected endogenous proteins like TRAF2, TRADD, RIP and caspase-8 via Western Blotting is described. Fusions of the proteins of interest with GFP were transiently expressed in Hela80 cells. In Figure 6.6A the GFP-X concentrations of the resulting lysates were determined by western blotting with rGFP of a known concentration (rGFP: Clonetech # 8365; ms α GFP: Boehringer Mannheim # 1814460). Those GFP-X lysates were then used as a standard to determine the concentration of endogenous X in whole cell lysates by blotting with αX. In Figure 6.6 X=TRAF2 is shown as an example (GFP-TRAF2: construct publication; first Ab:ms α TRAF2, Pharmingen #68411A and second Ab: HRP lsbeled gt α ms, Dianova #115-035-003; ECL: Pierce # 34075; film: Fujifilm SuperRX #10626). The Hela80 whole cell lysates were produced at a concentration of 1.85 x 10^7cells/ml lysate. Given the size of rGFP of 27kD and with Avogadro's Number, the number of molecules in HeLa cells results in 62 000 $\pm$ 2.2e4 TRAF2 molecules/cell.

Western blotting of caspase-8

For western blot analysis of caspase-8, lysates were prepared in RIPA buffer supplemented with a protease inhibitor cocktail stock solution (Roche Diagnostics GmbH, Germany) as recommended by the supplier. Cell debris was removed by centrifugation (10 000 x g, 10min) and the protein concentration was determined by the Bradford assay. Proteins 50μg) were resolved by sodium dodecyl sulfate-polyacryamide gel electrophoresis (SDS-PAGE) and transferred to nitrocellulose membranes by electroblotting. Blots were blocked for 1 hour at room temperature in TBS containing 0.05% Tween-20 and 3% (w/v) dry milk, washed and incubated with anti caspase-8 mouse mAb 1h at room temperature. Bound antibodies were visualized with alkaline phosphatase-conjugated goat anti-mouse/rat/rabit-IgG (Sigma, Deisenhofen, Germany) and NBT and BCIP as substrate.

In vitro caspase-3 activity assay

caspase-3 activity was measured in caspase activity assay buffer (30mM HEPES, pH 7.5, 10mM $CaCl_2$, 5mM DTT, 10% sucrose) with 20μM Ac-DEVD-AMC (Calbiochem, Cad Soden, Germany) as substrate. Activity was measured with a luminescence spectrometer (Aminco Bowman Series2) at excitation 380nm and emission at 450nm. Specificity of caspase-dependent Ac-DEVD-AMC cleavage was regularly controlled with the caspase inhibitors z-VAD-fmk and DEVD-fmk.

6.1.3 Single Cell Analysis of c-Fos Expression

The c-fos protooncogene is rapidly induced in response to a variety of extracellular stimuli including mitogenic signals. Activation of ERK-1/2 by mitogenic and stress signals leads to phosphorylation of the TCF proteins and, consequently, stimulate their transcriptional activity towards the c-fos promoter.

In Figure 6.7, activation of c-fos gene in response to various EGF concentrations is displayed. Noteworthy, a dose response pattern similar to that observed for ERK activation is also obtained for c-fos expression, with maximal c-fos induction after stimulation with 50, 5 and 0.5ng/ml EGF.

Approximately 2 x 10^4 HeLa cells were seeded on coverslips in RPMI with 5% fetal calf serum and then serum-starved for 24 hours. Afterwards cells were treated with different concentrations of EGF for 2 hours to induce c-fos expression. Cells were fixed with 3.7% formaldehyde in PBS for 20min at room temperature, rinsed once with PBS and permeabilized with 1% NP-40 for

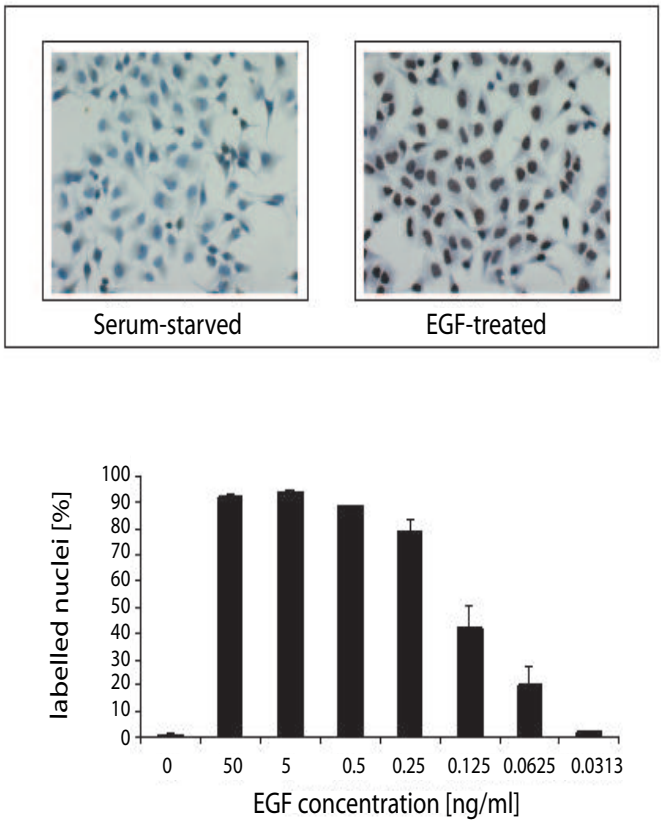

Fig. 6.7: c-fos expression in HeLa cells.

20min. Unspecific binding was avoided by 1 hour incubation with normal goat serum and then, coverslips were washed three times with PBS for 5min and incubated with anti-c-Fos rabbit polyclonal primary antibody (Santa Cruz) overnight at 4^{o}C. After washing three times with PBS for 5min, c-Fos protein was detected using Vectastain ABC kit and DAB (3,3´-diaminobenzidine) substrate kit for peroxidase according to the manufacturer´s instructions (Vector Laboratories). After counterstaining with hematoxiline (Sigma), coverslips were mounted on microscope slides using Mowiol 4.88 (Polysciences) and analyzed by optic microscopy. Immunocytochemistry for phosphorylated ERK-1/2 was performed as described above using rabbit anti-phospho ERK-1/2 primary antibody and goat anti-rabbit-FITC-conjugated secondary antibody.

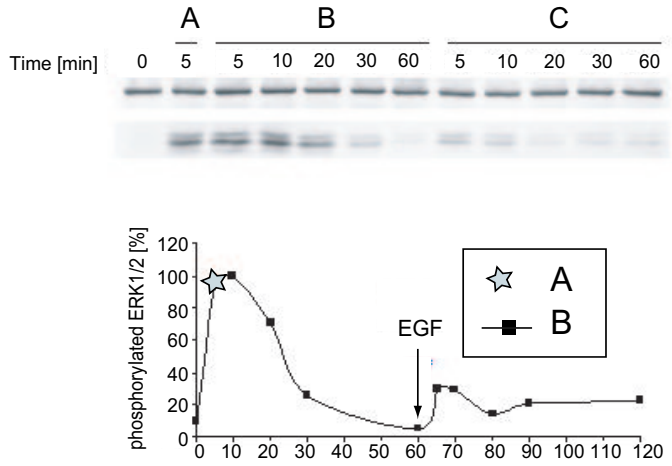

B: EGF (50ng/ml) for 1 min, washed, then lysed at 5, 10, 20, 30 and 60 min.

Fig. 6.8: Impulse-like stimulation and restimulation with EGF

6.1.4 Impulse-like stimulation with EGF

In Figure 6.8 the impulse-like stimulation of HeLa cells with 50ng/ml EGF is shown. Cells were serum-starved for 24 hours. B: cells were incubated with EGF (50ng/ml) for 1min, washed with PBS, and lysed after the times indicated. C: cells were stimulated with EGF (50ng/ml) for 1min, washed with PBS and after 60min cells were stimulated again with EGF (50ng/ml) for the times indicated. Western blot showing levels of phosphorylated forms of ERK-1/2 was immunostained using rabbit anti-phospho-ERK-1/2 primary antibody and goat anti-rabbit AP-conjugated- secondary antibody. Vinculin immunostaining was performed using mouse anti-vinculin primary antibody and goat anti-mouse AP-conjugated-secondary antibody to normalize for equal amounts of protein.

To verify the average time point when the cells reach the physiological pre-stimulation state, HeLa cells were stimulated with EGF for 5min Figure 6.9, lanes b to k, washed extensively to remove unbound EGF molecules from the medium and restimulated after 1 to 36 hours with

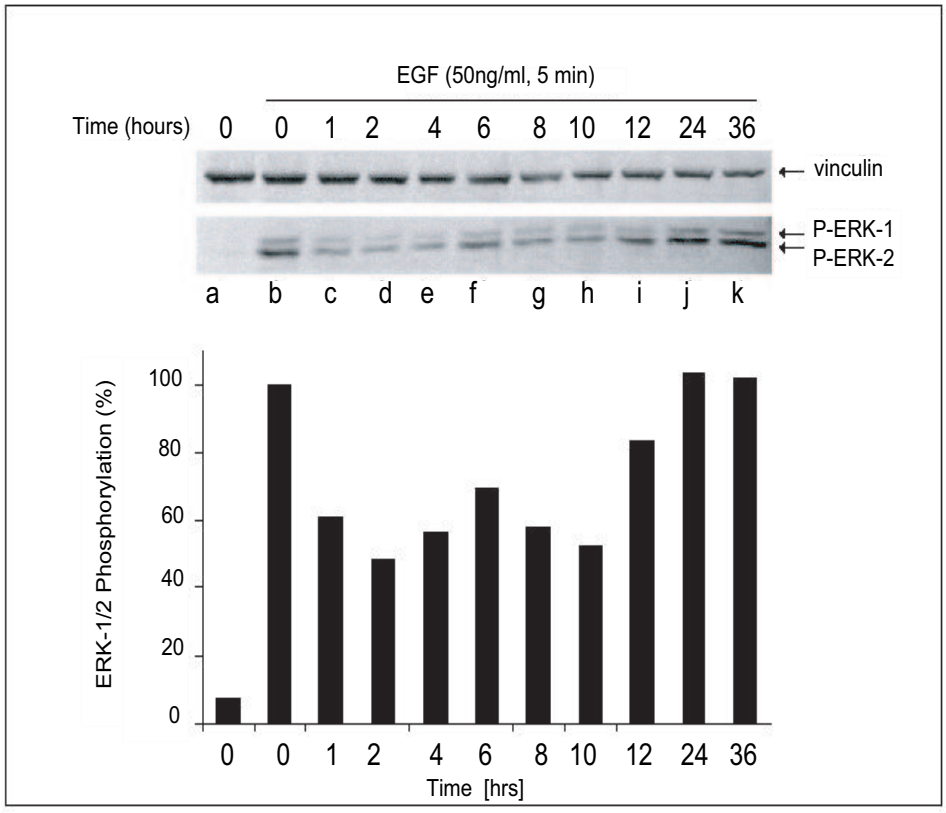

Fig. 6.9: Longterm kinetics of impulse-like stimulation and restimulation with EGF.

EGF for another 5min Figure 6.9 lanes c to k. As it can be observed, the cells were able to fully respond to the second EGF stimulation after a time lapse that ranges between 12 and 24 hours indicating their return to the pre-stimulation steady-state level.

Cells were serum-starved for 24 hours and stimulated with EGF (50ng/ml) for 5min. Samples from lanes c to k were washed with PBS and restimulated with EGF (50ng/ml) for 5min after the times indicated then lysed. Western blot showing levels of phosphorylated forms of ERK-1/2 was immunostained using rabbit anti-phospho-ERK-1/2 primary antibody and anti-rabbit AP-conjugated-secondary antibody. Vinculin immunostaining was performed using mouse anti-vinculin primary antibody and goat anti-mouse AP-conjugated-secondary antibody to normalize for equal amounts of protein.

List of Figures

List of Tables

Bibliography

[1] S. A. Aaronson. Growth factors and cancer. *Science*, 254:1146–1153, 1991.

[2] U. Alon, M. G. Surette, N. Barkai, and S. Leibler. Robustness in bacterial chemotaxis. *Nature*, 397:168–171, 1999.

[3] N. G. Anderson, T. Ahmead, K. Chan, R. Dobson, and N. J. Bundred. ZD1839 (IRESSA) a novel epidermal growth factor receptor EGFR tyrosine kinase inhibitor, potently inhibits the growth of EGFR-positive cancer cell lines with ot without ERBB2 overexpression. *Int. J. Cancer*, 94:774–782, 2001.

[4] M. A. Anonyak, D. K. Moscatello, and A. J. Wong. Constitutive activation of c-Jun n-terminal kinase by a mutant epidermal growth factor receptor. *The Journal of Biological Chemistry*, 273:2817–2822, 1998.

[5] M. Arrio-Dupont, G. Foucault, M. Vacher, P. F. Devaux, and S. Cribier. Translational diffusion of globular proteins in the cytoplasm of cultured muscle cells. *Biophys J*, 78:901–907, 2000.

[6] A. Ashkenazi and V. M. Dixit. Death receptors: Signaling and modulation. *Science*, 281(1305-1308), 1998.

[7] F. Authier, M. Metoui, A. Bell, and J. S. Mort. Negative regulation of epidermal growth factor signaling by selective proteolytic mechanism in the endosome mediated by cathepsin B. *J. Biol. Chem.*, 274:33723–33731, 1999.

[8] Z. Bajzer, A. C. Myers, and S. Vuk-Pavlovic. Binding, internalization, and intracellular processing of proteins interacting with recycling receptors. a kinetic analysis. *J Biol Chem*, 264:13623–31, 1989.

[9] Z. Bajzer and S. Vuk-Pavlovic. Rate transition and regulatory coupling in endocytosis of interferon-α in human epithelial tumor cells. *Journal of Cellular Biochemistry*, 48:203–214, 1992.

[10] A. S. Baldwin. The NF-kappaB and I-kappaB proteins: new discoveries and insights. *Annu. Rev. Immunol.*, 14:649, 1996.

[11] A. G. Batzer, P. Blaikie, K. Nelson, and J Schlessinger. The phosphotyrosine interaction domain of Shc binds an LXNPXY motif on the epidermal growth receptor. *Mol. Cell. Biol.*, 15:4403–4409, 1995.

[12] A. G. Batzer, D. Rotin, J. M. Urena, E. Y. Skolnik, and J. Schlessinger. Hierachy of binding sites for Grb2 and Shc on the epidermal growth factor receptor. *Mol. Cell. Biol.*, 14:5192–5201, 1994.

[13] J. A. M. Berkers, P. M. P. van Bergen en Henegouwen, and J. Boonstra. Three classes of epidermal growth factor receptors on HeLa cells. *The Journal of Biological Chemistry*, 266(2):922–927, 1991.

[14] A. Boiteux, B. Hess, and E. E. Selkov. Creative functions of instability and oscillations in metabolic systems. *Curr. Top. Cell. Regul.*, 17:171–203, 1980.

[15] M. Bos, J. Mendelson, Y.-M. Kim, J. Albanell, D. W. Fry, and J. Baselga. PD153035, a tyrosine kinase inhibitor, prevents epidermal growth factor receptor activation and inhibits growth of cancer cells in a receptor number-dependent manner. *Clin Cancer Res.*, 3:2099–2106, 1997.

[16] S. B. Bratton, B. Walker, S. M. Srinivasula, and X.-M. Sun. Recruitment, activation and retention of caspase-9 and -3 by Apaf-1 apoptosome and associated XIAP complexes. *The EMBO Journal*, 20(5):998–1009, 2001.

[17] D. Bray. Protein molecules as computational elements in living cells. *Nature*, 376:307–312, 1995.

[18] L. Buday and J. Downward. Epidermal growth factor regulates p21 ras throughout the formation of a complex receptor, Grb2 adaptor protein and Sos nucleotide exchange factor. *Cell*, 48:611–620, 1993.

[19] D. L. Cadena, C. Chan, and G. N. Gill. The intracellular tyrosine kinase domain of the epidermal growth factor undergoes a conformational change upon autophosphorylation. *J. Biol. Chem.*, 269:1–6, 1994.

[20] R. E. Carter and A. Sorkin. Endocytosis and functional epidermal growth factor receptor green flourescent protein chimera. *Journal of Biological Chemistry*, 273:35000–35007, 1998.

[21] F. K.-M Chan and M. J. Lenardo. A crucial role for p80 TNF-R2 in amplifying p60 TNF-R1 apoptosis signals in T lymphocytes. *Eur. J. Immunol.*, 30:652–660, 2000.

[22] J. C. Chung, N. Sciaky, and D. J. Gross. Heterogeneity of epidermal growth factor binding kinetics on individual cells. *Biophysical Journal*, 73:1089–1102, 1997.

[23] S. Corbalan-Garcia, S. M. Margarit, D. Gordonand, and S.-S. Yang. Regulation of Sos acitvity by intermolecular interactions. *Molecular and Cellular Biology*, 18(2):880–886, 1998.

[24] M. Delhase, M. Hayakawa, Yi Chen, and Michael Karin. Positive and negative regulation of IκB kinase subunit phosphorylation. *Science*, 284:309–313, 1999.

[25] C. DeLisi. The biophysics of ligand-receptor interactions. *Quaterly Reviews of Biophysics*, 13(2):201–230, 1980.

[26] P. Dent, D. B. Reardon, J. S. Park, G. Bowers, K. Valerie C. Logsdon, and R. Schmidt-Ullrich. Radiation-induced release of transforming growth factor α activates the epidermal growth factor receptor and mitogen-activated protein kinase pathway in carcinoma cells, leading to increased proliferation and protection from radiation-induced cell death. *Molecular Biology of the Cell*, 10:2493–2506, 1999.

[27] Q. L. Deveraux and J. C. Reed. IAP family proteins–suppressors of apoptosis. *Genes Dev.*, 13:239–259, 1999.

[28] Q. L. Deveraux, N. Roy, H. R. Stennicke, T. Van Arsdale, Q. Zhou, S. M. Srinivasula, E. S. Alnemri, G. S. Salvesen, and J. C. Reed. IAPs block apoptotic events induced by caspase-8 and cytochrome c by direct inhibition of distinct caspases. *The EMBO Journal*, 17:2215–2223, 1998.

[29] A. Devin, A. Cook, Y. Lin, Y. Rodriguez, M. Kelliher, and Z. Liu. The distinct roles of TRAF2 and RIP in IKK activation by TNF-R1: TRAF2 recruits IKK to TNF-R1 while RIP mediates IKK activation. *Immunity*, 12:419–429, 2000.

[30] J. R. Doedens and R. A. Black. Stimulation-induced down-regulation of tumor necrosis factor-alpha converting enzyme. *Journal of Biological Chemistry*, 275:14598–14607, 2000.

[31] J. Y. Dong and H. S. Wiley. Trafficking and proteolytic release of epidermal growth factor receptor ligands are modulated by their membrane-anchoring domain. *Journal of Biological Chemistry*, 275:557–564, 1999.

[32] J. C. H. Donovan, A. Milic, and J. M. Slingerland. Constitutive MEK/MAPK activation leads to p27^{Kip1} deregulation and antiestrogen resistance in human breast cancer cells. *The Journal of Biological Chemistry*, 276:40888–40895, 2001.

[33] C. S. Duckett and C. B. Thompson. CD30-dependent degradation of TRAF2: Implications for negative regulation of TRAF signaling and the control of cell survival. *Genes & Development*, 11:2810–2821, 1997.

[34] C. Eichler-Jonsson. *Aspects of mitogen-activated protein kinase activation by epidermal growth factor: its kinects and its crosstalk mechanism with tumor necrosis factor alpha*. PhD thesis, University of Stuttgart, 2002.

[35] M. Eigen. *Quantum Statistical Mechanics in the Natural Sciences*, chapter Diffusion Control in Biochemical Reactions, pages 37–61. Plenum Publishing Corporation, 1974.

[36] H. A. El-Masri and C. J. Portier. Replication potential of cells via the protein kinase C-MAPK, pathway: Application of a mathematical model. *Bulletin of Mathematical Biology*, 61:379–398, 1999.

[37] R. Eskes, S. Desagher, B. Antonsson, and J.-C. Martinou. Bid induces the oligomerization and insertion of Bax into the outer mitochondrial membrane. *Molecular and Cellular Biology*, 20(3):929–935, 2000.

[38] S. M. Kelsey F. Partheniou, S. M. Srinicasula, A. C. Newland, E. S. Alnemri, and L. Jia. C-IAP1 blocks TNFα mediated cytotoxicity upstream of caspase-dependent and -independent mitochondrial events in human leukemic cells. *Biochemical and Biophysical Research Communications*, 287:181–189, 2001.

[39] H. Z. Fan and R. Derynck. Ectodomain shedding of TGF-α and other transmembrane proteins is induced by receptor tyrosine kinase activation and MAP kinase signaling cascades. *EMBO Journal*, 18:6962–6972, 1999.

[40] Z. Fan, Y. Lu, X. Wu, and J. Mendelsohn. Antibody-induced epidermal growth factor receptor dimerization mediates inhibion of autocrine proliferation of A431 squamous carcinoma cells. *The Journal of Biological Chemistry*, 269:27595–27602, 1994.

[41] M. F. Favata, K. Y. Horiuchi, E. J. Manos, A. J. Daulerio, D. A. Stradley, W. S. Feeser, D.. E. Van Dyk, W. J. Pitts, R. A. Earl, F. Hoffs, R. A. Copeland, R. L. Mafolda, P. A. Scherle, and J. M Trzaskos. Identification of a novel inhibitor of mitogen-activated protein kinase kinase. *The Journal of Biological Chemistry*, 273(29):18623–32, 1998.

[42] J. E. Ferrel. Tripping the switch fantastic: How a protein kinase cascade can convert graded inputs into switch like outputs. *TIBS*, pages 460–466, December 1996.

[43] M. Fotin-Mleczek, F. Henkler, D. Samel, M. Reichwein, I. Parmryd, P. Scheurich, J. A. Schmid, and H. Wajant. Apoptotic crosstalk of TNF receptors: TNF-R2-induces depletion of TRAF2 and IAP proteins and accelerates TNF-R1-dependent activation of caspase-8. *Journall of Cell Science*, 2002.

[44] D. W. Fry, A. J. Kraker, A. Mc Michael, L. A. Ambroso, J. M. Nelson, W. R. Leopold, R. W. Connors, and A. J. Bridges. A specific inhibitor of the epidermal growth factor receptor kinase. *Science*, 265:1093–1095, 1994.

[45] M. Fussenegger, J. E. Bailey, and J. Varner. A mathematical model of caspase function in apoptosis. *Nature Biotechnology*, 18:768–774, 2000.

[46] C. Garbay, W.-Q. Liu, M. Vidal, and B. P. Roques. Inhibitors of RAS signal trasnsuction as antitumor agents. *Biochemical Pharmacology*, 60:1165–1169, 2000.

[47] M. Germain, E. B. Affar, D. D'Amours, V. M. Dixit, G. S. Salvesen, and G. G. Poirier. Cleavage of automidified poly(ADP-ribose) polymerase during apoptosis. *The Journal of Biological Chemistry*, 274(40):28379–28384, 1999.

[48] S. Gibson, S. Tu, R. Oyer, S. M. Anderson, and G. L. Johnson. Epidermal growth factor protects epithelial cells against Fas-induced apoptosis. *The Journal of Biological Chemistry*, 274:17612–17168, 1999.

[49] M. Ginkel, A. Kremling, F. Tränkle, E. D. Gilles, and M. Zeitz. Application of the process modeling tool ProMot to the modeling of metabolic networks. In *IMACS Symposium on Mathematical Modelling*, volume 2, pages 526–527, 2000.

[50] J. C. Goldstein, N. J. Waterhouse, P. Juin, G. I. Evan, and D. R. Green. The coordinate release of cytochrome c during apoptosis is rapid, complete and kinetically invariant. *Nature Cell Biology*, 2:156–162, 2000.

[51] M. Grell, E. Douni, H. Wajant, M. Lohden, M. Clauss, B. Maxeiner, S. Georgopoulos, W. Lesslauer, G. Kollias, and K. Pfizenmaier. The transmembrane form of tumor necrosis factor is the prime activating ligand of the 80 kda tumor necrosis factor receptor. *Cell*, 83:793–802, 1995.

[52] M. Grell, H. Wajant, G. Zimmermann, and P. Scheurich. The type 1 receptor (CD120a) is the high-affinity receptor for soluble tumor necrosis factor. *Proc. Natl. Acad. Sci.*, 95:570–575, 1998.

[53] M. Grinberg, R. Sarig, Y. Zaltsman, D. Frumkin, N. Grammatikakis, E. Reuveny, and A. Gross. tBID homooligomerizes in the mitochondrial membrane to induce apoptosis. *J Biol Chem*, (ahead of print), 2002.

[54] L. C. Groenen, E. C. Nice, and A. W. Burgess. Structure function relationships for the EGF/TGF -alpha family of mitogens. *Growth Factors*, 11:235–237, 1994.

[55] G. M. Di Gugelielmo, P. V. Baass, W.-J. Ou, B. I. Posner, and J. Bergeron. Compartimentalization of SHC GRB2 and mSOS and hyperphosphorylation of Raf-1 by EGF but not insulin in liver parenchyma. *The EMBO Journal*, 13:4269–4277, 1994.

[56] P. O. Hackel, E. Zwick, N. Prenzel, and A. Ullrich. Epidermal growth factor receptors critical mediators of multiple receptor pathways. *Curr. Opin. Cell Biol.*, 11:184–189, 1999.

[57] M. Haefele, A. Kienle, E. Klein, A. Kremling, C. Majer, M. Mangold, A. Spieker, E. Stein, R. Waschler, and K.P. Zeyer. User manual DIVA -3.9. Institute for Systems, 2000.

[58] S. H. Hansen, K. Sandvig, and B. van Deurs. The preensosomal compartment comprises distinct coated and noncoated endocytic vesicle populations. *J. Cell. Biol.*, 113:731–741, 1991.

[59] V. Haridas, B. G. Darnay, K. Natarajan, R. Heller, and B. B. Aggarwal. Overexpression of the p80 TNF receptor leads to TNF-dependent apoptosis, Nuclear Factor-κB activation and c-Jun kinase activation. *The Journal of Immunology*, 160:3152–3162, 1998.

[60] A. Hashimoto, M. Kurosaki, N. Gotoh, M. Shibuya, and T. Kurosaki. Shc regulates epidermal growth factor-induced activation of the JNK signaling pathway. *The Journal of Biological Chemistry*, 274:20139–20143, 1999.

[61] J. M. Haugh, A. C. Huang, H. S. Wiley, A. Wells, and D. Lauffenburger. Internalized epidermal growth factor receptors participate in the activation of p21ras in fibroblasts. *The Journal of Biological Chemistry*, 274:34350–34360, 1999.

[62] J. M. Haugh and D. A. Lauffenburger. Analysis of receptor internalization as a mechanism for modulating signal transduction. *J. theor. Biol.*, 195:187–218, 1998.

[63] J. M. Haugh, K. Schooler, A. Wells, H. S. Wiley, and D. A. Lauffenburger. Effect of epidermal growth factor receptor internalization on regulation of the phospholipase C-γ1 signaling pathway. *J. Biol. Chemistry*, 274:8958–8965, 1999.

[64] R. Heilker, F. Freuler, M. Vanek, R. Pulfer, T. Kobel, J. Peter, H.G.Zerwes, H. Hofstetter, and J. Eder. The kinetics of association and phosphorylation of IκB isoforms by IκB kinase 2 correlate with their cellular regulation in human endothelial cells. *Biochemistry*, 38:6231–6238, 1999.

[65] R. Heinrich and S. M. Rapoport. Metabolic regulation and mathematical models. *Prog. Biophys. Molec. Biol.*, 32:1–82, 1977.

[66] H. R. Herschman. Primary response genes induced by growth factors and tumor promoters. *Annu. Rev. Biochem.*, 60:281–319, 1991.

[67] B. Hess and A. Boiteux. Oscillatory phenomena in biochemistry. *Annu. Rev. Biochem.*, 40:237–258, 1971.

[68] H.-P. Hohmann, R. Remy, B. Pöschl, and A.P.G.M. van Loon. Tumor necrosis factor α and β bind to the same two types of tumor necrosis factor receptors and maximally activate the transcription factor NF-κB at low receptor occupancy and within minutes after receptor binding. *The Journal of Biological Chemistry*, 265:15183–15188, 1990.

[69] B. S. Hostager, I. M. Catlett, and G. A. Bishop. Recruitment of CD40 and tumor necrosis factor receptor associated factors 2 and 3 to membrane microdomains during CD40 signaling. *The Journal of Biological Chemistry*, 275:15392–15398, 2000.

[70] H. Hsu, J. Huang, H.-B. Shu, V. Baichwal, and D. V. Goeddel. TNF - dependent recruitment of the protein kinase RIP to the TNF receptor-1 signaling complex. *Immunity*, 4:387–396, 1996.

[71] C. F. Huang and J. E. Ferrell. Ultrasensitivity in the mitogen-activated protein kinase cascade. *Proc. Natl. Acad. Sci.*, 93:10078–10083, 1996.

[72] H.-K. Huang, C.A. Joazeiro, E. Bonfoco, S. Kamada, J.D. Leverson, and T. Hunter. The inhibitor of apoptosis, ciap2, functions as a ubiquitin-protein ligase and promotes in vitro monoubiquitination of caspases 3 and 7. *The Journal of Biological Chemistry*, 275:26661–4, 2000.

[73] Y. Huang, Y. C. Park, R. L. Rich, D. Segal, D. G. Myszka, and H. Wu. Structural basis of caspase inhibition by XIAP: Differential roles of the linker versus the BIR domain. *Cell*, 104:781–790, 2001.

[74] S. R. Hubbard, M. Mohammadi, and J. Schlessinger. Autoregulatory mechanisms in protein-tyrosine kinases. *J. Biol. Chem.*, 273:11987–11990, 1998.

[75] H. T. Idriss and J. H. Naismith. TNFα and the TNF receptor superfamily: structure-function relationships. *Microscopy Research and Technique*, 50:184–195, 2000.

[76] H.D. Jang, Y.M. Chung, J. H. Baik, Y. G. Choi, I. S. Park, Y. K. Jung, and S. Y. Lee. Caspase-cleaved TRAF1 negatively regulates the antiapoptotic signals of TRAF2 during TNF-induced cell death. *Biochem. Biophys. Res. Commun.*, 281:499–505, 2001.

[77] S. J. Jones, Elizabeth C. Ledgerwood, Johannes B. Prins, Jenny Galbraith, David R. Johnson, J. S. Pober, and John R. Bradley. TNF recruits TRADD to the plasma membrane but not the trans-golgi network the principal subcellular location of TNF-R1. *The Journal of Immunology*, 162:1042–1048, 1999.

[78] B. D. Kavanagh, P. Dent, P. Chen R. K. Schmidt-Ulrich, and R. B. Mikkelsen. Ca2+ dependent stimulation of mitogen activated protein kinase activity in A431 cells by low dose ionizing radiation. *Radiat. Res.*, 149:579–587, 1998.

[79] M. Kawada, S. Yamagoe, Y. Murakami, K. Suzuki, S. Mizuno, and Y. Uehara. Induction of p27kip1 degradation and anchorage independence by ras through the map kinase signaling pathway. *Oncogene*, 15, 1997.

[80] H. Keilhack, T. Tenev, E. Nyakatura, and F.-D. Boehmer. Phosphotyrosine 1173 mediates binding of the protein -tyrosine kinase phosphatase Shp-1 to the epidermal growth factor receptor and attenuation of receptor signaling. *J. Biol. Chem.*, 273:24839–24846, 1998.

[81] B. N. Kholodenko, O. V. Demin, Geisela Moehren, and Jan B. Hoek. Quantification of short term signaling by the epidermal growth factor receptor. *The Journal of Biological Chemistry*, 274:30169–30181, 1999.

[82] B. N. Kholododenko. Negative feedback and ultrasensitivity can bring about oscillations in the mitogen-activated protein kinase cascades. *Eur. J. Biochem*, 276:1583–1588, 2000.

[83] H. Kim and W. J. Muller. The role of the EGF receptor family in tumorgenesis and metastasis. *Exp. Cell Res.*, 253:78–87, 1999.

[84] P. H. Krammer. CD95's deadly mission in the immune system. *Nature*, 407(12):789–795, 2000.

[85] A. Kremling. The organization of metabolic reaction networks: a signal oriented approach to cellular models. *Metabolic Engineering*, 2:190–200, 2000.

[86] A. Kremling and E. D. Gilles. The organization of metabolic reaction networks. ii. signal processing in hierarchical structured functional units. *Metabolic Engineering*, 3:138–150, 2001.

[87] S. Kreuz, D. Siegmund, P. Scheurich, and H. Wajant. NF-kappaB inducers upregulate cFLIP, a cycloheximide-sensitive inhibitor of death receptor signaling. *Mol Cell Biol.*, 21:3964–3973, 2001.

[88] K.-M. V. Lai and T. Pawson. The ShcA phosphotyrosine docking protein sensitizes cardiovascular signaling in the mouse embryo. *Genes & Development*, 14:1132–1145, 2000.

[89] C. Lamaze and S. L. Schmid. Recruitment of epidermal growth factor receptors into coated pits requires their activated tyrosine kinase. *J. Cell Biol.*, 129:45–54, 1995.

[90] D. Lauffenburger. Cell signalling pathways as control modules: Complexity for simplicity. *PNAS*, 97(10):5031–5033, 2000.

[91] D. Lauffenburger and J. J. Linderman. *Receptors: Models for binding, trafficking and signaling*. Oxford University Press, 1993.

[92] D. A. Lauffenburger, G. T. Oehrtman, L. Walker, and H. S. Wiley. Real-time quantitative measurement of autocrine ligand binding indicates that autocrine loops are spatially localized. *Proc Natl Acad Sci*, (95):15368–15373, 1998.

[93] J. W. Lengeler. Metabolic networks: a signal-oriented approach to cellular models. *Biological Chem.*, 381:911–920, 2000.

[94] X. Li, Y. Yang, and J. D. Ashwell. TNF-RII and c-IAP1 mediate ubiquitination and degradation of TRAF2. *Nature*, 416:345–347, 2002.

[95] Y. lin, A. Devin, Y. Rodriguez, and Z. Liu. Cleavage of the death domain kinase RIP by Caspase-8 prompts TNF-induced apoptosis. *Genes & Development*, 13:2514–2526, 1999.

[96] K. A. Lund, L. K. Opresko, C. Starbuck, B. J. Walsh, and H. Wiley. Quantitative analysis of the endocytic system involved in hormone-induced receptor internalization. *J. Biol. Chem.*, 265:15713–15723, 1990.

[97] M. Maemura, Y. Iino, Y. Koibuchi, T. Yokoe, and Y. Morishita. Mitogen-activated protein kinase cascade in breast cancer. *Oncology*, 57:37–42, 1999. Suppl. 2.

[98] C. J. Marshall. Specificity of receptor tyrosine kinase signaling: tansient versus sustained extracellular signal-regulated kinase activation. *Cell*, 80:179–185, 1995.

[99] J. Massague and A. Pandiella. Membrane-anchored growth-factors. *Annual Review of Biochemistry*, 62:515–541, 1993.

[100] P. W. Mesner, K. C. Bible, L. M. Martins, T. J. Kottke, S. M. Srinivasula, Phyllis A. Svingen adn Tamie J. Chilcote, G.S. Basi, J. S. Tung, S. Krajewski, J. C. Reed, E. S. Alnemri, W. C. Earnshaw, and S. H. Kaufmann. Characterization of caspase processing and activation in HL-60 cell cytosol under cell-free conditions. *The Journal of Biolgical Chemistry*, 274(32):22635–22645, 1999.

[101] O. Micheau, S. Lens an dO. Gaide, K. Alevizopoulos, and J. Tschopp. NF-κB signals induce the expression of c-flip. *Molecular and Cellular Biology*, 21:5299–5305, 2001.

[102] N. Moghal and P. W. Sternberg. Multiple postive and negative regulators of signalling by the EGF receptor. *Curr. Opin. Cell. Biol.*, 11:190–196, 1999.

[103] D. K. Morrison and R. E. Cuttler. The complexity of Raf-1 regulation. *Curr. Opin. Cell. Biol.*, 9:174–179, 1997.

[104] G. Mueller, P. Storz, S. Bourteeleand H. Doppler, K. Pfizenmaier, H. Mischak, A. Philipp, C. Kaiser, and W. Kolch. Regulation of raf-1 kinase by TNF via its second messenger ceramide and cross-talk with mitogenicsignalling. *EMBO J.*, 17:732–742, 1998.

[105] L. O. Murphy, S. Smith, R. H. Chen, D. C. Fingar, and J. Blenis. Molecular interpretation of erk signal duration by immediate early gene products. *Nature Cell Biology*, 4:556–64, 2002.

[106] M. Muzio, B. R. Stockwell, H. R. Stennicke, G. S. Salvesen, and V. Dixit. An induced proximity model for caspase-8 activation. *The Journal of Biological Chemistry*, 273:2926–2930, 1998.

[107] H. Niv, O. Gutman, Y.I. Henis, and Y. Kloog. Membrane interactions of a constitutively active gfp-ki-ras 4b and their role in signaling. evidence from lateral mobility studies. *J Biol Chem.*, 274:16016–1613, 1999.

[108] G. T. Oehrtman, H. S. Wiley, and D. A. Lauffenburger. Escape of autocrine ligands into extracellular medium: Experimental test of theoretical model predictions. *Biotechnology and Bioengineering*, 57:571–582, 1998.

[109] S. Okada, K. Yamauchi, and J. E. Pessin. Shc isoform-specific tyrosine phosphorylation by the insulin and epidermal growth factor receptors. *The Journal of Biological Chemistry*, 270:20737–20741, 1995.

[110] Y. C. Park, H. Ye, C. Hsia, D. Segal, R. L. Rich, H. C. Liou, D. G. Myszka, and H. Wu. A novel mechanism of TRAF signaling revealed by structural and functional analyses of the TRADD-TRAF2 interaction. *Cell*, 101:777–787, 2000.

[111] D. Pennica, V. T. Lam, N. K. Mize, R. F. Weber, M. Lewis, B. M. Fenly, M. T. Lipari, and D. V. Goeddel. Biochemical properities of the 75 -kDa tumor necrosis factor receptor. Characterization of ligand binding, internalization, and receptor phosphorylation. *The Journal of Biological Chemistry*, 267:21172–21178, 1992.

[112] D. Perez and E. White. TNF α signals apoptosis through Bid-dependent conformational change in Bax that is inhibited by E1B 19K. *Molecular Cell*, 6:53–63, 2000.

[113] Felipe X. Pimentel-Muinos and Brian Seed. Regulated commitment of TNF receptor signaling: A molecular switch for death or activation. *Immunity*, 11:783–793, 1999.

[114] S. S. Pullen, M. E. Labadia, and R. H. Ingraham. High-affinity interactions of tumor necrosis factor receptor-associated factors TRAFs and CD40 require TRAF trimerization and CD40 multimerization. *Biochemistry*, 38:10168–10177, 1999.

[115] I. Rechenberg. *Evolutionsstrategie '94*. Frommann-Holzboog, Stuttgart, 1994.

[116] S.J. Riedl, M. Renatus, R. Schwarzenbacher, Q. Zhou, C. Sun, S. W. Fesik, R. C. Liddington, and G. S. Salvesen. Structural basis for the inhibition of caspase-3 by XIAP. *Cell*, 104:791–800, 2001.

[117] S. R. Ritland, S. J. Gendler, L. J. Burgart, D. W. Fry, J. M. Nelson, A. J. Bridges, L Andress, and W. E. Karnes. Inhibition of epidermal growth factor receptor tyrosine kinase fails to suppress adenoma formation in *apc*^{Min} mice but induces duodenal injury. *Cancer Research*, 60:4678–4681, 2001.

[118] M. Rothe, M. G. Pan, W. J. Henzel, T. M. Ayres, and D. V. Goeddel. The TNF-R2-TRAF signaling complex contains two novel proteins related to baculoviral inhibitor of apoptosis proteins. *Cell*, 83(7):1243–52, 1995.

[119] M. Rothe, S. C. Wong, W. J. Henzel, and D. V Goeddel. A novel family of putative signal transducers associated with the cytoplasmic domain of the 75 kda tumor necrosis factor receptor. *Cell*, 78:681–692, 1994.

[120] D. M. Rothwarf and M. Karin. The NF-kappa B activation pathway: a paradigm in information transfer from membrane to nucleus. *Sci STKE*, 5:RE1, 1999.

[121] W. Jr. Sabbagh, L. J. Flatauer, A. J. Bardwell, and Bardwell L. Specificity of map kinase signaling in yeast differentiation involves transient versus sustained mapk activation. *Molecular Cell*, 8(683-691), 2001.

[122] Y. Sako, S. Minoguchi, and T. Yanagida. Single molecule imaging of EGFR signaling on the surface of living cells. *Nature Cell Biology*, 2:168–172, 2000.

[123] G. S. Salvesen and C. S. Duckett. IAP proteins: blocking the road to death ś door. *Nature Reviews Molecular Cell Biology*, 3:401–410, 2002.

[124] K. Saso, Gisela Moehren, K. Hagashi, and J. B. Hoek. Differential inhibition of epidermal growth factor signaling pathways in rat hepatocytes by long-term ethanol treatment. *Gastroenterology*, 112:2073–2088, 1997.

[125] C. Scaffidi, I. Schmitz, J. Zha, S. J. Korsmeyer, and P.H. Krammer. Differential modulation of apoptosis sensitivity in CD95 type I and type II cells. *The Journal of Biological Chemistry*, 274:22532–22538, 1999.

[126] J. Schlessinger. Signal transduction by allosteric receptor oligomerization. *TIBS*, 13:443–447, 1988.

[127] J. Schlessinger and A. Ullrich. Growth factor signaling by receptor tyrosine kinases. *Neuron*, 9:383–391, 1992.

[128] J. S. Sebolt-Leopold, D. T. Dudley, R. Herrera, K. Van Beceleare, A. Wiland, R. C. Gowan, H. Tecle, S. D. Barret, A. Bridges, S. Przybranowski, W. R. Leopold, and A. R. Saltiel. Blockade of the map kinase pathway suppresses growth of colon tumors in vivo. *Nat. Med.*, 5:810 – 816, 1999.

[129] B. A. Sermon, P. N. Lowe, M. Strom, and J. F. Eccleston. The importance of two conserved arginine residues for catalysis by the RasGTPase-activating protein, neurofibromin. *The Journal of Biological Chemistry*, 273:9480–9485, 1998.

[130] B. Shapiro, A. Lechenko, and E. Mjolsness. Automatic model generation for signal transduction with applications to MAP-kinase pathways. In *In Proc. 1st International Conference on Systems Biology*, pages 64–74, 2000.

[131] S. Y. Shvartsman, P. Dent., H. S. Wiley, and D. A. Lauffenburger. Context dependent signaling in autocrine loops with positive feedback: modeling and experiments in the EGFR system. *submitted*, 2002.

[132] M. Sibilia, J. P. Steinbach, L. Stingl, A. Aguzzi, and Wagner E. F. A strain-independent postnatal neurodegeneration in mice lacking the EGF receptor. *EMBO J.*, 17:719–731, 1998.

[133] M. Sibilia and E. F. Wagner. Strain-dependent epthelial defects in mice lacking the EGF receptor. *Science*, 269:234–238, 1995.

[134] R. M. Siegel, F. K.-M. Chan, H. J. Chun, and M. J. Lenardo. The multifaceted role of Fas signaling in immune cell homeostasis and autoimmunity. *Nature Immunology*, 1(6):469–473, 2000.

[135] R. A. Smith and C. Baglioni. Multimeric structure of the tumor necrosis factor receptor of hela cells. *The Journal of Biochemistry*, 264:14646–14652, 1989.

[136] P. Smolen, D. A. Baxter, and J. H. Byrne. Mathematical modeling of gene networks. *Neuron*, 26:567–5880, 2000.

[137] M. B. Sporn and A. Roberts. Autocrine secretion -10 years later. *Annals of Internal Medicine*, 117:408–414, 1992.

[138] M. B. Sporn and G. J. Todaro. Autocrine secretion and malignant transformation of cells. *N. Eng. J. Med.*, 303:878–880, 1980.

[139] C. Starbuck. Mathematical model for the effects of epidermal growth factor receptor trafficking dynamics on fibroblast responses. *Biotechn. Prog.*, 8:132–143, 1992.

[140] J. Stelling, A. Kremling, M. Ginkel, K. Bettenbrock, and E. D. Gilles. *Towards a Virtual Biological Laboratory*, chapter 5. Foundations of Systems Biology. MIT Press, 2001. in press.

[141] Henning R. Stennicke, Quinn L. Deveraux, and Eric W. Humke et al. Caspase-9 can be activated without proteolytic processing. *The Journal of Biological Chemistry*, 274:8359–8362, 1999.

[142] Henning R. Stennicke, adn Hwain Shin Juliane M. Jürgensmeier, Quinn Deveraux, Beni B. Wolf, Xiaohe Yang, qiao Zhou, H. Michael Ellerby, Lisa M. Ellerby, Dale Bredesen, Douglas R.Green, John C. Reed, Christopher J. Froehlich, and G.S.Salvesen. Pro-caspase-3 is a major physiologic target of caspase 8. *The Journal of Biological Chemistry*, 273(42):27084–27090, 1998.

[143] S. M. Sun, M. MacFarlane, and J. Zhuang et. al. Distinct caspase cascades are initiated in receptor-mediated and chemical-induced apoptosis. *The Journal of Biological Chemistry*, 274:5053–50560, 1999.

[144] Jens R. Sydor, Martin Engelhard, Alfred Wittinghofer, Roger S. Goody, and Christiona Herrmannn. Transient kinetic studies on the interaction of ras and the ras-binding domain

of c-raf -1 reveal rapid equilibration of the complex. *Biochemistry*, 37:14292–14299, 1998.

[145] R. Takahashi, Q. Deveraux, and I. Tamm et al. A single BIR domain of XIAP sufficient for inhibiting caspases. *The Journal of Biological Chemistry*, 273:7787–7790, 1998.

[146] L. A. Tartaglia, D. Pennica, and D. V. Goeddel. Ligand passing: the 75-kDa tumor necrosis factor (TNF) receptor recruits TNF for signaling by the 55-kDa TNF receptor. *The Journal of Biological Chemistry*, 268(25):18543–18548, 1993.

[147] M. N. Teruel and T. Meyer. Translocation and reversible localization of signaling proteins a dynamic future for signal transduction. *Cell*, 103:181–184, 2000.

[148] S. Tokumaro, S. Higashiyama, T. Endo, T. Nakagawa, J.-I. Miyagawa, K. Yamamori, Y. Hanakawa, H. Ohmoto, K. Yoshino, Y. Shirakata, Y. Matsuzawa, K. Hashimoto, and N. Taniguchi. Ectodomain shedding of epidermal growth factor receptor ligands is required for keratinocyte migration in cutaneous wound healing. *J. Cell Biology*, 151:209–219, 2000.

[149] S. E. F. Tran, T. H. Holmström, M. Ahonen, V.-M. Kähäri, and J. E. Eriksson. MAPK/ERK overrides the apoptotic signaling from Fas, TNF, and TRAIL receptors. *The Journal of Biological Chemistry*, 276(19):16484–16490, 2001.

[150] S. Traverse, K. Seedorf, H. Paterson, C. J. Marshall, P. Cohen, and A. Ullrich. EGF triggers neuronal differentiation of PC12 cells that overexpress the EGF receptor. *Curr. Biol.*, 4:694–701, 1994.

[151] J. Tschopp, M. Irmler, and M. Thome. Inhibition of fas death signals by FLIPs. *Curr Opin Immunol*, 10(5):552–8, 1998.

[152] J. J. Tyson. Molecular, metabolic and genetic control: an introduction. *Chaos*, 11(1):81–83, 2001.

[153] J. J. Tyson and H. G. Ottmer. The dynamics of feedback control circuits in biochemical pathways. *Progr. Theor. Biol.*, 5:1–60, 1978.

[154] K. Ueki, S. Matsuda, K. Tobe, and T. Kadowaki. Feedback regulation of mitogen activated protein kinase kinase kinase activity of c-Raf-1 by phorbol ester stimulation. *J. Biol. Chem.*, 269:15756–15761, 1994.

[155] D. Veale, T. Ashcroft, C. Marsh, G. J. Gibson, and A. L. Harris. Epidermal growth factor receptors in non-small cell lung cancer. *Br. J. Cancer*, 55(513-516), 1987.

[156] I. M. Verma, J. K. Stevenson, E. M. Schwarz, D. Van Antwerp, and S. Miyamoto. Rel/NF-κB/IκB family: intimate tales of association and dissociation. *Genes & Development*, 55:2723–2735, 1995.

[157] G. von Dassow, E. Meir, E. M. Muro, and G. M. Odell. The segment polarity network is a robust developmental module. *Nature*, 406(188-192), 2000.

[158] H. Wajant. The Fas signaling pathway: More than a paradigm. *Science*, 296:1635–1636, 2002.

[159] E. Walter and L. Pronazto. *Identification of parametric models from experimental data*. Springer Verlag, 1997.

[160] C. Y. Wang, M. W. Mayo, R. G. Korneluk, D. V. Goeddel, and A. S. Baldwin. NF-kappaB antiapoptosis: induction of TRAF1 and TRAF2 and c-IAP1 and c-IAP2 to suppress caspase-8 activation. *Science*, 281:1680–1683, 1998.

[161] Z. Wang, P.S. Tung, and M. F. Moran. Association of p120rasGAP with endocytic components and colocalization with epidermal growth factor receptor in response to EGF stimulation. *Cell Growth Diff.*, 7:123–133, 1996.

[162] J. D. Wassermann and M. Freeman. An autoregulatory cascade of egf receptor autocrine signaling patterns in the *drosophila egg*. *Cell*, 95:355–364, 1998.

[163] H. Waterman, G. Levkowitz, I. Alroy, and Y. Yarden. The RING figner of c-Cbl mediates desensitation of the EGF receptor. *J. Biol. Chem.*, 274:22151–22154, 1999.

[164] S. B. Waters, D. Chen, A. W. Kao, S. Okada, K. H. Holt, and J. E. Pessin. Insulin and epidermal growth factor receptors regulate distinct pools of Grb2-SOS in the control of Ras activation. *The Journal of Biological Chemistry*, 271(30):18224–18230, 1996.

[165] M. C. Wei, W.-X. Zong, E. H.-Y. Cheng, T. Lindsten, and S. J. Kormeyer. Proapoptotic BAX and BAK: a requisite gateway to mitochondrial dysfunction and death. *Science*, 292(27):727–730, 2001.

[166] T. Weiss, M. Grell, K. Siemienski, F. Mühlenbeck, H. Dürkop, K. Pfizenmaier, P. Scheurich, and H. Wajant. TNFR80-dependent enhancement of TNFR60-induced cell death is me-

diated by TNFR-associated factor 2 and is specific for TNFR60. *The Journal of Immunology*, 161:3136–3142, 1998.

[167] Tilo Weiss, Matthias Grell, Behnam Hessabi, Soizic Bourteele, Gertraud Mueller, Peter Scheurich, and Harald Wajant. Enhancement of TNF receptor p60-mediated cytotoxicity by TNF receptor p80. *The Journal of Immunology*, 158:2398–2404, 1997.

[168] A. Wells, J. B. Welsh, C. S. Lazar, S. H. Wiley, G. N. Gill, and M. G. Rosenfeld. Ligand-induced transformation by a noninternalizing epidermal growth factor receptor. *Science*, 247:962–964, 1990.

[169] A. J. Whitmarsh, S. H. Yang, M. S. Su, A. D. Sharrocks, and R. J. Davis. Role of p38 and JNK mitogen-activated protein kinases in the activation of ternary complex factors. *Mol. Cell.*, 17:2360–2371, 1997.

[170] H. S. Wiley. Anomalous binding of epidermal growth factor to a431 cells is due to the efect of high receptor densities and a saturable endocytic system. *J. Cell Biol.*, 107:801–810, 1991.

[171] C. J. Wu, Z. Chen, A. Ullrich, M. I. Greene, and D. M. O'Rourke. Inhibition of EGFR mediated phophoinositide-3-oh kinase PI3-K signaling and glioblastoma phenotype by signal-regulatory proteins SIRPs. *Oncogene*, 19:3999–4010, 2000.

[172] W. Xie, A. J. Paterson, E. Chin, L. M. Nabell, and J. E. Kudlow. Targeted expression of a dominant negatice epidermal growth factor receptor in the mammary gland of transgenic mice inhibits pubertal mammary duct development. *Mol. Endocrinol*, 11:1766–1781, 1997.

[173] H. Yeh and H. Wu. Thermodynamic characterization of the interaction between TRAF2 and tumor neceorsis factor receptor peptides by isothermal titration calorimetry. *PNAS*, 97:8961–8966, 2000.

[174] Yonehara M. Yonehara S, Ishii A. A cell-killing monoclonal antibody (anti-fas) to a cell surface antigen co-downregulated with the receptor of tumor necrosis factor. *J. Exp. Med.*, 169:1747–56, 1989.

[175] J. M. Zapata, S. Matsuzawa, A. Godzik, E. Leo, S. A. Wasserman, and J. C. Reed. The Drosophila tumor necrosis factor receptor-associated factor-1 (DTRAF1) interacts with Pelle and regulates NFkappaB activity. *J Biol Chem*, 275:12102–7, 2000.

[176] H. Zou, Y. Li, X. Liu, and X. Wang. An APAF-1-cytochrome c multimeric complex is a functional apoptosome that activates procaspase-9. *The Journal of Biological Chemistry*, 274:11549–11556, 1999.